



MONASH University

The use of geodetic and geophysical observations and modelling to interpret ground deformation at the Okataina Volcanic Centre, North Island, New Zealand.

Lucas Holden

(BSc Hons RMIT University, MSc RMIT University)

A thesis submitted for the degree of *Doctor of Philosophy* at
Monash University in 2017

School of Earth, Atmosphere and Environment
Monash University, Clayton, Victoria, Australia

Copyright notice

I certify that I have made all reasonable efforts to secure copyright permissions for third-party content included in this thesis and have not knowingly added copyright content to my work without the owner's permission.

Abstract

The Taupo Volcanic Zone (TVZ) in the North Island of New Zealand is the world's most productive regions of rhyolitic volcanism and contains the highly active Okataina Volcanic Centre (OVC). The OVC is one of two large active rhyolite centres located in a tectonically active section of the TVZ, known as the Taupo Rift. The most recent volcanic unrest at the OVC includes the ~AD1315 Kaharoa and 1886 Tarawera eruptions. There has been significant research on the structural, volcanic and geophysical properties of the rift and OVC, but less focus on deformation using geodetic data and numerical modelling. The limited studies that have utilised geodetic data do not clearly resolve the present day distribution of deformation and strain rates within the rift and OVC. Further, the ground deformation patterns preceding volcanic activity the OVC are poorly constrained and restricted to predictions from basic modelling and comparison to other volcanoes worldwide. A better understanding of the deformation patterns preceding renewed volcanic activity, as well as contemporary background deformation patterns at the OVC and vicinity, is essential. This will ensure that any deformation signals from volcanic processes at the OVC are correctly identified and distinguished from those related to regional tectonic or local hydrothermal processes within the rift.

This study uses existing and new GPS campaign and continuous GPS (cGPS) data collected between 1998 and 2011 to present a picture of contemporary deformation at the OVC and within the surrounding rift in detail. The results show a highly heterogeneous deformation and strain rate field (both extension and shortening) through the study area, partitioned into different parts of the rift. In the OVC, a locally rotated horizontal velocity field is observed, as well as significant vertical deformation and variable strain rates across the caldera. In the Tarawera rift, elevated extension and shear rates are identified, which may have significant implications for volcanism there. Also, a shortening pattern is identified through the central rift, which is unexpected in an intra-arc rifting environment. This study also uses Finite element (FE) modelling techniques to investigate ground deformation patterns associated with hypothetical magma accumulation and diking processes at the OVC. The results show the modelled horizontal and vertical displacement fields have a number of key features, which include prominent lobe based regions extending northwest and southeast of the OVC. The results also show that the ring fault structure increases the magnitude of the displacements inside the caldera, in particular in the vicinity of the southern margin. As a result, some of the cGPS stations in the vicinity of the OVC are more important for measuring deformation related to volcanic processes than others. The results have important implications for how any future observed deformation at the OVC is observed and interpreted.

Declaration

This thesis contains no material which has been accepted for the award of any other degree or diploma at any university or equivalent institution and that, to the best of my knowledge and belief, this thesis contains no material previously published or written by another person, except where due reference is made in the text of the thesis.

Signature:



Print Name: *Lucas Holden*

Date: 31/05/2017

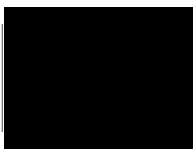
Publications during enrolment

I hereby declare that this thesis contains no material which has been accepted for the award of any other degree or diploma at any university or equivalent institution and that, to the best of my knowledge and belief, this thesis contains no material previously published or written by another person, except where due reference is made in the text of the thesis.

This thesis includes three original papers published in peer-reviewed journals. These papers comprise chapters 2, 3 and 4. The core theme of the thesis is the use of geodetic and geophysical observations and modelling to understand ground deformation patterns at the Okataina Volcanic Centre. The ideas, development and writing up of all the papers in the thesis were the principal responsibility of myself, the student, working within the School of Earth, Atmosphere and Environment under the supervision of Professor Ray Cas, Dr Laurent Ailleres and Dr Nico Fournier.

The inclusion of co-authors reflects the fact that the work came from active collaboration between researchers and acknowledges input into team-based research. In the case of chapters 2, 3 and 4 my contribution to the work involved the following:

Student signature:



Date:

29/05/2017

The undersigned hereby certify that the above declaration correctly reflects the nature and extent of the student's and co-authors' contributions to this work. In instances where I am not the responsible author I have consulted with the responsible author to agree on the respective contributions of the authors.

Main Supervisor signature:



Date: 7/06/2017

Acknowledgements

I first wish to thank my supervisors, Professor Ray Cas, Dr Laurent Ailleres and Dr Nico Fournier for their friendship, support and guidance during the period of this candidature. I am very grateful for the latitude provided to me to develop and undertake this research as well as their willingness to help at any point along the way. I am also very grateful for their patience, particularly with my limited background in the geological and geophysical aspects of the research. I would also like to thank my RMIT colleagues, David Silcock, Gita Pupedis, Colin Arrowsmith, Rod Deakin and Suelynn Choy for their support and assistance over the many years during this part time study. I am very grateful for their friendship and support. I am also very grateful for the friendship of my fellow PhD students, Dr Teagan Blaikie and Dr Jim Driscoll for their friendship and support. I have many fond memories of our time together in our Monash office.

Finally, I would like to thank GNS Science, New Zealand, for allowing me to join their GNSS campaign field survey in 2011, and then use the collected GNSS data and other campaign data for my study. I would like to personally thank Laura Wallace, (the late) John Beavan, Neville Palmer and Susan Ellis for their support and assistance over the last eight years.

Table of Contents

Copyright notice	ii
Abstract.....	iii
Declaration.....	vi
Publications during enrolment	vii
Acknowledgements.....	x
Table of Contents.....	xiii
List of Figures	xvii
List of Tables	xix

1 Introduction: A summary of research aims and methods and geological setting of the Taupo Volcanic Zone and the Okataina Volcanic Centre (OVC)..... 1

1.1 Introduction.....	2
1.2 Previous geodetic and numerical modelling studies at the OVC.....	4
1.3 Problem statement.....	6
1.4 Research aims	7
1.5 Research method.....	7
1.6 Thesis structure	8
1.7 Regional geology and tectonic setting of the OVC	9
1.7.1 Rift kinematics	9
1.7.2 Rift Structure.....	12
1.7.3 Lithospheric Structure of the Central North Island.....	15
1.7.4 Volcanism in the TVZ	16
1.7.5 Magmatism in the TVZ.....	17
1.7.6 Relationship between tectonic, magmatic and volcanic processes and rift structures	18
1.7.7 The Okataina Volcanic Centre.....	21
1.8 References.....	25

2 Contemporary ground deformation in the Taupo Rift and Okataina Volcanic Centre from 1998 to 2011, measured using GPS..... 34

2.1 Abstract.....	35
2.2 Introduction.....	36
2.3 Rift structure and kinematics	38

2.4	The Okataina Volcanic Centre.....	41
2.5	GPS data	44
2.6	GPS processing and velocity estimation.....	47
2.7	Results.....	51
2.7.1	Horizontal and vertical deformation	51
2.7.2	Strain rates.	55
2.8	Interpretation of results across study area.....	63
2.8.1	Outside the Rift.....	63
2.8.2	Inside the rift.....	64
2.8.3	Within the OVC	65
2.9	Discussion.....	65
2.9.1	Processes driving contemporary deformation in the Taupo Rift and OVC	65
2.9.2	Relationship of OVC deformation to volcanic, hydrothermal and tectonic processes and implications for geodetic monitoring.....	68
2.10	Conclusion	70
2.11	References.....	72

3 Evaluating a Campaign GNSS Velocity Field Derived From an Online Precise Point Positioning Service..... 79

3.1	Abstract.....	80
3.2	Introduction.....	80
3.3	Background.....	82
3.4	Data and Methodology.....	84
3.5	Results.....	88
3.5.1	CORS Data Results.....	88
3.5.1.1	Coordinate repeatabilities	88
3.5.1.2	Comparison to APREF or ITRF coordinate solutions	89
3.5.1.3	Velocity Results	90
3.5.2	NZ Campaign Data Results	91
3.5.2.1	Coordinate repeatabilities	91
3.5.2.2	Velocity Results	92
3.6	Discussion.....	94
3.6.1	How reliable are our results?	94

3.6.2	Can our results be used to observe various geophysical processes?	95
3.6.3	What implications do these results have for GNSS campaign fieldwork technique and post-processing and future geophysical research?	95
3.7	Conclusions.....	97
3.8	References.....	99
3.9	Electronic Supplemently Material	104
4	Ground deformation patterns associated with volcanic processes at the Okataina Volcanic Centre.....	114
4.1	Abstract.....	115
4.2	Introduction.....	115
4.3	Regional Geological Setting	117
4.4	The Okataina Volcanic Centre.....	119
4.4.1	Recent eruptive activity	121
4.4.2	Contemporary deformation at the OVC.....	121
4.4.3	Previous FE modelling at the OVC	122
4.5	Materials and methods	122
4.5.1	FE Models.....	122
4.5.2	FE ring fault structure	125
4.6	Results.....	126
4.6.1	The FE spherical magma chamber model.....	126
4.6.2	The FE rectangular magma chamber model	128
4.6.3	The FE 1 m wide dike model.....	128
4.6.4	Deformation results with ring fault structure	130
4.7	Discussion.....	133
4.7.1	Key characteristics of the modelling results	133
4.7.2	Can magma accumulation or emplacement occur at depth at the OVC without detection by the cGPS network?	134
4.7.3	Limitations of this research and directions for further research	136
4.8	Conclusions.....	137
4.9	Electronic Supplementary Material	140
4.10	References.....	146

5	Summary of results and research implications.....	154
5.1	Introduction.....	154
5.2	Summary of Chapter 2: Contemporary ground deformation in the Taupo Rift and Okataina Volcanic Centre from 1998 to 2011, measured using GPS.....	154
5.3	Summary of Chapter 3: Evaluating a Campaign GNSS Velocity Field Derived From an Online Precise Point Positioning Service.	156
5.4	Summary of Chapter 4: Ground deformation patterns associated with magma migration beneath the Okataina Volcanic Centre.....	157
5.5	Research Implications.....	158
5.5.1	Implications for rift processes and related deformation.....	158
5.5.2	Implications for volcanic processes at the OVC.....	159
5.5.3	Implications for geodetic monitoring at the OVC and other calderas worldwide.	160
5.5.4	Implications for GNSS data processing and field surveys.....	162
5.5.5	Suggestions for further research	162
5.6	References.....	165

List of Figures

Figure 1.1 – Location and generalised structure of the North Island and TVZ.	10
Figure 1.2 – Mechanism proposed by Wallace et al., (2004) for rotation of the eastern North Island and extension in the TVZ.	11
Figure 1.3 – Structural diagram of the Taupo Rift.....	13
Figure 1.4 –Schematic model of crust and upper mantle structure of the TVZ proposed by Stratford and Stern, (2006)..	16
Figure 1.5 – Relationship between tectonic faulting and dike intrusion in the Taupo rift and their contribution to extension across volcanic centres as proposed by Seebeck and Nichol, (2009).	21
Figure 1.6 – Location map and structural details of the OVC from Nairn (2002).....	22
Figure 2.1 – Structural diagram of the Taupo Rift.....	40
Figure 2.2 – Location map and structural details of the Okataina Volcanic Centre (OVC) from Nairn (2002)..	42
Figure 2.3 – Location and distribution of all GPS stations used in this processing.....	46
Figure 2.4 – Horizontal GPS velocities in the local fixed reference frame, defined by campaign stations west and northwest of the rift (see text for further details).....	52
Figure 2.5 – Vertical velocities for GPS stations in the local fixed reference frame.....	53
Figure 2.6 – Fitted surface of vertical velocities through the study area (produced using Triangulate command in GMT).....	54
Figure 2.7 – Horizontal principal strain rate axes derived from horizontal GPS velocity rate estimates using the Delaunay approach in SSPX software (Cardozo and Allmendinger 2009).....	56
Figure 2.8 – Dilation strain rate field derived from horizontal GPS velocity rate estimates using the Delaunay approach in SSPX software (Cardozo and Allmendinger 2009)..	58
Figure 2.9 – Shear strain rate field derived from horizontal GPS velocity rate estimates using the Delaunay approach in SSPX software (Cardozo and Allmendinger 2009)..	59
Figure 2.10 – Fitted surface to orthogonal velocities across the study site (produced using Triangulate command in GMT).....	61
Figure 2.11 – Velocity profiles produced for a) Whakatane, b) Okataina and c) Kapenga segments (Black lines) from plotting velocity components orthogonal to rift segments (in mm/yr) as a function of distance (in km)..	62
Figure 2.12 – De-trended time series plots for cGPS stations with study region..	70
Figure 3.1 – Classification of crustal deformation processes by rate (m/sec.) and duration (in seconds), from Massonnet and Feigl (1998)..	83

Figure 3.2 – Location and distribution of GNSS stations used in the Bernese and JPL APPS processing..	86
Figure 3.3 – Average day to day coordinate solution repeatabilities for IGS CORS station data..	89
Figure 3.4 – Average coordinate solution differences and their uncertainties for IGS CORS station data for each campaign..	90
Figure 4.1 – Regional geological setting and location and distribution of all GPS stations used in this study..	118
Figure 4.2 – Location map and structural details of the Okataina Volcanic Centre (OVC) from Nairn (2002)..	120
Figure 4.3 – A) Schematic 3D model of OVC ring fault structure used in the FE modelling (not to scale)..	124
Figure 4.4 – A) Horizontal and vertical displacement associated with a spherical cavity of 1.06 km radius at 6km depth. B) Horizontal and vertical displacement associated with a spherical cavity of 1.38km at 6km depth. C) Horizontal and vertical displacement associated with 1.06km radius spherical cavity, with ring fault structure. D) Horizontal and vertical displacement associated with 1.38km radius spherical cavity, with ring fault structure..	127
Figure 4.5 – The easting (A), northing (B) and vertical (C) displacement components associated with 10MPa overpressure of a rectangular magma chamber at 6km depth beneath the Tarawera Rift. The easting (D), northing (E) and vertical (F) displacement components associated with intrusion of a 1m wide vertical dike at 5km depth below the Tarawera Rift..	130
Figure 4.6 – The easting (A), northing (B) and vertical (C) displacement components associated with 10MPa overpressure of a rectangular magma chamber at 6km depth beneath the Tarawera Rift, in the presence of the OVC ring fault structure. The easting (D), northing (E) and vertical (F) displacement components associated with a 1m wide vertical dike at 5km depth below the Tarawera Rift in the presence of the OVC ring fault structure..	131
Figure 4.7 – Supplementary Material A – Comparison of horizontal (A) and vertical (B) displacements determined from Mogi analytical solution and Pylith FE solution for a 1.06 and 1.38 km radius spherical magma chamber (respectively) at 6 km depth. C - Comparison of horizontal and vertical displacements determined from Okada analytical solution and Pylith FE solution for a 4km long, 1m wide vertical dike from 5 to 1km depth.	141
Figure 4.8 – Supplementary Material B – The easting (A), northing (B) and vertical (C) displacement components associated with 10MPa overpressure of a 1.06 km radius spherical magma chamber at 6km depth with the OVC ring fault structure..	143
Figure 4.9 – Supplementary Material C – The easting (A), northing (B) and vertical (C) displacement components associated with 10MPa overpressure of a 1.38 km radius spherical magma chamber at 6km depth with the OVC ring fault structure..	145

List of Tables

Table 2.1 – History of occupation for campaign sites processed.....	44
Table 2.2 – GPS velocities of TVZ sites.....	50
Table 3.1 – Horizontal and vertical velocities and their differences and uncertainties for IGS CORS station data..	91
Table 3.2 – Horizontal and vertical velocities, their differences and uncertainties for the campaign data.....	94
Table 3.3 – Average coordinate solution repeatabilities, coordinate differences and their uncertainties for IGS CORS stations..	104
Table 3.4 – Average Bernese and APPS coordinate solution repeatability for each campaign.	105
Table 3.5 – Final coordinate solution repeatabilities, coordinate differences and their uncertainties for selected regional IGS stations..	107
Table 3.6 – 2000 Bernese and APPS campaign data coordinate solution repeatabilities..	108
Table 3.7 – 2005 Bernese and APPS campaign data coordinate solution repeatabilities.	109
Table 3.8 – 2007 Bernese and APPS campaign data coordinate solution repeatabilities.	111
Table 3.9 – 2011 Bernese and APPS campaign data coordinate solution repeatabilities..	113

1 Introduction: A summary of research aims and methods and geological setting of the Taupo Volcanic Zone and the Okataina Volcanic Centre (OVC)

1.1 Introduction

The signals emanating from volcanoes must be studied closely to determine whether an eruption is likely and to provide appropriate public warnings (Lowenstern et al., 2006). One of the major difficulties of identifying precursory signals of eruptions of large calderas is that no significant caldera eruption has occurred in recent history. These systems are capable of large-scale eruptions and exhibit frequent unrest, but have undergone only small eruptions historically (Newhall and Dzurisin, 1988). Although the research community has had some success in predicting small eruptions, the scarcity of great eruptions over the past one hundred and fifty years means that there is little experience understanding the prelude to major events (Lowenstern et al., 2006). This means that there are as yet no soundly based criteria for taking a given set of geophysical observations of unrest at a caldera volcano and using them to reliably predict the likelihood, size or timing of a future event (Ellis et al., 2007).

This process is especially difficult at large caldera systems that have complex geothermal systems or located in complex tectonic settings. Geothermal activity can mask changes in subsurface magma chambers, or generate ground subsidence and uplift, resulting in flawed interpretations or predictions of eruptive behaviour (Poland et al., 2006; Peltier et al., 2009b; Lowenstern et al., 2006). The Campi Flegrei caldera is a classic example of this behaviour and has undergone significant periods of ground deformation in the past, often without any major eruptions (De Natale et al., 2001). Similarly, the signals of an impending volcanic eruption may be disguised within regional tectonic activity (Cabral-Cano et al., 2008). For example, Cabral-Cano et al., (2008) identified that ground deformation signals observed at GPS stations on Popocatepétl volcano reflected regional aseismic transients related to the Middle America Trench subduction process rather than local volcanic activity.

Recently, scientists have considered that short-term eruption precursors are preceded by deeper and therefore more subtle magma changes, that nonetheless, can be measured at the surface (Dzurisin, 2003). If these subtle changes can be identified, the long-term behavior of volcanic systems can be better understood. A combination of geodetic instruments is often used to attempt this, including precise levelling, campaign and continuous GPS (cGPS) and satellite interferometry (InSAR). Complementing these surface observations are numerical modelling techniques such as Finite Element modelling (FE), which can be used to model stress and deformation in volcanoes. This is of fundamental importance for understanding unrest periods and for accurate forecasting volcano failure and instability, such as may result in large scale lateral and vertical collapses and eruptions (Walter et al., 2005; Gudmundsson et al., 2009). Numerical models can be also used to forward model changes in the volcano system and simulate the resulting surface deformation field. These provide new

important insights into the characteristics of the deformation associated with renewed volcanic activity, but also the sensitivity of the existing geodetic monitoring networks to detect the deformation.

The Okataina Volcanic Centre (OVC) is one of two large active rhyolite centres in the modern Taupo rift, within the Taupo Volcanic Zone (TVZ) in the central island of New Zealand. The TVZ is a region of active tectonic extension (Darby et al., 2000; Wallace et al., 2004), high heat flow and magmatism (Bibby et al., 1995) and is one of the most productive regions of rhyolitic volcanism in the world (Wilson et al., 1995; Sutton et al., 2000; Price et al., 2005). The OVC is one of seven large caldera centres in the TVZ that have produced very large eruptions and it is the most recently active volcanic region of the TVZ (Houghton et al., 1995; Wilson et al., 1995). The most recent volcanic unrest at the OVC includes the ~AD1315 Kaharoa and 1886 Tarawera eruptions, in which dike intrusion was a key eruption mechanism (Nairn and Cole, 1981; Sherburn and Nairn, 2001, 2004; Nairn et al., 2004; Nairn et al., 2005). Magma supply is considered plentiful in this part of the rift and has been linked to large-scale deformation patterns and variations in rift architecture (Rowland et al., 2010). Wilson et al., (2009) propose that in this region of the rift, complex interactions between magmatism and tectonic processes exist, whereby magma emplacement mediates crustal deformation, while rift related normal faulting can control magma emplacement. However, it is not clear how regional tectonic structure, rift kinematics and magmatic processes relate to deformation patterns and the style and timing of volcanism at the OVC.

Geodetic studies within the central Taupo rift have been limited, but have provided a better understanding of the regional velocity field (Beavan and Haines, 2001) and rifting rates (Darby et al., 2000; Wallace et al., 2004). However, these studies do not provide a detailed picture of the horizontal and vertical velocity and strain rate fields through the Taupo rift, and it remains difficult to identify ground deformation patterns within the OVC linked to volcanic processes there. The OVC is presently monitored using campaign and continuous GPS (cGPS), seismographs and lake levelling instrumentation. Surface deformation has been observed across the OVC (Scott, 1989), however there is no clear evidence that it is linked to renewed volcanic unrest. Further, since there has been no recent significant activity at the OVC, the ground deformation patterns preceding volcanic activity at the OVC are poorly constrained and have only been considered in a few studies (Sherburn and Nairn, 2001, 2004).

The last eruption within the OVC (the 1886 Tarawera eruption) was preceded by only one hour of felt earthquakes (Nairn 2002). Although seismicity is monitored at the OVC with a network of seismographs, increased seismic noise may be interpreted as normal tectonic activity, which characterizes this region (Bryan et al., 1999). As a result, seismic monitoring cannot be solely relied upon and should be used alongside other

techniques such as geodetic monitoring. Since there has been no recent significant activity at the OVC, the geodetic precursors leading to a volcanic crisis remain relatively unknown. Thus, an outstanding problem at the OVC is whether magma bodies could exist or accumulate at depth without being detected using modern geophysical techniques (Sherburn and Nairn, 2004).

1.2 Previous geodetic and numerical modelling studies at the OVC

Studies using geodetic data within New Zealand's North Island and Taupo rift have been limited, but have provided a better understanding of the regional velocity field (Beavan and Haines, 2001) and rifting rates (Darby et al., 2000; Wallace et al., 2004). Alongside geological studies, these have contributed significantly to studies regarding the large-scale structure of the Taupo rift. However they do not provide a detailed picture of the horizontal and vertical velocity and strain rate fields through the central Taupo rift and OVC. As a result, there is limited knowledge about deformation patterns through the Taupo rift and it remains difficult to identify ground deformation patterns within the OVC and relate these to volcanic processes there.

At the OVC, geodetic studies have primarily been limited to the use of a horizontal strain network at both Lake Rotomahana and Tarawera rift summit and lake levelling network at Lake Tarawera (Scott, 1989; Sherburn and Nairn 2001). These networks have measured a regional tilt (0.9 micro radians per year at an azimuth of 72°) in the lake levelling network and shear strain (1.66 ± 1.6 ppm yr⁻¹) and dilation (-4.33 ± 0.9 ppm yr⁻¹) across the strain networks, the source of which was not identified. The horizontal strain networks established at Lake Rotomahana and the Tarawera Rift are no longer surveyed (Sherburn and Nairn, 2004) and have been superseded by the introduction of GPS. Today, monitoring of ground deformation is primarily achieved using a network of cGPS receivers within and around the caldera, which are complemented by campaign GPS surveys. This cGPS network is a small part of the nationwide network of GPS and seismographs known as GeoNet.

The cGPS receivers are part of the two-strategy approach to monitoring undertaken on active volcanoes in NZ (Scott and Travers, 2009). They note that the first approach is to identify unrest at a volcano using a minimal level of monitoring and is typically undertaken at 'sleeping' volcanoes. The second approach is monitoring during an eruptive crisis, whereby instruments must be permanently deployed, as there is little opportunity to deploy instrumentation after an eruption. Regional InSAR studies through the Taupo Rift (Samsonov et al., 2011) have also documented very large vertical deformation rates in the OVC region.

The use of the numerical modelling (e.g. FE technique) has been limited and has been applied in other studies for other locations in the TVZ. This includes the Taupo caldera (Ellis et al., 2007; Peltier et al., 2009a), White Island volcano (Peltier et al., 2009b), but not specifically at the OVC. Sherburn and Nairn (2001, 2004) used the Mogi analytical model to predict ground deformation at the OVC. They model deformation related to a 1%, 5% and 15% volumetric increase in a 1.06 km spherical magma chamber at 6km depth. They conclude that the vertical deformation related to the 1% volumetric increase would be measureable across the lake levelling network, but if it were to occur at a steady rate across a number of years it would most likely be interpreted as tectonic in origin.

Sherburn and Nairn (2004), also consider the deformation field preceding a present day eruption similar to the Kaharoa 10m wide dike intrusion event. They consider that surface deformation linked to the rapidly increasing loss of magma at a deep reservoir would occur alongside deformation related to the dike intrusion at a shallower depth. As a result, they suggest that the total deformation signal would consist of a 'deep, longer wavelength deflation signal, upon which was superimposed a shallow short wavelength inflation'. They then speculate that this would be detectable by the monitoring sites on the upper slopes of Mt. Tarawera (which would record uplift), but that more distant sites would observe subsidence due to deflation of the deeper magma source.

Nairn, (1993) states that a basalt eruption within the OVC would probably occur within a short period of increased seismicity, detected over a few days, or at most weeks, before the eruption. He further concludes that this would be difficult to distinguish from the frequent non-volcanic earthquake swarms, which occur yearly without eruptions in the Okataina caldera. Alternatively, he highlights, that if a rhyolitic eruption were to occur at the OVC, it would be preceded by a long period (months to years) of increased seismicity, noticeable ground deformation, change in lake levels and increased hydrothermal activity.

1.3 Problem statement

The Okataina Volcanic Centre is situated in a complex tectonic setting. It is located in a region of tectonic extension (Darby et al., 2000; Wallace et al., 2004), an area of high heat flow (Bibby et al., 1995) and in one of the most productive regions of volcanic activity in the world (Price et al., 2005; Sutton et al., 1995; Wilson et al., 1995). Active geodetic monitoring is currently undertaken using cGPS, stationed permanently within and around the caldera. These are complemented with repeated campaign GPS surveys conducted by GNS Science NZ. Such monitoring must be accompanied by an understanding of what is likely to happen during a magma inflation event, as well as the ability to discriminate between such an event and background rifting processes (Ellis et al. 2007).

The last eruption within the OVC (the 1886 Tarawera event) was preceded by only one hour of felt earthquakes (Nairn and Cole, 1989; Nairn, 1993; Nairn 2002). Although, seismicity is monitored at the OVC with a network of seismographs, any increased seismic noise could be interpreted as normal tectonic activity, which characterizes this region (Bryan et al., 1999). As a result, seismic monitoring cannot be solely relied upon and must be coupled with other techniques such as ground deformation monitoring. However, if significant volumes of magma can accumulate in the crust below volcanoes and escape detection, even by extremely sensitive instruments, until a short time before an eruption, long term hazard mitigation becomes difficult (Dzurisin, 2003). If such slow aseismic magma accumulation were occurring at the OVC, it is possible that the present geodetic monitoring network may not sufficiently detect any associated ground deformation. A well-designed GPS network, is in some cases, the best means available to capture far-field deformation associated with relatively deep or distributed magmatic sources (Dzurisin, 2003).

Any geodetic data indicating ground deformation at the OVC must also be interpreted with caution. The use of GPS on volcanic systems using precise point-positioning GPS solutions implies that the observations will record both a local signal (assumed to be due to a magmatic process) and a regional tectonic signal (Cabral-Cano et al., 2008). Deformation identified in geodetic monitoring at the OVC, may be due to other geophysical processes such as regional rifting, magmatism, or even aseismic transient deformation events, that have been shown to occur at locations along the Hikurangi margin (Beavan et al., 2007). Thus, to properly interpret any geodetic data at the OVC, the regional geodynamic context must also be considered.

1.4 Research aims

The main aims of this research are:

- To use campaign and continuous GPS data to measure contemporary ground deformation patterns across the OVC and nearby Taupo rift region and consider these in the context of regional tectonic, magmatic and volcanic processes.
- To consider if an alternative GPS data processing technique, using an online Precise Point Positioning (PPP) service can provide coordinate and velocity solutions of suitable precision for geophysical studies.
- To use numerical modelling techniques to model the characteristics of ground deformation patterns associated with hypothetical renewed volcanic activity at the OVC.
- To consider how these modelled deformations might be detected in the existing cGPS network and the sensitivity of the network.

1.5 Research method

The research method will be divided into three main segments: data collection, data processing and numerical modelling.

Data collection: New GPS data will be collected in 2011, as part of the next GNSS field campaign planned by GNS Science New Zealand (GNS) through the central North Island of New Zealand. This field campaign will occupy the regional geodetic monuments within and around the OVC study site and through the Taupo rift. This data will be combined with prior campaign data collected by GNS science as well as regional cGPS stations.

Data processing: The data will be processed using standard GNSS data processing techniques in Bernese (ver. 4.0) software to obtain station coordinate solutions and velocities. From these, strain rates through the OVC region will be calculated. The same data will then be processed with an alternative data processing approach, using an online Precise Point Positioning (PPP) service to calculate the station velocities and compare these to the standard approach.

Numerical modelling: Numerical modelling will be used to simulate ground deformation patterns associated with hypothetical volcanic activity at the OVC. These models will also assist in determining how the modelled deformation fields might be observed in the cGPS network at the OVC and the limit of its sensitivity.

1.6 Thesis structure

This thesis structure includes an introduction and background chapter (chapter 1), three research chapters (chapter 2, 3 and 4) which are based on papers that have been published in a peer-reviewed journal and a discussion and conclusion chapter (chapter 5). Chapter 2, 3 and 4 are published papers. This format is permitted by Monash University for PhD thesis and results in some repetition within the thesis chapters. The content of chapters 2, 3 and 4 are identical to the published versions of the papers they are based on, however their formatting has been altered to ensure consistency through the thesis. Any electronic supplements associated with the published papers have been included in the appropriate chapters.

Chapter 1 – This chapter introduces the research problem and considers previous research and describes the selected methodology. A literature review of the geologic and tectonic setting of the OVC is included.

Chapter 2 – Chapter 2 is based on a paper published in the *Geophysical Journal International* entitled ‘*Contemporary ground deformation in the Taupo Rift and Okataina Volcanic Centre from 1998 to 2011, measured using GPS*’. This chapter presents the results of the processing of over ten years of campaign and continuous GPS data through the Taupo rift and OVC using Bernese software to derive station velocities. These velocities are used to derive strain rates through the study area using the SSPX software. The aim of this chapter is to better constrain the background deformation patterns across the OVC region and consider their link to regional tectonic or local volcanic processes.

Chapter 3 – Chapter 3 is based on a paper published in the *Geophysical Journal International* entitled ‘*Evaluating a Campaign GNSS Velocity Field Derived from an Online Precise Point Positioning Service*’. This chapter describes a new methodology and examines the use of a free online Precise Point Positioning (PPP) service to derive precise coordinate solutions for the GNSS data processed in chapter 2. This chapter then uses these solutions to calculate horizontal and vertical velocities for the geodetic stations within the study area. These are compared with the velocities calculated in chapter 2. The aim of this chapter is to consider if it is possible to obtain suitable coordinate and velocity solutions suitable for geophysical applications using a simpler GNSS processing technique than used in chapter 2.

Chapter 4 – Chapter 4 is based on a paper published in the Journal of Volcanology and Geothermal Research titled ‘*Ground deformation patterns associated with volcanic processes at the Okataina Volcanic Centre*’. This chapter uses the Finite Element (FE) modelling technique to model ground deformation patterns related to hypothetical renewed volcanic activity at the OVC. This includes a simulation of the ground deformation patterns associated with magma accumulation and diking processes at the OVC in greater detail. The ability of the present-day continuous GPS (cGPS) GeoNet monitoring network to detect or observe the modelled deformation is considered.

Chapter 5 – Chapter 5 presents a summary of the major conclusions presented in the research chapters 2, 3 and 4 and discusses the major point arising from these. These key points are considered in the context of the research aims of section 1.4 and discussed in the context of understanding deformation related to volcanic processes and geodetic monitoring at the OVC.

1.7 Regional geology and tectonic setting of the OVC

1.7.1 Rift kinematics

The North Island of New Zealand lies on an active plate boundary and is dominated by the subduction of oceanic crust of the Pacific plate beneath continental crust of the Australian plate (Cole, 1990). This zone of subduction is referred to as the Hikurangi margin and represents the southern ~ 10% portion of the 2800-km-long Tonga – Kermadec arc (Rowland et al., 2010). In the proximity of the North Island, the Pacific plate is subducting obliquely to the west at a rate of approximately 41mm/yr^{-1} (see Figure 1.1) (Henry et al., 2003). This includes a margin-parallel and margin-normal component between latitude of 36° to 41.5° S of $26\text{--}32\text{mm/yr}^{-1}$ and $27\text{--}33\text{mm/yr}^{-1}$ respectively (Beavan et al., 2002). The tectonics of the region are complex and involve considerable changes in tectonic style with time, which (Walcott, 1987) notes might be expected at the transition between subduction and transform zones and between oceanic and continental margins. Three processes dominate the active tectonics of the North Island; 1) subduction of the Pacific plate at the Hikurangi Trough, 2) back-arc rifting within the TVZ and 3) strike-slip faulting within the North Island Dextral Fault Belt (NIDFB) (Wallace et al., 2004).

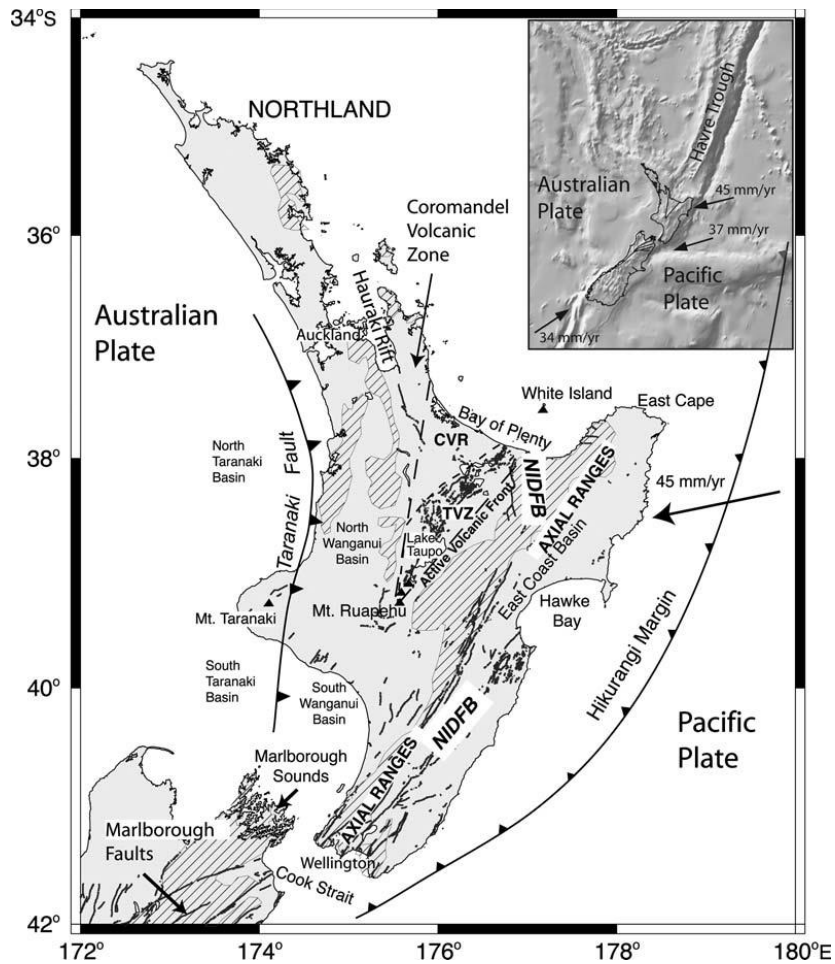


Figure 1.1 – Location and generalised structure of the North Island and TVZ (from Stern et al., 2009). The inset illustrates subduction rates along the Hikurangi margin, east of the TVZ.

Beavan and Haines, (2001) suggest that the inter-plate velocity variation along the Hikurangi margin is due to the close location of the Australian/Pacific pole of rotation and in part to the varying crustal thickness on either side of the plate boundary. They consider that seismic coupling is low and perhaps temporally variable along the northern section of the Hikurangi margin (on the North Island), but along the southern section of the North Island, the subduction boundary is highly coupled. Wallace et al., (2004) state that the combination of the southward increase of inter-seismic coupling along the Hikurangi margin and the varying thickness (and buoyancy) of the subducting oceanic plate, generates a torque effect; that is accommodated by a clockwise rotation of tectonic blocks in the overriding Australian plate of 0.5° - 3.8° Myr (relative to Australian plate) along the Eastern fore-arc of the North Island, as well as extension within the TVZ (schematically illustrated in Figure 1.2). Conversely, the area in the southwest of the eastern North Island is characterised by compression/contraction (Reyners et al., 2006; Nicol and Wallace, 2007). Geological studies (Beanland and

Haines, 1998; Nicol and Wallace, 2007) also support a tectonic block rotation along the eastern North Island, as well as identifying variations in strain rate and style across the wider North Island.

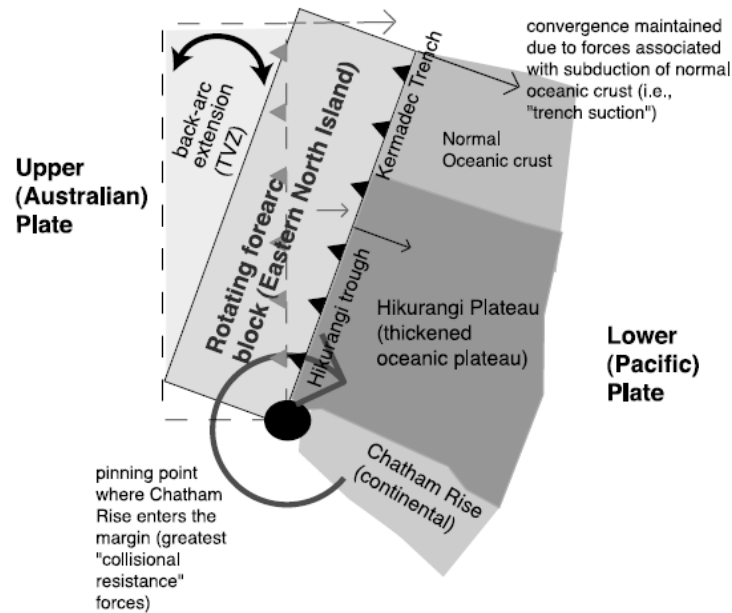


Figure 1.2 – Mechanism proposed by Wallace et al., (2004) for rotation of the eastern North Island and extension in the TVZ (from Wallace et al., 2004).

Within the TVZ, tectonic and volcanic deformation is very complex (Wallace et al., 2004) and is expressed as a zone of normal faults (Villamor and Berryman, 2001) originally referred to as the Taupo Fault Belt (Grindley, 1960), but more commonly the Taupo Rift (Acocella et al., 2003; Spinks et al., 2005; Villamor and Berryman, 2006). This region is characterised by a strain rate field that is primarily extensional (Beavan and Haines, 2001). Geodetic (GPS) observations have measured varying total rates of extension along the rift axis, from $\sim 15 \text{ mm/yr}^{-1}$ near the Bay of Plenty to $\sim 7 \text{ mm/yr}^{-1}$ in the Lake Taupo area (Wallace et al., 2004). Nicol and Wallace, (2007) also show that current geodetic and geological estimates of the rate of extension within the TVZ (Beanland and Haines, 1998; Villamor and Berryman, 2001; Nicol and Wallace, 2007) agree closely.

However, geodetic measurements may not sufficiently measure extension resulting from more rapid processes (on a geological time scale), such as dike intrusion and volcanic eruptions. For instance, Wallace et al., (2004) point out that in some locations within the TVZ, their predicted extension rates are twice as high as those documented by paleo-seismological studies (i.e. Villamor and Berryman, 2001). They associate this with slip on previously unrecognised faults and processes such as dike intrusion, which they consider that must

somehow contribute to the remaining extension budget in the TVZ. Rowland et al., (2010) note that these GPS velocities reflect bulk movement of the Eastern North Island away from the fixed Australian Plate and that the distribution and possible positioning of strain within the TVZ remains unresolved.

1.7.2 Rift Structure

The modern Taupo rift is divided into a number of offset and variably oriented rift segments that are either soft linked by accommodation zones of stress heterogeneity (Rowland and Sibson, 2001) or hard linked by transfer faults (Acocella et al., 2003). Following Acocella et al., (2003), these include the Whakatane, Okataina, Kapenga, Taupo and Ruapehu segments (see Figure 1.3). The axial part of the rift is roughly symmetrical with a central graben axis (Cole and Spinks, 2009). Shallow upper crustal seismicity is primarily concentrated within this area (Bibby et al., 1995). In the central Taupo rift, Rowland et al., (2010) propose that extensional mechanisms vary and include: pure tectonic faulting, mafic and rhyolitic dike intrusion, regional scale uplift and transient subsidence associated with inflation or deflation of mafic magma bodies, and regional-scale basin development in association with rhyolitic caldera-forming eruptions. They divide this region into two parallel zones: a cooler western belt that deforms by faulting (i.e., the TFB – see Figure 1.3) and a warmer zone (the Taupo Reporoa Basin – TRB) of little surface faulting, high heat flow and possibly partial melt in the upper crust. East of the Taupo rift lies the Axial Ranges, where strike-slip faulting dominates (e.g., Beanland and Haines, 1998) and largely coincides with the Axial Ranges (AXIR) tectonic block of Wallace et al., (2004).

Geological studies indicate different components of dextral shear and extension along the rift (Acocella et al., 2003) (see Figure 1.3). Segments with high extension rates (the Okataina and Taupo segments) correspond to the highly active rhyolitic Taupo and Okataina volcanic complexes, while segments with a high degree of trans-tensional shear (Whakatane, Kapenga and Ruapehu segments) coincide with more moderately eruptive andesitic stratovolcanoes (Spinks et al., 2005). The Okataina segment connects the neighbouring parallel Whakatane and Kapenga (Ngakuru) grabens by obliquely trending fault and vent lineations, which is accommodated by curved faults and is also characterised by a slight trend (~20 degrees) variation in the extension direction (orthogonal to Okataina structures with respect to neighbouring segments) (Acocella et al., 2003). This segment occurs at a structural step in the Taupo rift (Acocella et al., 2003; Seebeck et al., 2010). Rowland and Sibson (2001) consider these structural variations a result of stress heterogeneity linked to accommodation zones and question whether this is the cause of magmatic localisation at the OVC or an effect of magmatism. Acocella et al., (2003) suggest that the more easterly change in segment orientation is not

sufficient to account for all the trend rotation and propose the presence of a local rotation due to local readjustment of strain between the interacting Whakatane and Kapenga offset segments.

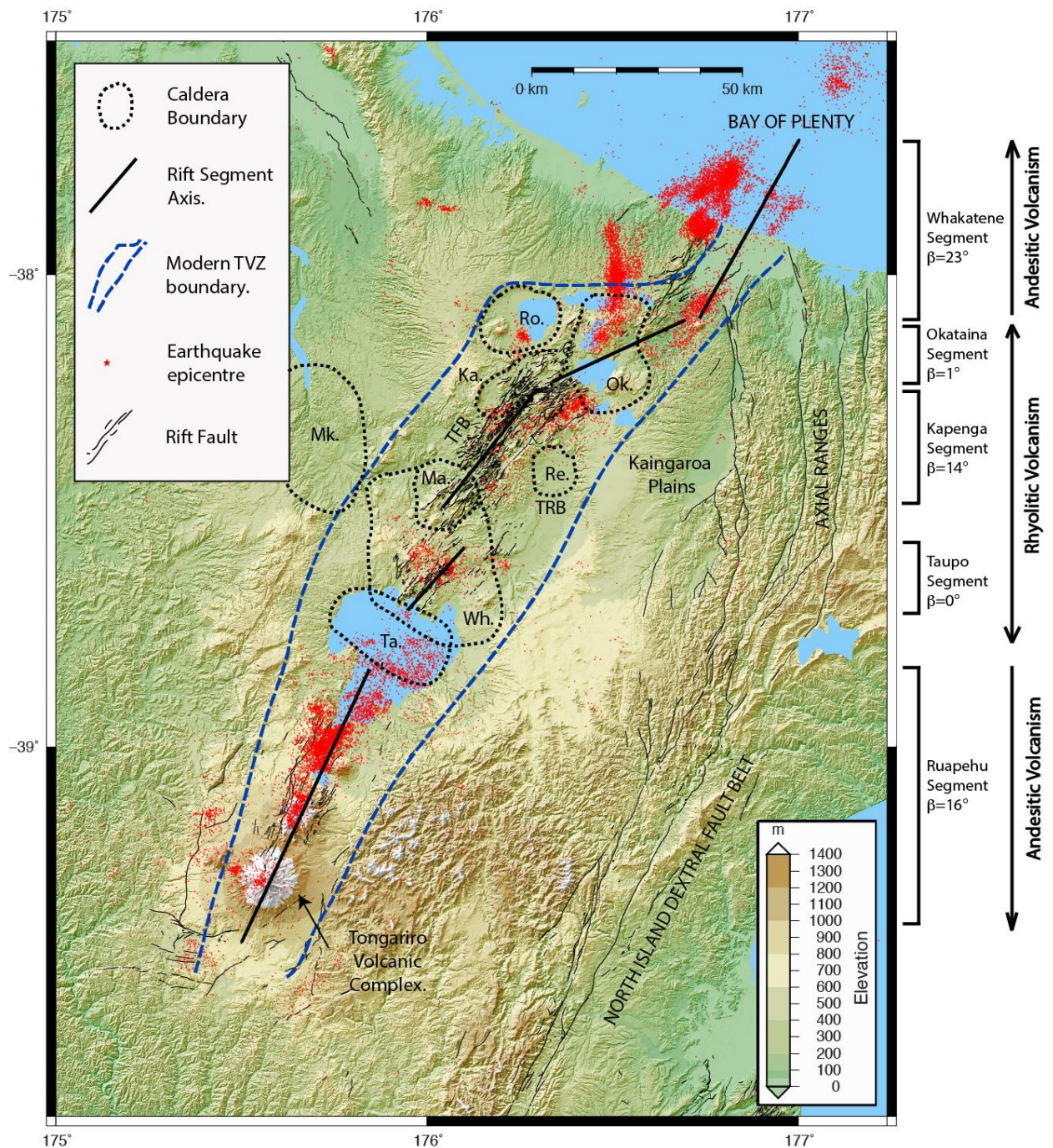


Figure 1.3 – Structural diagram of the Taupo Rift. The modern TVZ boundaries are approximate and from Cole (1990). Rift segment axis and strike-slip components (β) from Acocella et al., (2003). Light black lines are active rift faults from the GNS Science Active Faults Database. Epicentres plotted for shallow earthquakes

(<10km) between 1998 to 2011 from the GNS Science GeoNet Earthquake Database. DEM produced using LRIS Data Portal from NZ Landcare Research. Caldera boundary locations are shown as dashed grey lines and are approximate. Ro. Rotorua Caldera, Ok. Okataina Caldera, Mk. Mangakino Caldera, Ma. Maroa Caldera, Re. Reporoa Caldera, Ta. Taupo Caldera, To. Tongariro Volcanic Complex, Wk, Whakamaru Caldera. Dashed blue lines represent modern rift boundaries (from Acocella et al., 2003).

A broad wavelength (~250km), dome shaped pattern of rock uplift, centred east of Mt Ruapehu in the Tongariro Volcanic Complex, dominates the vertical tectonics of the central North Island (Pulford and Stern, 2004). They link this uplift to thermal processes in the underlying mantle wedge. In contrast, within the central rift, subsidence patterns are observed to vary in space and time and have been linked to rifting processes and magma availability (Villamor and Berryman, 2001; Manville and Wilson, 2003; Rowland et al., 2010). Subsidence in the Whakatane segment, associated with rifting, has been measured at $1\text{--}2\text{ mm/yr}^{-1}$ at the Bay of Plenty coast and uplift of $0.5\text{ to }1\text{ mm/yr}^{-1}$ at the eastern and western margins of the rift in this region (Wright, 1990). In the Kapenga segment, subsidence rates have locally been estimated at $-7.23 \pm 0.38\text{ mm/yr}^{-1}$ from fault displacement (Villamor and Berryman, 2001) and up to -10 mm/yr^{-1} from repeated precise levelling (Blick and Otway, 1995). Immediately north of Taupo caldera, local vertical deformation is small (relative to the Taupo rift further northwards), appears to be episodic on a scale between 1 to 10 years, and is often associated with magma migration (Manville and Wilson, 2003).

TVZ seismicity is defined by short periods of localised activity, separated by extended periods of quiescence (Sherburn 1992). The majority of seismicity occurs at depths between 2 to 8 km (Byran et al., 1999; Sherburn et al., 2003) and is concentrated along a 30km wide belt immediately northwest of the TVZ eastern boundary, mostly overlapping with the Taupo Fault Belt (in the central Rift). However, elevated and localised seismicity has also been closely linked with geothermal field activity. Bibby et al., (1995) and Bryan et al., (1999) estimate the depth of the brittle/ductile transition zone beneath the TVZ to be generally between 6 to 9km depth.

1.7.3 Lithospheric Structure of the Central North Island

Stern et al., (2006) state that based on 25 years of seismic exploration, it is currently considered that two distinct spatial domains of crustal structure exist across the North Island of NZ. The first is west, northwest and through central North Island (terminating at Mt Ruapehu – see Figure 1.1), where the crust is thinner than normal to depths of 20 to 25 km. The second is south and east of a line connecting Mt Ruapehu and Mt Taranaki, as well as central North Island where crustal thickness approaches 35km. North of the Taupo Rift, the crust thickens to over 40km (Rowland et al., 2010). The 3D crustal structure through the central rift has also been inferred from numerous geophysical observations (Harrison and White 2004; Stratford and Stern 2004; Stratford and Stern 2006; Harrison and White 2006; Bannister et al., 2007; Behr et al., 2011; Stern and Benson 2011). From these studies, it is generally agreed that the uppermost shallow 2-3 km of crust consists of low-density, low-velocity and low-porosity rocks such as pyroclastic sediments and ignimbrites, with low v_p velocities (between 1.5 to 3.0km/s) (see Figure 1.4). Between depths of approx. 3 to 15km, v_p velocities range between 5 to 6.5 kms⁻¹ and have been interpreted as either igneous (Harrison and White, 2006), basement greywacke (Cole et al., 1995), or cooling granitoid intrusions (Rowland and Sibson, 2004). The structure of lower depths (between 15 to 25km) is still not well constrained, but recent data suggest the presence of a ‘pillow-like’ large mafic intrusive body (Stern and Benson 2011). Seismic velocities through the caldera centres are lower than surrounding areas and considered to represent volcano infill (Bibby et al., 1995; Sherburn et al., 2003).

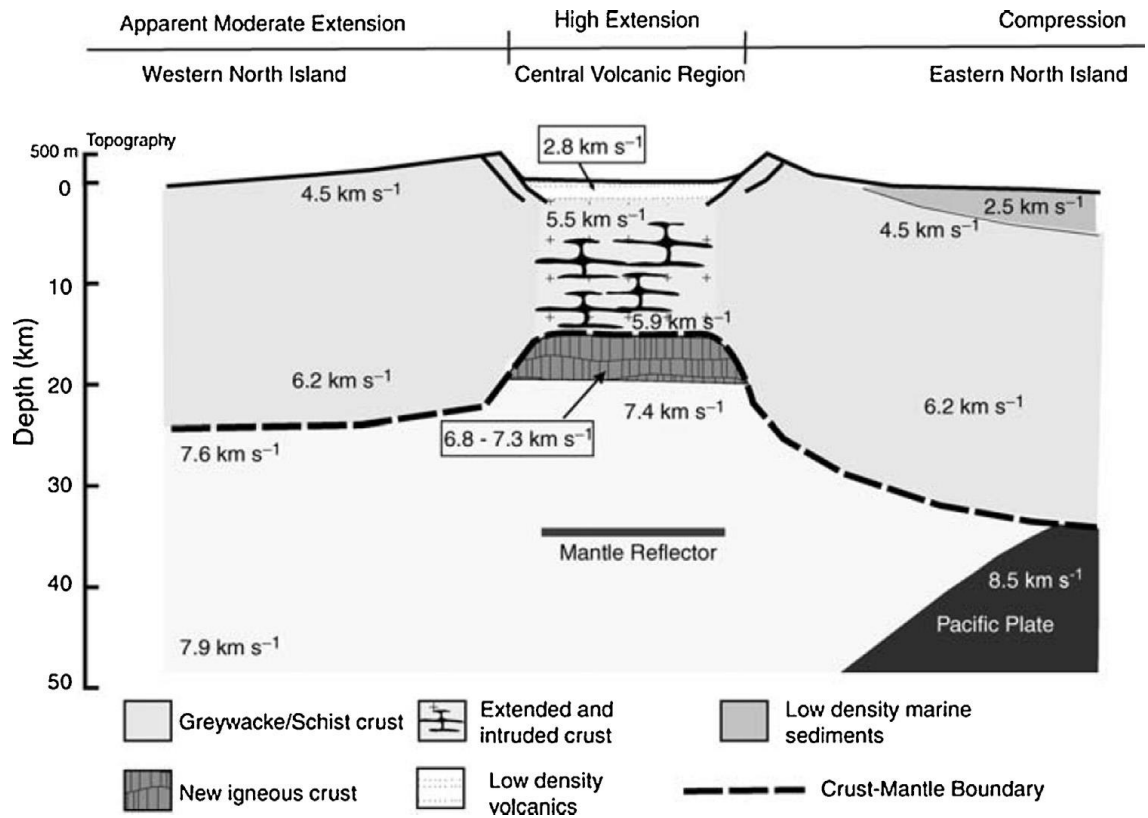


Figure 1.4 –Schematic model of crust and upper mantle structure of the TVZ proposed by Stratford and Stern, (2006) (from Stratford and Stern, 2006). Mantle velocities under the western North Island and slab velocities are from Stern et al., (1987) and Reyners et al., (1999) respectively. All velocities are in km s^{-1} .

1.7.4 Volcanism in the TVZ

Earliest volcanism in the TVZ has been identified as andesitic, and began at c. 2 Ma, followed and dominated by at least 31 caldera forming rhyolitic eruptions since 1.6 Ma in the central section (Darby et al., 2000; Price et al., 2005). Based on the onset of volcanism, Wilson et al., (1995) divides the TVZ into three temporal categories:

- the old TVZ, classifying eruptions that represents activity from the inception of the zone (c. 2 Ma) up to the onset of the Whakamaru group eruptions (c 0.24 Ma), and
- the young TVZ, classifying eruptions from 0.34 Ma (after the Whakamaru eruptions) to present, and
- the modern TVZ, describing activity since c. 65 ka to the current state of the zone.

In the TVZ, andesitic and dacite composite volcanoes are primarily located in the southern and northern extremities of the TVZ, while rhyolitic caldera systems are located within the central 125km by 60km segment (Houghton et al., 1995) (see Figure 1.3). The largest and most active andesitic volcanic centres include the Tongariro-Ruapehu massif at the southern tip of the TVZ, White Island in the offshore northern TVZ and Mt Taranaki in the west (Price et al., 2005). In the central TVZ, volcanism has been identified as pre-dominantly bimodal and dominated by rhyolite and basaltic volcanism (Deering et al., 2008). The central TVZ is also one of the most productive silicic magmatic systems on earth, producing between approximately 15000 to 20000 km³ of eruptive material in the last 2 Ma (Wilson et al., 1995). This activity is associated with a number of rhyolitic centres (and associated calderas) (see Figure 1.3) that includes Kapenga, Mangakino, Okataina, Reporoa, Taupo, Rotorua, Whakamaru and Maroa (Wilson et al., 1995; Cole et al., 1995; Houghton et al., 1995). In the last 0.20 Ma, activity in the central region has been dominated by rhyolitic dome formation, explosive eruptions and the eruption of ignimbrites at the Okataina and Taupo centres (Cole et al., 1995). These two volcanic centres are among the most productive and active rhyolitic volcanoes documented (Wilson et al., 1995) and over the last 61ka, are responsible for 99% of all volcanic output in the central TVZ (Wilson et al., 2009).

1.7.5 Magmatism in the TVZ

Natural heat flow within the central Taupo rift is anomalously high and greater than the continental average (Stern, 1985; Bibby et al., 1995; Hochstein 1995). This heat is primarily discharged at the surface as geothermal fluids within geothermal fields. Some of these geothermal fields are also located near or within active calderas (Bibby et al., 1995) or within major accommodation zones and the intervening regions of second-order segmentation (Rowland and Sibson, 2004). Geophysical surveys have suggested the presence of various magma bodies in the crustal structure through the central rift. Reyners et al (2006) produced a large-scale detailed 3D seismic velocity model of the Hikurangi subduction zone using data from the Central North Island Geophysical Transect (CNIPSE) experiment (Henrys et al., 2003) and the New Zealand National Seismograph Network. Alongside results from other MT/resistivity (Ogawa, 1999; Heise et al., 2007) and shear wave observations (Bannister et al., 2004), it is now considered that;

- The mantle wedge is a low v_p , high v_p/v_s feature, with significant changes along strike of the subduction zone, which suggest represents variations in partial melt which are consistent with changes in volcanism seen at the surface (Reyners et al., 2006).

- An interconnected melt fraction (<4%) in the lower crust exists underneath the central TVZ region (Ogawa 1999; Heise et al., 2007) at a depth of approximately 10km. Ogawa et al., (1999) note that the width of this zone is similar to that denoted as the young TVZ by Wilson et al., (1995).
- There is an increased concentration of melt below the quartzofeldspathic crust (>16km depth) near the eastern side of TVZ (Heise et al., 2007).
- Two bodies of partial melt (between depths of 6 to 16km, extend laterally over approximately 10 to 20km), one located just south near the Roturua caldera and the other on the eastern side of the central TVZ near the Reporoa caldera (Bannister et al., 2004).
- A region of significant partial melt in the mantle wedge exists north-west of Lake Taupo (evident through low v_p (high v_p/v_s) observations), which meets the base of the crust close to the volcanic front in the Taupo Region (Reyners et al., 2006).
- These low v_p and high v_p/v_s anomalies become more subdued in the region near the boundary of the rhyolite dominated central TVZ and the northern andesite dominated section, while in the southwest they end abruptly (Reyners et al., 2006).

Studies by Price et al., (2005) and Reyners et al., (2006) also highlight important differences in the deeper plumbing systems of rhyolitic and andesitic magmatism in the central TVZ. Reyners et al., (2006) believe that in the rhyolite dominated central rift segment there is no partial melt in the upper crust but most likely regions of partial melt in the lower crust. In contrast, they believe that in the andesite dominated south-west section of the TVZ, there is no evidence for the presence of partial melt in the crust, but rather magma appears to be ponding at the base of the crust. They state that the lack of rhyolites in this region is therefore due to the lack of significant intrusion into the crust. Price et al., (2005) consider that earlier formed andesitic systems are recycled and overwhelmed by rhyolitic storage systems at shallow depths, due to rising advection associated with crustal extension and thinning. They believe that following progressive under-plating associated with crustal thickening, arc magmatism becomes more complex, crustal recycling more significant and compositions of erupted material switch from basaltic to andesitic and eventually rhyolitic.

1.7.6 Relationship between tectonic, magmatic and volcanic processes and rift structures

Wilson et al., (2009) note that in the long and short-term history of the central TVZ, there is emerging evidence for an exceedingly complex set of three-way interactions between volcanic, magmatic and tectonic processes. Based on their own observations and from other studies, they summarise the key features of these interactions. Some of these are briefly summarised and listed here as follows (the reader is directed to Wilson et al., (2009) for more detailed explanations);

- *Between tectonism and volcanism*: that faulting, e.g., externally driven rifting events, can trigger volcanic eruptions and vice versa, caldera collapse may trigger faulting, stress changes accompanying eruptions may trigger other eruptions through changes in the regional stress field.
- *Between tectonism and magmatism*: that the presence of magma may control crustal deformation and rift related normal faulting might mediate magma emplacement in the crust.
- *Between magmatism and volcanism*: that there exist contrasts between the location of volcanism and magmatism (deep plutonism) unrepresented by volcanism (e.g. surface vents).

Studies supporting these relationships in the TVZ are many and varied. Acocella et al., (2003), Spinks et al., (2005), Cole and Spinks (2009) and Cole et al., (2010), consider that in the TVZ, upper crustal tectonic processes can control the location of magma storage and extrusion, based on the following observations;

- Eruptive vents for all styles of volcanism in the TVZ, including at Taupo and Okataina calderas, are typically aligned to regional structure. This indicates that magma which has risen to the mid crust depths near the ductile/brittle zone finds passage to surface vents through local faulting.
- The geometry of these calderas indicates strong tectonic influence on caldera formation, evolution and collapse,
- the extension axes for the Taupo and Okataina segments are consistent with the overall extension direction for the TVZ.
- Rift segments with higher dextral shear are associated with lower eruptive volumes, i.e., stratovolcanoes, whereas segments with smaller shear (and greater extension) are associated with larger eruptive volumes, i.e., calderas. Acocella et al., (2003) consider that the higher rates of orthogonal extension in these segments locally enhance upward flow of magma.

Spinks et al., (2005) and Cole and Spinks (2009), also propose that based on their location in relation to the Taupo Rift (and regional tectonic structure), two types of calderas occur in the TVZ. These are (1) extra-rift calderas which are located outside the main bounding faults of the TVZ, simple, small and sub-circular in structure and monogenetic; and (2) and intra-rift caldera complexes, which are large, have rectangular geometry and multiple collapse structures that are coupled to regional structure and broadly homogenous magmas.

Manville and Wilson (2003), Gravely et al., (2007) and Rowland et al., (2010) also provide evidence for interactions between volcanism, rifting and surface deformation in the TVZ, particularly focusing on the role of magmatism. Manville and Wilson (2003), note that in the vicinity north of Taupo caldera, inter-eruption

rifting is occurring without apparent subsidence or normal faulting and propose that magma addition below seismogenic depth may compensate for this. Gravley et al., (2007) suggest that paired eruptions between historic caldera forming eruptions may be due to enhanced rifting linked to a period of magmatism in the central TVZ. In both studies, the authors speculate that syn-eruptive, or post-eruptive fault displacement or significant subsidence outside the calderas may be linked to lateral magma migration or withdrawal, e.g. drainage of the magma chamber towards the collapse centre.

Seebeck and Nichol (2009) and Rowland et al., (2010) consider how rifting related extension is accommodated in the TVZ. Seebeck and Nichol (2009) consider that the approximately constant total regional extension is comprised of both a varying component (along the rift) of dike-driven extension within the volcanic centres, and a varying component of extension from tectonically driven faulting outside the caldera centres (see Figure 1.5). In their model, they believe that extension on rift faults decreases across the boundary of the volcanic centres and the contribution of extension due to dike intrusion increases by a similar proportion to maintain a uniform extension rate along the rift. They also consider that dike intrusion within the OVC is generally not sufficient to produce fault slip or extension outside the OVC. Rowland et al., (2010) consider that extension is accommodated differently through the TVZ according to how mafic and silicic magmatic systems interact and relate to tectonic processes. In the northern and southern TVZ segments this may include tectonic and mafic dike intrusion respectively and is related to two-way coupling between mafic magmatism and tectonism. They also consider that in the magma plentiful central TVZ region, a more complex interaction between mafic and silicic magmatism and regional tectonics exists, in which extension may be accommodated by magmatic and volcanic processes (e.g. dike intrusion, regional scale uplift and subsidence and co-volcanic fault-slip linked to large rhyolitic caldera eruptions, as well as pure tectonic faulting).

These interactions within the central North Island have also been linked to rift evolution and rift-scale structure. Villamor and Berryman (2006) consider the southwards evolution of the Taupo rift is stepwise and correlated with periods of redistribution of faulting in the central segment, and initiation of volcanism in the southern part of the rift. In their study they also note the coincidence of the initiation of significant faulting of <400 ka with large-volume ignimbrite eruptions at around 0.34 - 0.32 Ma.

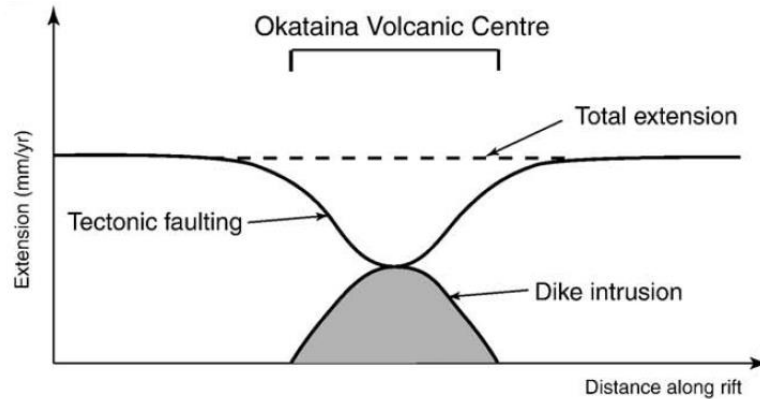


Figure 1.5 – Relationship between tectonic faulting and dike intrusion in the Taupo rift and their contribution to extension across volcanic centres as proposed by Seebeck and Nichol, (2009) (from Seebeck and Nichol, 2009).

1.7.7 The Okataina Volcanic Centre

The OVC is a rectangular caldera structure whose long axis trends roughly perpendicular to the Okataina segment axis (Spinks et al., 2005) and is located at a ~10km left step in the Taupo Rift (Seebeck et al., 2010). It consists of overlapping and nested caldera structures filled with post-caldera rhyolites, which includes the larger Haroharo caldera, containing the Haroharo and Tarawera volcanic complexes (Nairn, 2002) (see Figure 1.6). The major structures that are adjacent to and reside within the OVC are mapped and described in detail by Nairn, (2002). These include the Kapenga caldera, the Okataina ring structure, the Haroharo, Tarawera and Rotoma calderas, the Puhipuhi basin, Okareku embayment and the Rerewhakaaitu and Rotokawau-Rotoatua fissures (see Figure 1.6). Dispersed amongst these features are a number of lakes, which form a moat around the western and northern sides of the caldera floor, and have formed between the caldera margins and caldera-filling post-caldera constructional volcanism (Cole and Spinks, 2009).

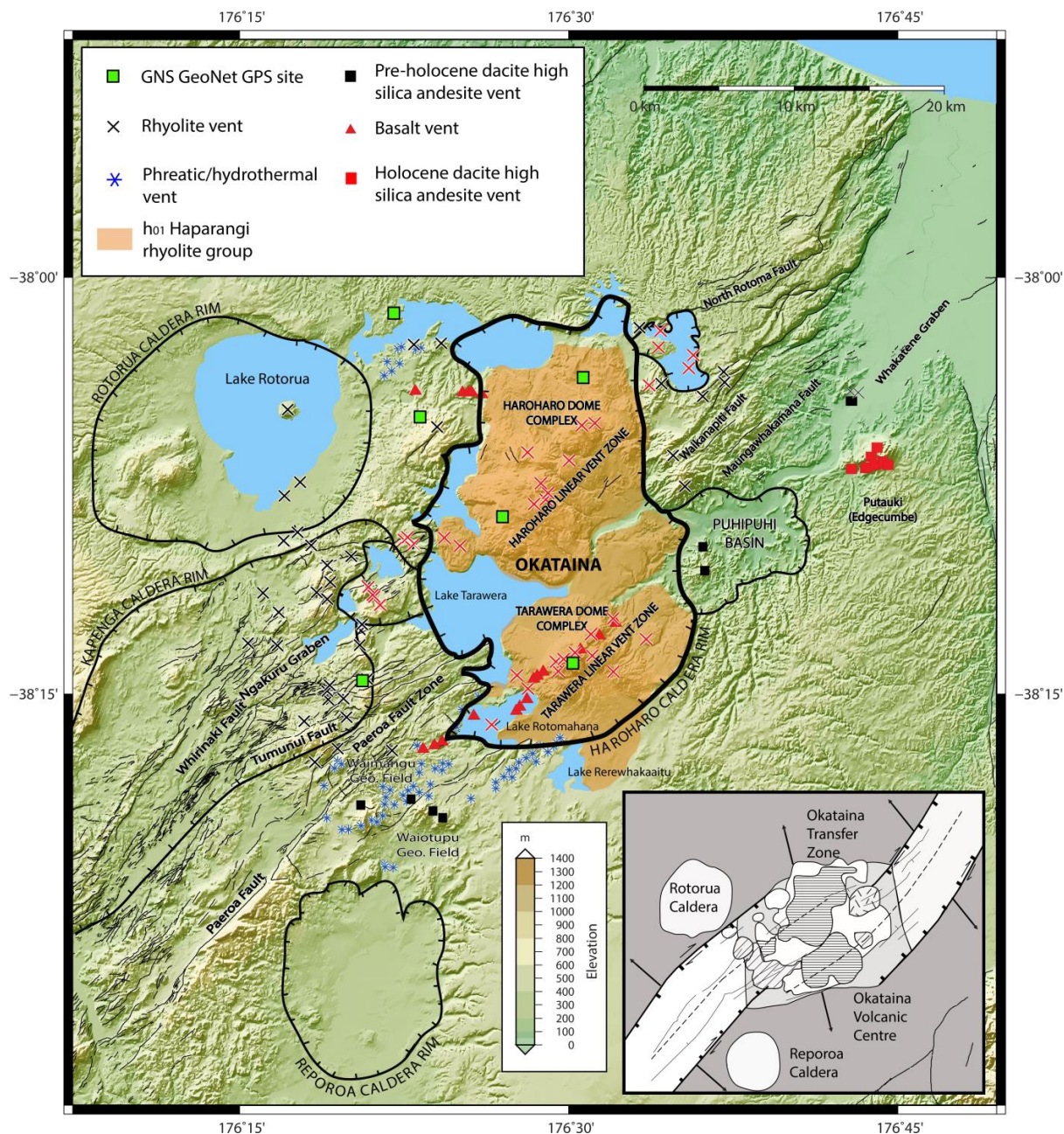


Figure 1.6 – Location map and structural details of the Okataina Volcanic Centre (OVC) based on Nairn (2002). Caldera boundary locations are shown as dashed grey lines and from Spinks et al., (2005). Bottom right inset shows interaction of the Okataina rift segment and OVC with the neighbouring Kapenga and Whakatane rift segments (from Cole et al., 2010).

Eruptive vents post 25ka are well mapped and define two broad linear zones; the Tarawera and Haroharo linear vent zones (Nairn, 2002). These lineations are roughly axial to the Whakatane and Kapenga segments and considered to mark their continuation into the Okataina area (Spinks et al., 2005). Volcanic activity within

the last 26ka has been linked to post-caldera rhyolitic dome building, primarily along these linear vent zones (Nairn, 2002; Cole et al., 2010). Recent activity includes the ~AD 1315 Kaharoa rhyolite ($>5\text{km}^3$) and 1886 Tarawera basalt dike eruptions (Nairn, 2002). The Kaharoa eruption was primed and triggered by multiple basalt intrusions into an existing stratified rhyolitic magma body (Leonard et al., 2002; Nairn, 2002; Sherburn and Nairn, 2004). Today the most intense hydrothermal activity is located outside the caldera, within the Lake Rotomahana, Waimangu and the Waiotapu geothermal fields, and it is closely related with the southwest extension of the Tarawera vent lineations and 1886 AD rift (Nairn, 2002). A number of small to moderate hydrothermal explosions have occurred within these fields since 1886 (Scott, 1992; Scott, 1994; Vandemeulebrouck et al., 2008).

The Okataina caldera also coincides with a large negative gravity anomaly, trending north-south, consistent with the shape of the caldera and located within its margins (Rogan, 1982; Nairn, 2002; Seebeck et al., 2010), as well as a zone of low v_p velocities in the upper crust (Sherburn et al., 2003). Regional fault structures have strongly influenced OVC caldera structure (Cole et al., 2010; Seebeck et al., 2010). Gravity observations show that the northwest and southeast structural boundaries are controlled by normal rift faults (dip 55 to 75°), while the east and west boundaries are defined by near vertical north-south striking faults (dip 70 to 90°) (Seebeck et al., 2010). Other studies indicate that the depth of the collapse structure beneath the caldera is approximately 3 to 4 km and filled with volcanoclastic materials, underlain by a highly fractured greywacke basement (Bibby et al., 1995; Sherburn et al., 2003; Heise et al., 2007; Bibby et al., 2008; Seebeck et al., 2010).

The formation of the Okataina caldera is attributed to the Quartz-biotite (Pre ca. 325ka), Matahina (ca. 325 ka) and Rotoiti (65 ka) ignimbrite eruptions and accompanying subsidence, and has filled with large volumes of eruptives and sediments (Houghton et al., 1995; Wilson et al., 1995; Nairn, 2002; Sherburn and Nairn, 2004; Cole et al., 2010). Smith et al., (2005) state that following these large caldera forming episodes, changes in the style, activity, composition and vent location occurred at the OVC, and imply that either regional controls or that the voluminous caldera forming episodes adjusted the regional stress field. The OVC has erupted $\sim 80\text{km}^3$ of rhyolitic magma in the last 21ka (Nairn, 2002). An average recurrence interval between eruptions (2200 years) and average eruption rate of (0.004km^3) over this period relates to a chamber volume of 2000 km^3 (Jellinak and DePaulo, 2003). However, post caldera eruptions at the OVC are not considered to come from a single large magma chamber, but rather from diverse small to moderate magma sources (Charlier and Wilson, 2010). Most of these rhyolite magma bodies form at depths between 8 to 5 km beneath the Tarawera and Haroharo complexes (Smith et al., 2004,2006; Shane et al., 2007).

Little surface hydrothermal activity presently occurs within the Haroharo caldera. The most intense activity is located outside the caldera at Lake Rotomahana and the Waimangu, Waiotapu and Kawerau geothermal fields (see Figure 1.6). The Lake Rotomahana, Waimangu and Waitupu fields are considered closely related with the southwest extension of the Tarawera vent lineations and 1886 AD Rift (Nairn, 2002). Using estimates of erupted volumes at 0.7 ka (from Tarawera) and 5 ka (from Haroharo), Nairn, (2002), believe that magma bodies related to these eruptions have not had time to cool via convection and probably still exist. Small earthquake sequences in this region are considered to be a result of ongoing regional deformation, rather than active volcanism (Sherburn, 1992). There have been few earthquakes ($M_L > 3$) near Mt Tarawera since 1992, and no evidence exists for significant seismicity in the last 50 years (Bryan, 1999). However, Bryan, (1999) do note that clusters of earthquakes have occurred in space at time in the OVC, southwest of the Kawerau and Waiotapu-Waimangu geothermal areas over this period. They note however, that these results do not suggest that geothermal systems lie over areas of intruded volcanism.

1.8 References

- Acocella, V., Spinks, K., Cole, J., Nicol, A., 2003. Oblique back arc rifting of Taupo Volcanic Zone, New Zealand. *Tectonics*, 22, 1045. doi: 10.1029/2002TC001447
- Bannister, S.C., Bryan, C.J., Bibby, H.M., 2004. Shear wave velocity variation across the Taupo Volcanic Zone, New Zealand, from receiver function inversion. *Geophysical Journal International*, 159(1), 291-310. doi: <https://doi.org/10.1111/j.1365-246X.2004.02384.x>
- Bannister, S.C., Reyners, M.E., Stuart, G., Savage, M., 2007. Imaging the Hikurangi subduction zone, New Zealand, using teleseismic receiver functions : crustal fluids above the forearc mantle wedge. *Geophysical Journal International*, 169(2): 602-616; doi: 10.1111/j.1365-246X.2007.03345.x
- Beanland, S., Haines, J., 1998. The kinematics of active deformation in the North Island, New Zealand, determined from geological strain rates. *New Zealand Journal of Geology and Geophysics*, 41, 311-323. doi:<http://dx.doi.org/10.1080/00288306.1998.9514813>
- Beavan, J., Wallace, L., Fletcher, H., Douglas, A., 2007. Slow slip events on the Hikurangi subduction interface, New Zealand, in *Monitoring and Understanding a Dynamic Planet With Geodetic and Oceanographic Tools*, IAG Symposium, Cairns, Australia, 22 – 26 August, 2005, Int. Assoc. of Geod. Symp., vol. 130, edited by P. Tregoning and C. Rizos, pp. 438 – 444, Springer, Berlin
- Beavan, J., Haines, J., 2001. Contemporary horizontal velocity and strain rate fields of the Pacific-Australian plate boundary zone through New Zealand. *J Geophys Res-Sol Ea*, 106(B1): 741-770. doi:10.1029/2000JB900302
- Beavan, J., Tregoning, P., Bevis, M., Kato, T., Meertens, C., 2002. Motion and rigidity of the Pacific Plate and implications for plate boundary deformation. *Journal of Geophysical Research-Solid Earth*, 107(B10).doi:10.1029/2001JB000282.
- Behr, Y., Townend, J., Bannister, S., Savage, M. K., 2011. Crustal shear wave tomography of the Taupo Volcanic Zone, New Zealand, via ambient noise correlation between multiple three - component networks, *Geochem. Geophys. Geosyst.*, 12, Q03015. doi:10.1029/2010GC003385.
- Blick, G.H., Otway, P.M., 1995. Regional vertical deformation from repeated precise levelling in the Taupo Volcanic Zone. *Institute of Geological & Nuclear Sciences Limited*, Lower Hutt, N.Z.
- Bibby, H. M., Caldwell, T. G., Davey, F. J., Webb, T. H., 1995. Geophysical evidence on the structure of the Taupo Volcanic Zone and its hydrothermal circulation. *Journal of Volcanology and Geothermal Research*, 68, 29-58. doi:[http://dx.doi.org/10.1016/0377-0273\(95\)00007-H](http://dx.doi.org/10.1016/0377-0273(95)00007-H)
- Bryan, C. J., Sherburn, S., Bibby, H. M., Bannister, S. C., Hurst, A. W., 1999. Shallow seismicity of the central Taupo Volcanic Zone, New Zealand: its distribution and nature. *New Zealand Journal of Geology and Geophysics*, 42, 533-542. doi:<http://dx.doi.org/10.1080/00288306.1999.9514859>

- Cabral-Cano, E., Correa-Mora, F., Meertens, C., 2008. Deformation of Popocatepetl volcano using GPS: Regional geodynamic context and constraints on its magma chamber. *Journal of Volcanology and Geothermal Research*, 170, 24-34. doi:<http://dx.doi.org/10.1016/j.jvolgeores.2007.09.008>
- Charlier, B.L.A., Wilson, C.J.N., 2010. Chronology and Evolution of Caldera-forming and Post-caldera Magma Systems at Okataina Volcano, New Zealand from Zircon U-Th Model-age Spectra. *Journal of Petrology*, 51(5), 1121-1141. doi:<https://doi.org/10.1093/petrology/egq015>
- Cole, J. W., 1990. Structural Control and Origin of Volcanism in the Taupo Volcanic Zone, New-Zealand. *Bulletin of Volcanology*, 52, 445-459. doi:10.1007/BF00268925
- Cole, J.W., Spinks, K.D., 2009. Caldera volcanism and rift structure in the Taupo Volcanic Zone, New Zealand. In: J.B. Murphy, J.D. Keppie and A.J. Hynes (Editors), *Ancient Orogens and Modern Analogues*. Geological Society Special Publication, pp. 9-29. doi: 10.1144/SP327.2
- Cole, J. W., Darby, D. J., Stern, T., 1995. Taupo Volcanic Zone and Central Volcanic Region -Backarc Structures of the North Island, New Zealand. In Taylor, B. (Ed.) *Backarc Basins: Tectonics and Magmatism*. New York, Plenum Press. doi:10.1186/BF03351838
- Cole, J.W., Spinks, K.D., Deering, C.D., Nairn, I.A., Leonard, G.S., 2010. Volcanic and structural evolution of the Okataina Volcanic Centre; dominantly silicic volcanism associated with the Taupo Rift, New Zealand. *Journal of Volcanology and Geothermal Research*, 190(1-2): 123-135. doi:10.1016/j.jvolgeores.2009.08.011
- Darby, D. J., Hodgkinson, K. H., Blick, G. H., 2000. Geodetic measurement of deformation in the Taupo Volcanic Zone, New Zealand: the North Taupo Network revisited. *New Zealand Journal of Geology and Geophysics*, 43, 157-170. doi:<http://dx.doi.org/10.1080/00288306.2000.9514878>
- De Natale, G., Troise, C., Pingue, F., 2001. A mechanical fluid-dynamical model for ground movements at Campi Flegrei caldera. *Journal of Geodynamics*, 32, 487-517. doi:[http://dx.doi.org/10.1016/S0264-3707\(01\)00045-X](http://dx.doi.org/10.1016/S0264-3707(01)00045-X)
- Deering, C. D., Cole, J. W., Vogel, T. A., 2008. A Rhyolite Compositional Continuum Governed by Lower Crustal Source Conditions in the Taupo Volcanic Zone, New Zealand. *Journal of Petrology*, 49, 2245-2276. doi:<https://doi.org/10.1093/petrology/egn067>
- Dzurisin, D., 2003. A comprehensive approach to monitoring volcano deformation as a window on the eruption cycle. *Reviews of Geophysics*, 41, 1001, doi:10.1029/2001RG000107
- Dzurisin, D., 2007. *Volcano deformation: geodetic monitoring techniques* Springer-Verlag Berlin Heidelberg, 442 p., ISBN: 978-3-642-51763-1. doi:10.1007/978-3-540-49302-0
- Ellis, S. M., Wilson, C. J. N., Bannister, S., Bibby, H. M., Heise, W., Wallace, L., Patterson, N., 2007. A future magma inflation event under the rhyolitic Taupo volcano, New Zealand: Numerical models based

- on constraints from geochemical, geological, and geophysical data. *Journal of Volcanology and Geothermal Research*, 168, 1-27. doi:<http://dx.doi.org/10.1016/j.jvolgeores.2007.06.004>
- Gravley, D.M., Wilson, C.J.N., Leonard, G.S., Cole, J.W., 2007. Double trouble: paired ignimbrite eruptions and collateral subsidence in the Taupo Volcanic Zone, New Zealand. *Geol. Soc. Am. Bull.* 119(1-2),18-30. doi: 10.1130/B25924.1
- Grindley, G., 1960. Sheet 8 - Taupo. Geological Map of New Zealand 1:250000. Wellington, New Zealand: Department of Scientific and Industrial Research.
- Gudmundsson, A., Acocella, V., Vinciguerra, S., 2009. Understanding stress and deformation in active volcanoes. *Tectonophysics*, 471, 1-3. doi: 10.1016/j.tecto.2009.04.014
- Harrison, A. J., White, R. S., 2004. Crustal structure of the Taupo Volcanic Zone, New Zealand: Stretching and igneous intrusion. *Geophysical Research Letters*, 31, L13615. doi:10.1029/2004GL019885
- Harrison, A., White, R. S., 2006. Lithospheric structure of an active backarc basin: The Taupo Volcanic Zone, New Zealand. *Geophysical Journal International*, 167, 968-990. doi:10.1111/j.1365-246X.2006.03166.x
- Heise, W., Bibby, H.M., Caldwell, T.G., Bannister, S.C., Ogawa, Y., Takakura, S., Uchida, T., 2007. Melt distribution beneath a young continental rift: The Taupo Volcanic Zone, New Zealand. *Geophysical Research Letters*, 34(14): L14313. doi:10.1029/2007GL029629
- Henry, S. A., Reyners, M., Bibby, H., 2003. Exploring the Plate Boundary Structure of the North Island, New Zealand. *Eos Trans. AGU*, 84(31), 289–295, doi:10.1029/2003EO310002.
- Hochstein, M. P., 1995. Crustal Heat-Transfer in the Taupo Volcanic Zone (New-Zealand) - Comparison with Other Volcanic Arcs and Explanatory Heat-Source Models. *Journal of Volcanology and Geothermal Research*, 68, 117-151. doi:10.1016/0377-0273(95)00010-R
- Houghton, B. F., Wilson, C. J. N., McWilliams, M. O., Lanphere, M. A., Weaver, S. D., Briggs, R. M., Pringle, M. S., 1995. Chronology and Dynamics of a Large Silicic Magmatic System - Central Taupo Volcanic Zone, New-Zealand. *Geology*, 23, 13-16. doi:10.1130/0091-7613(1995)023<0013:CADOAL>2.3.CO;2
- Jellinek, A.M., DePaolo, D.J., 2003. A model for the origin of large silicic magma chambers: precursors of caldera-forming eruptions. *Bulletin of Volcanology*, 65(5): 363-381. doi:10.1007/s00445-003-0277-y.
- Leonard, G.S., Cole, J.W., Nairn, I.A., Self, S., 2002. Basalt triggering of the c. AD 1305 Kaharoa rhyolite eruption, Tarawera Volcanic Complex, New Zealand. *Journal of Volcanology and Geothermal Research*, 115(3-4), 461-486. doi:[http://dx.doi.org/10.1016/S0377-0273\(01\)00326-2](http://dx.doi.org/10.1016/S0377-0273(01)00326-2)
- Lowenstern, J. B., Smith, R. B., Hill, D. P., 2006. Monitoring super-volcanoes: geophysical and geochemical signals at Yellowstone and other large caldera systems. *Philosophical Transactions of the Royal Society a-Mathematical Physical and Engineering Sciences*, 364, 2055-2072. doi:10.1098/rsta.2006.1813

- Manville, V., Wilson, C.J.N., 2003. Interactions between volcanism, rifting and subsidence: implications of intracaldera palaeoshorelines at Taupo volcano, New Zealand. *J Geol Soc London*, 160, 3-6. doi:10.1144/0016-764902-103
- Mogi, K., 1958. Relations between the eruptions of various volcanoes and the deformation of the ground surface around them. *Bull. Earthquake Res. Inst. Univ. Tokyo*, 36, 99-134.
- Nairn, I.A., 1993. Volcanic hazards at Okataina Centre. 3rd ed. [Palmerston North, NZ]: Ministry of Civil Defence. Volcanic hazards information series 2. 29, [1] p. available at <https://www.gns.cri.nz/Home/Learning/Science-Topics/Volcanoes/New-Zealand-Volcanoes/Volcano-Geology-and-Hazards/Okataina-Volcanic-Centre-Geology>. Accessed on 18/3/2017.
- Nairn, I.A., 2002. Geology of the Okataina Volcanic Centre. In: I.o.G.a.N. Sciences (Editor). Institute of Geological and Nuclear Sciences Ltd., Lower Hutt, New Zealand, pp. Geological Map 25. 21 sheet + 156p.
- Nairn, I.A., Cole, J.W., 1981. Basalt dikes in the 1886 Tarawera Rift, New Zealand *Journal of Geology and Geophysics*, 24(5-6), 585-592, doi:10.1080/00288306.1981.10421534
- Nairn, I. A., Shane, P. R., Cole, J. W., Leonard, G. J., Self, S., Pearson, N., 2004. Rhyolite magma processes of the similar to AD 1315 Kaharoa eruption episode, Tarawera volcano, New Zealand. *Journal of Volcanology and Geothermal Research*, 131, 265-294. [http://dx.doi.org/10.1016/S0377-0273\(03\)00381-0](http://dx.doi.org/10.1016/S0377-0273(03)00381-0).
- Nairn, I. A., Hedenquist, J. W., Villamor, P., Berryman, K. R., Shane, P. A., 2005. The similar to AD1315 Tarawera and Waiotapu eruptions, New Zealand: contemporaneous rhyolite and hydrothermal eruptions driven by an arrested basalt dike system? *Bulletin of Volcanology*, 67, 186-193. doi: doi:10.1007/s00445-004-0373-7
- Newhall, C., Dzurisin, D., 1988. Historical Unrest at Large Calderas of the World. U.S. Geological Survey Bulletin 1855. 1108 p.
- Nicol, A., Wallace, L. M., 2007. Temporal stability of deformation rates: Comparison of geological and geodetic observations, Hikurangi subduction margin, New Zealand. *Earth and Planetary Science Letters*, 258, 397-413. doi: <http://dx.doi.org/10.1016/j.epsl.2007.03.039>
- Ogawa, Y., Bibby, H. M., Caldwell, T. G., Takakura, S., Matsushima, N., Bennie, S. L., Tosha, T., Nishi, Y., 1999, Wide-band magnetotelluric measurements across the Taupo volcanic zone: Preliminary results, *Geophys. Res. Lett.*, 26, 3673–3676. doi: 10.1029/1999GL010914
- Peltier, A., Hurst, T., Scott, B., Cayol, V., 2009a. Structures involved in the vertical deformation at Lake Taupo (New Zealand) between 1979 and 2007: New insights from numerical modelling, *J. Volcano. Geotherm. Res.* 181(3-4), 173-184. <http://dx.doi.org/10.1016/j.jvolgeores.2009.01.017>

- Peltier, A., Scott, B., Hurst, T., 2009b. Ground deformation patterns at White Island volcano (New Zealand) between 1967 and 2008 deduced from levelling data, *J. Volcano. Geotherm. Res.*, 181(3-4), 207-219.
<http://dx.doi.org/10.1016/j.jvolgeores.2009.01.020>
- Poland, M., Hamburger, M., & Newman, A., 2006. The changing shapes of active volcanoes: History, evolution, and future challenges for volcano geodesy. *Journal of Volcanology and Geothermal Research*, 150, 1-13. doi:10.1016/j.jvolgeores.2005.11.005. doi:10.1016/j.jvolgeores.2005.11.005
- Price, R. C., Gamble, J. A., Smith, I. E. M., Stewart, R. B., Eggins, S., Wright, I. C., 2005. An integrated model for the temporal evolution of andesites and rhyolites and crustal development in New Zealand's North Island. *Journal of Volcanology and Geothermal Research*, 140, 1-24.
doi:<http://dx.doi.org/10.1016/j.jvolgeores.2004.07.013>
- Pulford, A., Stern, T., 2004. Pliocene exhumation and landscape evolution of central North Island, New Zealand: The role of the upper mantle. *Journal of Geophysical Research*, 109, F01016,
doi:10.1029/2003JF000046.
- Reyners, M., Eberhart-Phillips, D., Stuart, G., 1999. A three-dimensional image of shallow subduction: crustal structure of the Raukumara Peninsula, New Zealand, *Geophys. J. Int.*, 137(3), 873-890.
doi:<https://doi.org/10.1046/j.1365-246x.1999.00842.x>
- Reyners, M., Eberhart-Phillips, D., Stuart, G., Nishimura, Y. 2006. Imaging subduction from the trench to 300 km depth beneath the central North Island, New Zealand, with Vp and Vp/Vs. *Geophysical Journal International*, 165, 565-583. doi:10.1111/j.1365-246X.2006.02897.x
- Rogan, M., 1982. A Geophysical-Study of the Taupo Volcanic Zone New-Zealand. *Journal of Geophysical Research*, 87(Nb5): 4073-4088.
- Rowland, J.V., Sibson, R.H., 2001. Extensional fault kinematics within the Taupo Volcanic Zone, New Zealand: soft-linked segmentation of a continental rift system. *New Zeal J Geol Geop*, 44(2), 271-283.
doi:<http://dx.doi.org/10.1080/00288306.2001.9514938>
- Rowland, J. V., Sibson, R. H., 2004. Structural Controls On Hydrothermal Flow In A Segmented Rift System, Taupo Volcanic Zone, New Zealand. *Geofluids*, 4, 259-283. doi: 10.1111/j.1468-8123.2004.00091.x
- Rowland, J. V., Wilson, C. J. N., Gravley, D. M., 2010. Spatial and temporal variations in magma-assisted rifting, Taupo Volcanic Zone, New Zealand: *Journal of Volcanology and Geothermal Research*, v. 190, no. 1-2, p. 89-108. Samsonov, S., Beavan, J., Gonzalez, P.J., Tiampo, K. and Fernández, J., 2011. Ground deformation in the Taupo Volcanic Zone, New Zealand, observed by ALOS PALSAR interferometry. *Geophys J Int*, 187(1), 147-160. doi:<http://dx.doi.org/10.1016/j.jvolgeores.2009.05.004>
- Samsonov, S., Beavan, J., Gonzalez, P., Tiampo, K., Fernández, J., 2011. Ground deformation in the Taupo Volcanic Zone, New Zealand, observed by ALOS PALSAR Interferometry. *Geophysical Journal International*, 187(1), 147-160. 10.1111/j.1365-246X.2011.05129.x

- Scott, B., Travers, J., 2009. Volcano monitoring in NZ and links to SW Pacific via the Wellington VAAC. *Natural Hazards*, 51: 263. doi:10.1007/s11069-009-9354-7
- Scott, B. J., 1989. Geodetic and geophysical monitoring of the 1886 Tarawera rift. In Latter, J. H., (Ed.) *Volcanic Hazards assessment and monitoring*. Springer-Verlag. Berlin, Heidelberg, http://dx.doi.org/10.1007/978-3-642-73759-6_34
- Scott, B.J., 1992. Characteristics of cyclic activity in Frying Pan and Inferno Crater Lakes, Waimangu, New Zealand Geothermal Workshop. Institute of Geological & Nuclear Sciences contribution Auckland, pp. 253-258.
- Scott, B.J., 1994. Cyclic Activity in the Crater Lakes of Waimangu Hydrothermal System, New-Zealand. *Geothermics*, 23(5-6),555-572. doi:[http://dx.doi.org/10.1016/0375-6505\(94\)90019-1](http://dx.doi.org/10.1016/0375-6505(94)90019-1)
- Seebeck, H., 2008. The inter-relationships between faulting and volcanism in the Okataina Volcanic Centre, New Zealand. Victoria University of Wellington. PhD Thesis.
- Seebeck, H., Nicol, A., 2009. Dike intrusion and displacement accumulation at the intersection of the Okataina Volcanic Centre and Paeroa Fault zone, Taupo Rift, New Zealand. *Tectonophysics*, 475(3-4), 575-585. <http://dx.doi.org/10.1016/j.tecto.2009.07.009>
- Seebeck, H., Nicol, A., Stern, T.A., Bibby, H.M., Stagpoole, V., 2010. Fault controls on the geometry and location of the Okataina Caldera, Taupo Volcanic Zone, New Zealand. *J. Volcanol. Geoth. Res.*, 190(1-2), 136-151. doi: <http://dx.doi.org/10.1016/j.jvolgeores.2009.04.011>
- Sherburn, S., 1992. Seismicity of the Lake Taupo region, New Zealand, 1985–90, *New Zealand Journal of Geology and Geophysics*, 35(3), 331-335, doi: 10.1080/00288306.1992.9514526
- Sherburn, S., Nairn, I. A., 2001. A scenario of geophysical events inferred to have preceded the 1300AD Kaharoa eruption: lessons for the future, *Inst. Geol. Nucl. Sciences Science Report 2001/26*, 57 pp. Lower Hutt, New Zealand.
- Sherburn, S., Nairn, I. A., 2004. Modelling Geophysical Precursors To The Prehistoric C. Ad1305 Kaharoa Rhyolite Eruption Of Tarawera Volcano, New Zealand. *Natural Hazards*, 32,37-58. doi:10.1023/B:NHAZ.0000026791.16566.96
- Sherburn, S., Bannister, S., Bibby, H., 2003. Seismic velocity structure of the central Taupo Volcanic Zone, New Zealand, from local earthquake tomography. *J. Volcanol. Geoth. Res.*, 122(1-2), 69-88. [http://dx.doi.org/10.1016/S0377-0273\(02\)00470-5](http://dx.doi.org/10.1016/S0377-0273(02)00470-5)
- Spinks, K. D., Acocella, V., Cole, J. W., Bassett, K. N., (2005) Structural control of volcanism and caldera development in the transtensional Taupo Volcanic Zone, New Zealand. *Journal of Volcanology and Geothermal Research*, 144(1-4), 7-22. doi:<http://dx.doi.org/10.1016/j.jvolgeores.2004.11.014>

- Smith, V.C., Shane, P., Nairn, I.A., 2004. Reactivation of a rhyolitic magma body by new rhyolitic intrusion before the 15.8 ka Rotorua eruptive episode: Implications for magma storage in the Okataina volcanic center, *Journal of the Geological Society*, (161),757–772. doi: 10.1144/0016-764903-092
- Smith, V.C., Shane, P., Nairn, I.A., 2005. Trends in rhyolite geochemistry, mineralogy, and magma storage during the last 50 kyr at Okataina and Taupo volcanic centres, Taupo Volcanic Zone, New Zealand. *Journal of Volcanology and Geothermal Research*, 148(3-4),372-406. doi:http://dx.doi.org/10.1016/j.jvolgeores.2005.05.005
- Smith, V.C., Shane, P., Nairn, I.A., Williams, C.M., 2006. Geochemistry and magmatic properties of eruption episodes from Haroharo Linear Vent Zone, Okataina volcanic center, New Zealand during the last 10 ka, *Bulletin of Volcanology*, (69),57–88. doi:10.1007/s00445-006-0056-7.
- Shane, P., Martin, S.B., Smith, V.C., Beggs, K.F., Darragh, M.B., Cole, J.W., Nairn, I.A., 2007. Multiple rhyolite magmas and basalt injection in the 17.7 ka Rerewhakaaitu eruption episode from Tarawera volcanic complex, New Zealand: *Journal of Volcanology and Geothermal Research*, (164),1–26. doi: 10.1016/j.jvolgeores.2007.04.003
- Stern, T. A., 1985. A Back-Arc Basin Formed within Continental Lithosphere - the Central Volcanic Region of New-Zealand. *Tectonophysics*, 112(1-4), 385-409. doi: http://dx.doi.org/10.1016/0040-1951(85)90187-8
- Stern, T.A., 2009. Reconciling short- and long-term measures of extension in continental back arcs: heat flux, crustal structure and rotations within central North Island, New Zealand. In U. Ring & B. Wernicke (Eds.), *Extending a Continent: Architecture, Rheology and Heat Budget*. Geol. Soc. Spec. Publ., (321)73–87. doi:10.1029/2011JB008337
- Stern, T., Benson, A., 2011. Wide angle seismic imaging beneath an andesitic arc: Central North Island, New Zealand. *Journal of Geophysical Research* 116, B09308. http:// dx.doi.org/10.1029/2011JB008337.
- Stern, T. A., Stratford, W. R., Salmon, M. L., 2006. Subduction evolution and mantle dynamics at a continental margin: Central North Island, New Zealand. *Reviews of Geophysics*, 44, RG4002, doi:10.1029/2005RG000171.
- Stern, T.A., Smith, E.G.C., Davey, F.J., Muirhead, K.J., 1987. Crustal and upper mantle structure of the northwestern North Island, New Zealand, from seismic refraction data, *Geophys. J. R. astr. Soc.*, 91(3), 913-936. doi:https://doi.org/10.1111/j.1365-246X.1987.tb01674.x
- Stratford, W. R., Stern, T. A., 2004. Strong Seismic Reflections And Melts In The Mantle Of A Continental Back-Arc Basin. *Geophysical Research Letters*, 31, L06622. doi:10.1029/2003GL019232
- Stratford, W. R., Stern, T. A., 2006. Crust And Upper Mantle Structure Of A Continental Backarc: Central North Island, New Zealand. *Geophysical Journal International*, 166: 469–484. doi:10.1111/j.1365-246X.2006.02967.x

- Sutton, A. N., Blake, S., Wilson, C. J. N., 1995. An outline geochemistry of rhyolite eruptives from Taupo volcanic centre, New Zealand. *Journal of Volcanology and Geothermal Research*, 68, 153-175. doi: [http://dx.doi.org/10.1016/0377-0273\(95\)00011-I](http://dx.doi.org/10.1016/0377-0273(95)00011-I)
- Vandemeulebrouck, J., Hurst, A.W., Scott, B.J., 2008. The effects of hydrothermal eruptions and a tectonic earthquake on a cycling crater lake (Inferno Crater Lake, Waimangu, New Zealand). *Journal of Volcanology and Geothermal Research*, 178(2), 271-275. doi: <http://dx.doi.org/10.1016/j.jvolgeores.2008.06.021>
- Villamor, P., Berryman, K., 2001. A late Quaternary extension rate in the Taupo Volcanic Zone, New Zealand, derived from fault slip data. *New Zeal J Geol Geop*, 44(2): 243-269. doi: <http://dx.doi.org/10.1080/00288306.2001.9514937>
- Villamor, P., Berryman, K.R., 2006. Evolution of the southern termination of the Taupo Rift, New Zealand. *New Zeal J Geol Geop*, 49(1), 23-37. doi: <http://dx.doi.org/10.1080/00288306.2006.9515145>
- Villamor, P., Berryman, K.R., Nairn, I., Van Dissen, R., Begg, J., Lee, J., 2008. Late Pleistocene surface rupture history of the Paeroa Fault, Taupo Rift, New Zealand. *New Zeal J Geol Geop*, 51(1), 135-158. doi: <http://dx.doi.org/10.1080/00288300809509855>
- Walcott, R. I., 1987, Geodetic Strain and the Deformational History of the North Island of New Zealand during the Late Cainozoic. *Philosophical Transactions of the Royal Society of London. Series A, Mathematical and Physical Sciences*, 321, 163-181. doi: 10.1098/rsta.1987.0009
- Wallace, L. M., Beavan, J., McCaffrey, R., Darby, D., 2004. Subduction zone coupling and tectonic block rotations in the North Island, New Zealand. *Journal of Geophysical Research-Solid Earth*, 109, B12406. doi: 10.1029/2004JB003241
- Walter, T.R., Troll, V.R., Cailleau, B., Belousov, A., Schminke, F., Amelung, F., v.v Bogaard, P., 2005. Rift zone reorganisation through flank instability in ocean volcanoes: an example from Tenerife, Canary Islands. *Bulletin of Volcanology*, 37, 281-291. doi: 10.1007/s00445-004-0352-z.
- Wilson, C. J. N., Houghton, B., F., McWilliams, M. O., Lanphere, M. A., Weaver, S. D., Briggs, R. M., 1995. Volcanic and structural evolution of Taupo Volcanic Zone, New Zealand: a review. *Journal of Volcanology and Geothermal Research*, 68, 1-28. doi: [http://dx.doi.org/10.1016/0377-0273\(95\)00006-G](http://dx.doi.org/10.1016/0377-0273(95)00006-G)
- Wilson, C.J.N., Gravley, D.M., Leonard, G.S., Rowland, J.V., 2009. Volcanism in the central Taupo Volcanic Zone, New Zealand : tempo, styles and controls. p. 225-247 In: Thordarson, T.; Self, S.; Larsen, G.; Rowland, S.K.; Hoskuldsson, A. (eds) *Studies in volcanology : the legacy of George Walker*. London: Geological Society. Special publications of the International Association of Volcanology and Chemistry of the Earth's Interior 2.

Wright, C., 1990. Late Quaternary faulting of the offshore Whakatane Graben, Taupo Volcanic Zone, New Zealand, *New Zealand Journal of Geology and Geophysics*, 33(2), 245-256, doi: 10.1080/00288306.1990.10425682

2 Contemporary ground deformation in the Taupo Rift and Okataina Volcanic Centre from 1998 to 2011, measured using GPS.

L. Holden¹, L. Wallace², J. Beavan^{3,5}, N. Fournier³,
R. Cas¹, L. Ailleres¹, D. Silcock⁴

¹*Monash University, School of Earth, Atmosphere & Environment, Melbourne, Victoria, Australia*

²*Institute for Geophysics, The University of Texas at Austin, United States*

³*GNS Science, New Zealand,*

⁴*School of Mathematical and Geospatial Science, RMIT University, Melbourne, Australia*

⁵*Deceased*

Corresponding Author: lucas.holden@monash.edu

PUBLISHED IN: GEOPHYSICAL JOURNAL INTERNATIONAL

Volume 202, Issue 3, pages 2082-2105

doi:10.1093/gji/ggv243

Citation: Holden, L., Wallace, L., Beavan, J., Fournier, N., Cas, R., Ailleres, L. & Silcock, D., 2015. Contemporary ground deformation in the Taupo Rift and Okataina Volcanic Centre from 1998 to 2011, measured using GPS, *Geophysical Journal International*, 202(3), 2082-2105, doi: 10.1093/gji/ggv243.

2.1 Abstract

The Taupo Volcanic Zone (TVZ) is one of the world's most productive regions of rhyolitic volcanism and contains the highly active Okataina Volcanic Centre (OVC). Within the TVZ, intra-arc extension is expressed as normal faulting within a zone known as the Taupo rift. The OVC is located within a complex part of the rift, where volcanism and deformation is considered influenced by rift structure and kinematics. There has been significant research on the structural, volcanic and geophysical properties of the rift and OVC, but less focus on deformation using geodetic data. The limited studies that have utilised geodetic data do not clearly resolve the distribution of deformation and strain rates within the rift and OVC. This is essential to ensure that deformation signals from volcanic processes at the OVC are correctly identified and distinguished from those related to regional tectonic or local hydrothermal processes within the rift.

In this paper, we present a picture of contemporary deformation at the OVC and within the surrounding rift in detail, using existing and new GPS campaign and continuous GPS (cGPS) data collected between 1998 and 2011. The results show a highly heterogeneous deformation and strain rate field (both extension and shortening) through the study area, partitioned into different parts of the rift. Our results agree well with earlier geodetic studies, as well as identify new features, but some deformation patterns conflict with long-term geological observations. In the OVC, we observe a locally rotated horizontal velocity field, significant vertical deformation and variable strain rates across the caldera. In the Tarawera rift, we identify elevated extension and shear rates, which may have significant implications for volcanism there. A shortening pattern is identified through the central rift, which is unexpected in an intra-arc rifting environment. We attempt to explain the source/s of shortening and extension and discuss their implications for geodetic monitoring efforts in the OVC.

KEYWORDS – satellite geodesy, crustal strain rates, volcanic arc processes, New Zealand

2.2 Introduction

Within large caldera systems, geodetic observations can provide accurate measurements of ground deformation. These observations can be studied to better understand magma system dynamics and related volcanic processes. However, they must be interpreted within the regional context, as tectonic, magmatic or hydrothermal activity can mask volcanic deformation signals. In magmatically active rift systems this is challenging, as studies have implied the presence of complex inter-relationships between magmatism, tectonics and volcanism, whereby magmatism and upper crustal deformation can feedback on one another (Manville and Wilson, 2003; Spinks et al., 2005; Wilson et al., 2010; Kogan et al., 2012; Keir et al., 2013). To interpret local deformation at large caldera systems in active rift settings, accurate models of the regional velocity and strain rate field are necessary.

The Okataina Volcanic Centre (OVC) is a large inter-rift caldera, located in a complex tectonic rift setting known as the Taupo Volcanic Zone (TVZ). This is a region of active tectonic extension (Darby et al., 2000; Wallace et al., 2004), high heat flow and magmatism (Bibby et al., 1995) and is one of the most productive regions of rhyolitic volcanism in the world (Wilson et al., 1995; Sutton et al., 2000; Price et al., 2005). The OVC is one of seven large caldera centres in the TVZ that have produced very large eruptions and it is the most recently active volcanic region of the TVZ (Houghton et al., 1995; Wilson et al., 1995). Geodetic monitoring at the OVC is currently undertaken using cGPS stationed permanently within and around the caldera. These are complemented with repeated campaign style GPS surveys. This monitoring must be accompanied by an understanding of what is likely to happen during renewed activity, as well as the ability to discriminate between such activity and background rifting processes (Ellis et al., 2007).

The last eruption within the OVC (the 1886 Tarawera eruption) was preceded by only one hour of felt earthquakes (Nairn 2002). Although seismicity is monitored at the OVC with a network of seismographs, increased seismic noise may be interpreted as normal tectonic activity, which characterizes this region (Bryan et al., 1999). As a result, seismic monitoring cannot be solely relied upon and should be used alongside other techniques such as geodetic monitoring. However, geodetic data indicating ground deformation must be interpreted with caution. Since there has been no recent significant activity at the OVC, the geodetic precursors leading to a volcanic crisis remain relatively unknown. Also, the use of precise GPS monitoring of volcanic systems implies that the observations will record both a local signal (assumed to be due to magmatic and/or hydrothermal processes) and a regional tectonic signal (Cabral-Cano et al., 2008). Further, a number of highly active geothermal fields exist within and around the OVC, whose recurrent activity must be considered when interpreting deformation.

In the TVZ, intra-arc extension is accommodated pre-dominantly by a zone of normal faulting, dike intrusion and extensional fracturing, known as the Taupo rift (Acocella et al., 2003; Villamor and Berryman, 2006). Studies suggest that the rift is divided into discrete segments with variable extension rates and styles as well as different upper crustal properties (Rowland and Sibson, 2001; Acocella et al., 2003; Rowland et al., 2010). The Okataina segment occurs at the largest stepover in the Taupo rift (see Figure 2.1) and is considered to be either a structurally complex transfer zone related to local strain adjustment (Acocella et al., 2003) or an accommodation zone that reflects stress field heterogeneity (Rowland and Sibson, 2001; Rowland et al., 2010).

It is not clear how regional tectonic structure, rift kinematics and magmatic processes relate to deformation patterns and volcanism at the OVC. Wilson et al., 2009 propose that in this region of the rift, complex interactions between magmatism and tectonic processes exist, whereby magma emplacement mediates crustal deformation, while rift related normal faulting can control magma emplacement. Seebeck and Nicol (2009) propose that crustal extension is tectonic outside the OVC and induced by dike intrusion within the caldera boundary. Rift structure and kinematics have been linked to OVC caldera structure and development, eruptive behaviour and volcanism (Cole et al., 2005; Smith et al., 2005; Cole and Spinks, 2009; Cole et al., 2010; Smith et al., 2010). Rowland and Sibson (2001) question whether the magma localisation at the OVC is a result of stress heterogeneity in the Okataina segment (linked to a step in rift structure) or if there is another cause still remains uncertain.

Studies using geodetic data within New Zealand's North Island and Taupo rift have been limited, but have provided a better understanding of the regional velocity field (Beavan and Haines, 2001) and rifting rates (Darby et al., 2000; Wallace et al., 2004). Recently, Differential Radar Interferometry (InSar) data has been utilised to examine the broad scale patterns between surface uplift and subsidence and magmatism at a large scale across the central North Island (Samsonov et al., 2011; Hamling et al., 2015). However, these studies do not provide a detailed picture of the horizontal and vertical velocity and strain rate fields through the entire central Taupo rift. As a result, there is limited knowledge about deformation patterns through the Taupo rift and it remains difficult to identify ground deformation patterns within the OVC linked to volcanic processes there.

In this paper we reprocess 11 years of continuous and campaign GPS data (including new data) for the central and northern Taupo rift and OVC. Incorporating this new data, we present a new picture of contemporary crustal deformation through this region and across the OVC. This includes the first published strain field for the TVZ from a comprehensive GPS velocity field. We consider and discuss the various origins of the

deformation patterns and their implication for monitoring volcanic processes at the OVC. Specifically, we address the following specific questions; 1) what is the nature of contemporary ground deformation through the OVC and in the surrounding Taupo rift and 2) is deformation in the OVC related to volcanic activity or linked to background tectonic processes or local hydrothermal activity? Finally, we discuss the implications of our results for geodetic monitoring of volcanic activity in the OVC.

2.3 Rift structure and kinematics

Intra-arc rifting processes in the Taupo rift have been linked to rapid tectonic block rotation along the eastern North Island (Wallace et al., 2004). This region is characterised by a strain rate field that is primarily extensional (Beavan and Haines, 2001). Geodetic (GPS) observations have measured varying total rates of extension along the rift axis, from $\sim 15 \text{ mm/yr}^{-1}$ near the Bay of Plenty to $\sim 7 \text{ mm/yr}^{-1}$ in the Lake Taupo area (see Figure 2.1) (Wallace et al., 2004). Wallace et al., (2004) interpret these results to indicate a uniformly decreasing (southwards) wedge based extension model though the central North Island. Rowland et al., (2010) correctly point out that these results reflect bulk movement of the Eastern North Island away from the fixed Australian Plate and that the distribution and distribution of contemporary strain within the TVZ is not well resolved in the previously published geodetic studies. Alternatively, Villamor and Berryman (2001) and Villamor and Berryman (2006) propose a more parallel-sided extension model with abrupt changes at specific locations along the rift axis, although with an overall northward increase in extension rates. Mouslopoulou et al., (2007) propose that the increase in extension rate near the Bay of Plenty (see Figure 2.1) is a result of the interaction and transfer of strike-slip fault motion from the North Island Dextral Fault Belt (NIDFB) (see Figure 2.1) into the rift structure.

The modern Taupo rift is divided into a number of offset and variably oriented rift segments that are either soft linked by accommodation zones of stress heterogeneity (Rowland and Sibson, 2001) or hard linked by transfer faults (Acocella et al., 2003). Following Acocella et al., (2003), these include the Whakatane, Okataina, Kapenga, Taupo and Ruapehu segments (see Figure 2.1). The axial part of the rift is roughly symmetrical with a central graben axis (Cole and Spinks, 2009) and contains a dense array of normal faults between the Okataina and Taupo Volcanic Centres, known as the Taupo Fault Belt (TFB) (Grindley, 1960) (see Figure 2.1). Shallow upper crustal seismicity is primarily concentrated within this area (Bibby et al., 1995; Ellis et al., 2007). In the central TVZ, Rowland et al., (2010) propose that extensional mechanisms vary and include: pure tectonic faulting, mafic and rhyolitic dike intrusion, regional scale uplift and transient subsidence associated with inflation or deflation of mafic magma bodies and regional-scale basin development in association with rhyolitic caldera-forming eruptions. They divide this region into two parallel zones (see Figure 2.1): a cooler

western belt that deforms by faulting (i.e., the TFB) and a warmer zone (the Taupo Reporoa Basin - TRB) of little surface faulting, high heat flow and possibly partial melt in the upper crust. East of the Taupo rift lies the Axial Ranges (see Figure 2.1), where strike-slip faulting dominates (e.g., Beanland and Haines, 1998) and largely coincides with the Axial Ranges (AXIR) tectonic block of Wallace et al., (2004).

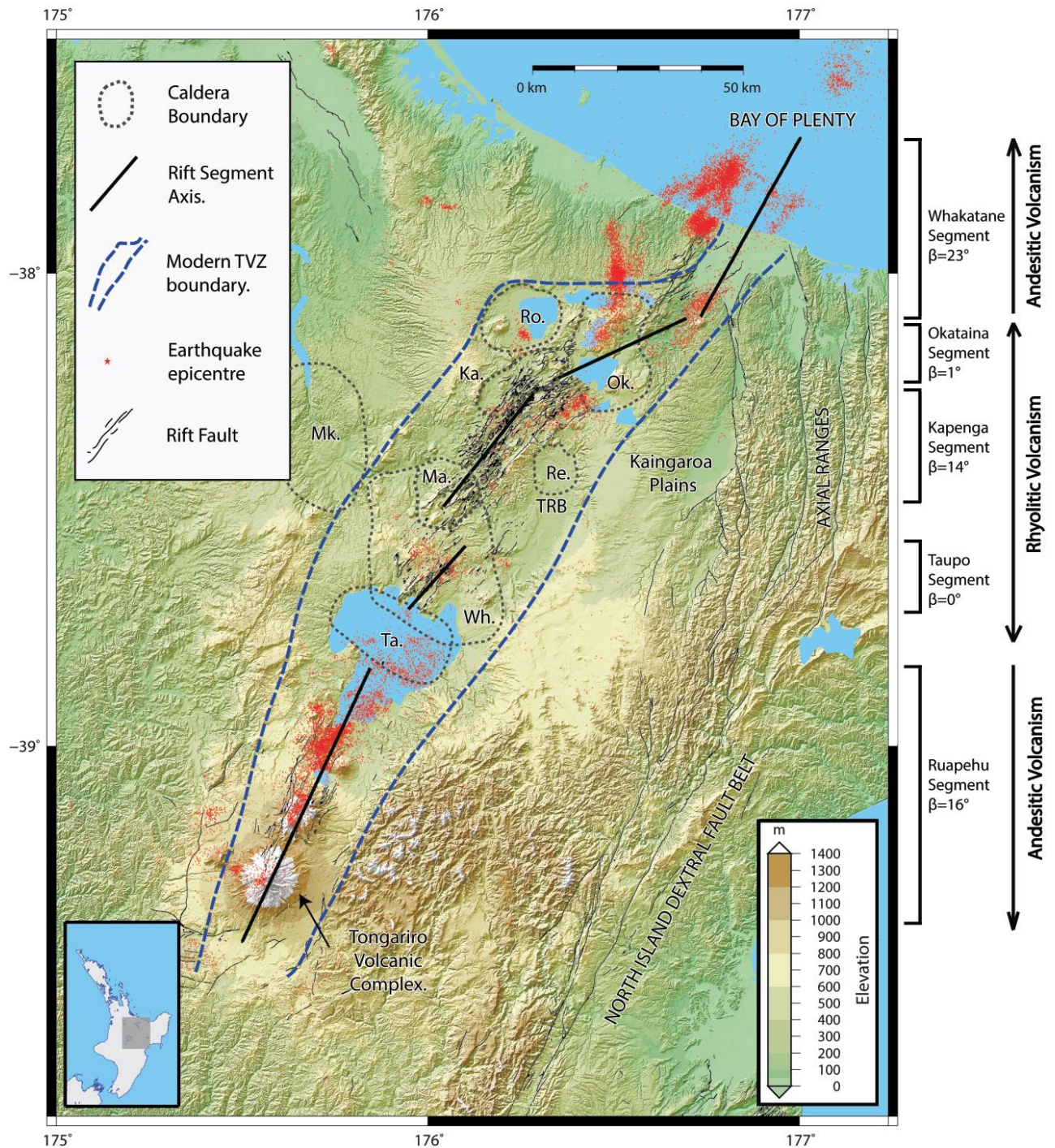


Figure 2.1 – Structural diagram of the Taupo Rift. The modern TVZ boundaries are approximate and from Cole (1990). Rift segment axis and strike-slip components (β) from Acocella et al., (2003). Light black lines are active rift faults from the GNS Science Active Faults Database. Epicentres plotted for shallow earthquakes (<10km) between 1998 to 2011 from the GNS Science GeoNet Earthquake Database. DEM produced using LRIS Data Portal from NZ Landcare Research. Caldera boundary locations are shown as dashed grey lines and are approximate. Ro. Rotorua Caldera, Ok. Okataina Caldera, Mk. Mangakino Caldera, Ma. Maroa Caldera, Re. Reporoa Caldera, Ta. Taupo Caldera, To. Tongariro Volcanic Complex, Wk, Whakamaru Caldera. Dashed blue lines represent modern rift boundaries (from Acocella et al., 2003). Bottom left inset shows location of study area.

Geological studies indicate different components of dextral shear and extension along the rift (see Figure 2.1) (Acocella et al., 2003). Studies also show that segments with high extension rates (the Okataina and Taupo segments) correspond to the highly active rhyolitic Taupo and Okataina volcanic complexes, while segments with a high degree of trans-tensional shear (Whakatane, Kapenga and Ruapehu segments) coincide with more moderately eruptive andesitic stratovolcanoes (Acocella et al., 2003; Spinks et al., 2005). The Okataina segment connects the neighbouring parallel Whakatane and Kapenga (Ngakuru) grabens by obliquely trending fault and vent lineations, which is accommodated by curved faults and is also characterised by a slight trend (~20 degrees) variation in the extension direction (orthogonal to Okataina structures with respect to neighbouring segments) (Acocella et al., 2003). This segment occurs at the largest step in the Taupo rift (Rowland and Sibson, 2001; Acocella et al., 2003; Cole and Spinks, 2009; Cole et al., 2010). Rowland and Sibson (2001) consider these structural variations a result of stress heterogeneity linked to accommodation zones and question whether this is the cause of magmatic localisation at the OVC or an effect of magmatism. Acocella et al., (2003) suggest that the more easterly change in segment orientation is not sufficient to account for all the trend rotation and propose the presence of a local rotation due to local readjustment of strain between the interacting Whakatane and Kapenga offset segments.

A broad wavelength (~250km), dome shaped pattern of rock uplift, centred east of Mt Ruapehu in the Tongariro Volcanic Complex (see Figure 2.1), dominates the vertical tectonics of the central North Island (Pulford and Stern, 2004). They link this uplift to thermal processes in the underlying mantle wedge. In contrast, within the central rift, subsidence patterns are observed to vary in space and time and have been linked to rifting processes and magma availability (Villamor and Berryman, 2001; Manville and Wilson, 2003; Rowland et al., 2010; Hamling et al., 2015). Subsidence in the Whakatane segment, associated with rifting, has been measured at 1-2 mm/yr⁻¹ at the Bay of Plenty coast and uplift of 0.5 to 1 mm/yr⁻¹ at the eastern and

western margins of the rift in this region (Wright, 1990). In the Kapenga segment, subsidence rates have locally been estimated at $-7.23 \pm 0.38 \text{ mm/yr}^{-1}$ from fault displacement (Villamor and Berryman, 2001) and up to -10 mm/yr^{-1} from repeated precise levelling (Blick and Otway, 1995). Immediately north of Taupo caldera, local vertical deformation is small (relative to the Taupo rift further northwards), appears to be episodic on a scale between 1 to 10 years, and is often associated with magma migration (Manville and Wilson, 2003). InSAR has also identified localised regions of subsidence linked to geothermal exploitation (Hole et al., 2005; 2007; Samsonov et al., 2011).

2.4 The Okataina Volcanic Centre

The OVC is a rectangular caldera structure whose long axis trends roughly perpendicular to the Okataina segment axis (see Figure 2.2) (Spinks et al., 2005). It consists of overlapping and nested caldera structures filled with post-caldera rhyolites, which includes the larger Haroharo caldera (delineated by the bold line in Figure 2.2), containing the Haroharo and Tarawera volcanic complexes (Nairn, 2002). Eruptive vents post 25ka are well mapped and define two broad linear zones; the Tarawera and Haroharo linear vent zones (see Figure 2.2) (Nairn, 2002). These lineations are roughly axial to the Whakatane and Kapenga segments and considered to mark their continuation into the Okataina area (Spinks et al., 2005). Volcanic activity within the last 26ka has been linked to post-caldera rhyolitic dome building (Cole et al., 2010), primarily along these linear vent zones (Nairn, 2002). Recent volcanic activity includes the 1886 AD Tarawera-Rotomahana-Waimangu basalt dike intrusion eruption from the Tarawera volcanic complex. Today the most intense hydrothermal activity is located outside the caldera, within the Lake Rotomahana, Waimangu and the Waiotapu geothermal fields (see Figure 2.2), and it is closely related with the southwest extension of the Tarawera vent lineations and 1886 AD rift (Nairn, 2002). A number of small to moderate hydrothermal explosions have occurred within these fields since 1886 (Scott, 1992; Scott, 1994; Vandemeulebrouck et al., 2008).

<u>Site</u>	<u>Occupation details</u>							
	1998	1999	2000	2001	2005	2007	2009	2011
1291			XX		XX	XX		XX
2308			XXX	XX	XX		XX	
2309			XX		XX	XX		XX
2313			XXX		XX	XXXX		XX
2318			XX		XX	XX		XX
2344			XX		XXX	XX		XX
2348			XX		XX	XX		XX
2350			X		XX	XX		XX
2351			X		XX	XX		XX
2382					XXX	XX		XX
2383			XX		XX	XX		XX
2401				X	X	XXXX		
2405			XX		X			
3002			XX		XXX	XX		XX
3006			XX		XX	XX		XX
3051	XXX	XXXXXX*	XXXXXX*	XXXXXX*	XX	XX		XX
3052			XX		XX	XX		XX
3056			XX		XX	XX		XX
3061			XX		XX	XX		XX
3063			XX		XX	XX		XX
3066			XX		XX	XX		XX
3067			XX		XX	XX		XX
3077			XX		XX	XX		XX
3078			XXX		XX	XX		XX
3079			XX		XX	XX		XX
3080	XX	XXXXXX*	XXXXXX*	XXXXXX*	XX	XX		XX
3081			XX		XX	XX		XX
3093			XX		XX	XX		XX
3094			XX		XX	XX		XX
6881						XX	XX	XX
A4K6						XX	XX	XX
A7LF			XX		XX	XX		XX
A7LJ			XX		XX	XX		XX
A86L			XX		XX	XX		XX
A86T						XXX	XX	XX
A86W						XX	XX	XX
A87P						XX	XX	XX
A88G			XX		XX	XX		XX
A88H			XX		XX	XX		XX
A886						XXX	XX	XX
A89V			XX		XX			
AGB9						XX	XX	XX
A9BM				XX	XX	XX		XX
AGUG					X	XX		XX
AH9J						XX	XX	XX
B26Q			XX		XX	XX		XX
B4DP					XX	XX		XX
B4HJ					X	XX		XX
BE2T			XX			XX	XX	XX
BEVJ	XX	XXXXXX*	XXXXXX*	XXXXXX*	XX	XX		XX
CBWR			XX		XX	XX		XX
CBWU			XXX		XXX	XX		XX
CBWV			XX	XX	XXX	XX		XX
CBWW			XX		XX	XX	XX	
EAXX						XX	XX	XX
EAXY						XX	XX	XX
E4MH						XXX	XX	XX

Table 2.1 - History of occupation for campaign sites processed. SITE: four-character code description of campaign site. X: each X represents one daily occupation each year with the exception of some 1998/1999 campaigns. XXXXX* indicates that more than five occupations were observed in the calendar year of the campaign. This is the case when two or more campaigns are conducted at different times in the calendar year.

The 1886 AD eruption was preceded by only one hour of felt earthquakes and no eyewitness reports exist of pre-eruptive ground deformation patterns (Nairn and Cole, 1981; Nairn 2002). Sherburn and Nairn (2004) hypothesise two types of ground deformation might precede a surface dike intrusion at the OVC similar to the 1886 event: the first reflecting the rapidly increasing loss of magma at depth, and the second reflecting dike intrusion much closer to the surface. They believe this signal would consist of a longer wavelength, deep deflation signal, superimposed by shallow shorter wavelength inflation. They suggest that monitoring sites on the upper slopes of Mt. Tarawera would probably record uplift (due to the dike intrusion); however more distant sites would only detect the effect of the deeper deflation source, and measure subsidence. They further note that a small (1 per cent) volumetric inflation of the rhyolitic magma chamber would be detected by the lake levelling network, however if this inflation occurred at a steady rate over several years, it would initially be interpreted as tectonic in origin.

Geodetic observations, including lake and tilt levelling measurements plus horizontal strain rate network measurements have measured ground deformation within the caldera (Scott, 1989). Scott (1989) measured significant shear strain rate ($1.66 \pm 1.6 \text{ ppm/yr}^{-1}$) and dilation ($-4.33 \pm 0.9 \text{ ppm/yr}^{-1}$) near Lake Rotomahana (see Figure 2.2), (where negative dilational strain rate is linked to contraction). Scott (1989) emphasised that these results may have been biased by short observation intervals, but still concluded that significant deformation was occurring within the Tarawera rift. cGPS sites are operated by GeoNet (www.geonet.org.nz) within the caldera. At present, there are seven cGPS receivers stationed within and around the OVC (see Figure 2.3). However it should be noted that some of these instruments have only been in operation since 2009. Recent studies using InSAR (Samsonov et al., 2011; Hamling et al., 2015) has detected broad subsidence across the OVC region, which these studies interpret to be of volcanic or magmatic origin.

2.5 GPS data

GNS Science has surveyed a large geodetic network in the central North Island since the early 1990's (Darby and Williams, 1991; Darby and Meerten, 1995). Various sections of this network have been measured every 1-4 by GPS campaign surveys. The majority of geodetic stations in this network consist of concrete blocks with brass plaques anchored in bedrock. In addition, an extensive network of cGPS sites has also been installed and

operated across NZ by GeoNet (www.geonet.org.nz) and Land Information New Zealand (LINZ), for both geodetic/surveying and geophysical monitoring applications. We analyse data collected from eight GPS campaign surveys (57 geodetic stations) conducted between 1998 and 2011 and data from the two continuous networks (21 stations in total) of the same time period. The location of all these stations is illustrated in Figure 2.3. The occupation details of the geodetic stations occupied in these campaigns are shown in Table 2.1. For campaign surveys from 2000 to 2011, stations were occupied for two days consecutively (20 - 24 hours each day). For earlier campaigns, before 2000, some sessions are 7 - 8 hours in length. Trimble GPS receivers (Trimble 4000 series, 5700, and R7s) and Trimble antennas (mostly Zephyr Geodetic, but some Choke rings for the earlier measurements) have been used predominantly for all campaign surveys and continuous sites, with some Ashtech receivers used in the earlier campaigns.

We also include regional cGPS data from IGS sites in New Zealand, Australia and the southwest Pacific in our processing in order to obtain GPS velocities as a consistent solution in a well-defined reference frame (see Figure 2.3). GPS processing was performed using International Geodynamics Service (IGS) *Repro1* products (precise orbits, clock corrections and Earth rotation parameters). These products are the result of the re-analysis of all GPS data collected by the IGS network since 1994 using a consistent approach (International GNSS Service, 2012). The benefit of these products is that they are all aligned with one reference frame and account for absolute antenna calibrations. The final station coordinates and velocities for this study are in the IGS08 reference frame. We then transform these results to a local fixed reference frame to better identify the ground deformation within the study area (this is described in more detail in the next section).

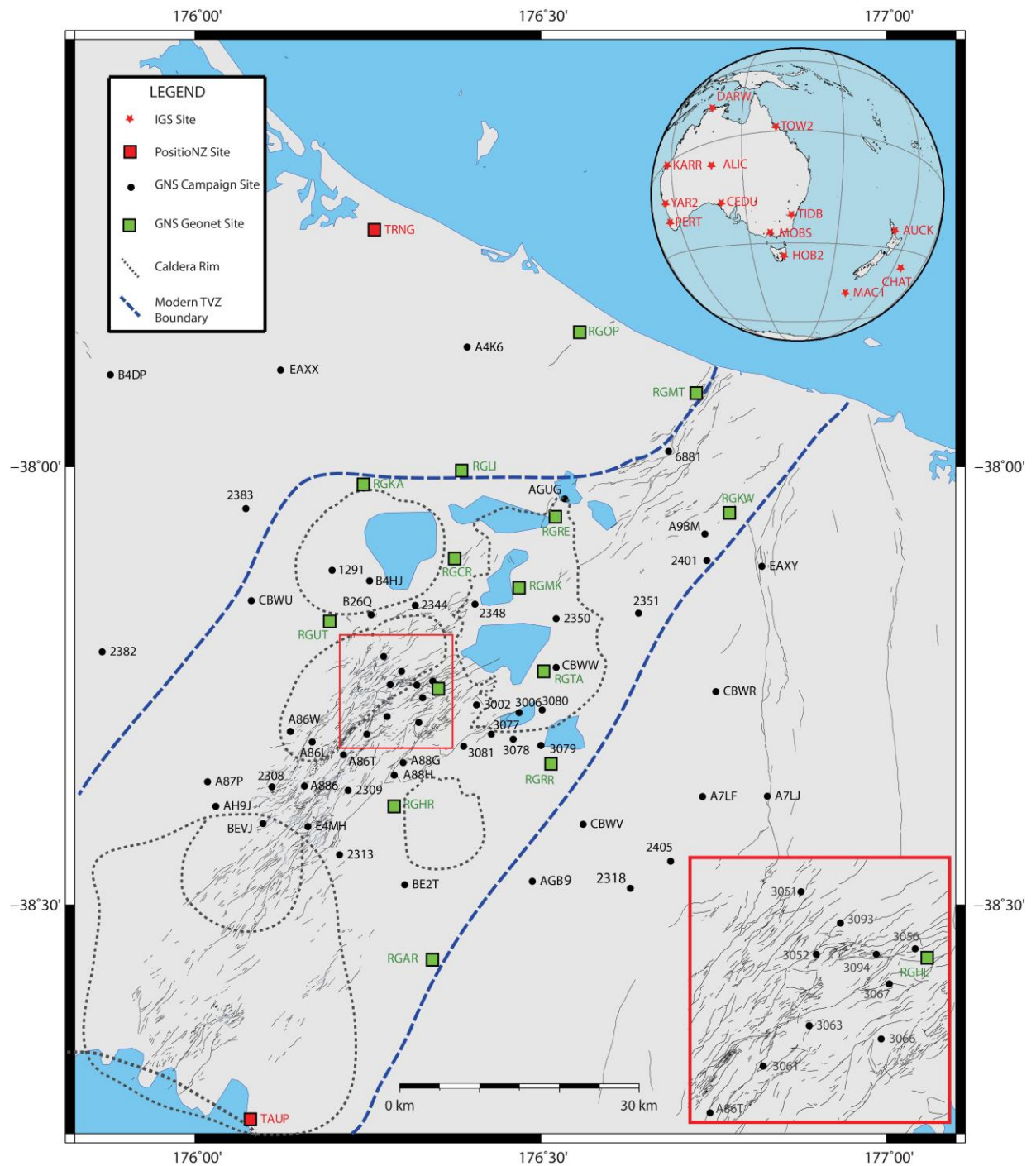


Figure 2.3 – Location and distribution of all GPS stations used in this processing. Locations of calderas are shown as dashed grey lines and are approximate. Modern TVZ boundaries are approximate. IGS GPS stations are plotted on globe at top right. Bottom right inset shows GPS stations south-west of OVC in greater detail.

2.6 GPS processing and velocity estimation

We use standard high precision processing procedures for the GPS phase processing in Bernese GPS software (BSW) version 5 (Dach et al., 2007). In the first part of the processing we obtain daily coordinate estimates and their associated covariance matrices using the double difference baseline processing strategy. We use IGS antenna phase centre models to account for different antenna types. Phase ambiguities are fixed using the quasi-ionospheric free (QIF) resolution strategy. We use an elevation cut-off angle of 3 degrees and elevation dependent weighting in the observation modelling and parameter estimation. The DRY_NIELL model (Neil, 1996) was used to estimate tropospheric parameters at 4-hr intervals. Normal equations were generated without fixing stations to their a-priori coordinates.

The normal equations are then combined (using the ADDNEQ2 option in BSW) in order to calculate station velocities. In ADDNEQ2, we first minimally constrain regional (Australia and NZ) IGS stations to their ITRF coordinates and velocities to identify any inconsistencies and check repeatability in these reference stations. Following this, we estimate final station velocities for our NZ campaign and continuous stations by tightly constraining the velocities of the IGS stations in ADDNEQ2. The results indicated that stations west and northwest of the Taupo rift (e.g. stations 2381, 2383, B4DP and EAXX which are shown west and northwest of Rotorua caldera in Figure 2.3) move with similar horizontal velocities (to within 1.1 mm/yr^{-1}). We use these sites to define a local reference frame for the TVZ velocity field. We then determine GPS velocities through the study area relative to this local reference frame, through a transformation, minimising their velocities to zero.

A recent study (Tregoning et al., 2013) shows some small motion of cGPS stations along the west coast of the North Island, relative to the fixed Australian plate. Given the possibility that the western North Island has some motion relative to the Australian Plate (e.g., Tregoning et al., 2013) we prefer to view the velocity field relative to the stable crustal block just to the west of the TVZ, rather than relative to a fixed Australian Plate, as this gives us clearer insight into the kinematics within the central North Island. The sites we choose for our local reference frame are well suited for this, as they are observed for the full study period and the variations we observe between these stations are very small relative to the large displacements in the rift. In this study, we choose not to use GeoNet cGPS sites west of our study area to define our reference frame since many were not available at the start of our campaign data. Moreover, the determination of strain rates from GPS velocities is independent of reference frame (Sagiya et al., 2004) and we find our velocities to be in excellent agreement with the results presented in Beavan and Haines (2001) and Wallace et al., (2004) and cGPS sites maintained by GeoNet.

It is well documented that GPS formal velocity errors resulting from Bernese ADDNEQ2 are under-estimated and at present there is no standard approach for appropriately rescaling these values (Hugentobler et al., 2001; Geirsson, 2003; Kashani et al., 2004). Further, Bernese (BSW) 5.0 is unable to rescale the covariance matrices in the ADDNEQ2 process (Dach et al., 2007). Subsequently, our rescaling of the GPS formal velocity errors was performed externally of BSW. The use of Bernese variance-covariance matrices for estimation of GPS velocity uncertainties results in underestimation, since no consideration is given to time-dependant errors such as random walk error and time independent error such as white noise. The magnitude of these errors can be assessed using spectral analysis or maximum likelihood estimation (MLE) of suitably long continuous GPS time series (see for example, Zhang et al., 1997; Mao et al., 1999; Dixon et al., 2000; Williams et al., 2004 and Beavan, 2005). According to Zhang et al., (1997), velocity uncertainty related to random walk noise $(\sigma_{\dot{r}})_{WN}$ (mm/yr) is proportional to the magnitude of white noise (a_{WN}) in millimetres, and inversely proportional to the total observation interval T (years) and the square root of the number of measurements N , as shown in equation 1 below;

$$(\sigma_{\dot{r}})_{WN} = \frac{2\sqrt{3}a_{WN}}{N^{1/2}T}$$

(Eq. 1)

Zhang et al., (1997) estimate the component of velocity uncertainty related to random walk error $(\sigma_{\dot{r}})_{RWN}$ using equation 2;

$$(\sigma_{\dot{r}})_{RWN} = \frac{b_{RWN}}{T^{1/2}}$$

(Eq. 2)

whereby $(\sigma_{\dot{r}})_{RWN}$ (mm/yr) is proportional to the magnitude of random walk noise amplitude b_{RWN} (mm/yr^{-1/2}) and inversely proportional to the square root of the total time span T . a_{WN} and b_{RWN} are obtained empirically from the MLE or spectral analysis techniques aforementioned.

In this study we are unable to empirically derive a_{WN} and b_2 from our campaign GPS data since our sampling number and sampling interval are poor (e.g. we do not have a suitably long continuous GNSS time series over the span of our study to estimate reliable results). As a result, our velocity uncertainties incorporate the estimates of Beavan (2005), who analysed the long-term noise characteristics of geodetic monuments in our study area. These are typical of, and in some cases are the same geodetic monuments we use in our study. Beavan (2005) derives mean white noise values (a_{WN}) of 1.1, 1.1 and 3.7 mm/yr⁻¹ in the east, north and up components respectively. He also derives median random walk noise amplitudes (b_2) of 1.8, 2.1 and 4.1

mm/year^{1/2} in the east, north and up components. We incorporate these values into our uncertainty estimates in Table 2.2.

Our horizontal and vertical velocities are illustrated in Figure 2.5 and Figure 2.5. These results are also presented in detail in Table 2.2 along with their uncertainties. The horizontal velocities are in good agreement with those presented in (Beavan and Haines, 2001; Wallace et al., 2004; Beavan and Litchfield, 2012; Tenzer et al., 2012). We observe a small uniform rotation from their solutions due to selection of difference reference frames, as most of the previous velocity fields were shown in an Australian Plate fixed reference frame. We interpret our vertical velocities with caution, due to their inherently larger uncertainties, particularly from campaign style GPS data. In some instances our estimates are larger than prior estimates from geological measurements. However, we find an excellent agreement with the vertical velocities from differential levelling (Darby et al., 2000) and cGPS sites maintained by GeoNet (www.geonet.org.nz) and those presented in Samsonov et al., (2011) and Hamling et al., (2015), which indicates consistency in our approach.

Site	Long.	Lat.	V _E	V _N	V _{UP}	σ _{VE}	σ _{VN}	σ _{VUP}	V _{hor}	σ V _{hor}
HAMT	175.1092	-37.8068	-0.4	1.6	0.4	0.8	0.9	1.7	1.6	0.9
KTIA	173.2731	-35.0689	4.4	3.9	-0.8	1.2	1.3	2.7	5.9	1.2
MAHO	174.8541	-38.5130	-0.7	2.9	-2.4	0.8	0.9	1.7	3.0	0.9
RGAR	176.3430	-38.5620	-0.9	-4.0	-3.6	1.4	1.5	3.2	4.1	1.5
RGCR	176.3780	-38.1047	0.5	-3.8	-3.2	1.2	1.3	2.7	3.8	1.3
RGHL	176.3523	-38.2519	-4.3	-4.3	-19.6	1.4	1.5	3.2	6.1	1.4
RGHR	176.2880	-38.3858	-2.2	-4.6	-7.5	1.2	1.3	2.7	5.1	1.3
RGKA	176.2441	-38.0201	0.4	-1.6	-0.9	1.2	1.3	2.7	1.6	1.3
RGKW	176.7728	-38.0525	0.0	-10.4	-0.8	1.4	1.5	3.2	10.4	1.5
RGLI	176.3857	-38.0033	0.6	-3.4	-2.1	1.2	1.3	2.7	3.5	1.3
RGMK	176.4671	-38.1383	0.6	-9.0	-17.9	0.8	0.9	1.7	9.0	0.9
RGMT	176.7247	-37.9154	0.2	-8.2	10.4	1.4	1.5	3.2	8.2	1.5
RGOP	176.5563	-37.8459	-3.4	-2.0	4.5	1.2	1.3	2.7	3.9	1.2
RGRE	176.5212	-38.0573	-1.4	-5.3	-2.1	1.2	1.3	2.7	5.5	1.3
RGRR	176.5146	-38.3389	-1.4	-5.8	-1.9	1.2	1.3	2.7	6.0	1.3
RGTA	176.5061	-38.2338	-3.7	-2.6	-13.8	1.2	1.3	2.7	4.5	1.2
RGUT	176.1942	-38.1766	3.7	-3.4	-6.0	0.8	0.9	1.7	5.0	0.8
TAUP	176.0810	-38.7427	3.6	-4.5	1.6	0.8	0.9	1.7	5.8	0.8
TRNG	176.2609	-37.7288	1.1	-0.1	-0.9	0.8	0.9	1.7	1.1	0.8
WHNG	174.3146	-35.8038	2.4	2.3	0.3	0.8	0.9	1.7	3.3	0.8
1291	176.1979	-38.1184	1.6	-1.2	-5.5	0.5	0.6	1.2	2.0	0.6
2308	176.1110	-38.3652	4.1	-5.0	-9.1	0.8	0.9	1.9	6.5	0.8
2309	176.2211	-38.3693	-1.1	-4.3	-11.9	0.5	0.6	1.2	4.4	0.6
2313	176.2086	-38.4424	-3.1	-3.3	-19.4	0.7	0.7	1.6	4.5	0.7
2318	176.6344	-38.4847	1.0	-8.6	-2.1	0.5	0.6	1.2	8.7	0.6
2344	176.3181	-38.1582	-0.3	-4.8	-5.7	0.6	0.7	1.3	4.8	0.7
2348	176.4048	-38.1570	2.1	-3.5	-3.8	0.5	0.6	1.2	4.1	0.6
2350	176.5221	-38.1736	1.1	-5.6	-9.7	0.5	0.6	1.1	5.7	0.6
2351	176.6411	-38.1673	1.2	-6.6	-5.7	0.5	0.6	1.1	6.7	0.6
2382	175.8654	-38.2111	-0.6	-0.2	0.5	1.1	1.3	3.3	0.6	1.2
2383	176.0731	-38.0478	-0.1	-0.2	0.4	0.5	0.6	1.2	0.2	0.6
2401	176.7401	-38.1069	5.6	-4.2	-6.9	1.0	1.1	2.7	7.0	1.1
2405	176.7027	-38.4544	1.5	-9.4	2.5	0.8	0.9	1.9	9.5	0.9
3002	176.4069	-38.2719	2.0	-2.1	-19.4	0.6	0.7	1.3	2.9	0.6

3006	176.4683	-38.2807	-2.2	-3.9	-2.2	0.5	0.6	1.2	4.5	0.6
3051	176.2725	-38.2166	2.1	-4.7	-11.0	1.0	1.2	4.3	5.1	1.1
3052	176.2822	-38.2486	1.8	-3.4	-13.5	0.5	0.6	1.2	3.8	0.6
3056	176.3459	-38.2463	-1.2	-4.7	-14.0	0.5	0.6	1.2	4.9	0.6
3061	176.2483	-38.3054	0.6	-1.7	-12.9	0.5	0.6	1.2	1.8	0.6
3063	176.2779	-38.2850	1.2	-0.7	-12.2	0.5	0.6	1.2	1.4	0.6
3066	176.3235	-38.2917	0.2	-1.2	-12.0	0.5	0.6	1.2	1.2	0.6
3067	176.3291	-38.2640	-0.3	-2.4	-15.0	0.5	0.6	1.2	2.4	0.6
3077	176.4283	-38.3051	-1.7	-3.4	-6.8	0.5	0.6	1.2	3.8	0.6
3078	176.4598	-38.3112	-0.7	-4.7	-3.4	0.6	0.7	1.3	4.8	0.7
3079	176.5003	-38.3183	-0.6	-5.5	-10.7	0.5	0.6	1.2	5.5	0.6
3080	176.5017	-38.2776	-1.2	-5.2	-4.2	1.0	1.2	4.3	5.3	1.2
3081	176.3881	-38.3192	-1.3	-3.4	-3.4	0.5	0.6	1.2	3.6	0.6
3093	176.2983	-38.2335	1.8	-4.0	-8.1	0.5	0.6	1.2	4.4	0.6
3094	176.3207	-38.2492	-0.2	-4.0	-13.4	0.5	0.6	1.2	4.0	0.6
6881	176.6847	-37.9821	-0.6	-6.7	1.7	1.9	2.2	7.2	6.7	2.2
A4K6	176.3932	-37.8628	0.1	-1.6	0.6	1.9	2.2	7.2	1.6	2.2
A7LF	176.7340	-38.3764	1.1	-9.3	-1.9	0.5	0.6	1.2	9.4	0.6
A7LJ	176.8272	-38.3757	-1.1	-10.4	-0.2	0.5	0.6	1.2	10.5	0.6
A86L	176.1690	-38.3140	3.7	-4.6	-9.1	0.5	0.6	1.2	5.9	0.6
A86T	176.2143	-38.3289	-0.3	-3.4	-12.4	2.1	2.5	9.6	3.4	2.5
A86W	176.1377	-38.3020	3.1	-4.2	-8.5	2.1	2.5	9.6	5.2	2.3
A87P	176.0179	-38.3596	2.2	-2.8	-4.5	2.1	2.5	9.6	3.6	2.3
A886	176.1582	-38.3643	3.5	-6.1	-12.3	2.1	2.5	9.6	7.0	2.4
A88G	176.3007	-38.3376	0.0	-1.8	-10.3	0.5	0.6	1.2	1.8	0.6
A88H	176.2877	-38.3520	-1.1	-2.3	-9.3	0.5	0.6	1.2	2.5	0.6
A9BM	176.7371	-38.0765	1.2	-7.2	-0.7	0.5	0.6	1.2	7.3	0.6
AGB9	176.4878	-38.4725	-0.3	-7.6	0.8	1.3	1.5	4.1	7.6	1.5
AGUG	176.5345	-38.0364	-0.8	-4.3	-1.0	0.9	1.0	2.2	4.4	1.0
AH9J	176.0301	-38.3875	4.3	-4.3	-5.3	1.9	2.2	7.2	6.1	2.0
B26Q	176.2547	-38.1689	2.9	-4.4	-8.7	0.5	0.6	1.2	5.3	0.6
B4DP	175.8775	-37.8943	-0.3	1.3	-0.8	1.0	1.1	2.7	1.3	1.1
B4HJ	176.2525	-38.1304	1.8	-4.7	-4.9	0.9	1.0	2.2	5.0	1.0
BE2T	176.3028	-38.4768	-2.4	-4.7	-9.1	0.5	0.5	1.0	5.3	0.5
BEVJ	176.0981	-38.4070	4.6	-4.5	-12.2	1.0	1.2	4.3	6.4	1.1
CBWR	176.7530	-38.2566	1.2	-9.3	1.8	0.5	0.6	1.2	9.4	0.6
CBWU	176.0813	-38.1529	0.6	-0.8	-0.8	0.6	0.7	1.5	1.0	0.7
CBWV	176.5608	-38.4079	0.3	-7.2	-1.4	0.7	0.7	1.6	7.2	0.7
CBWW	176.5220	-38.2292	-2.4	-3.4	-7.2	0.5	0.6	1.2	4.2	0.6
E4MH	176.1632	-38.4107	0.8	-4.3	-15.5	2.1	2.5	9.6	4.4	2.4
EAXX	176.1238	-37.8892	0.5	0.1	-2.1	1.9	2.2	7.2	0.5	1.9
EAXY	176.8194	-38.1136	2.0	-10.3	-1.0	1.9	2.2	7.2	10.5	2.2

Table 2.2- GPS Velocities of TVZ Sites (in millimetre per year, in the local fixed reference frame.) Site: four digit site code, Long.: Longitude of station (°), Lat.: Latitude of station (°), $V_E/V_N/V_{UP}$ are east, north and up velocity respectively, $\sigma_{V_E}/\sigma_{V_N}/\sigma_{V_{UP}}$ are the 1σ uncertainty of the respective velocities.

2.7 Results

2.7.1 Horizontal and vertical deformation

Figure 2.4, Figure 2.5 and Figure 2.6 illustrate our horizontal and vertical deformation results. Sites east and southeast of the Taupo rift, towards the AXIR tectonic block, move coherently southwards up to 15mm/yr^{-1} with negligible vertical movement. In the Whakatane segment, velocities coherently trend southerly (e.g. stations RGMT and 6881), at rates between 7 to 9mm/yr^{-1} , which increase towards the AXIR tectonic block (e.g. stations RGKW and EAXY in Figure 2.4). Sparse resolution in this segment means our results add little insight to previous geological estimates of ground uplift or subsidence there. An exception is station RGMT, near the Bay of Plenty (see Figure 2.1), where an uplift of 10mm/yr^{-1} is observed.

In general, horizontal velocities in the OVC region (see Figure 2.4) show a subtle variation in direction southwards through the caldera. This is most pronounced through the Tarawera volcanic complex (particularly near the Tarawera Rift and geothermal fields south of the OVC) where we observe a more rapid clockwise rotation. With the exception of station RGMK, little change in horizontal velocity rate occurs alongside these rotations. We also observe a broad pattern of subsidence in this area and increased subsidence rates in the geothermal areas south of the OVC (see Figure 2.4 and Figure 2.5). The sparse data at the intersection of the Okataina and Whakatane segments does not allow us to constrain deformation well in this region.

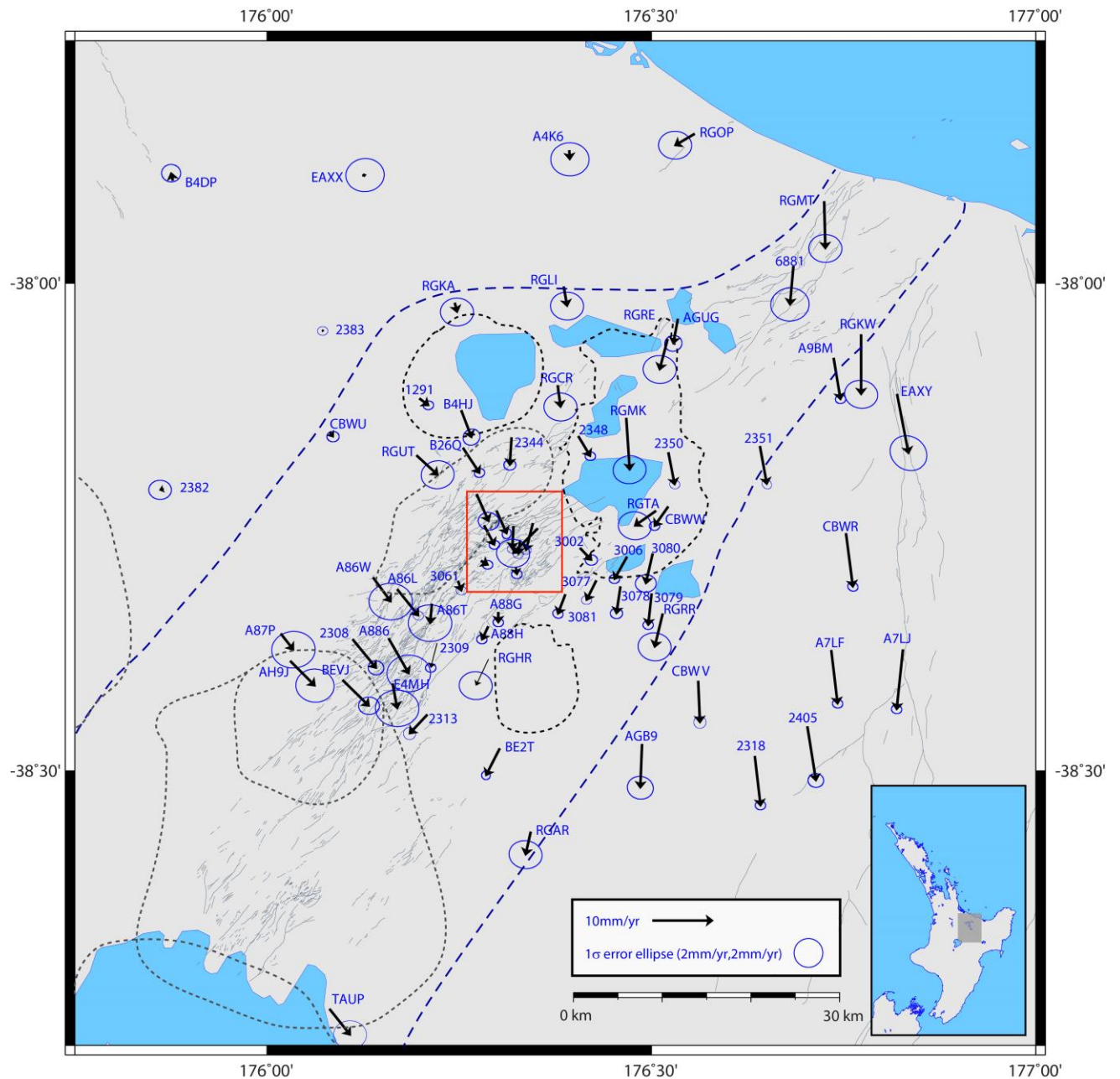


Figure 2.4 – Horizontal GPS velocities in the local fixed reference frame, defined by campaign stations west and northwest of the rift (see text for further details). Locations of calderas are shown as dashed grey lines and are approximate. Red inset same as Figure 2.3. Dashed blue lines represent approximate location of modern rift boundaries. Bottom right inset show location of study area.

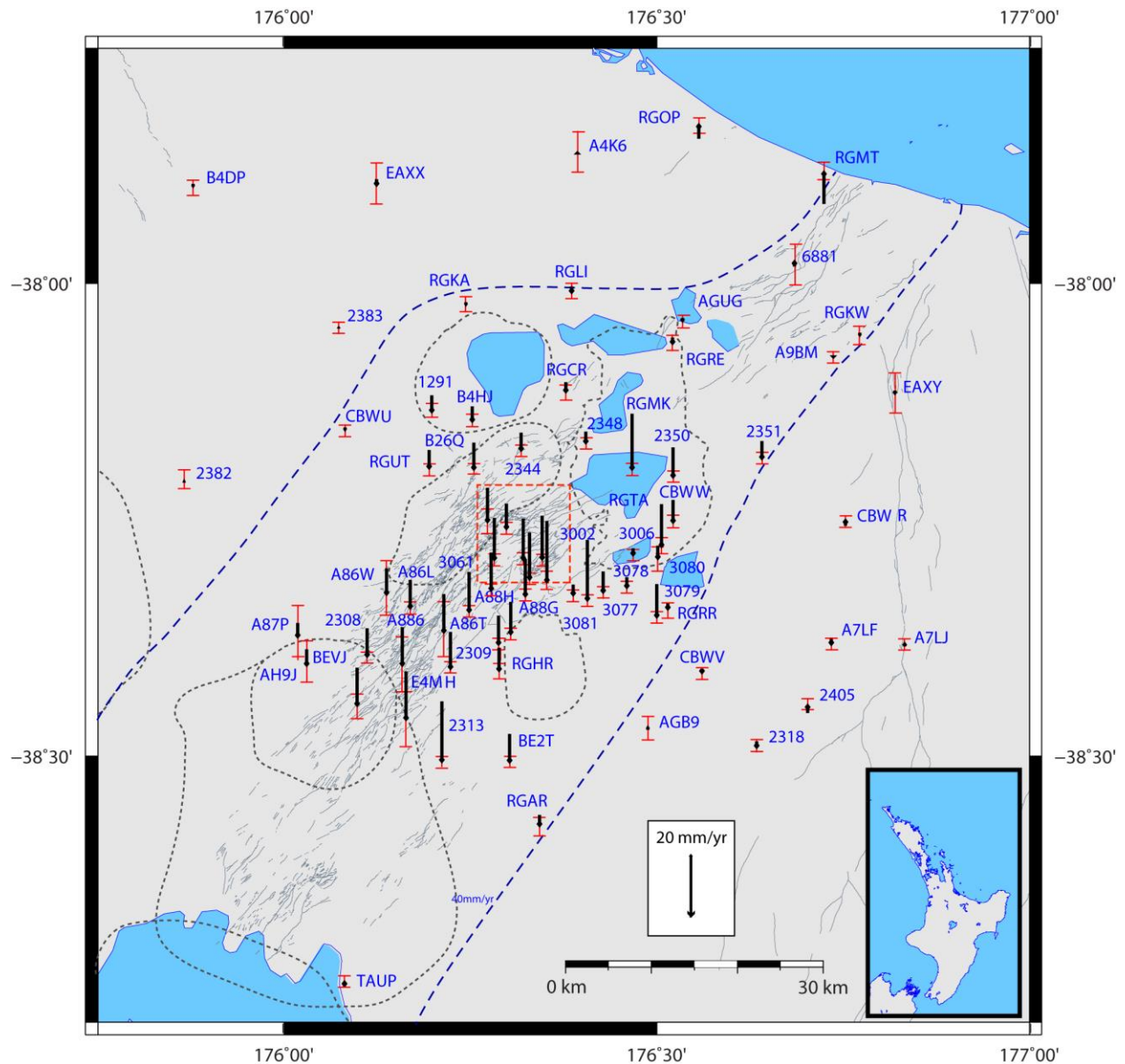


Figure 2.5 – Vertical velocities for GPS stations in the local fixed reference frame. Vertical error-bars indicate 68% standard deviation. Light black lines are active rift faults from the GNS Science Active Faults Database. Locations of calderas are shown as dashed grey lines and are approximate. Red inset same as Figure 2.3. Dashed blue lines represent approximate location of modern Rift boundaries (Acocella et al., 2003). Bottom right inset shows location of study area.

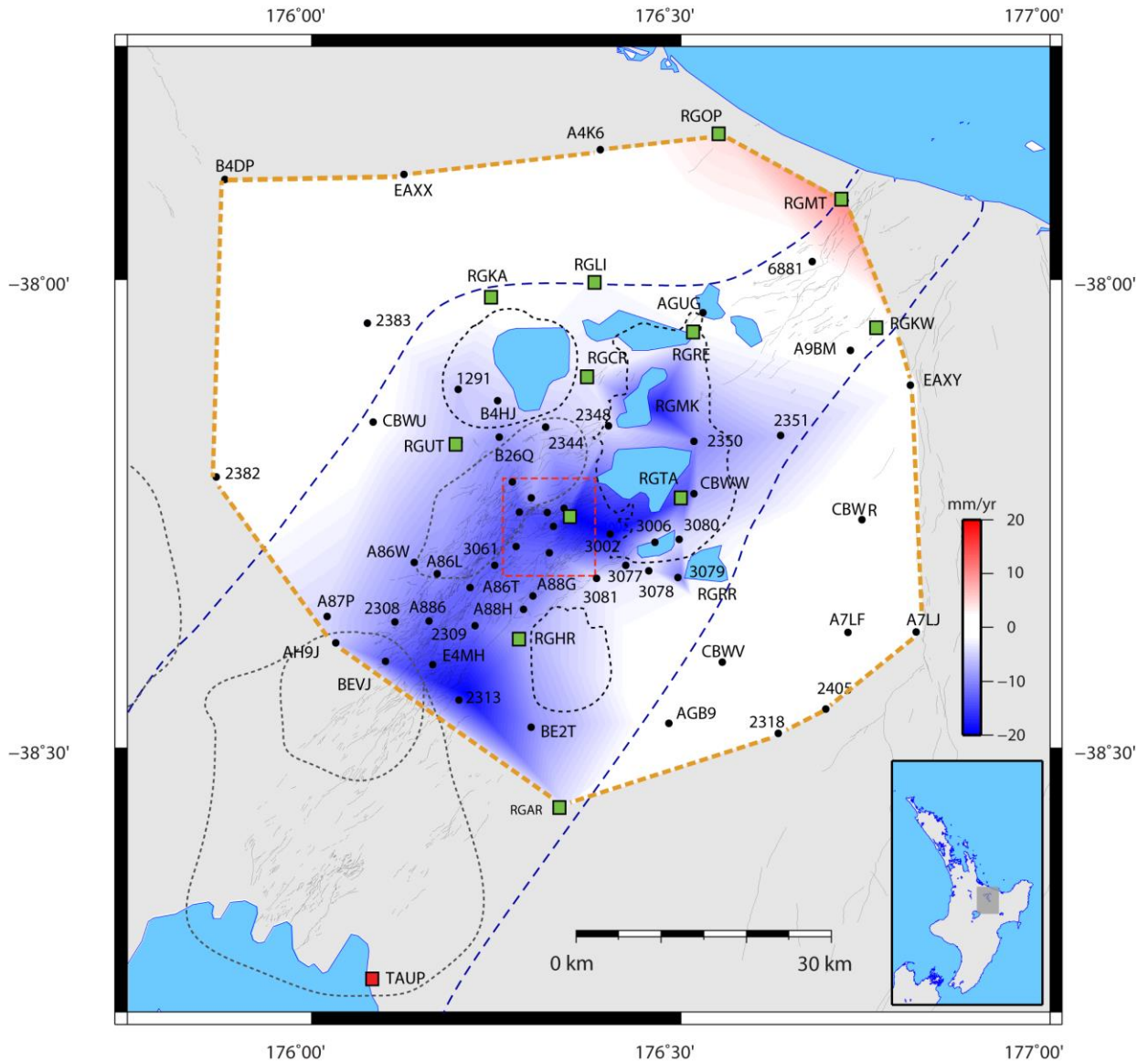


Figure 2.6 – Fitted surface of vertical velocities through the study area. Color-coded scale for velocities is included at bottom right. Dashed orange lines represent limit of triangulation modelling. Dashed blue lines represent approximate location of modern rift boundaries (Acocella et al., 2003). Caldera boundary locations are shown as dashed grey lines are approximate. Red inset same as Figure 2.3. Bottom right inset shows location of study area.

Outside and along the western boundary of the Kapenga segment (see Figure 2.1) (e.g. near stations AH9J, A87P and A86W), horizontal velocities are oriented perpendicular to the segment axis (trending south-east), between 3.6 to 6.5 mm/yr⁻¹ (see Figure 2.4). This pattern extends northwards into the Rotorua caldera (e.g. station RGUT). Figure 2.4 also shows that stations along the eastern side of the Kapenga segment (e.g. stations

A88G, A88H and 2309) trend south to southwest at slower rates. Eastern Kapenga segment border faults (including the Paeroa fault) appear to define a kinematic boundary, which divides southeast trending velocities within the TFB from the southerly or south-westerly motions east of the rift (see Figure 2.4). The horizontal deformation field described by these velocities suggest significant contraction within this segment. We discuss this in more detail in the following section.

We identify a regional subsidence signal through the central rift, with rates varying from -4.5 to -15 mm/yr^{-1} (see Figure 2.5 and Figure 2.6). Exceptions include very large subsidence rates ($>-15 \text{ mm/yr}^{-1}$) measured at station 2313 and RGHL. Excluding these exceptions, our subsidence pattern agrees well at a first order, with the pattern defined by precise levelling (Blick and Otway, 1995). We have no GPS stations within the TRB but note that the precise levelling of Blick and Otway (1995) measure significant subsidence there too. We observe a localised and complex horizontal ground deformation pattern immediately southwest of the OVC in the vicinity of northern strands of the Whirinaki, Tumanui and Paeroa faults (see Figure 2.2). Here, velocities decrease rapidly (from northwest to southeast) to only a few millimetres per year, alongside a pronounced clockwise rotation of their trend direction (see Figure 2.4). Significant subsidence rates are also observed throughout this region.

2.7.2 Strain rates.

We computed the areal strain rate through the study area using the velocities derived from the GPS position time series and the SSPX software (Cardozo and Allmendinger, 2009). SSPX uses 2D (or 3D) horizontal velocity components to determine best fitting strain tensors. Because of the spatially highly variable GPS network density, we opted to discretise the domain using a Delaunay triangulation instead of a regularly gridded domain. Each cell's nodes are GPS stations and an areal strain rate is computed for each cell. The triangulation approach allows some preservation of information in high network density areas while avoiding interpolation in sparse regions. One limitation of this approach is that spurious velocity values at a single station can substantially affect strain calculations for all adjacent cells. Caution must therefore be exercised when interpreting individual local and maximum strain rates for given cells as those are best interpreted in the context of values at neighbouring cells. The strain computation process can be summarised as first solving a set of linear equations for the displacement gradient tensor G_{ij} and then compute the Lagrangian strain tensor E_{ij} . Finding the principal strain components equates to compute the eigenvalues and eigenvectors of E_{ij} . The reader is referred to Cardozo and Allmendinger (2009) and Means (1976) for more detailed information about strain computation.

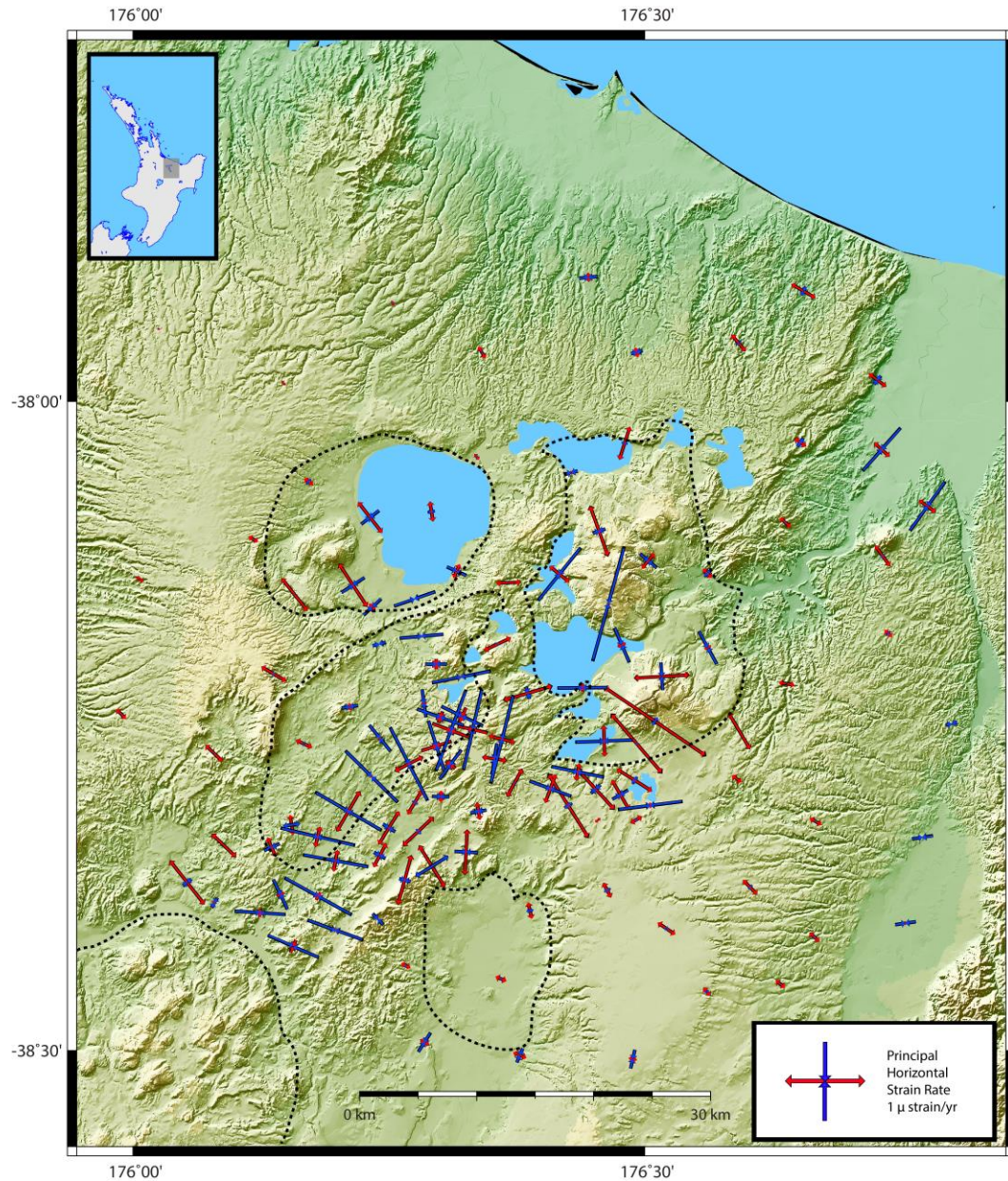


Figure 2.7 – Horizontal principal strain rate axes derived from horizontal GPS velocity rate estimates using the Delaunay approach in SSPX software (Cardozo and Allmendinger, 2009). Caldera boundary locations are shown as dashed black lines and are approximate. Top left inset shows location of study area.

Horizontal principal strain rates are shown in Figure 2.7. The estimated dilation and maximum shear strain rates are illustrated in Figure 2.8 and Figure 2.9 respectively. In general, the main features of the principal strain rate field are lower strain rates (less than approx. $0.2 \times 10^{-6}/\text{yr}^{-1}$) outside the Taupo rift (both NW and SE of the rift) and increased (up to approx. $1.5 \times 10^{-6}/\text{yr}^{-1}$) and more variable rates within the Taupo rift,

particularly within the Kapenga and Okataina segments. In the west and northwest of the study region, lower rates are evident in the maximum principal strain rate axes (see Figure 2.7). Figure 2.7 also suggests extensional strain rates (0.2 to $0.4 \times 10^{-6}/\text{yr}^{-1}$) along much of the eastern border of the Kapenga segment extending into the Rotorua caldera. Shear strain rates are also lower (relative to those within the rift) along this region (see Figure 2.9) and the directions of the maximum principal strain rate axes are rift orthogonal. Some shear strain rates are also observed in the southwest of the Rotorua caldera. Across the Kaingaroa plain, lower strain rates are observed (approximately $0.2 \times 10^{-6}/\text{yr}^{-1}$) and the directions of maximum principal strain rate axes are rift orthogonal.

The most striking aspects of the horizontal strain rate field through the central rift are (1) the presence and localisation of significant shortening rates within and along the Kapenga segment (see Figure 2.7) and (2) the strong contrast of this contraction to the elevated horizontal extension strain rates near the Tarawera rift. Shortening within the Kapenga segment is localised to a narrow zone coinciding with the Ngakuru, Maleme and Whirinaki fault zones (see Figure 2.2). Shortening rates here are remarkably uniform in magnitude (approximately $-1 \times 10^{-6}/\text{yr}^{-1}$) and the direction of the minimum strain rate axes trends rift perpendicular. Strain rates though the OVC and its vicinity are not uniform in rate or orientation. In general, significant shortening is measured in the Haroharo complex (trending N-S) and elevated extension through the Tarawera Dome Complex and south through Lake Rotomahana (see Figure 2.2). The largest principal strain rate we observe in the Tarawera rift is approximately $1.5 \times 10^{-6}/\text{yr}^{-1}$, trending rift orthogonal. The magnitude of this strain rate is large, but matches that estimated by Scott (1989). We also determine elevated positive dilation (between approx. 0.5 to $1.5 \times 10^{-6}/\text{yr}^{-1}$) and significant shear strain rates through the Tarawera rift and negative dilation (compression) across Lake Tarawera. South of the OVC, at the intersection of the Kapenga segment, we also observe elevated amounts of horizontal shear (see Figure 2.9), which appears to occur along much of the length the Paeroa fault leading towards the OVC.

Although we have sparser distribution of data across the Whakatane segment, lower and more uniform strain rates are observed there. We also find anomalous minimum principal strain rates in the vicinity of stations RGKW and A9BM (see Figure 2.3) whose axes are closely aligned with the rift segment axis. They most likely reflect poor geodetic resolution through this region, as well as poor spatial sampling in the Delaunay triangulation. Some shear strain rates are also modelled through this region, which might be related to shortening identified there. No significant dilation (relative to within the rift) is evident in this region (see Figure 2.8).

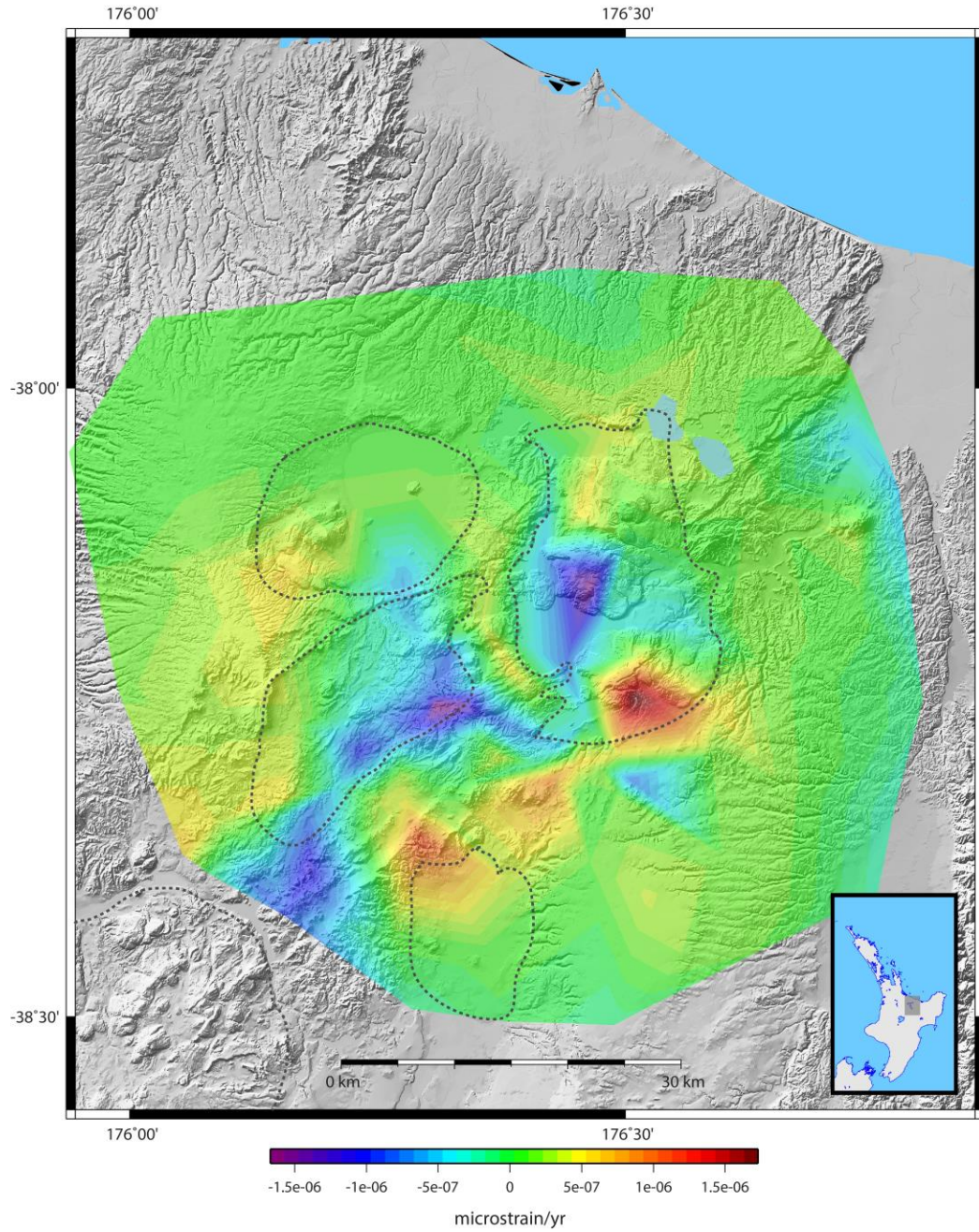


Figure 2.8 – Dilation strain rate field derived from horizontal GPS velocity rate estimates using the Delaunay approach in SSPX software (Cardozo and Allmendinger, 2009). Caldera boundary locations are shown as dashed grey lines and are approximate. Bottom right inset shows location of study area.

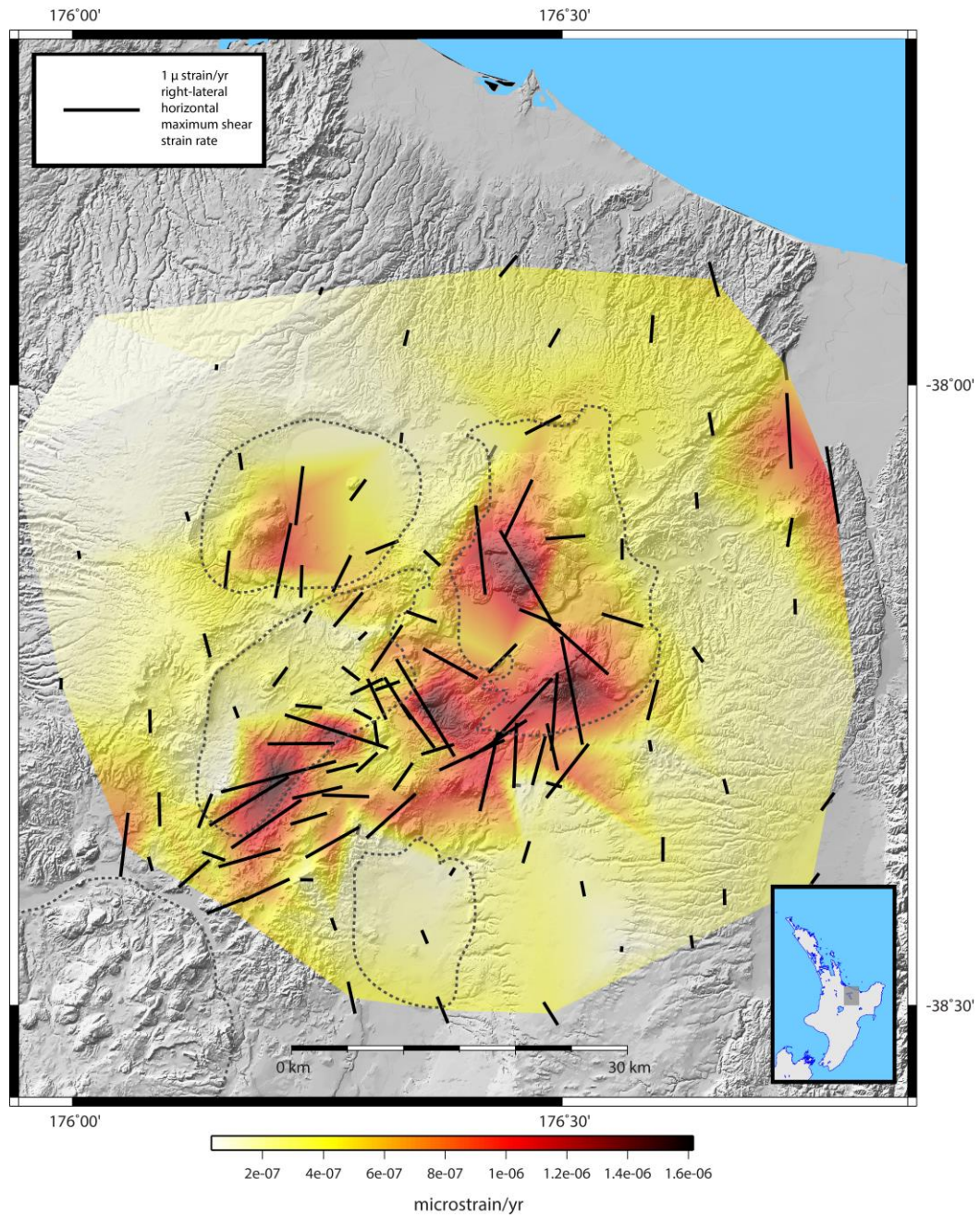


Figure 2.9 – Shear strain rate field derived from horizontal GPS velocity rate estimates using the Delaunay approach in SSPX software (Cardozo and Allmendinger, 2009). Shear strain rate lines are right lateral. Caldera boundary locations are shown as dashed grey lines and are approximate. Bottom right inset shows location of study area.

Geodetic strain rates determined from the SSPX software provide a good insight into spatial patterns of extension and contraction through horizontal velocity fields. This approach can, however, be influenced by velocity uncertainties (for three-node Delaunay triangulation) and geometry effects (e.g. averaging effects) (Serpelloni et al., 2006). Following Vigny et al., (2007), Payne et al., (2012) and Kogan et al., (2012), we generate horizontal GPS velocities profiles (see Figure 2.11) to estimate strain rates across the study area without the geometry effects of SSPX triangulation. To do this we project our horizontal velocities onto 2D profiles orthogonal (trending 120°) to the inferred rift axis (30° E from Acocella et al., (2003)). As these transects are perpendicular to the inferred rift axis, they allow us to estimate rift perpendicular strain rates across the study area (see Figure 2.10). We fit a surface through these rift-perpendicular velocities to examine patterns of rifting through the study area. We then produce velocity profiles through the Whakatane, Okataina and Central segment (see Figure 2.11a, Figure 2.11b, Figure 2.11c). Using least squares linear regression we also determine strain rate estimates from velocity gradients in these figures (dark green lines and text in Figure 2.11). Positive slopes therefore reflect extension and negative slopes shortening.

Figure 2.11a suggests a rift-perpendicular extension rate across the Whakatane graben of 4.5 mm/yr^{-1} . A maximum rate of 7 mm/yr^{-1} is measured in the vicinity of the AXIR tectonic block. The velocities across the Whakatane graben show an estimated strain rate of $0.24 \pm 0.08 \times 10^{-6}$ (estimated over approximately 17 km distance). However, if we consider the 2 mm/yr^{-1} velocity of station RGOP away from the rift axis, our total rifting estimate across the Whakatane profile is 9 mm/yr^{-1} . This compares well with the geodetic estimate of Walcott (1987) of 12 mm/yr^{-1} but less than that predicted by Wallace et al., (2004) of 15 mm/yr^{-1} , although we note that their total extension rate was for the North Island fore-arc relative to the Australian Plate.

Rift-perpendicular extension rates across the Okataina profile are varied (see Figure 2.11b). We do not attempt to determine a single regression estimate there, due to the heterogeneous nature of these velocities and the possible influence of transient velocities within the caldera. In general, extension increases from east to west, where we observe a maximum rate of 5.5 mm/yr^{-1} towards the AXIR tectonic block. However, locally increased velocities are observed near the Rotorua and Haroharo caldera (4 and 5 mm/yr^{-1} respectively). Figure 2.11b also shows decreased horizontal velocities in the vicinity of the Tarawera rift, which could be interpreted to indicate contraction there. However, we consider this an artefact of projecting the locally rotated horizontal velocities in the Tarawera rift onto the Okataina line profile. We also note that the projected velocities in Figure 2.10, do not account for rift segment axis variations, particularly through the Okataina segment, which has a more easterly orientation than neighbouring segments. For these reasons, the use of 2D velocity profiles to estimate strain rates across this part of the Taupo rift may be limited.

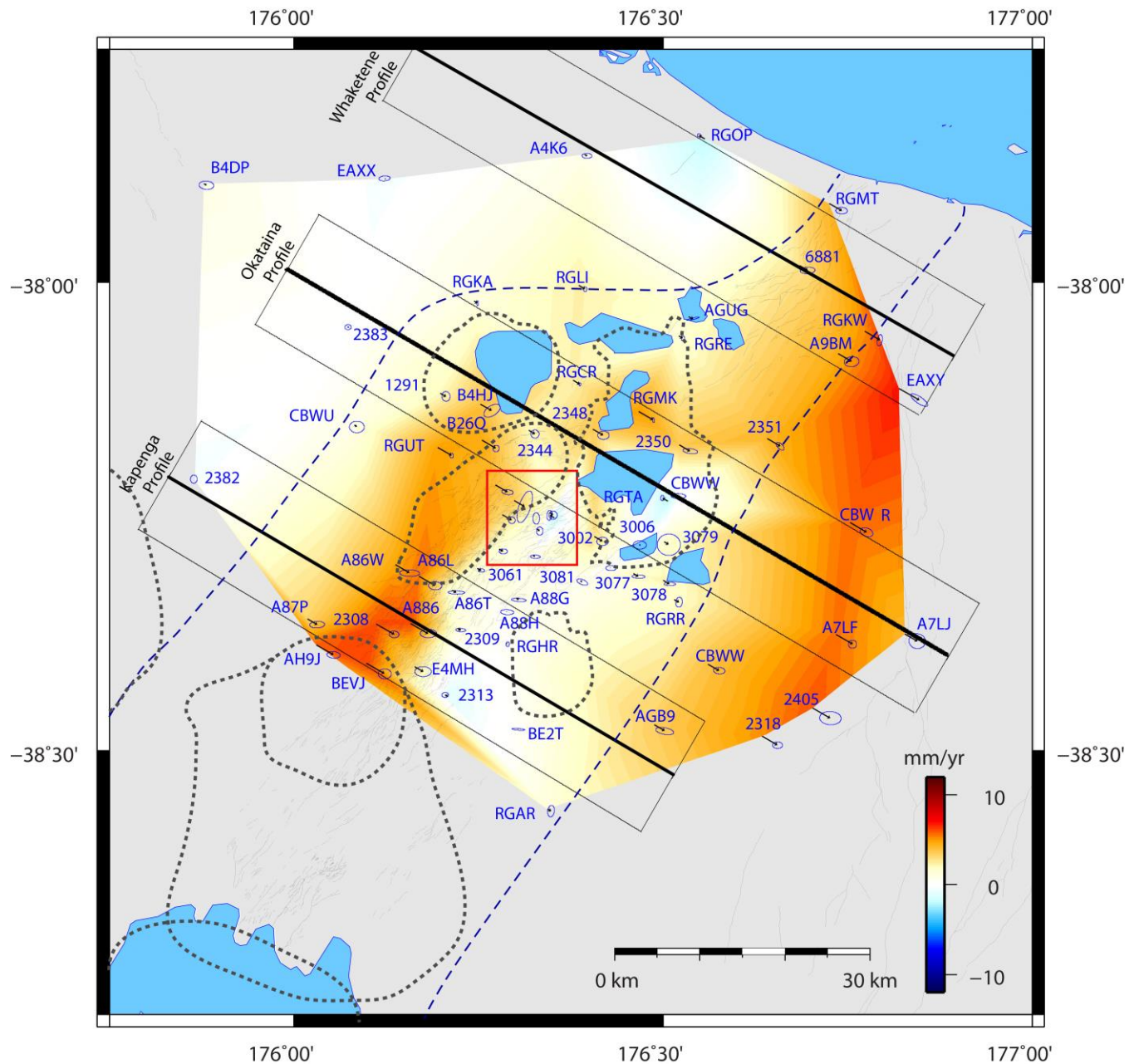


Figure 2.10 - Fitted surface to orthogonal velocities across the study site (produced using *Triangulate* command in GMT). Dashed blue lines represent approximate location of modern rift boundaries (Acocella et al., 2003). Caldera boundary locations are approximate.

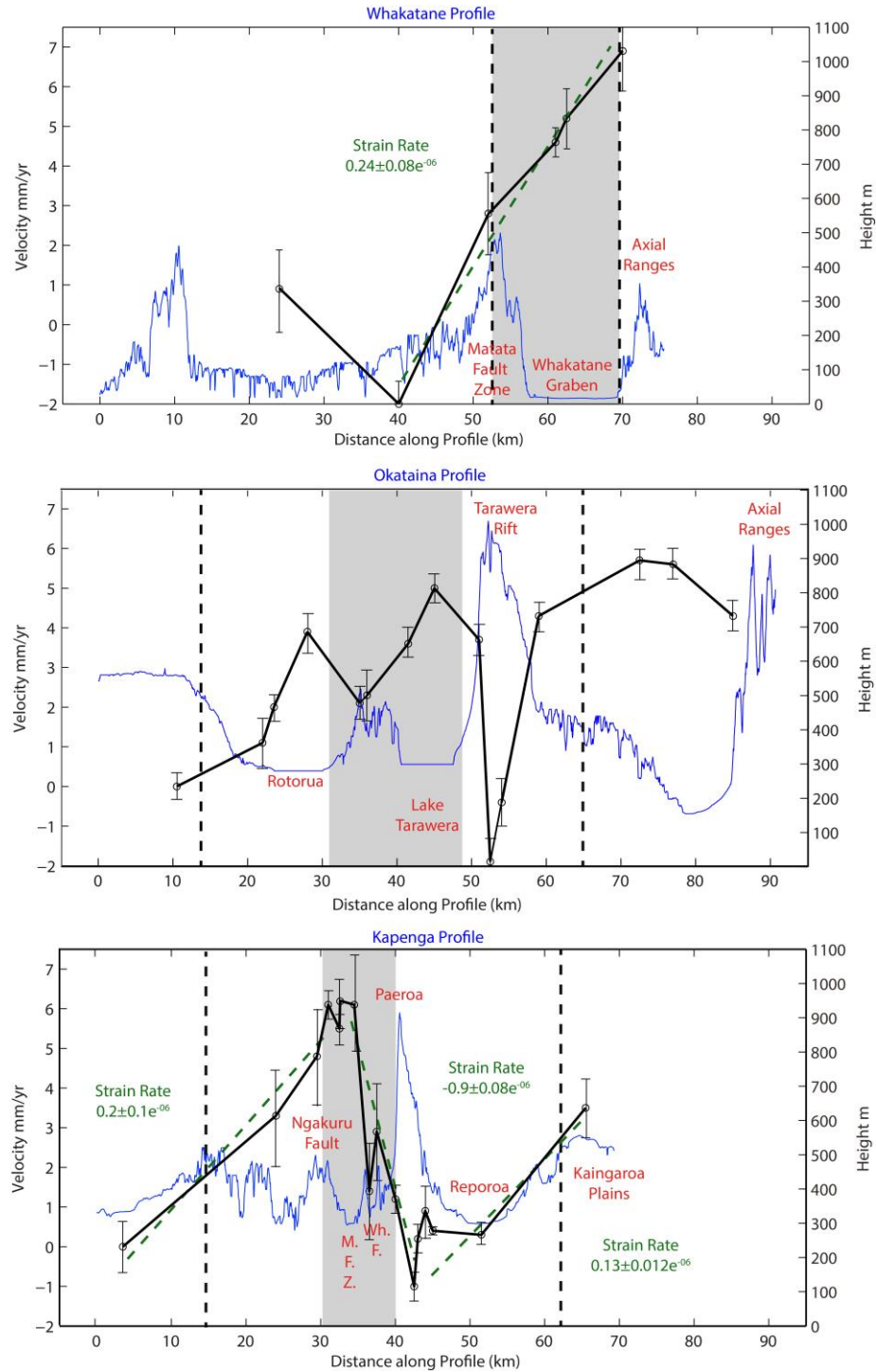


Figure 2.11 – Velocity profiles produced for a) Whakatane, b) Okataina and c) Kapenga segments (Black lines) from plotting velocity components orthogonal to rift segments (in millimetre per year) as a function of distance (in km). Error-bars indicate 68% standard deviation. Solid black lines represent interpolated horizontal velocity between stations in each profile. Green dashed lines represent best fit horizontal velocity

estimates using least squares regression approach for different sections of profile. The strain rate values associated with each estimate are shown in green text. The topography of each profile is also overlain as blue lines. Dashed vertical lines represent the approximate location of the TVZ boundaries. Caldera boundary locations are approximate. Grey shaded area represents the approximate location of rift-related normal faulting.

Estimates of rift related extension across the Kapenga profile must also be made with caution due to the probable influence of magmatic or hydrothermal processes there. The velocity profile shown in Figure 2.11c reflects this. However, orthogonal extension across this profile appears to be focussed immediately west of the TVZ (see Figure 2.4 and Figure 2.11c). In this region velocities rapidly increase eastwards, and then abruptly decrease east of the central axis. The estimated strain rate (determined from the profile velocity gradient) here is $0.20 \pm 0.1 \times 10^{-6}$ (estimated over approximately 27km distance). Across the central axis of the Kapenga segment, the faster south-east velocities west of the axis, compared to the slower southerly motions along the eastern side suggest shortening between the Ngakuru graben to the Paeroa fault zone of 6mm/yr^{-1} . A shortening strain rate of $-0.99 \pm 0.08 \times 10^{-6}$ (estimated over approximately 10km distance) is estimated for this section of the profile. This shortening observed in the GPS is at odds with the longer-term extension observed on the Paeroa fault and Ngakuru Graben (Villamor and Berryman, 2001, 2006), suggesting that is related to non-tectonic (e.g. volcanic and/or magmatic) processes. East of the Reporoa caldera and across the Kaingaroa plain, velocities increase suggesting extension rates of approximately 3.5mm/yr^{-1} . An extension rate of $0.13 \pm 0.012 \times 10^{-6}$ (estimated over approximately 22km distance) is derived for this section of the Kapenga velocity profile.

2.8 Interpretation of results across study area

2.8.1 Outside the Rift

The horizontal strain rates across the study area show a distinction between lower rates (outside the Taupo rift), compared with higher rates (both extension and shortening) within the rift. We interpret this to differentiate deformation processes related to magmatic and tectonic deformation within the rift from regional deformation processes outside the rift. Strain rates outside the rift are typically smaller than 0.2×10^{-6} , while those within the rift are larger and can be up to (on average) approximately 1 to 1.5×10^{-6} . This distinction is also visible in the vertical velocities (see Figure 2.5 and Figure 2.6), although to a lesser degree in the Whakatane graben. We find that our strain rate estimates outside the rift are in good agreement with that of Darby et al., (2000), who estimate strain rates of 0.21×10^{-6} across a similar region. The strain rate identified

using regression in Figure 2.11 is also similar to their estimate. However, their strain rate estimate is based on data with a much lower spatial resolution and as such we cannot compare results in greater detail.

Outside the rift, we can link our results to a number of regional tectonic structures or magmatic processes. First, we locate the tectonically stable western North Island, northwest of the Taupo rift, based on the coherent horizontal and vertical motion observed in this region. Second, we consider the coherent horizontal motions, decreased vertical velocities and increased extension in the east and southeast of the study area to be linked to clockwise rotation of the AXIR block (Wallace et al., 2004). Lower strain rates east of the Paeroa fault may also reflect background tectonic processes and structure, as the magnitude of strain rate in this region is significantly less than that within the Taupo rift. The Paeroa fault is a major rift scale structure, with a fast slip rate and no common recurrence interval (Villamor et al., (2008). Our results suggests that the Paeroa fault zone might play an important role in controlling deformation in this part of the rift and, geodetically at least, may delineate an eastern boundary of rift related deformation in this region, despite the fact that we currently observe contraction in the region of this fault. Magnetotelluric data indicates that shallow melt may exist just below and east of the Paeroa fault (Bertrand et al., 2012). Contraction in the central rift has been linked to magma cooling (Hamling et al., 2015) and it is likely that the strain rate pattern we observe through this region reflects this. A similar association may also explain the lack of significant surface deformation we observe in our geodetic data across the Reporoa caldera (and vicinity). The results there do not provide evidence to confirm that significant extension is currently accommodated across the TRB as proposed by Rowland et al., (2010).

2.8.2 Inside the rift

In general, we interpret the high rates and broad scale subsidence rates within the rift to delineate the zone of active deformation related to rifting. The 2-3mm/yr⁻¹ extension rate decrease between the Whakatane and central segment agrees with that predicted in the wedge-shaped extension model of Wallace et al., (2004). This supports tectonic block rotation along the eastern North Island as a regional mechanism for driving rifting in the Taupo rift (Wallace et al., 2004). However, within the Kapenga and Okataina segments, subsidence rates are too large to be linked purely to rifting and it is likely that hydrothermal or magmatic system processes contribute significantly. This is reflected in the highly heterogeneous horizontal strain rate and velocity fields in the Kapenga and Okataina segments we identify, which are difficult to link to an individual source. For instance, the significant change in orientation of the principal strain rate axis between the Kapenga (contraction) and the Okataina segment (i.e. extension at the Tarawera rift) (see Figure 2.7) could be

interpreted as geodetic evidence to support a variation in rift structure. However, such heterogeneity is likely related to transient deformation from magmatic and hydrothermal activity, particularly at this location in the rift, where magma emplacement into the upper crust is considered possible.

Only in the Whakatane graben, can we confidently interpret strain rates and velocities to reflect rift-perpendicular extension. Our extension rate there of 9mm/yr^{-1} using GPS is less than that predicted by Wallace et al., (2004). We attribute this difference to our measurements not sampling the entire AXIR tectonic block, which they use in their modelling. However, we associate the coherent pattern of gradually increasing velocities towards the AXIR tectonic block to clockwise rotation of this block. We interpret the local uplift signal observed at station RGMT to be linked to seismicity and fault movement in the Matata Fault Zone (Wright, 1990; Beanland and Haines, 1998, Mouslopoulou and Hristopolos 2011).

2.8.3 Within the OVC

Interpreting the results in the OVC is more difficult and requires caution due to the OVC's location within both a rift setting and an active caldera. In general we associate the highly heterogeneous strain rates and velocity field to either regional tectonic and/or local magmatic processes. For example, the broad scale clockwise rotation of horizontal principle strain rate axes across the caldera (see Figure 2.7) could be linked to rift structure variation. The more localised elevated strain rates along the Tarawera rift (and vicinity) we interpret to either tectonic or possibly volcanic origin, which we discuss in the following section. We attribute the large subsidence rates across Lake Tarawera, Lake Rotomahana, south of the OVC, as related to active magmatic and/or hydrothermal subsidence. Such large rates are not unusual and have been documented in other hydrothermal areas within the rift (Allis et al., 2009; Bromley et al., 2009).

2.9 Discussion

2.9.1 Processes driving contemporary deformation in the Taupo Rift and OVC

Our results constrain the pattern of ground deformation through the central rift in greater detail than previous studies using GPS data and indicate that it is not uniform in rate or distribution. This is indicated by the presence of a number of remarkable features, which include 1) significant contraction within the Kapenga segment and extension offset westwards from the zone of normal faulting, 2) rapid changes of principle strain rate axis orientations at the intersection of the Kapenga and Okataina segments, 3) elevated extension and shear strain rates at the Tarawera rift within the OVC, 4) very large subsidence rates in the central rift (up to -

1.94 cm/yr⁻¹) and 5) lower extensional strain rates than previously documented in the Whakatane graben (Wallace et al., 2004).

It is not clear why we observe contraction within the normal fault system of the Ngakuru graben and Paeroa fault, and extension up to approximately 15 km west of the main rift axis. A similar pattern was also observed north and northwest of Lake Taupo (30km south of our study region) by Darby et al., (2000) using GPS data from 1986 to 1997. This pattern does not agree with abundant geological estimates of normal faulting in the central rift. Hamling et al., (2015) link the large subsidence rates in this part of the rift to cooling of large-scale magma bodies at approximately 6km depth. A magma cooling mechanism would explain the mismatch we observe between contemporary contraction from our GPS data and the long-term geological estimates in that region. This would suggest that present day magmatic processes are masking geological observations of long-term normal faulting in the Kapenga segment and are also responsible for the observed extension west of the main rift axis. Subsequently, in this part of the rift we cannot confidently link ground deformation patterns to upper crustal faulting from our geodetic data.

The deformation pattern at the intersection of the Kapenga and Okataina segments (and the south-western border of the OVC) is the most complex in the study area. This includes significant principle strain rate axis rotations (up to tens of degrees) (see Figure 2.7), elevated shear strain rates (approximately 1 to 1.4 x 10⁻⁶/yr⁻¹) (see Figure 2.9) and large vertical velocities (up to -1.97 cm/yr⁻¹). This heterogeneity could accommodate the extension rate decrease we observe southwards through the rift and/or the proposed bend in rift architecture across the Okataina segment (Rowland and Sibson, 2001; Acocella et al., 2003; Rowland et al., 2010; Seebeck and Nicol, 2009; Seebeck et al., 2009). However, the subsidence rates are greater than those expected from rifting processes alone and it is more likely that magmatic processes contribute significantly. This conclusion is supported by the good agreement between our principal strain rate axes rotations and those modelled just south of Okataina by Ellis et al., (2014). They model clockwise rotations of extension axes due to the presence of a large accumulation of partial melt orientated NW-SE south of Okataina. It is also likely that the elevated levels of upper crustal seismicity and the highly energetic hydrothermal fields in this part of the rift would also suggest that our deformation field may also reflect a transition between different sets of hydrothermal and/or magmatic processes. Similar associations are often attributed to hydrothermal fluid pressurisation and movement at other large caldera systems, including Taal, (Lowry et al., 2001; Bartel et al., 2003), Campi Flegrei (Battaglia et al., 2006) and Yellowstone caldera (Puskas et al., 2007).

To the north of the OVC (in the Whakatane graben), we observe horizontal velocities similar to those in the AXIR tectonic block (see Figure 2.4). Other than a small step change in velocity rates, there is little geodetic

evidence of a significant discontinuity between the Whakatane segment and AXIR tectonic block. Also, the vertical velocities do not yield evidence for such a boundary. We consider this good evidence in support of the non-rotational strike slip fault termination model of Mouslopoulou et al., (2007). A key component of their model is that the 4mm/yr^{-1} strike-slip transferred into the Taupo rift in the Whakatane segment from the NIDFB occurs without any block rotation at the terminating faults (e.g. at the western side of the Whakatane graben). Our horizontal velocities show no evidence of such rotations (at least on a scale larger than tens of kilometres). We consider that the small uniform increase in horizontal velocities across this region reflects the influence of rotation of the AXIR tectonic block. This would explain the increased dextral shear we observe across the Whakatane graben (in agreement with Acocella et al., 2003).

The intermittent nature of our campaign data only provides a snapshot of surface deformation between major eruptive and/or tectonic episodes in the Taupo rift and makes it very difficult to identify transient ground deformation patterns. Given the plentiful supply of magma and presence of energetic hydrothermal fields in central Taupo Rift, it is unlikely that the GPS velocities and strain rate features we identify there are representative of long-term tectonic processes. Therefore to consider the temporal stability of our results, we analyse the de-trended daily position time series plots of the cGPS sites within the study area (see Figure 2.3 and Figure 2.12 – also available at www.geonet.org.nz). They show evidence of transient ground deformation patterns for all cGPS stations, but in particular stations TAUP (within the Taupo caldera) and RGHL (at the intersection of the Kapenga and Okataina segments). Both stations undergo significant rapid uplift (TAUP) and subsidence (RGHL) over approximately 5 years, as well as two more rapid displacement periods (highlighted in yellow in Figure 2.12). Given the short term time period associated with these deformation features, we attribute their source to magmatic, or hydrothermal processes. This implies that the highly heterogeneous horizontal velocities and strain-rates seen in the vicinity of station RGHL from our campaign data may also accommodate some shorter-term transient deformation patterns. Further, the uplift and subsidence deformation patterns concurrently measured at different parts of the central rift provides evidence that magmatic processes vary spatially within this region, in agreement with earlier studies (Manville and Wilson, 2003; Rowland et al., 2010).

2.9.2 Relationship of OVC deformation to volcanic, hydrothermal and tectonic processes and implications for geodetic monitoring

The co-location of high extension and shear strain rates (see Figure 2.7 and Figure 2.9) with the location of the most recent volcanic activity (at the Tarawera rift) supports a causal relationship between magmatic/volcanic processes and ground deformation at the OVC. This deformation pattern provides a highly suitable environment for diking and magma emplacement in the upper crust and agrees well with the observed patterns of left stepping en-echelon diking related to the 1886 Tarawera eruption shown in the geological record (Nairn et al., 1988). Therefore, it is tempting to link the elevated extension and shear strain rates in this region as a local driver for the AD 1886 Tarawera eruption. However, our results do not indicate if this deformation is a response to or has encouraged magma localisation (e.g. upper-crust diking) in the Tarawera rift.

The elevated extension and shear strain rates through the Tarawera rift could also be interpreted to support propagation of the Whakatane graben axis into the OVC caldera (e.g. a tectonic driver of deformation in the OVC) (Spinks et al., 2005). A puzzling aspect of this interpretation is the absence of significant upper crustal seismicity (at least during our study period) associated with the elevated strain rates in the Tarawera rift (see Figure 2.1). This seismicity is also low in comparison to the southwest boundary of the OVC and within the Haroharo dome complex. Similar (poor) correlations between deformation and seismicity have also been observed at other large calderas, including Yellowstone (Puskas et al., 2007). We propose that extensional and shear strain rates through the Tarawera rift are presently accommodated with little significant upper crustal seismicity. Given that upper crustal seismicity might not be relied upon solely for evidence of magma migration to the surface here, any ground deformation in this region must be interpreted with caution. Deformation patterns in the vicinity of the Tarawera rift must be watched closely.

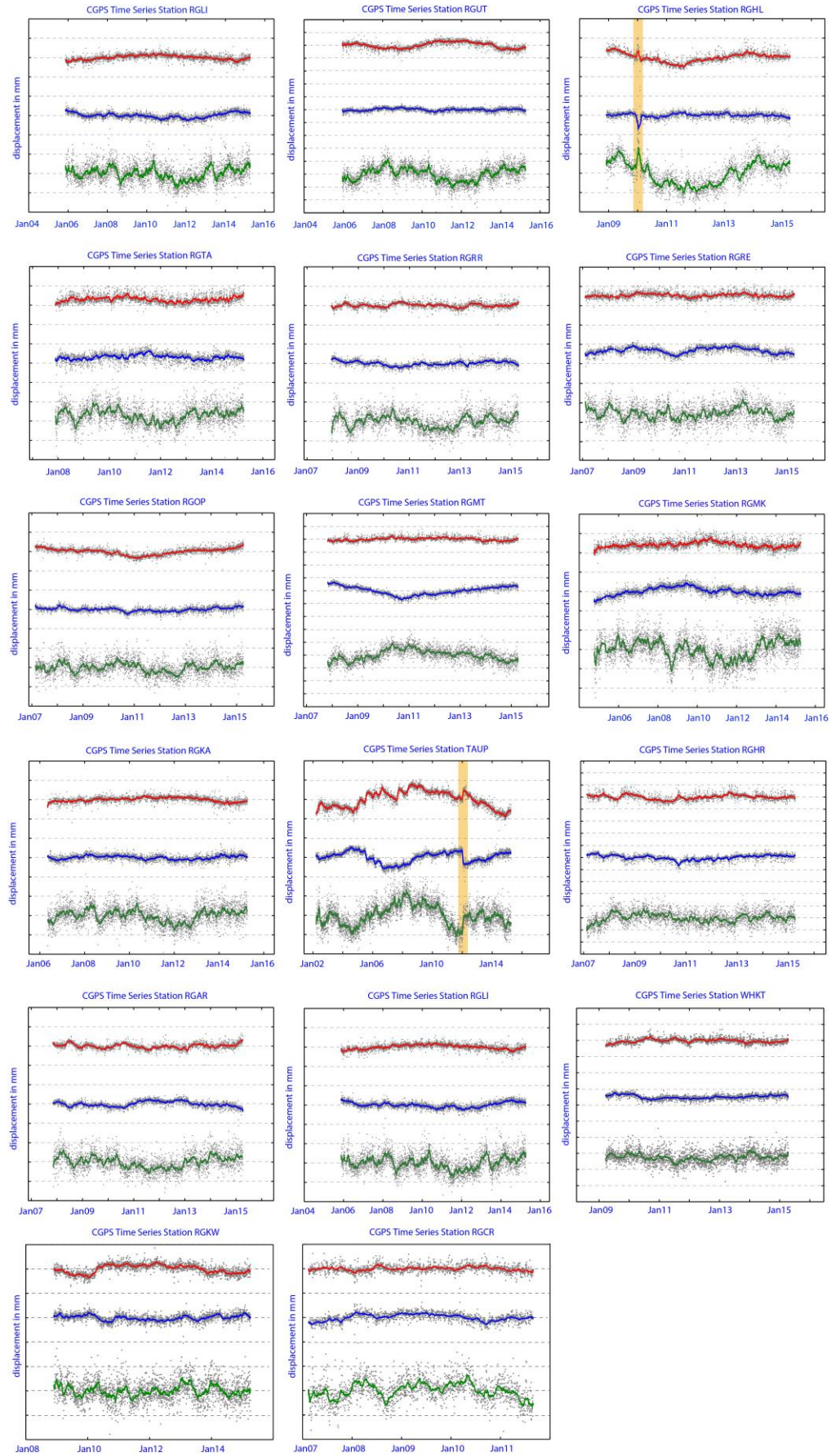


Figure 2.12 – De-trended time series plots for cGPS stations with study region. The red, blue and green lines represent smoothed displacements from initial position in the easting, northing and height components respectively. Each time series has been offset for visual clarity. Spacing between grey horizontal grid lines in each plot represents 10mm. Yellow vertical bands represent suspected transient displacement episodes at stations RGHL and TAUP. See Figure 2.3 for station locations. Information regarding the removal of the regional signal from the data was available at the GeoNet webpage.

We cannot confidently identify a volcanic signal within our OVC deformation field from the campaign data for the study period. This is likely due to either 1) the contamination of any volcanic geodetic signal by local tectonic and/or hydrothermal processes within the caldera and or 2) the poor temporal resolution of the campaign GPS data, which may not have detected transient deformation related to local volcanic and hydrothermal activity. Moreover, little evidence of significant transient deformation is evident in the cGPS time series of stations inside the OVC (RGRE, RGMK and RGTA - see Figure 2.3 and Figure 2.12). Only at station RGHL south of the OVC, outside the caldera boundary, is there evidence for a local magmatic deformation signal (at the start of 2010, highlighted in yellow in Figure 2.12).

It has been hypothesised that preceding an OVC eruption, broad subsidence and local uplift signals would be observed in the geodetic data in the far and near fields respectively. It is therefore prudent to consider if these signals might be discernable within the contemporary deformation field using GPS data. Considering the dominant subsidence signal in the central rift, we suggest that a broad subtle subsidence signal would be difficult to observe in regional campaign GPS data. Campaign GPS data are better suited for longer-term (e.g., several years or more) deformation studies of overall processes, rather than observing short-term transient deformation that often occurs within calderas. cGPS data are required for the latter. Given that no volcanic crisis has occurred since the installation of the cGPS receivers in the OVC, and the short time span of their operation, reconciling any modern transient behaviour detected there with geological observations in the rift remains difficult.

2.10 Conclusion

In this study we use new and existing campaign and cGPS data collected from 1998 to 2011 to measure contemporary deformation within the Taupo rift and OVC. These results identify a heterogeneous velocity and strain rate field through the study area. We find a good agreement with existing geodetic estimates of extension rates in the study area. The major new contributions presented in this paper include (1) the identification of large contraction within a large portion of the central Taupo rift, which has not been

previously highlighted or recognized, (2) revised rates of rifting in the Whakatane area, which appear to be slightly slower than in previously presented (Wallace et al., (2004), (3) a detailed description and presentation of variations in crustal kinematics in the Okataina caldera, and its relationship to magmatic and tectonic processes and, (4) the first published strain and velocity field for the TVZ from a comprehensive GPS dataset.

In the central rift, we consider the contemporary deformation patterns to be dominated by magmatic sources. As a result, we observe a significant mismatch between the well-documented long-term geological estimates of fault movements (e.g. extension related to normal faulting in the central rift) with those predicted from our GPS velocities, as the current high GPS shortening rates may reflect cooling of a magma body (e.g., Hamling et al., 2015). As a result areas currently showing contraction from GPS (e.g. in the Ngakuru graben) probably shift to extension in the long term. While, areas undergoing extremely rapid subsidence through the central rift may be buoyed up by magma in the longer term and shift to uplift as magma migration patterns change. The Whakatane graben is the only location that may be appropriate for comparisons between the GPS and geological deformation rates, where the contemporary deformation patterns from GPS are in good agreement with those expected from geological studies.

In the OVC, we find no clear evidence of active volcanic processes. However, in the Tarawera rift we identify a strain rate environment highly suitable for magma migration and diking through the upper crust. We are unable to confidently determine if this is related to volcanic and magmatic processes, given the nearby hydrothermal activity and likely influence of regional tectonic structure. However, given the recent history of volcanism in this part of the OVC, future deformation there must be interpreted cautiously. Our results therefore provide a useful baseline study from which any local volcanic signals might be compared in the future.

Acknowledgments: This paper is dedicated to John Beavan whose generosity and willingness to discuss and assist in any aspect of the geodetic processing and interpretation of TVZ deformation will always be appreciated. All figures (except Figure 2.11 and Figure 2.12) were produced using *Generic Mapping Tools* software. We thank the two anonymous reviewers for their comments which significantly improved this paper.

2.11 References

- Acocella, V., 2010, Coupling volcanism and tectonics along divergent plate boundaries: Collapsed rifts from central Afar, Ethiopia. , *Bull. Geol. Soc. Am.*, 122(9–10), 1717–1728.
- Acocella, V., Spinks, K., Cole, J. and Nicol, A., 2003. Oblique back arc rifting of Taupo Volcanic Zone, New Zealand. *Tectonics*, 22(4), 1045, doi:10.1029/2002TC001447.
- Allis, R., Bromley, C. and Currie, S., 2009. Update on subsidence at the Wairakei-Tauhara geothermal system, New Zealand. *Geothermics*, 38(1): 169-180.
- Bartel, B.A., Hamburger, M.W., Meertens, C.M., Lowry, A.R. and Corpuz, E., 2003. Dynamics of active magmatic and hydrothermal systems at Taal Volcano, Philippines, from continuous GPS measurements. *J. Geophys. Res.-Solid Earth*, 108(B10), 2475, doi:10.1029/2002JB002194.
- Battaglia, M., Troise, C., Obrizzo, F., Pingue, F. and De Natale, G., 2006. Evidence for fluid migration as the source of deformation at Campi Flegrei caldera (Italy). *Geophys. Res. Lett.*, 33(1), L01307, doi:10.1029/2005GL024904.
- Beanland, S. and Haines, J., 1998. The kinematics of active deformation in the North Island, New Zealand, determined from geological strain rates. *N. Z. J. Geol. Geophys.*, 41(4), 311–323.
- Beavan, J., 2005, Noise properties of continuous GPS data from concrete pillar geodetic monuments in New Zealand and comparison with data from U.S. deep drilled braced monuments. *J. Geophys. Res.-Solid Earth*, 110, B08410, doi:10.1029/2005JB003642.
- Beavan, J. and Haines, J., 2001. Contemporary horizontal velocity and strain rate fields of the Pacific-Australian plate boundary zone through New Zealand. *J. Geophys. Res.-Solid Earth*, 106(B1), 741–770.
- Beavan, R.J. and Litchfield, N.J., 2012. Vertical Land Movement Around the New Zealand Coastline: Implications for Sea-Level Rise. 9781972192153, GNS Science, New Zealand.
- Bertrand, E., Caldwell, T., Hill, G., Wallin, E., Bennie, S., Cozens, N., Onacha, S., Ryan, G., Walter, C., Zaino and A., Wameyo, P. (2012). Magnetotelluric imaging of upper-crustal convection plumes beneath the Taupo Volcanic Zone, New Zealand. *Geophys. Res. Lett.* 39(2), L02304, doi:10.1029/2011GL050177.
- Bibby, H.M., Caldwell, T.G., Davey, F.J. and Webb, T.H., 1995. Geophysical evidence on the structure of the Taupo Volcanic Zone and its hydrothermal circulation. *J. Volc. Geotherm. Res.*, 68(1–3), 29–58.
- Blick, G.H. and Otway, P.M., 1995. Regional vertical deformation from repeated precise levelling in the Taupo Volcanic Zone. Institute of Geological & Nuclear Sciences Limited, Lower Hutt, N.Z.
- Bromley, C.J., Currie, S., Manville, V.R. and Rosenberg, M.D., 2009. Recent ground subsidence at Crown Road, Tauhara and its probable causes. *Geothermics*, 38(1), 181–191.

- Bryan, C.J., Sherburn, S., Bibby, H.M., Bannister, S.C. and Hurst, A.W., 1999. Shallow seismicity of the central Taupo Volcanic Zone, New Zealand: its distribution and nature. *N. Z. J. Geol. Geophys.*, 42(4), 533–542.
- Cabral-Cano, E., Correa-Mora, F. and Meertens, C., 2008. Deformation of Popocatepetl volcano using GPS: Regional geodynamic context and constraints on its magma chamber. *J. Volc. Geotherm. Res.*, 170(1–2), 24–34.
- Cardozo, N., and Allmendinger, R.W., 2009. SSPX: A program to compute strain from displacement/velocity data. *Comput. Geosci.*, 35(6), 1343–1357., doi: 10.1016/j.cageo.2008.05.008.
- Charlier, B.L.A. and Wilson, C.J.N., 2010. Chronology and Evolution of Caldera-forming and Post-caldera Magma Systems at Okataina Volcano, New Zealand from Zircon U-Th Model-age Spectra. *J Petrol*, 51(5): 1121-1141.
- Cole, J.W., 1990. Structural Control and Origin of Volcanism in the Taupo Volcanic Zone, New-Zealand. *Bull. Volcanol.*, 52(6), 445–459.
- Cole, J.W. and Spinks, K.D., 2009. Caldera volcanism and rift structure in the Taupo Volcanic Zone, New Zealand. in *Ancient Orogens and Modern Analogues*, pp. 9–29, eds Murphy, J.B., Keppie, J.D. & Hynes, A.J., Geological Society Special Publication.
- Cole, J.W., Milner, D.M. and Spinks, K.D., 2005. Calderas and caldera structures: a review. *Earth-Sci. Rev.*, 69(1–2), 1–26.
- Cole, J.W., Spinks, K.D., Deering, C.D., Nairn, I.A. and Leonard, G.S., 2010. Volcanic and structural evolution of the Okataina Volcanic Centre; dominantly silicic volcanism associated with the Taupo Rift, New Zealand. *J. Volc. Geotherm. Res.*, 190(1–2), 123–135.
- Dach, R., Hugentobler, U., Fridez, P. and Meindl, M., 2007. Bernese GPS Software Version 5.0. Stampfli Publications AG, Astronomical Institute, University of Bern.
- Darby, D. J., and Williams, R. O., 1991. A New Geodetic Estimate of Deformation in the Central Volcanic Region of the North Island, New-Zealand. *N. Z. J. Geol. Geophys.*, 34, 127–136.
- Darby, D. J., and Meertens, C. M., 1995. Terrestrial and GPS measurements of deformation across the Taupo back arc and Hikurangi forearc regions in New Zealand, *J. Geophys. Res.*, 100(B5), 8221–8232.
- Darby, D.J., Hodgkinson, K.H. and Blick, G.H., 2000. Geodetic measurement of deformation in the Taupo Volcanic Zone, New Zealand: the North Taupo Network revisited. *N. Z. J. Geol. Geophys.*, 43(2), 157–170.
- Dixon, T. H., Miller, M., Farina, F., Wang, H. Z., and Johnson, D., 2000, Present-day motion of the Sierra Nevada block and some tectonic implications for the Basin and Range province, North American Cordillera, *Tectonics*, 19(1), 1–24.

- Ellis, S.M., Wilson, C.J.N., Bannister, S., Bibby, H.M., Heise, W., Wallace, L. and Patterson, N., 2007. A future magma inflation event under the rhyolitic Taupo volcano, New Zealand: Numerical models based on constraints from geochemical, geological, and geophysical data. *J. Volc. Geotherm. Res.*, 168(1–4), 1–27.
- Ellis, S., Heise, W., Kissling, W., Villamor, P., Schreurs, G. 2014. The effect of crustal melt on rift dynamics: Case study of the Taupo Volcanic Zone, N. Z. *J. Geol. Geophys.*, 57(4), 453–458.
- Geirsson, H., 2003. Continuous GPS measurements in Iceland 1999–2002. Icelandic Meteorological Office, Reykjavik, Rep, 3014, 94 pp.
- Grindley, G., 1960. Sheet 8 - Taupo. In: D.o.S.a.I. Research (Editor), Wellington, New Zealand.
- Hamling, I.J., Hreinsdottir, S., and Fournier, N., 2015. The ups and downs of the TVZ: Geodetic observations of deformation around the Taupo Volcanic Zone, New Zealand. *J. Geophys. Res.-Solid Earth*, doi:10.1002/2015JB012125.
- Hole, J.K., Stevens, N.F. and Wadge, G., 2005. Surface Deformation at Rotorua, New Zealand Measured by InSAR, 1996-2003 (345), Envisat & ERS symposium, Salzburg, Austria.
- Houghton, B.F., Wilson, C.J.N., McWilliams, M.O., Lanphere, M.A., Weaver, S.D., Briggs, R.M. and Pringle, M.S., 1995. Chronology and Dynamics of a Large Silicic Magmatic System - Central Taupo Volcanic Zone, New-Zealand. *Geology*, 23(1), 13-16.
- Hugentobler, U., Schaer, S., Fridez, P., Beutler, G., Bock, H., Brockmann, E., Dach, R., Gurtner, W., Ineichen, D., Johnson, J., Meindl, M., Mervart, L., Rothacher, M., Springer, T. and Weber, R., 2001. Bernese GPS Software, Version 4.2, Astronomical Institute, University of Berne, Berne, Switzerland.
- Kashani, I., Wielgosz, P. and Grejner-Brzezinska, D.A., 2004. On the reliability of the VCV matrix: A case study based on GAMIT and Bernese GPS software. *Gps. Solut.*, 8(4), 193–199.
- Keir, D., Bastow, I.D., Pagli, C. and Chambers, E.L., 2013. The development of extension and magmatism in the Red Sea rift of Afar. *Tectonophysics*, 607(0), 98-114.
- Kogan, L., Fisseha, S., Bendick, R., Reilinger, R., McClusky, S., King, R. and Solomon, T., 2012. Lithospheric strength and strain localization in continental extension from observations of the East African Rift. *J. Geophys. Res.-Solid Earth*, 117, B03402, doi:10.1029/2011JB008516.
- Lowry, A.R., Hamburger, M.W., Meertens, C.M. and Ramos, E.G., 2001. GPS monitoring of crustal deformation at Taal Volcano, Philippines. *J. Volc. Geotherm. Res.*, 105(1–2), 35–47.
- Manville, V. and Wilson, C.J.N., 2003. Interactions between volcanism, rifting and subsidence: implications of intracaldera palaeoshorelines at Taupo volcano, New Zealand. *J. Geol. Soc. Lond.*, 160, 3–6.
- Mao, A. L., Harrison, C. G. A., and Dixon, T. H., 1999, Noise in GPS coordinate time series, *J. Geophys. Res.-Solid Earth*, 104(B2), 2797–2816.

- Means, W. D., 1976. Stress and Strain. New York, NY: Springer-Verlag., <http://doi.org/10.1007/978-1-4613-9371-9>
- Mouslopoulou, V. and Hristopulos, D., 2011. Patterns of tectonic fault interactions captured through geostatistical analysis of microearthquakes. , *J. Geophys. Res.*, 116, B07305, doi:10.1029/2010JB007804.
- Mouslopoulou, V., Nicol, A., Little, T.A. and Walsh, J.J., 2007. Terminations of large strike-slip faults: an alternative model from New Zealand. , in *Tectonics of Strike-Slip Restraining and Releasing Bends*, pp. 387– 415, eds Cunningham, W.D. & Mann, P., Geological Society Special Publication.
- Nairn, I.A., 2002. Geology of the Okataina Volcanic Centre. In: I.O.G.a.N. Sciences (Editor). Institute of Geological and Nuclear Sciences Ltd., Lower Hutt, New Zealand, pp. Geological Map 25. 21 sheet + 156p.
- Nairn, I.A. and Cole, J.W., 1981. Basalt Dikes in the 1886 Tarawera Rift. *N. Z. J. Geol. Geophys.*, 24(5–6), 585–592.
- Neil, A. E., 1996. Global Mapping for the Atmospheric Delay at Radio Wavelengths. *J. Geophys. Res.*, 111(B2), 3227–3246.
- Payne, S.J., McCaffrey, R., King, R.W., Kattenhorn, S.A., 2012. A new interpretation of deformation rates in the Snake River Plain and adjacent basin and range regions based on GPS. *Geophys. J. Int.*, 118(1), 101– 122.
- Price, R.C., Gamble, J.A., Smith, I.E.M., Stewart, R.B., Eggins, S. and Wright, I.C., 2005. An integrated model for the temporal evolution of andesites and rhyolites and crustal development in New Zealand's North Island, *J. Volc. Geotherm. Res.*, 140(1–3), 1–24.
- Pulford, A., Stern, T., 2004. Pliocene exhumation and landscape evolution of central North Island, New Zealand: The role of the upper mantle. *J. Geophys. Res.-Solid Earth*, 109, F01016, doi:10.1029/2003JF000046.
- Puskas, C.M., Smith, R.B., Meertens, C.M. and Chang, W.L., 2007. Crustal deformation of the Yellowstone-Snake River Plain volcano-tectonic system: Campaign and continuous GPS observations, 1987-2004. *J. Geophys. Res.-Solid Earth*, 112(B3), B03401, doi:10.1029/2006JB004325.
- Rowland, J.V. and Sibson, R.H., 2001, Extensional fault kinematics within the Taupo Volcanic Zone, New Zealand: soft-linked segmentation of a continental rift system. *N. Z. J. Geol. Geophys.*, 44(2), 271–283.
- Rowland, J. V., Wilson, C. J. N., and Gravley, D. M., 2010, Spatial and temporal variations in magma-assisted rifting, Taupo Volcanic Zone, New Zealand. *J. Volc. Geotherm. Res.*, 190(1–2), 89–108.
- Sagiya, T., Miyazaki, S., and Tada, T., 2000, Continuous GPS array and present-day crustal deformation of Japan, *Pure appl. Geophys.*, 157(11–12), 2303–2322.

- Samsonov, S., Beavan, J., Gonzalez, P.J., Tiampo, K. and Fernández, J., 2011. Ground deformation in the Taupo Volcanic Zone, New Zealand, observed by ALOS PALSAR interferometry. *Geophys. J. Int.*, 187(1), 147–160.
- Scott, B.J., 1989. Geodetic and geophysical monitoring of the 1886 Tarawera rift. In: J.H. Latter (Editor), *Volcanic Hazards assesment and monitoring. IAVCEI Proceedings in Volcanology.*, pp. 575–584, ed. Latter, J.H., Springer-Verlag.
- Scott, B.J., 1992. Characteristics of cyclic activity in Frying Pan and Inferno Crater Lakes, Waimangu, New Zealand Geothermal Workshop. Institute of Geological and Nuclear Sciences contribution., Auckland, 253–258 pp.
- Scott, B.J., 1994. Cyclic Activity in the Crater Lakes of Waimangu Hydrothermal System, New-Zealand. *Geothermics*, 23(5–6), 555–572.
- Seebeck, H. and Nicol, A., 2009, Dike intrusion and displacement accumulation at the intersection of the Okataina Volcanic Centre and Paeroa Fault zone, Taupo Rift, New Zealand, *Tectonophysics*, 475(3–4), 575–585.
- Seebeck, H., Nicol, A., Stern, T.A., Bibby, H.M. and Stagpoole, V., 2009. Fault controls on the geometry and location of the Okataina Caldera, Taupo Volcanic Zone, New Zealand. *J. Volc. Geotherm. Res.*, 190(1–2), 136–151.
- Serpelloni, E., Anzidei, M., Baldi, P., Casula, G. and Galvani, A., 2006. GPS measurement of active strains across the Apennines. *Ann. Geophys.-Italy*, 49(1), 319–329.
- Sherburn, S. and Nairn, I.A., 2004. Modelling geophysical precursors to the prehistoric c. AD1305 Kaharoa rhyolite eruption of Tarawera volcano, New Zealand. *Nat. Hazards*, 32(1), 37–58.
- Smith, V.C., Shane, P. and Nairn, I.A., 2005. Trends in rhyolite geochemistry, mineralogy, and magma storage during the last 50 kyr at Okataina and Taupo volcanic centres, Taupo Volcanic Zone, New Zealand. *J. Volc. Geotherm. Res.*, 148(3–4), 372–406.
- Smith, V., Shane, P. and Nairn, I., 2010. Insights into silicic melt generation using plagioclase, quartz and melt inclusions from the caldera-forming Rotoiti eruption, Taupo volcanic zone, New Zealand. *Contrib Mineral Petr*, 160(6), 951–971.
- Spinks, K.D., Acocella, V., Cole, J.W. and Bassett, K.N., 2005. Structural control of volcanism and caldera development in the transtensional Taupo Volcanic Zone, New Zealand, *J. Volc. Geotherm. Res.*, 144(1–4), 7–22.
- Sutton, A.N., Blake, S., Wilson, C.J.N. and Charlier, B.L.A., 2000. Late Quaternary evolution of a hyperactive rhyolite magmatic system: Taupo volcanic centre, New Zealand, *J. geol. Soc. Lond.*, 157, 537–552.
- Tenzer, R., Stevenson, M. and Denys, P., 2012. A Compilation of a Preliminary Map of Vertical Deformations in New Zealand from Continuous GPS Data. *Iag Symp*, 136, 697–703.

- Tregoning, P., R. Burgette, S.C. McClusky, S. Lejeune, H. McQueen and C.S. Watson, 2013, A decade of horizontal deformation from great earthquakes, *J. geophys. Res.-Solid Earth*, 118, doi:10.1002/jgrb.50154.
- Vandemeulebrouck, J., Hurst, A.W. and Scott, B.J., 2008. The effects of hydrothermal eruptions and a tectonic earthquake on a cycling crater lake (Inferno Crater Lake, Waimangu, New Zealand). *J. Volc. Geotherm. Res.*, 178(2), 271–275.
- Vigny, C., de Chabali r, J.B., Ruegg, J.C., Huchon, P., Feigl, K.L., Cattin, R., Asfaw, L. and Kanbari, K., 2007. Twenty-five years of geodetic measurements along the Tadjoura-Asal rift system, Djibouti, East Africa. *J. geophys. Res.-Solid Earth*, 112, B06410, doi:10.1029/2004JB003230.
- Villamor, P. and Berryman, K., 2001. A late Quaternary extension rate in the Taupo Volcanic Zone, New Zealand, derived from fault slip data. *N. Z. J. Geol. Geophys.*, 44(2), 243–269.
- Villamor, P. and Berryman, K.R., 2006. Evolution of the southern termination of the Taupo Rift, New Zealand. *N. Z. J. Geol. Geophys.*, 49(1), 23–37.
- Villamor, P. and Berryman, Nairn, I., Van Dissen, R., Begg, J., Lee, J., K.R., 2008. Late Pleistocene surface rupture history of the Paeroa Fault, Taupo Rift, New Zealand. *N. Z. J. Geol. Geophys.*, 51(1), 135–158.
- Walcott, R.I., 1987. Geodetic Strain and the Deformational History of the North Island of New Zealand during the Late Cainozoic. *Phil. Trans. R. Soc. Lond., A*, 321(1557), 163–181.
- Wallace, L.M., Beavan, J., McCaffrey, R. and Darby, D., 2004. Subduction zone coupling and tectonic block rotations in the North Island, New Zealand. *Geophys. Res.-Solid Earth*, 109(B12), B12406, doi:10.1029/2004JB003241.
- Wessel, P. and Smith, W.H.F., 1995. New Version of the Generic Mapping Tools Released. *EOS, Trans. Am. Geophys. Un.*, 79(47), 579.
- Williams, S. D. P., Bock, Y., Fang, P., Jamason, P., Nikolaidis, R. M., Prawirodirdjo, L., Miller, M., and Johnson, D. J., 2004, Error analysis of continuous GPS position time series, *J. Geophys. Res.-Solid Earth*, 109(B3), B03412, doi:10.1029/2003JB002741.
- Wilson, C.J.N. and Charlier, B.L.A., 2009. Rapid Rates of Magma Generation at Contemporaneous Magma Systems, Taupo Volcano, New Zealand: Insights from U-Th Model-age Spectra in Zircons. *J Petrol*, 50(5), 875-907.
- Wilson, C.J.N., Gravley, D.M., Leonard, G.S., Rowland, J.V., 2009. Volcanism in the central Taupo Volcanic Zone, New Zealand : tempo, styles and controls. p. 225-247 In: Thordarson, T.; Self, S.; Larsen, G.; Rowland, S.K.; Hoskuldsson, A. (eds) *Studies in volcanology : the legacy of George Walker*. London: Geological Society. Special publications of the International Association of Volcanology and Chemistry of the Earth's Interior 2.

- Wilson, C.J.N., Houghton, B.F., McWilliams, M.O., Lanphere, M.A., Weaver, S.D. and Briggs, R.M., 1995. Volcanic and structural evolution of Taupo Volcanic Zone, New Zealand: a review. *J. Volc. Geotherm. Res.*, 68(1–3), 1–28.
- Wright, I.C., 1990. Late Quaternary faulting of the offshore Whakatane Graben, Taupo Volcanic Zone, New Zealand. *N. Z. J. Geol. Geophys.*, 33(2), 245–256.
- Zhang, J., Bock, Y., Johnson, H., Fang, P., Williams, S., Genrich, J., Wdowinski, S., and Behr, J., 1997, Southern California Permanent GPS Geodetic Array: Error analysis of daily position estimates and site velocities. *Geophys. Res.-Solid Earth*, 102(B8), 18035-18055.
- Zhang, J., Bock, Y., Johnson, H., Fang, P., Williams, S., Genrich, J., Wdowinski, S. & Behr, J., 1997. Southern California permanent GPS geodetic array: error analysis of daily position estimates and site velocities, *J. Geophys. Res.-Solid Earth*, 102(B8), 18 035–18 055.

3 Evaluating a Campaign GNSS Velocity Field Derived From an Online Precise Point Positioning Service

L. Holden¹, D. Silcock², S. Choy², R. Cas¹, L. Ailleres¹ N. Fournier³

¹*Monash University, School of Earth, Atmosphere & Environment, Melbourne, Victoria, Australia*

²*School of Mathematical and Geospatial Science, RMIT University, Melbourne, Australia*

³*GNS Science, Taupo, New Zealand,*

PUBLISHED IN: GEOPHYSICAL JOURNAL INTERNATIONAL

Volume 208 Issue 1 pages 246-256

doi: 10.1093/gji/ggw372

Citation: Holden, L., Silcock, D., Choy, S., Cas, R., Ailleres, L., Fournier, N., 2016. Evaluating a campaign GNSS velocity field derived from an online precise point positioning service. *Geophys. J. Int.* 208 (1), 246–256. <http://dx.doi.org/10.1093/gji/ggw372>.

3.1 Abstract

Traditional processing of Global Navigation Satellite System (GNSS) data using dedicated scientific software has provided the highest levels of positional accuracy, and has been used extensively in geophysical deformation studies. To achieve these accuracies a significant level of understanding and training is required, limiting their availability to the general scientific community. Various online GNSS processing services, now freely available, address some of these difficulties and allow users to easily process their own GNSS data and potentially obtain high quality results. Previous research into these services has focused on Continually Operating Reference Station (CORS) GNSS data. Less research exists on the results achievable with these services using large campaign GNSS datasets, which are inherently noisier than CORS data. Even less research exists on the quality of velocity fields derived from campaign GNSS data processed through online PPP services. Particularly, whether they are suitable for geodynamic and deformation studies where precise and reliable velocities are needed.

In this research, we process a very large campaign GPS dataset (spanning ten years) with the online Jet Propulsion Laboratory (JPL) Automated Precise Positioning Service (APPS) service. This dataset is taken from a GNSS network specifically designed and surveyed to measure deformation through the central North Island of New Zealand (NZ). This includes regional CORS stations. We then use these coordinates to derive a horizontal and vertical velocity field. This is the first time that a large campaign GPS dataset has been processed solely using an online service and the solutions used to determine a horizontal and vertical velocity field. We compared this velocity field to that of another well utilised GNSS scientific software package. The results show a good agreement between the CORS positions and campaign station velocities obtained from the two approaches. We discuss the implications of these results for how future GNSS campaign field surveys might be conducted and how their data might be processed.

Key Words: Satellite geodesy, space geodetic surveys, reference systems, New Zealand, GPS, GNSS, precise point positioning

3.2 Introduction

Well-established high precision GNSS field techniques and data analysis procedures are used in geodetic and geophysical applications. GNSS users can now routinely achieve very high positional repeatabilities (a few millimetres in the easting and northing coordinates) using long period data (e.g. up to 24 hours), while larger

repeatabilities (tens of millimetres) are often observed in the height component (Dixon, 1991; Zumberge et al., 1997; Langbein, 2003; Sagiya, 2004; Shimada, 2005). Such precisions are achieved using well established field survey techniques (e.g. GNSS field campaigns), and/or Continually Operating Reference stations (CORS), as well as sophisticated scientific software packages like GIPSY (Lichten et al., 1995), BERNESSE (Dach et al., 2007) and GAMIT (King and Bock, 1999) to process the GNSS data (Kouba, 2009). These incorporate differential positioning and/or Precise Point Positioning (PPP) processing techniques (Zumberge et al., 1997) and depend on the availability of reliable precise satellite corrections and sophisticated atmospheric correction models.

Each technique has inherent strengths and weaknesses. Differential positioning provides reliable results, since a number of GNSS error sources are mitigated or cancelled. However, the use of this technique places a number of practical limitations on how the GNSS campaign fieldwork is carried out. There is a limit to the maximum separation distance between GNSS receivers, the receivers need to be deployed simultaneously and a poor geometry of the GNSS receiver network can bias positioning results (Leick 1990). In addition, to use differential processing, the user requires a significant level of experience and knowledge (Tsakiri 2008). The PPP technique determines the position of a single GNSS receiver in a geocentric reference frame, but achieving high precision results typically requires a long observation sessions. PPP is also dependent upon reliable GNSS satellite and clock products. The availability and continuing improvement of these products, means that the PPP technique is currently being investigated as a viable alternative to differential positioning.

A number of free online PPP processing services are now available (Ghoddousi-Fard et al., 2006). These include the Jet Propulsion Laboratory (JPL) Automated Precise Positioning Service (APPS) (Jet Propulsion Laboratory., 2015), and the Natural Resources Canada (NRC) CSRS-PPP service (Natural Resources Canada., 2015). These provide open access to the PPP technique and the potential for the broader research community to easily process their own data and achieve high precision coordinates (Tsakiri, 2008). Studies using online PPP services to specifically observe deformation related to geophysical processes are limited (Kouba 2005), and restricted to using CORS data, but have shown promising results. Only Ebner and Featherstone (2008) have investigated the results obtained from processing campaign GPS data with an online PPP service (the CSRS-PPP). As a result, it is not well known how these online PPP services can account for the quality of GNSS campaign data and whether the results are suitable for geophysical studies. Our study addresses this issue and represents the first use of results from an online PPP processing service to derive horizontal and vertical velocities of a large campaign GPS dataset (spanning ten years). We consider the suitability of the derived velocities for geophysical studies and their implications for future GNSS campaign field practice and data processing.

3.3 Background

Achieving geodetic quality coordinates suitable for deformation studies is not trivial. Careful consideration must be given to 1) the limitations of the geodetic instruments and data processing technique used, 2) the expected strain rate range and the spatial scale of the deformation field, and 3) the local and regional geological setting of the study area, to ensure that any deformation signal/s can be reliably identified from background noise. This is because geophysical processes occur over a variety of spatial and temporal scales. Massonnet and Feigl, (1998) illustrate this concept and classify different phenomena by their respective deformation rate and duration (see Figure 3.1). For example, the plot shows that glacial processes may have associated deformation rates of meters per day, while inter-seismic and post-seismic deformation may occur at rates of mm/yr to cm/yr. It is worth noting that the values in Figure 3.1 are an approximate guide, as exceptionally large co-seismic and post-seismic displacements have been observed following large plate boundary earthquakes (Briggs et al., 2006; Sato et al., 2011; Simons et al., 2011; Vigny et al., 2005; Vigny et al., 2011).

The final decision of which processing technique and geodetic instrument to choose is ultimately that of the researcher, but is now greatly assisted by the variety of geodetic infrastructure and data analysis services available. CORS networks now exist in many parts of the world, including across major subduction zones, and have provided important insights into large-scale geophysical processes in these regions. In particular, the silent tremor or silent slip phenomenon identified along some major subduction zones (Dragert et al., 2001; Rogers and Dragert, 2003, Wallace and Beavan 2006). However, CORS station spacing (resolution) is typically not suitable for faulting related deformation (Rizos et al., 2000). This is because many CORS networks are designed for regional studies and typically not sufficiently dense enough to observe localised deformation, such as that in volcanic rifts. Also, regional CORS stations may be displaced during a large earthquake, leading to erroneous results (Li et al., 2013). Subsequently, campaign style GNSS surveys still provide an important tool supplementing CORS networks for dense deformation measurements, and to respond to rapid transient deformation processes.

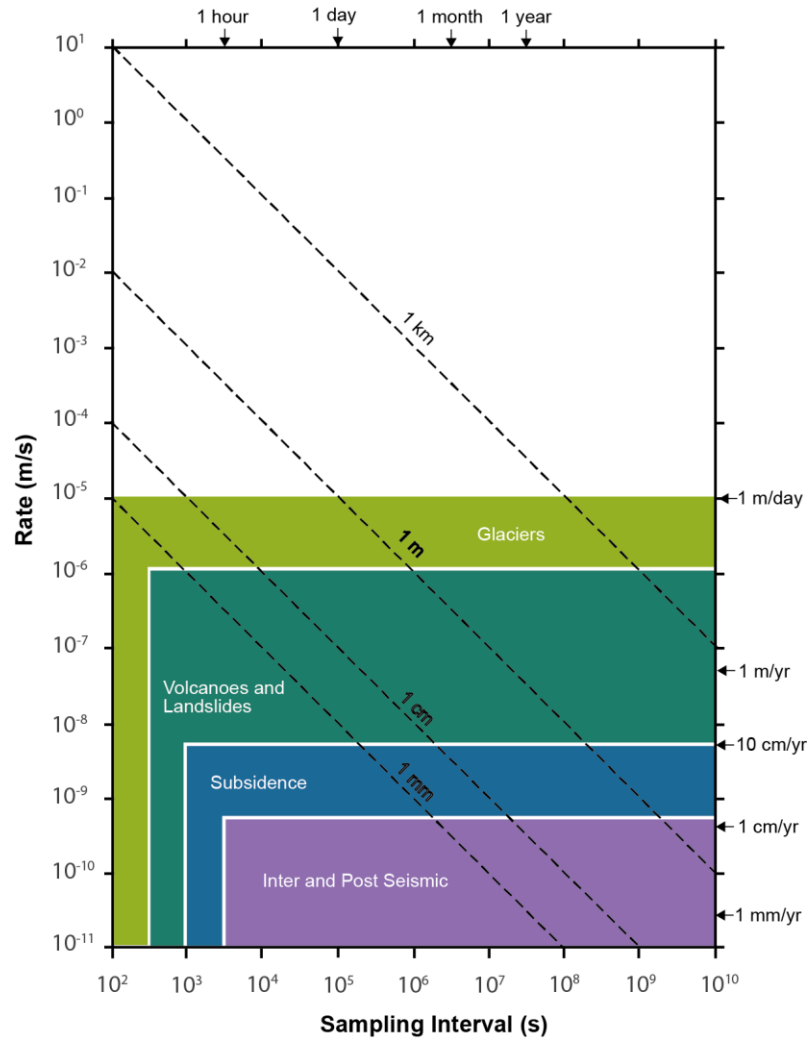


Figure 3.1 - Classification of crustal deformation processes by rate (m/sec.) and duration (in seconds), from Massonnet and Feigl (1998). The product of rate (m/s) and duration (s) gives the total amount of displacement over a given time (shown as dashed diagonal lines). The dashed lines have been added by the authors.

The greater flexibility and mobility associated with campaign GNSS surveys comes at the potential cost of greater repeatabilities in individual daily coordinate solutions. These can arise because of 1) errors in manually centring the antenna above the monument, 2) errors due to the change in ground reflections of the GPS signal (multipath) when the antenna is positioned at different heights above the ground each time the tripod is set up, 3) error due to movement of the tripod during each campaign (tripod settling, ground moisture, freeze-thaw or heavy winds), 4) monument instability, and 5) collecting data shorter than twenty four hours (Hammond et al., 2011). For these reasons campaign data are inherently noisier than CORS reference data. Therefore, it is

important to continually update the efficiency of field campaign surveys as well as simplify the data processing requirements.

Processing GNSS campaign data with an online PPP service can potentially offer numerous advantages for data processing and fieldwork. First, since the PPP technique computes positions relative to a global datum, absolute displacements can be determined (Li et al., 2013). As a result, regional GNSS reference stations are not required for datum definition. This also negates any local distortions associated with the use of local coordinates at reference stations when using differential positioning (Rizos et al., 2012). Second, the PPP solution is homogeneous and not influenced by any network adjustment biases and error correlation, which are inherent to differential processing. Third, when using differential positioning to determine velocities, the motions of regional GNSS reference stations must be modelled using very accurate tectonic plate motion models. PPP positions are independent of these models and any errors they may contain. In fact, PPP can be directly used to estimate the velocities, without consideration of regional plate motions (and motions of CORS stations on those plates). However, as new and innovative techniques are introduced, they need to be robustly tested before being accepted by the research community.

3.4 Data and Methodology

In NZ, Geological and Nuclear Science (GNS Science) has surveyed a large geodetic network in the central North Island since the early 1990s. Various sections of this network have been measured repeatedly through GPS campaign surveys. The majority of geodetic stations in this network consist of concrete pillars and brass plaques anchored in bedrock. The location and distribution of these stations is illustrated in Figure 3.2. The GPS campaign data used in this research were collected between day of year (DOY) 52 to 62 in the year 2000, DOY 39 to 47 in year 2005, DOY 58 to 71 in year 2007, and DOY 30 to 50 in year 2011. Within these campaigns, stations were typically occupied twice. The total occupation time for each station in each campaign is presented in Table 3.6 to Table 3.9 (see supplementary material). These indicate that the occupation time for the campaign sites is quite uniform and average between 40 to 48 hours. Data from stations only occupied once in any campaign were not used in this research. Trimble GPS receivers (Trimble 4000, 5700, and R7s series), and Trimble antennas (mostly Zephyr Geodetic, but some Choke rings for the earlier measurements) have been used exclusively for all the campaign survey data used in this study. We also included daily (24hr) GPS data from five regional International GNSS Service (IGS) CORS stations from New Zealand, Australia and southwest Pacific (see Figure 3.2). These include Wellington (WGTN), Auckland

(AUCK), Chatham Island (CHAT), Hobart (HOB2) and Tidbinbilla (TIDB). Data was obtained for these stations to cover the full time span of each of the GNS Science campaigns.

In this research we only used the GPS data, which were processed in the following manner. First, the campaign data were processed using standard high precision differential processing procedures for GPS phase processing in Bernese GPS software (BSW) version 5 (Dach et al., 2007). We used the regional IGS CORS stations to provide a well-defined reference frame for our velocity solutions. We also used the IGS *Repro1* products (precise orbits, clock corrections and Earth rotation parameters). The consistent use of these products ensured that the velocities were in the ITRF08 reference frame (Steigenberger et al., 2006). Further details of this processing are presented in Holden et al., (2015). We then rescaled the internally propagated Bernese GPS velocity formal estimation errors externally of Bernese to account for time-dependant errors such as random walk error and time independent error such as white noise. This process is also presented in detail in Holden et al., (2015).

Daily PPP coordinate solutions were then obtained (in ITRF08) for all the campaign and five regional IGS CORS data using the JPL APPS service. We note that the use of the *Repro1* products in our Bernese processing ensured that the Bernese results were compatible with the APPS solutions (see IGS mail #6475). The repeatabilities of the APPS coordinate solutions for the campaign data were determined by computing the standard deviation of the population of the day-to-day daily position estimates for each station within each campaign. We acknowledge that these estimates are limited since only two daily solutions for each station are available in each campaign. This is a limitation of the dataset and ideally future research would utilise a much larger dataset to better constrain the repeatabilities associated with campaign GNSS data processed in APPS. The individual repeatabilities for each station in each campaign are not presented here but available in the supplementary material (see Table 3.6 to 3.9). As a result, we primarily considered the repeatabilities of the IGS CORS data, which were derived in the same manner, but based on longer datasets than the campaign repeatabilities, to investigate the positional accuracy and reliability provided by the APPS service (this will be discussed shortly).

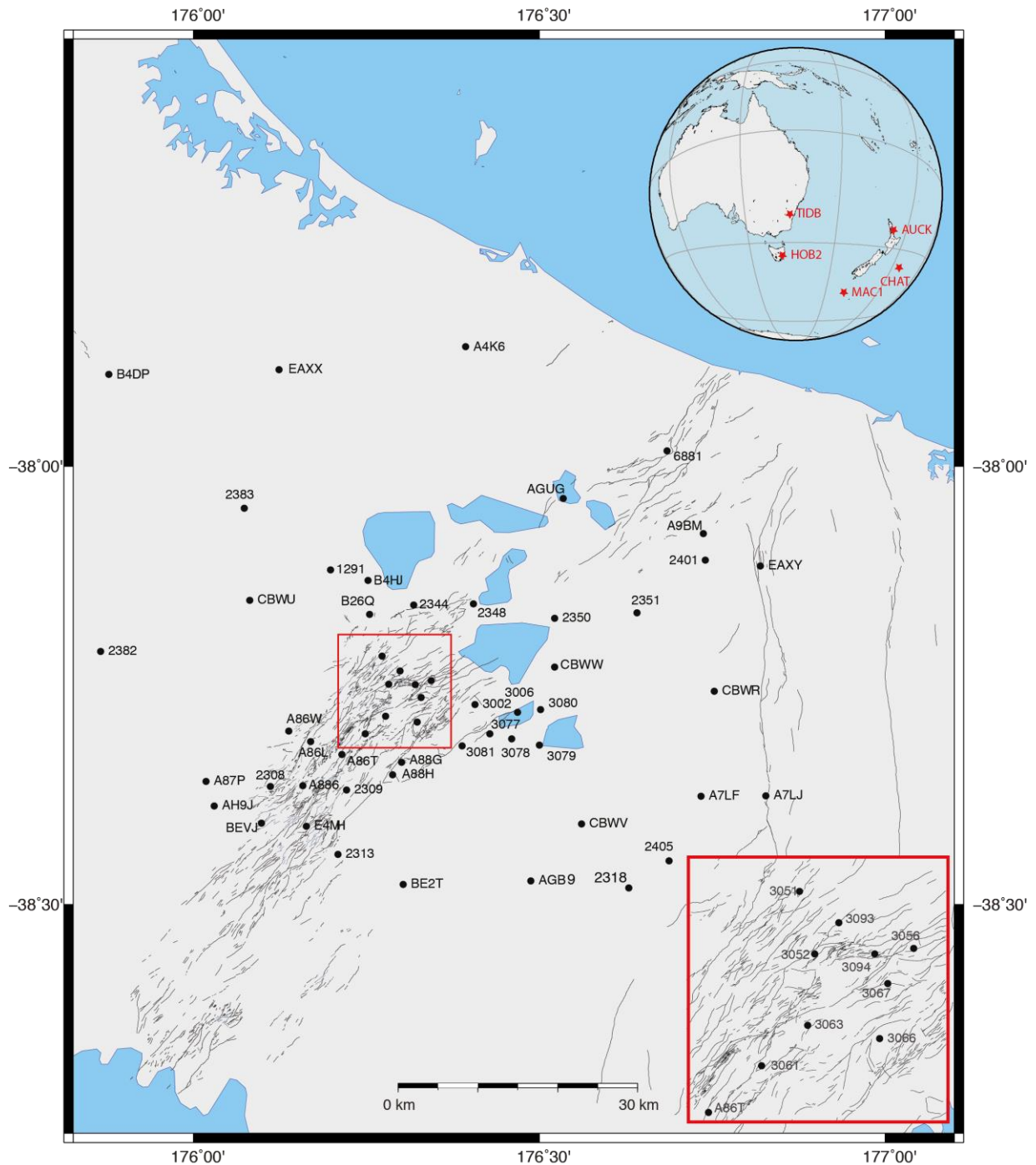


Figure 3.2 – Location and distribution of GNSS stations used in the Bernese and JPL APPS processing. IGS GPS stations are plotted on globe at top right. Inset shows GPS stations labels in greater detail. Plot produced using Generic Mapping Tools (Wessel et al., 2013).

The horizontal velocities of the campaign and CORS stations determined from the JPL APPS coordinates were estimated using Combined Least Squares (CLS) linear regression. Vertical velocities were estimated using standard linear regression (line fitting of height and epoch). CLS allows least squares linear regression estimation of the direct station velocity using both the easting and northing positions together, as well as considering their different and varying precisions. This involves observation equations (in matrix form) where;

$$Ax + B\delta x = f$$

(Eq. 3)

$$\text{where } \hat{l} = l + v \text{ and } \hat{x} = x + \delta x$$

The coefficient matrices A and B are design matrices containing partial derivatives of the function, evaluated using the observations l and the "observed" parameters x . v is a vector of small residuals or small corrections and δx is a vector of small corrections. Observations l have an apriori cofactor matrix Q_{ll} containing estimates of the variances and covariances of the observations. The weight matrices reflect the quality of the coordinate and are defined as the inverse of the cofactor matrix, or $W = Q^{-1}$. The least squares solution of eq. 3 is obtained by minimising the scalar function ϕ , where k is a vector of m Lagrange multipliers (eq. 4). The uncertainties of the velocities were also estimated in this process.

$$\phi = v^T W v + \delta x^T W_{xx} \delta x - 2k^T (Av + B\delta x - f)$$

(Eq 4.)

To examine the quality of the APPS coordinate solutions and the velocities derived from these, we analysed the results in a number of steps. First, we compared the APPS coordinate solutions of the IGS CORS data with the Asia-Pacific Reference Frame (APREF) sinex solutions (coordinates and repeatabilities) (Hu et al., 2011) provided from Geoscience Australia. The APREF is a consistent geodetic reference frame for the Asia-Pacific region defined using GNSS data and compatible with the ITRF (Hu et al., 2011). When APREF solutions were not available, we used the ITRF solutions provided by the International Earth Rotation and Reference Systems Service (IERS) (International Earth Rotation and Reference Service, 2016). This occurred for all the IGS CORS stations in the year 2000, and station WGTN in the year 2011. The day-to-day repeatabilities of the IGS CORS coordinate APPS solutions were also examined to consider the reliability of the APPS service. Propagation of error theory was used to calculate the uncertainties associated with the coordinate differences.

We then compared the IGS CORS velocities calculated from the APPS solutions with those obtained from the ITRF. The ITRF velocities are based on numerous space geodesy techniques and very long high-fidelity GNSS datasets. Because station WGTN has no ITRF velocity solution it was excluded from the velocity comparisons for the IGS CORS data. We also compared the horizontal and vertical velocities for the campaign data calculated from the APPS coordinate solutions, with the campaign velocities derived from Bernese to examine the closeness of the two sets of solutions. We consider the Bernese campaign station velocities as suitable for comparison, since historically Bernese software has been used extensively at GNS Science to process their campaign surveys (Beavan and Haines 2001; Wallace et al., 2004; Holden et al., 2015) and has shown to produce reliable results. Propagation of error theory was used to calculate the uncertainties associated with the coordinate differences.

3.5 Results

3.5.1 CORS Data Results

3.5.1.1 Coordinate repeatabilities

The average east, north and height coordinate repeatabilities (± 2.1 , ± 2.7 and ± 4.2 mm respectively) for the IGS CORS data solutions from APPS are presented in Figure 3.3. The individual CORS station results are presented in Table 3.3 and Table 3.5 in the supplementary material. The averages are similar in magnitude to those reported by Kouba (2005), Ocalan et al., (2013), Ebner and Featherstone (2008) and Kalita et al., (2014). Figure 3.3 indicates that the average east and north coordinate repeatability of the IGS CORS data in 2000 processed using APPS are higher than the average east and north repeatability of the other campaign years. No appreciable improvement in the APPS height repeatability is evident from the earlier to later campaign results. The individual results for each IGS CORS station in each campaign year are not presented here, but are included in the supplementary material (see Table 3.5).

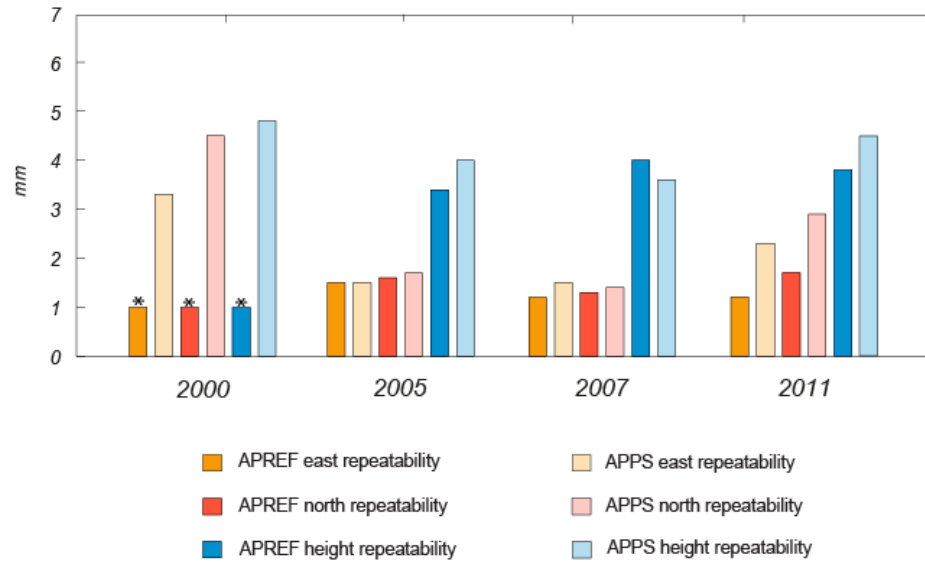


Figure 3.3 - Average day-to-day coordinate solution repeatabilities for IGS CORS station data. All units are in mm. These repeatabilities are also listed in Table 3 and 5 in the supplementary material. The 2000 campaign easting, northing and height repeatabilities (marked by the * symbol) are obtained from ITRF solutions.

3.5.1.2 Comparison to APREF or ITRF coordinate solutions

When compared to the APREF or ITRF coordinates (see Figure 3.4), the APPS coordinate solutions for the IGS CORS data differ in the east (ΔE) north (ΔN) and height (ΔH) components on average by 2.2mm, 2.4 mm and 3.0 mm respectively. If we consider the APREF and ITRF solutions as ‘true’ coordinates, since these solutions are based on long continuous daily time series of high-fidelity data, we estimate the overall accuracy of our APPS coordinate solutions for the IGS CORS data to be approximately 2.5mm in the horizontal and 3 mm in height. These are also similar in magnitude to those differences observed in Ocalan et al., (2013) (up to 6.5 mm in XY and Z components), Ebner and Featherstone (2008) (3.3mm in the east, 4.8mm in the north and 7.8 mm in height) and Guo (2014) (3.5mm in east, 2.1mm in north and 8.6mm in height). However, we note that the uncertainties associated with our differences (see Figure 3.4) are significant and indicate that the differences may be underestimated.

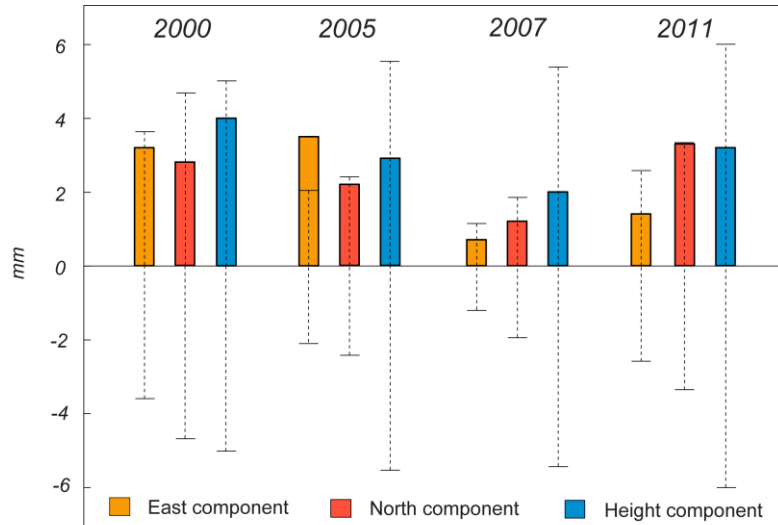


Figure 3.4 - Average coordinate solution differences and their uncertainties for IGS CORS station data for each campaign. All units are in mm. The differences and uncertainties are also listed in Table 4 in the supplementary material.

3.5.1.3 Velocity Results

When compared to the ITRF velocities, the horizontal and vertical velocities of the IGS CORS stations derived from the APPS coordinate solutions are on average different by 0.4 mm/yr^{-1} and 0.9 mm/yr^{-1} respectively (see Table 3.1). The average uncertainty error for these velocities is $\pm 1.7 \text{ mm/yr}^{-1}$ and $\pm 5.8 \text{ mm/yr}^{-1}$ respectively. The larger magnitude of the vertical uncertainty reflects the larger repeatabilities associated with the APPS height solutions for the IGS CORS stations as shown in Table 3.3 and Table 3.5 (see supplementary material).

Velocity Comparisons for IGS CORS Data

<i>Stn</i>	<i>ITRF</i>			<i>CLS</i>			<i>H_z</i>			<i>ITRF</i>			<i>L.R.</i>			<i>Vert</i>		
	<i>H_z vel</i>	$\pm \sigma$		<i>H_z vel</i>	$\pm \sigma$		<i>Vel Δ</i>	$\pm \sigma$		<i>Vert vel</i>	$\pm \sigma$		<i>Vert vel</i>	$\pm \sigma$		<i>Vel Δ</i>	$\pm \sigma$	
AUCK	40.2	0.1		40.5	1.3		-0.3	1.3		-0.8	0.2		-0.8	4.1		0.0	4.1	
CHAT	52.3	0.1		53.3	2.9		-1.0	2.9		-0.4	0.2		0.9	7.6		-1.3	7.6	
HOB2	57.6	0.1		57.6	1.4		0.0	1.4		0.3	0.5		-0.7	5.2		1.0	5.3	
TIDB	58.4	0.1		58.5	1.2		-0.1	1.2		0.6	0.3		-0.9	6.5		1.5	6.5	
Average		0.1			1.7		0.4	1.7		0.3				5.8		0.9	5.9	

Table 3.1 – Horizontal and vertical velocities and their differences and uncertainties for IGS CORS station data. *The column order is as follows:* Station name, ITRF horizontal velocity and uncertainties, Combined Least Squares (CLS) horizontal velocity and uncertainties using APPS horizontal coordinate solutions, horizontal velocity differences and uncertainties, ITRF vertical velocity and uncertainties, Linear regression (L.R.) vertical velocity and uncertainties calculated using APPS height solutions, vertical velocity differences and their uncertainties. All units are in mm/yr⁻¹.

3.5.2 NZ Campaign Data Results

3.5.2.1 Coordinate repeatabilities

Although restricted by the availability of data within each campaign, the average repeatabilities for the campaign solutions obtained from APPS are worth considering (see Table 3.4 in supplementary). The results indicate that these average $\pm 1.7\text{mm}$, $\pm 1.9\text{mm}$ and $\pm 5.0\text{ mm}$ for the east, north and height coordinates respectively. These are similar to the average repeatabilities calculated for all the campaign data using Bernese, which is $\pm 1.1\text{mm}$ in the east, $\pm 1.1\text{mm}$ in the north and $\pm 3.9\text{mm}$ for the height, although Kashani et al., (2004) consider the magnitude of Bernese internally-propagated formal sigma errors to be under-estimated. Larger repeatabilities occur in the individual station results for the APPS results (see Table 3.6 to Table 3.9 in supplementary material). These occur primarily in the height component (e.g. a height repeatability of $\pm 25.8\text{mm}$ for station 2351 in the 2011 campaign), but also occur in the horizontal repeatabilities (e.g. a easting repeatability of $\pm 36.8\text{mm}$ for station A88H in the 2005 campaign). Close examination of the APPS results for these stations indicates large variability between the different daily solutions within the campaigns. In general, where very large repeatabilities occur in the APPS campaign coordinate results, large repeatabilities are also identified in the Bernese campaign coordinate results, particularly in the height solutions. Possible reasons for these might include antenna height measurement error, GPS antenna dislevelment or local site characteristics.

3.5.2.2 Velocity Results

The average uncertainty associated with the Bernese horizontal and vertical velocities derived from the campaign data are $\pm 1.0 \text{ mm/yr}^{-1}$ and $\pm 2.3 \text{ mm/yr}^{-1}$ respectively (see Table 3.2). The average uncertainties of the horizontal and vertical velocities derived from the APPS coordinate solutions are $\pm 1.7 \text{ mm/yr}^{-1}$ and $\pm 5.6 \text{ mm/yr}^{-1}$ respectively. However, much larger individual uncertainties are associated with some of the velocity calculations derived from the APPS results, particularly the vertical velocities (e.g. stations B4HJ and EAXY for the horizontal velocities and station 2318 for the vertical velocities in Table 3.2). As a result, for a number of the vertical velocities determined using the APPS heights, their uncertainty is much larger than magnitude of their velocity (e.g. station 2318), placing their reliability in question. This may reflect the inherent inaccuracy associated with the vertical component of GPS, as well as the higher repeatabilities associated with the APPS campaign data height solutions (see Table 3.6 to Table 3.9 in supplementary material). However, similarly large uncertainties for the vertical velocities were also identified for CORS velocities derived from the APPS service, suggesting that any height errors associated with campaign GNSS survey field practices may not solely be responsible.

When compared to the Bernese velocities (see Table 3.2), the horizontal and vertical velocities or the campaign data, derived from the APPS coordinates, are on average different by $0.6 \pm 2.0 \text{ mm/yr}^{-1}$ and $1.0 \pm 6.4 \text{ mm/yr}^{-1}$. The largest difference between the two sets of horizontal velocities is -3.1 mm/yr^{-1} of station 6881 and -4.9 mm/yr^{-1} for the vertical velocities of station B4HJ. Although these two sets of campaign velocities are similar, the uncertainty error associated with these comparisons is in some instances quite large. This again reflects the large repeatability associated with some of the APPS coordinate solutions for the campaign data (see Table 3.6 to Table 3.9 in supplementary material).

Velocity Comparisons for Campaign Data

<i>Stn</i>	<i>Bernese</i>		<i>CLS</i>		<i>Hz</i>		<i>Bernese</i>		<i>L.R.</i>		<i>Vert</i>	
	<i>Hz vel</i>	$\pm \sigma$	<i>Hz vel</i>	$\pm \sigma$	<i>Vel A</i>	$\pm \sigma$	<i>Vert vel</i>	$\pm \sigma$	<i>Vert vel</i>	$\pm \sigma$	<i>Vel A</i>	$\pm \sigma$
1291	36.8	0.6	36.2	0.8	0.6	1.0	-5.5	2.7	-5.0	7.4	-0.5	7.8
2308	33.5	0.9	33.7	0.8	-0.2	1.2	-9.1	1.0	-9.1	4.1	0.0	4.3
2309	33.5	0.6	33.4	1.8	0.1	1.9	-11.9	1.0	-10.4	3.1	-1.5	3.3
2313	34.4	0.7	34.5	0.5	-0.1	0.9	-19.4	2.4	-19.6	6.3	0.2	6.7
2318	29.4	0.6	29.3	0.7	0.1	0.9	-2.1	2.6	-2.2	18.2	0.1	18.3
2344	33.0	0.7	32.4	0.5	0.6	0.8	-5.7	0.5	-5.1	5.7	-0.6	5.7
2348	34.6	0.6	34.5	0.4	0.1	0.7	-3.8	0.6	-3.5	3.0	-0.3	3.1
2350	32.4	0.6	31.9	2.1	0.5	2.1	-9.7	1.9	-12.0	5.3	2.3	5.6
2351	31.4	0.6	31.9	1.0	-0.6	1.2	-5.7	1.7	-4.0	0.1	-1.7	1.7
2382	37.6	1.3	38.5	0.9	-1.0	1.6	0.5	1.2	-0.1	1.9	0.6	2.3
2383	37.6	0.6	37.4	0.0	0.2	0.6	0.4	0.8	0.7	2.8	-0.3	2.9
3002	35.9	0.7	35.6	1.1	0.4	1.3	-19.4	2.6	-21.9	0.9	2.5	2.7
3006	33.8	0.6	34.6	0.8	-0.8	1.0	-2.2	1.8	-4.8	0.7	2.6	1.9
3051	33.4	1.2	34.1	0.5	-0.7	1.3	-11.0	1.6	-11.4	0.7	0.4	1.7
3052	34.6	0.6	34.0	0.4	0.7	0.7	-13.5	0.9	-12.9	3.5	-0.6	3.7
3056	33.0	0.6	32.0	0.5	1.1	0.8	-14.0	0.7	-13.5	7.7	-0.5	7.7
3061	36.2	0.6	35.8	0.4	0.4	0.7	-12.9	0.7	-12.8	3.7	-0.1	3.8
3063	37.2	0.6	37.4	1.0	-0.2	1.2	-12.2	0.5	-13.4	8.8	1.2	8.8
3066	36.6	0.6	35.7	1.3	1.0	1.4	-12.0	0.7	-11.0	1.6	-1.0	1.8
3067	35.4	0.6	34.7	0.4	0.7	0.7	-15.0	0.7	-15.0	10.1	0.0	10.1
3077	34.3	0.6	34.2	0.5	0.1	0.8	-6.8	1.1	-6.1	12.3	-0.7	12.4
3078	33.1	0.7	32.8	1.0	0.3	1.2	-3.4	0.4	-2.5	6.1	-0.9	6.2
3079	32.3	0.6	32.0	0.8	0.3	1.0	-10.7	4.6	-10.0	0.6	-0.7	4.6
3080	32.5	1.2	33.1	2.9	-0.6	3.2	-4.2	1.9	-6.0	1.9	1.8	2.7
3081	34.3	0.6	34.4	1.5	-0.1	1.6	-3.4	5.5	-4.0	0.0	0.6	5.5
3093	34.0	0.6	34.3	1.2	-0.3	1.3	-8.1	8.3	-8.2	13.8	0.1	16.1
3094	33.8	0.6	34.1	1.8	-0.3	1.9	-13.4	1.0	-14.0	1.0	0.6	1.4
6881	31.1	2.2	34.2	2.2	-3.1	3.1	1.7	1.5	-1.6	4.3	3.3	4.5
AK46	36.2	2.2	37.5	2.2	-1.3	3.1	0.6	1.6	0.8	16.7	-0.2	16.8
A7LF	28.7	0.6	28.9	1.1	-0.2	1.3	-1.9	1.3	-1.4	0.3	-0.5	1.3
A7LJ	27.4	0.6	27.0	1.1	0.4	1.2	-0.2	1.0	0.5	4.2	-0.7	4.3
A86L	33.8	0.6	33.1	2.5	0.7	2.5	-9.1	1.1	-9.5	2.8	0.4	3.0
A86T	34.4	2.5	34.6	1.4	-0.2	2.8	-12.4	2.5	-13.7	4.1	1.3	4.8
A86W	34.1	2.4	35.7	3.6	-1.7	4.3	-8.5	2.5	-9.6	7.2	1.1	7.6
A87P	35.3	2.4	36.6	4.1	-1.3	4.7	-4.5	1.7	-4.9	6.5	0.4	6.7
A886	32.3	2.4	33.6	5.9	-1.3	6.4	-12.3	3.5	-13.0	4.5	0.7	5.7
A88G	36.0	0.6	36.1	2.0	-0.1	2.1	-10.3	1.1	-12.0	10.5	1.7	10.5
A88H	35.5	0.6	36.6	0.4	-1.2	0.7	-9.3	1.4	-9.5	4.8	0.2	5.0
A9BM	30.8	0.6	31.8	3.3	-1.0	3.3	-0.7	0.6	-2.4	6.9	1.7	6.9
AGB9	30.2	1.5	31.4	2.2	-1.2	2.7	0.8	2.3	-0.2	7.3	1.0	7.7
AGUG	33.5	1.0	34.0	1.4	-0.5	1.7	-1.0	4.0	1.1	1.0	-2.1	4.1
B26Q	33.8	0.6	33.7	0.8	0.1	1.0	-8.7	0.9	-9.7	6.8	1.0	6.8
B4DP	39.1	1.1	39.1	0.9	-0.1	1.5	-0.8	2.2	-2.0	12.4	1.2	12.6
B4HJ	33.3	1.0	36.0	8.9	-2.7	9.0	-4.9	4.9	0.0	6.1	-4.9	7.8
BET2	33.0	0.5	32.8	1.0	0.2	1.1	-9.1	8.9	-8.1	4.2	-1.0	9.8
BEVJ	34.1	1.2	34.1	2.5	0.0	2.7	-12.2	2.2	-10.8	6.2	-1.4	6.5
CBWR	28.7	0.6	29.1	1.5	-0.4	1.6	1.8	6.4	1.7	4.2	0.1	7.6
CBWU	37.1	0.7	36.8	0.5	0.3	0.9	-0.8	1.4	-0.5	7.9	-0.3	8.0
CBWW	30.7	0.7	31.0	0.8	-0.3	1.1	-1.4	3.0	-2.7	7.8	1.3	8.4
CBWW	34.3	0.6	34.4	0.7	-0.1	0.9	-7.2	0.8	-7.5	1.5	0.3	1.7
E4MH	33.6	2.4	34.9	1.0	-1.3	2.6	-15.5	3.5	-18.1	7.7	2.6	8.4
EAXX	38.0	2.2	38.9	3.1	-0.9	3.8	-2.1	4.0	-1.6	5.9	-0.5	7.2
EAXY	27.9	2.2	29.8	6.9	-2.0	7.3	-1.0	8.5	-2.7	11.8	1.7	14.5
Average		1.0		1.7	0.6	2.0	2.3	5.6		1.0	6.4	

Table 3.2 – Horizontal and vertical velocities, their differences and uncertainties for the campaign **data**. *Column order is as follows:* Station name, Bernese horizontal velocity and uncertainties, Combined Least Squares (CLS) horizontal velocity and uncertainties, horizontal velocity differences and uncertainties, Bernese vertical velocity and uncertainties, Linear regression (L.R.) vertical velocity and uncertainties, vertical velocity differences and their uncertainties. All units are in mm/yr^{-1} .

3.6 Discussion

3.6.1 How reliable are our results?

The results suggest that the APPS coordinate solutions are accurate with respect to the published APREF or ITRF coordinates for the IGS CORS data. Further, the repeatabilities of these solutions indicate that APPS can provide reliable results, with respect to stable CORS stations. The horizontal velocity field that we model from our APPS results for the campaign data compares well with that from network based Bernese modelling. A notable aspect of these comparisons is that although some significant differences occur between the campaign data horizontal and height coordinates using the Bernese software and APPS (see Table 3.6 to Table 3.9 in supplementary material), the horizontal and vertical velocities are still remarkably close in magnitude. We link this to the consistency of the relative differences between coordinate results of the two approaches (e.g. Bernese differencing and the APPS PPP technique). We suggest that although each technique has likely biases in their approaches and the coordinates from each technique might differ, the relative differences for each station between each campaign coordinate solution are similar. Therefore, the resultant velocities calculated from the relative differences are similar.

We cannot comment fully on the reliability of the APPS campaign coordinate solutions with confidence, since their repeatabilities were determined from the limited data samples available. To some extent this also limits the uncertainty associated with the velocities derived from these coordinates. Nonetheless, the average uncertainty we estimate for the campaign data horizontal velocities derived from the APPS coordinate solutions ($\pm 1.7 \text{ mm/yr}^{-1}$) are similar to that of the Bernese horizontal velocities ($\pm 1.5 \text{ mm/yr}^{-1}$). Considered alongside the small differences we observe between the APPS and Bernese horizontal velocities, this suggests that the APPS horizontal velocities are reliable. Less reliability can be placed on the vertical velocities derived from the APPS height solutions, as in some cases their uncertainty is significantly larger than the magnitude of their velocity. There is little published research literature available that estimate velocity repeatabilities from online PPP from which we can independently compare our results to.

3.6.2 Can our results be used to observe various geophysical processes?

If we consider our horizontal and vertical velocity uncertainties with respect to the expected deformation rates shown in Figure 3.1, we can comment on their ability to observe deformation related to various geophysical processes. In general, the average level of uncertainty associated with calculated horizontal and vertical velocities presented in this research is generally less than the expected deformation rates associated with subsidence, volcanic, landslide and glacial processes. Therefore, we consider that our APPS and Bernese velocities could be used to measure deformation associated with these particular processes with a high level of confidence.

Our average APPS and Bernese horizontal velocity uncertainties (± 1.5 and $\pm 1.7\text{mm/yr}^{-1}$ respectively) are of a similar magnitude to the velocities expected for inter and post-seismic deformation (see Figure 3.1). This implies that they could measure inter and post-seismic deformation, but that to achieve this with a suitable degree of confidence, careful field planning and practice, repeated GNSS campaigns and rigorous processing procedures must be used. For examples, our results have significantly benefited from the long-term decadal data spans that were available from GNS. Over this period of time, any long-term tectonic signal is more likely to have emerged from the background and measurement noise. As a result we place a high level of confidence in the calculated horizontal velocities. It is possible that a shorter GNSS dataset (e.g. perhaps only two sets of campaign data separated over only a few years) might provide a similar result, but the velocities would lack reliability. Similarly, the larger uncertainties (an average of $\pm 5.6\text{mm/yr}^{-1}$) associated with the vertical velocities calculated from the APPS height solutions, would limit their use to the measurement of gross vertical displacement (where upwards of tens of mm/yr^{-1} or greater movement may occur).

3.6.3 What implications do these results have for GNSS campaign fieldwork technique and post-processing and future geophysical research?

The online PPP approach used in this research offers an alternative to the use of sophisticated scientific GNSS software packages. Although the velocities achieved using this approach are not superior to those derived from the Bernese software, the method used to calculate these provides a number of benefits that might appeal to various research groups and individuals. First, since the APPS service has shown to provide geodetic quality results in an absolute sense, large fleets of GNSS receivers would not need to be deployed simultaneously, as required when using differential positioning. This would require less personnel and resources in the field, significantly reducing operating costs. This would also provide more flexibility to when the fieldwork could be conducted, since the receivers could be deployed when needed or required. For example, a small field crew

could be employed to establish and/or regularly reoccupy geodetic monuments within a geodetic network regularly throughout the year, or as time permits. However, it is critical that there is a repeated observation schedule during the survey period in order to determine coordinate repeatabilities.

Second, this research has also shown that high precision geodetic results can be achieved with an online PPP service without significant training in scientific GNSS software and post-processing. The use of the JPL orbit and clock products by APPS provides absolute and consistent solutions, which greatly simplifies the GNSS data processing procedure. This may benefit various organisations, particularly Government scientific organisations in developing countries, where the number of personnel appropriately trained in GNSS data processing is often limited, due to the associated expensive costs and high level of experience required. However, we suggest that some knowledge of the different orbit and clock products, ITRF reference frame realisations and GNSS processing is still necessary to interpret the PPP results correctly. This includes the ability to decide if the measurement repeatabilities are reliable and also to determine if a ‘misbehaving’ station (or anomalous velocity) is due to a processing error, a field survey error or a local deformation signal. It is critical that all GNSS data be processed through online PPP services after the final orbit and clock products have become available.

The quality of results we achieved is a testament to the good field techniques GNS Science incorporate in their GNSS campaign surveys. This includes long time-span daily observation sessions, increased redundancy from repeated monument occupations, the consistent use of well recognised and calibrated GNSS antenna types and station monuments with maximum sky visibility and local stability. The use of these techniques for any future campaign surveys processed with APPS is highly recommended. However, a limitation of our research is the availability of only two daily (a minimum) coordinate solutions for many stations in each campaign. As a result the source/s any large differences between these two solutions provided by APPS could not be resolved. Although, such differences also affect the differential GPS baseline approach, the ability to perform a network adjustment using the redundant GPS baselines allows outlier detection. In the future, using the PPP approach, these troublesome solutions could be addressed by obtaining another APPS solution by conducting a third GNSS occupation of that station. Since the PPP technique is absolute, only this station would only have to be occupied. Although this results in extra fieldwork (which could be conducted as soon as the initial anomalous coordinate solutions is detected), this would be offset by the simpler data processing used to obtain this new coordinate solution.

Finally, differential positioning typically requires connection to CORS for datum definition and access to plate tectonic models. It is unlikely that that government funded CORS networks will achieve a density suitable to

observe deformation related to all geophysical processes. As a result differential GNSS surveys in very remote regions (no CORS infrastructure) still require baseline observations of lengths of hundreds and sometimes thousands of kilometres, which reduce the quality of the results achieved. Since station velocities can be derived directly from absolute PPP positions, deformation surveys can be conducted without the need for CORS networks. This has significant implications for geophysical research in remote locations, such as that related to glacial movement in the arctic regions.

3.7 Conclusions

In this research, we processed a very large campaign GPS dataset (spanning ten years) with the online JPL APPS service. This dataset was taken from a GPS network specifically designed and surveyed to measure deformation through the central North Island of New Zealand. This is the first time that such a significant campaign GPS dataset has been processed solely using an online PPP service. The resulting coordinates were then used to determine horizontal and vertical velocities. The quality of these velocities is considered by comparing them to Bernese GPS derived horizontal and vertical solutions. We find a good agreement between velocities obtained from the two approaches. The major contributions of this paper are to show that, 1) reliable horizontal and height solutions can be derived using the JPL APPS processing service and 2) the quality of the velocities derived from these positions indicate they can be used to measure deformation related to a variety of geophysical processes, 3) the uncertainties associated with these must still be considered carefully in the context of the expected deformation associated with these processes.

These findings may have significant implications for how future campaign GNSS surveys are conducted in the field and their data processed. First, campaign GNSS surveys can be undertaken in remote regions with no CORS infrastructure without numerous GNSS receivers being deployed. This has considerable cost savings associated with field equipment, logistics and personnel. Second, the JPL APPS service is freely available and users without access to other commercial scientific GNSS software now have the opportunity to obtain high quality coordinates. Third, there is no need to use CORS stations to define local reference frames for deformation measurements, whose velocities need to be modelled using complex plate tectonics.

A present limitation of our analysis is that no post-survey network adjustment is possible and outliers can only be identified using repeated monument occupation. Further, it is still recommended that users of online PPP processing services have some understanding of the underlying issues with the GNSS and online processing services. This is essential, since it is the users responsibility to select an appropriate geodetic instrument and/or technique when attempting to measure deformation. Ultimately, the user must decide if the chosen technique

can be reliably used to detect the deformation signal at the expected rate in the presence of measurement noise. This fundamental problem is an issue for all geodetic instruments and techniques when used in geodynamic and deformation studies.

It is anticipated that with the increase in multi-frequency, multi-constellation GNSS, PPP performance is expected to improve significantly, providing better position accuracy, availability and reliability with shorter convergence time (Bisnath and Gao, 2009; Li et al., 2015a; Li et al., 2015c; Li et al., 2015d). There are now several online PPP processing services that process multi-GNSS data, which are expected to provide improved position solutions, particularly for near real-time and kinematic applications (Wright et al., 2012; Li et al., 2013; Li et al., 2015b). These include the Trimble RTX (Trimble Centerpoint RTX Post-Processing 2016), MagicGNSS (MagicGNSS 2016) and the CSRS-PPP services. The research presented here has only focussed on GPS campaign data. Further research is needed on multi-GNSS campaign datasets using these online PPP services. Gains in campaign data processing and fieldwork efficiency are likely to be achieved, which may have significant benefits for geophysical studies. It is recommended that researchers use APPS in conjunction with their existing GNSS campaign data processing routine. This will provide an independent check on their results, as well as more research into the quality of results achieved using APPS for a broader variety of GNSS datasets and applications.

3.8 References

- Beavan, J. and Haines, J., 2001. Contemporary horizontal velocity and strain rate fields of the Pacific-Australian plate boundary zone through New Zealand. *J Geophys Res-Sol Ea*, **106**(B1): 741-770, doi: 10.1029/2000JB900302
- Bisnath, S. & Gao, Y., 2009. Current State of Precise Point Positioning and Future Prospects and Limitations, *Observing Our Changing Earth*, **133**, 615-623, doi: 10.1007/978-3-540-85426-5_71.
- Briggs, R. W., Sieh, K., Meltzner, A. J., Natawidjaja, D., Galetzka, J., Suwargadi, B., Hsu, Y. J., Simons, M., Hananto, N., Suprihanto, I., Prayudi, D., Avouac, J. P., Prawirodirdjo, L. & Bock, Y., 2006. Deformation and slip along the Sunda Megathrust in the great 2005 Nias-Simeulue earthquake: *Science*, **311**(5769), 1897-1901, doi: 10.1126/science.1122602.
- Dach, R., Hugentobler, U., Fridez, P. & Meindl, M., 2007. *Bernese GPS Software Version 5.0* Stamfli Publications AG, Astronomical Institute, University of Bern.
- Dawson, J., Govind, R. & Manning, J., (2004), The AUSLIG online GPS processing system (AUSPOS), The Australian surveying and land information group (AUSLIG).
- Dixon, T. H., 1991. An Introduction to the Global Positioning System and Some Geological Applications, *Reviews of Geophysics*, **29**(2), 249-276, doi: 10.1029/91RG00152.
- Dragert, H., Wang, K. L. & James, T. S., 2001. A silent slip event on the deeper Cascadia subduction interface, *Science*, **292**(5521), 1525-1528, doi: 10.1126/science.1060152.
- Ebner, R. & Featherstone, W., 2008. How well can online GPS PPP post-processing services be used to establish geodetic survey control networks?, *Journal of Applied Geodesy*, **2**(3), 149-157, doi: 10.1515/JAG.2008.017
- Ghoddousi-Fard, R. & Dare, P., 2006. Online GPS processing services: an initial study, *Gps Solutions*, **10**(1), 12-20, doi: 10.1007/s10291-005-0147-5.
- Guo, Q., 2014. Precision comparison and analysis of four online free PPP services in static positioning and tropospheric delay estimation, *GPS Solutions*, **19**(4), 537-544, doi: 10.1007/s10291-014-0413-5.
- Hammond, W., Blewitt, J., Kreemer, C., Murray-Moraleda, J. R. & Svarc, J. L., 2011. Global Positioning System Constraints on Crustal Deformation Before and During the 21 February 2008 Wells, Nevada M 6.0 Earthquake, in dePolo, C.M. & LaPoint, D., eds., a compendium of earthquake-related investigations prepared by the University of Nevada, Reno, Special Publication, Nevada Bureau of Mines and Geology, 181-196.

- Holden, L., Wallace, L., Beavan, J., Fournier, N., Cas, R., Ailleres, L. & Silcock, D., 2015. Contemporary ground deformation in the Taupo Rift and Okataina Volcanic Centre from 1998 to 2011, measured using GPS, *Geophysical Journal International*, **202**(3), 2082-2105, doi: 10.1093/gji/ggv243.
- Hu, D., Dawson, J., Jia, M., Deo, M., Ruddick, R., Johnston, G., 2011. Towards the Densification of the International Terrestrial Reference Frame in the Asia and Pacific Region – Asian Pacific Reference Frame (APREF), in *Advances in Geoscience*, **31**, 23-31, eds., Ching-Hua Lo et al., World Scientific Publishing Company, Singapore.
- Jet Propulsion Laboratory., 2015, *The JPL APPS service*, accessed 5 July 2015, <http://apps.gdgps.net/>
- Kalita, J., Rzepecka, Z. & Szuman-Kalita, I., 2014. The application of Precise Point Positioning in Geosciences, *Selected papers of the 9th International Conference Environmental Engineering*, 1-7, Available from http://leidykla.vgtu.lt/conferences/ENVIRO_2014/Articles/5/215_Kalita.pdf accessed 4 Feb 2016.
- Kashani, I., Wielgosz, P. & Grejner-Brzezinska, D. A., 2004. On the reliability of the VCV matrix: A case study based on GAMIT and Bernese GPS software, *Gps Solutions*, **8**(4), 193-199, doi: 10.1007/s10291-004-0103-9.
- King, R. W. & Bock, Y., 1999. *Documentation for the MIT GPS analysis software: GAMIT*, Dept. Earth, Atmos., and Planet. Sci., Massachusetts Institute of Technology.
- Kouba, J., 2005. A possible detection of the 26 December 2004 great Sumatra-Andaman Islands Earthquake with solution products of the international GNSS service, *Studia Geophysica et Geodaetica*, **49**(4), 463-483, doi: 10.1007/s11200-005-0022-4.
- Kouba, J., 2009, *A guide to using international GPS service (IGS) products*, accessed 5 Feb 2016, <https://igscb.jpl.nasa.gov/components/usage.html>.
- Langbein, J., 2003. Deformation of the Long Valley Caldera, California: inferences from measurements from 1988 to 2001, *Journal of Volcanology and Geothermal Research*, **127**(3-4), 247-267, doi: 10.1016/S0377-0273(03)00172-0.
- Leick, A., 1995. GPS Satellite Surveying, John Wiley and Sons, USA.
- Li, X., Ge, M. R., Zhang, Y., Zhang, X., Guo, B., Klotz, J. & Wickert, J., 2013. Real-time high-rate co-seismic displacement from ambiguity-fixed precise point positioning: Application to earthquake early warning, *Geophysical Research Letters*, **40**(2), 295-300, doi:10.1002/grl.50138.
- Li, X., Ge, M., Dai, X., Ren, X., Fritsche, M., Wickert, J. & Schuh, H., 2015a. Accuracy and reliability of multi-GNSS real-time precise positioning: GPS, GLONASS, BeiDou, and Galileo, *Journal of Geodesy*, **89**(6), 607-635, doi: 10.1007/s00190-015-0802-8.

- Li, X., Zus, F., Lu, C., Ning, T., Dick, G., Ge, M., Wickert, J. & Schuh, H., 2015b. Retrieving high-resolution tropospheric gradients from multi-constellation GNSS observations, *Geophysical Research Letters*, **42**(10), 4173-4181, doi: 10.1002/2015GL063856.
- Li, X., Zus, F., Lu, C., Dick, G., Ning, T., Ge, M., Wickert, J. & Schuh, H., 2015c. Retrieving of atmospheric parameters from multi-GNSS in real time: Validation with water vapor radiometer and numerical weather model. *Journal of Geophysical Research: Atmospheres*, **120**(14), 7189-7204, doi: 10.1002/2015JD023454.
- Li, X., Zhang, X., Ren, X., Fritsche, M., Wickert, J. & Schuh, H., 2015d. Precise positioning with current multi-constellation Global Navigation Satellite Systems: GPS, GLONASS, BeiDou, and Galileo, *Scientific Reports*, **5**(8328), 1-14, doi: 10.1038/srep08328.
- Lichten, S., Yoazar-Sever, W., Bertiger, M., Hurst, K., Muellersehoen, R. J., Wu, S. C., Yunck, T. & Zumberge, J., 1995. *GIPSY-OASIS II: A high precision GPS data processing system and general satellite orbit*, technical report 95 -1323, Jet Propulsion Laboratory, Pasadena, California.
- Massonnet, D. & Feigl, K. L., 1998. Radar interferometry and its application to changes in the earth's surface, *Reviews of Geophysics*, **36**(4), 441-500, doi: 10.1029/97RG03139.
- MagicGNSS, 2016, *Quality Data, Algorithms and Products for the GNSS User Community*, accessed 9 Feb 2016, <http://magicgnss.gmv.com/>.
- Natural Resources Canada., 2015. *Precise Point Positioning*, Accessed Feb 6 2015, <http://webapp.geod.nrcan.gc.ca/geod/tools-outils/ppp.php?locale=en>
- Ocalan, T., Erdogan, B. & Tunalioglu, N., 2013. Analysis of Web-Based Online Services for Gps Relative and Precise Point Positioning Techniques, *Boletim De Ciencias Geodesicas*, **19**(2), 191-207, doi: 10.1590/S1982-21702013000200003.
- Rizos, C., Han, S. W., Ge, L. L., Chen, H. Y., Hatanaka, Y. & Abe, K., 2000, Low-cost densification of permanent GPS networks for natural hazard mitigation: First tests on GSI's GEONET network, *Earth Planets and Space*, **52**(10), 867-871, doi:10.1186/BF03352297.
- Rogers, G. & Dragert, H., 2003. Episodic tremor and slip on the Cascadia subduction zone: The chatter of silent slip: *Science*, **300**(5627), 1942-1943, doi: 10.1126/science.1084783.
- Sagiya, T., 2004. A decade of GEONET: 1994-2003 - The continuous GPS observation in Japan and its impact on earthquake studies, *Earth Planets and Space*, **56**(8), xxix-xli, doi: 10.1007/3-540-27432-4_4.
- Sato, M., Ishikawa, T., Ujihara, N., Yoshida, S., Fujita, M., Mochizuki, M. & Asada, A., 2011, Displacement Above the Hypocenter of the 2011 Tohoku-Oki Earthquake: *Science*, **332**(6036), 1395-1395, doi: 10.1126/science.1207401
- Shimada, S., 2005. Vertical repeatability of GPS measurements in the Tsukuba GPS/MET dense-network campaigns, in *A Window on the Future of Geodesy*, 21-25, eds., Sanso, F., Proceedings of the

- International Association of Geodesy IAG General Assembly Sapporo, Japan, June 30 – July 11, 2003, doi: 10.1007/3-540-27432-4_4.
- Simons, M., Minson, S. E., Sladen, A., Ortega, F., Jiang, J. L., Owen, S. E., Meng, L. S., Ampuero, J. P., Wei, S. J., Chu, R. S., Helmberger, D. V., Kanamori, H., Hetland, E., Moore, A. W. & Webb, F. H., 2011, The 2011 Magnitude 9.0 Tohoku-Oki Earthquake: Mosaicking the Megathrust from Seconds to Centuries, *Science*, 332(6036), 1421-1425, doi: 10.1126/science.1206731.
- Steigenberger, P., Rothacher, M., Dietrich, R., Fritsche, M., Rulke, A. & Vey, S., 2006. Reprocessing of a global GPS network, *Journal of Geophysical Research-Solid Earth*, **111**(B05402), doi: 10.1029/2005JB003747
- Trimble Centerpoint RTX Post-processing Service, 2016, accessed 9 Feb 2016, <http://www.trimblertx.com/UploadForm.aspx>.
- Tsakiri, M., 2008, GPS Processing Using Online Services, *Journal of Surveying Engineering-Asce*, **134**(4), 115-125, doi:10.1061/(ASCE)0733-9453.
- Vigny, C., Simons, W. J. F., Abu, S., Bamphenyu, R., Satirapod, C., Choosakul, N., Subarya, C., Socquet, A., Omar, K., Abidin, H. Z. & Ambrosius, B. A. C., 2005. Insight into the 2004 Sumatra-Andaman earthquake from GPS measurements in southeast Asia, *Nature*, **436**(7048), 201-206, doi: 10.1038/nature03937
- Vigny, C., Socquet, A., Peyrat, S., Ruegg, J. C., Metois, M., Madariaga, R., Morvan, S., Lancieri, M., Lacassin, R., Campos, J., Carrizo, D., Bejar-Pizarro, M., Barrientos, S., Armijo, R., Aranda, C., Valderas-Bermejo, M. C., Ortega, I., Bondoux, F., Baize, S., Lyon-Caen, H., Pavez, A., Vilotte, J. P., Bevis, M., Brooks, B., Smalley, R., Parra, H., Baez, J. C., Blanco, M., Cimbaro, S. & Kendrick, E., 2011. The 2010 M-w 8.8 Maule Megathrust Earthquake of Central Chile, Monitored by GPS: *Science*, **332**(6036), 1417-1421, doi: 10.1126/science.1204132
- Wallace, L.M., Beavan, J., McCaffrey, R. and Darby, D., 2004. Subduction zone coupling and tectonic block rotations in the North Island, New Zealand. *J Geophys Res-Sol Ea*, 109(B12), 12406-, doi: 10.1029/2004JB003241
- Wallace, L. M., & R. J. Beavan, 2006. A large slow slip event on the central Hikurangi subduction interface beneath the Manawatu region, North Island, New Zealand, *Geophysical Research. Letters*, **33**(11), doi: 10.1029/2006GL026009.
- Wessel, P., W. H. F. Smith, R. Scharroo, J. F. Luis, & F. Wobbe. 2013. Generic Mapping Tools: Improved Version Released, *EOS Transactions, AGU*, **94**(45), 409-410, doi: 10.1002/2013EO450001.
- Wright, T. J., Houlie, N., Hildyard, M., & Iwabuchi, T. 2012, Real-time, reliable magnitudes for large earthquakes from 1Hz GPS precise point positioning The Tohoku-Oki (Japan) earthquake, *Geophysical Research Letters*, **39**(12), 12302-, doi:10.1029/2012GL051894

Zumberge, J. F., Heflin, M. B., Jefferson, D. C., Watkins, M. M., & Webb, F. H., 1997, Precise point positioning for the efficient and robust analysis of GPS data from large networks, *Journal of Geophysical Research-Solid Earth*, 102(B3), 5005-5017, doi: 10.1029/96JB03860

3.9 Electronic Supplemently Material

IGS CORS Data Coordinate Solution Repeatabilities and Differences

<i>Year</i>	$\pm\sigma$	APREF E /ITRF $\pm\sigma$	APREF N /ITRF $\pm\sigma$	APREF H /ITRF $\pm\sigma$	APPS E $\pm\sigma$	APPS N $\pm\sigma$	APPS H ΔE	$\pm\sigma$	ΔN	$\pm\sigma$	ΔH	$\pm\sigma$
2000	1.0	1.0	1.0	3.3	4.5	4.8	3.2	3.6	2.8	4.7	4.0	4.9
2005	1.5	1.6	3.4	1.5	1.7	4.0	3.5	2.1	2.2	2.4	2.9	5.5
2007	1.2	1.3	4.0	1.5	1.4	3.6	0.7	1.2	1.2	2.0	2.0	5.5
2011	1.2	1.7	3.8	2.3	2.9	4.5	1.4	2.6	3.3	3.4	3.2	6.0
Average	1.2	1.4	3.0	2.1	2.7	4.2	2.2	2.4	2.4	3.1	3.0	5.5

Table 3.3– Average coordinate solution repeatabilities, coordinate differences and their uncertainties for IGS CORS stations. *The column order for 2011 to 2005 results are as follows:* Campaign year, APREF easting repeatability, northing repeatability and height repeatability respectively, APPS easting repeatability, northing repeatability and height repeatability respectively, easting difference (ΔE), northing difference (ΔN) and their uncertainty and height difference (ΔH) and its uncertainty. *The column order for 2000 is as follows:* Campaign year, ITRF easting and repeatability, northing and repeatability, height and repeatability, respectively, all remaining columns are the same as 2011 to 2005. All units are in mm.

Campaign Data Average Coordinate Solution Repeatabilities

	<i>Bernese E</i>	<i>Bernese N</i>	<i>Bernese H</i>	<i>APPS E</i>	<i>APPS N</i>	<i>APPS H</i>
<u><i>Year</i></u>	<u>$\pm\sigma$</u>	<u>$\pm\sigma$</u>	<u>$\pm\sigma$</u>	<u>$\pm\sigma$</u>	<u>$\pm\sigma$</u>	<u>$\pm\sigma$</u>
2000	1.4	1.6	3.4	1.4	2.0	4.4
2005	1.0	1.2	3.7	2.9	2.2	5.5
2007	1.1	0.7	3.8	1.2	1.3	5.0
2011	1.0	1.1	4.7	1.4	1.9	5.0
Average	1.1	1.1	3.9	1.7	1.9	5.0

Table 3.4— Average Bernese and APPS coordinate solution repeatability for each campaign. *Column order is as follows:* Campaign year, Bernese easting repeatability, northing repeatability and height repeatability, APPS easting repeatability, northing repeatability and height repeatability respectively. All units are in mm.

2000 IGS Data Coordinate Solution Repeatabilities and Differences

<i>Stn</i>	<i>ITRF E</i> $\pm\sigma$	<i>ITRF N</i> $\pm\sigma$	<i>ITRF H</i> $\pm\sigma$	<i>APPS E</i> $\pm\sigma$	<i>APPS N</i> $\pm\sigma$	<i>APPS H</i> $\pm\sigma$	ΔE	$\pm\sigma$	ΔN	$\pm\sigma$	ΔH	$\pm\sigma$
AUCK	1.0	1.0	1.0	2.4	7.0	3.0	4.0	2.6	-4.9	7.1	-3.7	3.2
CHAT	1.0	1.0	1.0	8.4	6.8	7.7	7.1	8.4	0.9	6.9	6.2	7.7
HOB2	1.0	1.0	1.0	1.3	2.7	3.7	0.9	1.7	-2.7	2.9	-2.8	3.9
TIDB	1.0	1.0	1.0	1.2	1.6	4.6	0.7	1.6	-2.6	1.9	-3.5	4.7
Average	1.0	1.0	1.0	3.3	4.5	4.8	3.2	3.6	2.8	4.7	4.0	4.9

2005 IGS Data Coordinate Solution Repeatabilities and Differences

<i>Stn</i>	<i>APREF E</i> $\pm\sigma$	<i>APREF N</i> $\pm\sigma$	<i>APREF H</i> $\pm\sigma$	<i>APPS E</i> $\pm\sigma$	<i>APPS N</i> $\pm\sigma$	<i>APPS H</i> $\pm\sigma$	ΔE	$\pm\sigma$	ΔN	$\pm\sigma$	ΔH	$\pm\sigma$
AUCK	1.5	1.2	4.4	1.4	2.8	2.0	-3.2	2.1	-1.9	3.0	-2.9	4.8
CHAT	1.4	1.4	3.1	0.9	1.2	3.9	-2.4	1.7	-3.4	1.9	-3.1	5.0
HOB2	1.9	2.2	3.6	1.6	1.2	3.7	-3.8	2.5	-2.3	2.5	1.4	5.2
TIDB	1.6	2.0	4.8	1.1	1.2	4.9	-3.3	1.9	-1.2	2.3	-2.1	6.9
WGTM	1.0	1.0	1.0	2.4	2.2	5.5	-5.0	2.6	-1.9	2.4	-4.9	5.6
Average	1.5	1.6	3.4	1.5	1.7	4.0	3.5	2.1	2.2	2.4	2.9	5.5

2007 IGS Data Coordinate Solution Repeatabilities and Differences

<i>Stn</i>	<i>APREF E</i> $\pm\sigma$	<i>APREF N</i> $\pm\sigma$	<i>APREF H</i> $\pm\sigma$	<i>APPS E</i> $\pm\sigma$	<i>APPS N</i> $\pm\sigma$	<i>APPS H</i> $\pm\sigma$	ΔE	$\pm\sigma$	ΔN	$\pm\sigma$	ΔH	$\pm\sigma$
AUCK	1.2	1.2	3.5	1.2	1.4	3.0	-1.0	1.7	0.9	1.9	2.4	4.6
CHAT	1.7	0.9	3.3	1.5	1.5	3.9	0.1	2.2	0.8	1.8	-0.5	5.1
HOB2	0.9	1.0	5.1	1.6	1.6	2.4	0.1	1.8	-0.2	1.9	-1.0	5.7
TIDB	0.8	1.2	3.1	1.0	1.2	3.5	-1.2	1.3	3.0	1.7	3.4	4.7
WGTM	1.5	2.3	5.2	2.1	1.5	5.3	-1.2	2.6	1.2	2.7	2.6	7.4
Average	1.2	1.3	4.0	1.5	1.4	3.6	0.7	1.9	1.2	2.0	2.0	5.5

2011 IGS Data Coordinate Solution Repeatabilities and Differences

<i>Stn</i>	<i>APREF E</i> $\pm\sigma$	<i>APREF N</i> $\pm\sigma$	<i>APREF H</i> $\pm\sigma$	<i>APPS E</i> $\pm\sigma$	<i>APPS N</i> $\pm\sigma$	<i>APPS H</i> $\pm\sigma$	ΔE	$\pm\sigma$	ΔN	$\pm\sigma$	ΔH	$\pm\sigma$
AUCK	1.2	1.5	4.0	1.8	2.8	4.2	1.0	2.2	-3.8	3.2	3.6	5.8
CHAT	1.1	1.9	4.7	1.9	2.6	3.2	-2.5	2.2	-2.1	3.2	-3.3	5.7
HOB2	1.2	1.6	4.8	2.8	3.1	4.4	-1.1	3.1	-4.4	3.4	-2.4	6.5
TIDB	1.5	2.5	4.5	2.4	3.1	5.4	-2.1	2.8	-4.2	4.0	-1.8	7.0
WGTM	1.0	1.0	1.0	2.4	3.2	5.1	-0.4	2.6	-2.0	3.4	4.9	5.2
Average	1.2	1.7	3.8	2.3	2.9	4.5	1.4	2.6	3.3	3.4	3.2	6.0

Table 3.5 – Final coordinate solution repeatabilities, coordinate differences and their uncertainties for selected regional IGS stations. *Column order for 2011 to 2005 is as follows:* Campaign year, APREF easting repeatability, northing repeatability and height repeatability respectively, JPL APPS easting repeatability, northing repeatability and height repeatability respectively, easting difference (ΔE), northing difference (ΔN) and its uncertainty and height difference (ΔH) and its uncertainty. *Column order for 2000 is as follows:* Campaign year, ITRF easting and repeatability, northing and repeatability, height and repeatability, respectively, all remaining columns are the same as 2011 to 2005 columns. All units are in mm.

2000 Campaign Data Coordinate Solution Repeatabilities

<i>Stn</i>	<i>Total Obs. Time</i>	<i>Bernese E ±σ</i>	<i>Bernese N ±σ</i>	<i>Bernese H ±σ</i>	<i>APPS E ±σ</i>	<i>APPS N ±σ</i>	<i>APPS H ±σ</i>
1291	45.1750	2.7	0.1	7.0	2.5	1.2	3.5
2308	66.0991	1.5	1.0	1.7	0.6	1.2	3.6
2309	46.7494	0.9	1.7	2.0	2.3	1.5	0.3
2313	69.4167	1.3	1.4	2.0	0.8	0.8	6.5
2318	44.2084	0.4	2.2	3.3	2.5	1.6	4.6
2344	42.6917	1.2	0.5	1.9	0.8	1.3	2.8
2348	44.9750	3.0	0.9	4.8	0.6	1.2	1.0
2351	47.8744	0.4	1.5	3.3	1.1	2.3	0.8
2383	44.9083	2.0	2.1	4.5	0.9	0.3	0.1
2405	35.4833	0.1	2.7	4.6	1.6	0.8	4.7
3002	44.7344	1.3	1.2	3.9	0.2	3.5	8.8
3006	43.7417	2.7	1.9	2.9	0.2	1.7	1.1
3051	327.233	3.6	8.3	4.1	3.4	8.1	7.4
3052	45.7911	0.7	0.7	1.6	1.1	0.4	3.7
3056	45.1083	0.9	0.3	0.7	0.3	1.1	2.7
3061	44.9917	0.8	0.7	1.7	1.1	0.4	4.0
3063	42.8245	1.3	0.8	2.4	2.1	2.0	6.5
3066	47.9494	0.4	0.7	4.9	0.8	2.9	13.3
3067	42.7917	2.9	1.5	1.5	2.0	0.8	8.7
3077	42.4084	1.4	1.2	2.1	1.4	0.8	1.8
3078	64.2992	1.6	1.5	2.4	0.1	2.3	1.4
3079	44.1167	1.4	2.0	1.8	1.5	1.3	6.0
3080	421.814	1.4	1.3	3.3	4.3	8.1	9.5
3093	43.8917	0.7	0.6	4.2	1.3	1.3	9.6
A7LF	44.5250	0.1	2.9	7.6	0.5	3.3	0.1
A7LJ	47.9417	0.4	1.9	2.5	1.3	2.7	3.3
A86L	45.2745	0.7	1.2	2.5	2.6	0.2	3.0
A88H	43.3833	1.8	1.9	5.1	1.1	0.3	2.4
B26Q	44.8833	2.6	0.4	1.1	1.1	0.9	7.4
BET2	43.5645	1.1	0.6	0.5	0.9	2.0	3.3
BEVJ	362.092	1.7	1.9	8.4	3.9	6.7	4.8
CBWR	42.1333	0.4	2.8	4.0	1.1	4.2	4.5
CBWU	68.3500	1.1	0.2	0.9	1.0	0.7	8.0
CBWV	39.0334	1.3	2.4	11.2	0.6	1.4	2.6
CBWW	41.8334	1.2	1.8	3.7	0.7	1.6	1.3
Average		1.4	1.6	3.4	1.4	2.0	4.4

Table 3.6 – 2000 Bernese and APPS campaign data coordinate solution repeatabilities. *Column order is as follows:* Station name, Total observation time (hours), Bernese easting repeatability, northing repeatability and height repeatability, respectively, JPL APPS easting repeatability, northing repeatability and height repeatability respectively. All units are in mm.

2005 Campaign Data Coordinate Solution Repeatabilities

<i>Stn</i>	<i>Total Obs. Time</i>	<i>Bernese E ±σ</i>	<i>Bernese N ±σ</i>	<i>Bernese H ±σ</i>	<i>APPS E ±σ</i>	<i>APPS N ±σ</i>	<i>APPS H ±σ</i>
1291	47.9344	0.6	1.0	6.1	2.1	0.0	2.8
2308	46.3411	1.6	1.3	1.9	0.0	3.5	6.4
2309	43.7664	1.5	0.5	5.7	1.4	4.2	9.1
2313	47.9334	0.4	0.3	4.1	1.4	1.4	3.5
2318	41.9744	0.2	0.5	4.2	5.0	3.5	19.1
2344	50.3333	0.9	2.1	2.1	4.0	5.3	12.9
2348	47.9334	0.4	2.6	1.8	3.5	0.0	0.7
2350	45.9911	0.9	1.4	7.7	0.7	0.7	13.0
2382	68.8659	0.4	1.5	2.8	2.8	0.7	0.0
2383	43.7083	0.3	0.7	5.0	2.1	2.8	5.0
3002	71.2575	0.3	0.2	0.4	5.1	0.6	2.9
3006	42.6666	0.4	0.7	4.5	3.5	7.1	2.1
3051	59.6917	0.5	1.0	4.8	2.6	6.4	12.2
3056	41.7666	0.6	1.3	4.4	0.0	0.0	5.7
3061	45.6244	1.5	0.8	5.1	5.7	4.2	5.0
3063	45.0328	1.7	1.1	6.9	5.7	5.0	0.7
3067	46.5911	1.7	0.6	6.7	4.2	2.8	10.6
3077	46.2667	1.4	1.3	4.1	4.2	2.1	7.1
3078	44.0417	0.3	0.6	3.2	0.7	1.4	2.8
3079	45.0083	2.5	0.9	5.2	2.8	0.0	5.7
3081	47.9666	1.5	0.6	5.5	0.0	0.7	6.4
3093	44.1417	2.0	3.3	13.1	1.4	2.1	5.0
3094	41.9250	0.9	1.4	0.8	1.4	1.4	3.5
A7LF	41.9500	0.6	1.2	5.3	1.4	2.1	4.2
A7LJ	45.7167	1.4	2.7	1.8	2.1	1.4	3.5
A86L	47.0161	0.9	0.5	2.7	0.0	0.7	4.2
A88G	45.2828	1.8	0.9	2.6	1.4	2.1	2.8
A88H	43.6662	2.1	0.8	0.8	36.8	12.7	10.6
A9BM	42.3578	0.5	0.9	4.2	1.7	0.0	3.5
B26Q	45.3916	0.6	0.9	1.8	0.0	1.4	3.5
B4DP	45.4245	0.4	0.9	1.6	0.0	1.4	1.4
CBWR	43.9584	1.4	0.2	0.9	7.1	11.3	0.7
CBWU	69.8749	2.1	4.0	5.2	3.5	0.6	5.3
CBWV	44.4667	2.6	2.0	9.8	2.0	0.6	10.8
CBWW	47.9500	0.8	4.3	4.0	5.7	0.7	5.0
Average		1.0	1.2	3.7	2.9	2.2	5.5

Table 3.7 – 2005 Bernese and APPS campaign data coordinate solution repeatabilities. *Column order is as follows:* Station name, Total observation time (hours), Bernese easting repeatability, northing repeatability and height repeatability, respectively, JPL APPS easting repeatability, northing repeatability and height repeatability respectively. All units are in mm.

2007 Campaign Data Coordinate Solution Repeatabilities

<i>Stn</i>	<i>Total Obs. Time</i>	<i>Bernese E ±σ</i>	<i>Bernese N ±σ</i>	<i>Bernese H ±σ</i>	<i>APPS E ±σ</i>	<i>APPS N ±σ</i>	<i>APPS H ±σ</i>
1291	43.4250	0.4	0.6	7.4	0.1	0.8	5.1
2309	45.9250	0.7	0.7	1.9	1.8	0.1	0.1
2313	92.9667	2.1	0.9	2.6	2.5	1.7	5.3
2318	44.9750	1.2	0.3	3.4	1.1	2.3	2.8
2344	42.1583	0.9	0.2	1.4	3.0	0.1	6.6
2348	42.9333	0.7	0.6	3.1	1.0	2.1	5.7
2350	41.5667	1.6	0.4	7.5	2.3	2.8	13.1
2351	47.9500	0.8	0.6	2.0	0.7	0.3	0.4
2382	45.6833	0.6	1.2	5.8	0.2	1.1	7.8
2383	43.2750	0.2	0.6	2.0	0.4	0.9	5.7
2401	93.2166	1.6	1.5	2.3	1.0	0.8	2.5
3002	44.5416	0.8	0.1	2.2	2.1	1.0	4.4
3006	42.1750	0.9	0.5	2.4	2.1	0.2	0.7
3051	44.3083	1.0	0.5	3.5	1.3	0.6	2.1
3052	47.9500	0.8	0.6	2.8	0.1	1.3	2.3
3056	47.4250	0.8	0.7	2.0	0.1	1.3	1.1
3061	42.9583	1.5	1.1	2.9	1.4	1.8	3.5
3063	42.3000	0.7	0.8	1.5	2.4	0.0	0.9
3066	45.6500	0.7	0.6	1.5	1.3	0.2	0.0
3067	46.2000	0.7	0.5	2.2	0.0	0.9	0.4
3077	47.9500	1.1	0.2	5.2	2.1	1.2	6.4
3078	47.9666	1.0	0.6	5.8	2.3	1.8	7.3
3079	46.8916	1.1	0.3	6.2	2.8	2.3	8.8
3080	42.4417	0.8	0.6	1.6	2.9	0.5	1.8
3081	43.0917	1.4	0.3	6.1	1.1	0.8	12.2
3093	40.5333	1.8	0.4	3.0	2.3	3.7	6.7
3094	45.0583	0.7	0.4	2.0	0.4	0.5	3.4
6881	44.2917	2.9	2.0	1.5	1.8	2.4	1.3
A4K6	42.7667	1.1	0.9	4.5	0.0	2.4	5.1
A7LF	44.9083	0.4	0.5	1.1	1.4	1.1	6.0
A7LJ	44.8250	0.9	0.5	1.9	0.2	0.6	3.7
A86L	42.3250	0.6	0.3	5.8	1.7	0.1	6.9
A86T	67.0583	1.4	0.3	2.3	0.9	1.0	1.0
A86W	47.8417	2.4	0.3	2.3	0.4	1.6	0.6
A87P	45.6500	2.2	0.8	5.8	0.2	1.0	2.3
A886	68.2083	1.9	0.3	4.4	1.5	0.0	1.8
A88G	45.6584	1.3	0.6	8.3	2.5	2.0	11.1
A88H	43.5834	1.1	0.3	7.0	0.4	2.3	9.6
A9BM	44.3750	0.8	1.4	0.6	0.4	0.5	7.4
AGB9	44.0417	1.5	1.0	1.8	0.0	0.9	0.3
AGUG	41.4917	0.3	0.5	1.5	0.4	0.2	1.2
B26Q	43.4083	0.7	2.1	3.3	0.4	3.0	6.4
B4DP	46.1334	0.9	1.6	6.5	0.4	0.2	1.4
B4HJ	17.3833	1.0	0.2	5.5	2.1	9.2	23.0
BE2T	45.3333	0.4	1.6	14.1	0.5	0.8	19.7
BEVJ	43.8416	0.9	0.4	3.2	2.0	0.1	5.7
CBWR	42.9084	0.6	1.1	9.5	1.9	2.3	15.9
CBWU	43.2666	1.4	1.0	3.3	0.1	0.4	7.5
CBWV	43.7417	1.8	0.8	5.2	0.1	1.9	3.4
CBWW	44.9083	0.8	0.7	3.7	1.2	0.1	3.3
E4MH	70.5667	1.7	0.6	4.0	1.2	0.3	1.7
EAXX	40.6750	0.2	0.8	3.0	0.1	1.0	1.5
EAXY	45.8416	0.7	1.3	1.5	1.1	0.8	2.8
Average		1.1	0.7	3.8	1.2	1.3	5.0

Table 3.8 – 2007 Bernese and APPS campaign data coordinate solution repeatabilities. *Column order is as follows:* Station name, Total observation time (hours), Bernese easting repeatability, northing repeatability and height repeatability, respectively, JPL APPS easting repeatability, northing repeatability and height repeatability respectively. All units are in mm.

2011 Campaign Data Coordinate Solution Repeatabilities

<i>Sta</i>	<i>Total Obs. Time</i>	<i>Bernese E ±σ</i>	<i>Bernese N ±σ</i>	<i>Bernese H ±σ</i>	<i>APPS E ±σ</i>	<i>APPS N ±σ</i>	<i>APPS H ±σ</i>
1291	45.5833	2.3	2.9	2.8	1.3	1.8	7.3
2308	44.4333	0.2	0.1	3.5	1.1	2.0	2.8
2309	45.6500	0.7	2.1	2.6	3.7	4.7	3.4
2313	44.6500	0.7	0.7	3.4	0.9	1.1	2.3
2318	44.7667	1.0	2.6	5.2	1.6	0.3	19.4
2344	45.0000	1.3	0.3	4.3	0.0	1.4	5.6
2348	26.4500	2.8	2.6	3.7	3.0	0.2	3.2
2350	42.8666	1.1	0.9	6.9	2.1	3.5	9.8
2351	44.7584	1.0	0.4	12.4	1.1	1.7	25.8
2382	47.9666	0.4	0.5	2.6	1.1	1.4	1.1
2383	45.3583	1.3	1.0	1.2	0.8	0.4	3.0
3002	43.8917	1.0	1.3	5.9	0.8	1.4	4.3
3006	44.2250	2.4	1.5	3.1	0.3	0.8	7.1
3051	45.2000	0.7	2.3	4.3	2.4	0.3	1.0
3052	46.3000	0.8	1.5	0.6	1.1	0.6	1.2
3056	46.0083	1.0	1.7	11.4	1.5	0.6	8.0
3061	45.6833	0.6	0.8	2.9	0.2	1.2	0.7
3063	44.9666	1.0	0.7	3.7	1.5	2.0	7.1
3066	44.5833	0.9	0.5	3.4	1.2	2.0	11.6
3067	44.6416	0.4	1.3	7.9	0.8	0.3	6.9
3077	46.1666	1.4	0.8	4.5	1.3	0.8	13.4
3078	44.4500	0.6	0.1	3.3	0.3	2.0	6.6
3079	46.4500	0.6	0.2	3.3	0.4	2.0	3.7
3080	44.5750	2.0	0.6	7.0	2.1	2.1	16.9
3081	43.6333	0.8	1.7	4.5	1.3	1.8	0.2
3093	41.2583	0.1	2.8	5.5	8.1	3.4	11.7
3094	42.0083	0.9	2.3	17.8	0.9	1.6	4.7
6881	44.5167	0.8	0.4	3.1	0.4	1.0	1.1
A4K6	47.4750	1.1	0.1	4.3	1.8	0.8	4.3
A7LF	46.4583	0.1	1.1	3.4	0.8	0.7	0.3
A7LJ	43.9250	0.9	1.5	1.3	1.8	0.3	3.2
A86L	44.3416	2.6	1.9	5.6	3.5	7.3	0.4
A86T	47.9666	0.5	1.2	2.2	0.2	1.3	1.3
A86W	44.4333	0.4	1.0	3.8	1.8	3.3	2.8
A87P	42.6750	1.7	0.3	7.3	0.8	3.6	1.2
A886	44.9334	1.3	1.8	5.5	2.9	6.1	0.1
A88G	46.0083	1.8	0.6	8.1	0.8	0.4	5.8
A88H	45.9666	1.1	0.7	6.6	0.4	1.1	4.7
A9BM	44.1750	0.8	1.7	1.8	4.0	4.9	2.1
AGB9	44.3750	1.0	2.2	2.3	0.1	1.7	2.9
AGUG	43.8000	0.4	0.6	6.0	4.3	2.1	3.8
AH9J	45.2000	2.0	0.8	6.3	1.6	4.2	1.9
B26Q	40.6167	0.4	1.7	5.3	1.0	2.3	0.3
B4DP	44.4750	0.3	0.2	6.4	0.1	1.3	7.4
B4HJ	14.6000	1.0	0.3	2.2	1.2	1.1	7.6
BE2T	44.0167	0.8	1.6	6.3	0.1	2.1	3.2
BEVJ	44.0250	1.0	0.7	4.0	0.1	1.0	4.7
CBWR	44.0833	0.7	0.8	6.0	0.9	1.5	0.6
CBWU	43.6083	0.2	0.7	1.3	2.0	1.0	3.3
CBWV	44.8000	0.7	0.8	5.0	2.1	1.6	8.2
CBWW	45.0666	0.7	1.1	2.2	0.1	0.4	0.9
E4MH	43.7083	0.9	0.5	5.0	0.8	0.8	2.5
EAXX	45.9250	2.0	0.4	4.6	0.6	3.0	1.8
EAXY	42.4833	0.6	1.1	2.5	3.2	6.8	3.7
Average		1.0	1.1	4.7	1.4	1.9	5.0

Table 3.9 – 2011 Bernese and APPS campaign data coordinate solution repeatabilities. *Column order is as follows:* Station name, Total observation time (hours), Bernese easting repeatability, northing repeatability and height repeatability, respectively, JPL APPS easting repeatability, northing repeatability and height repeatability respectively. All units are in mm.

4 Ground deformation patterns associated with volcanic processes at the Okataina Volcanic Centre.

L. Holden¹, R. Cas¹, N. Fournier², L. Ailleres¹,

¹*Monash University, School of Earth, Atmosphere & Environment, Melbourne, Victoria, Australia*

²*GNS Science, New Zealand,*

Corresponding Author: lucas.holden@monash.edu

**PUBLISHED IN: JOURNAL OF VOLCANOLOGY AND GEOTHERMAL
RESEARCH (UPCOMING SPECIAL EDITION – MEASURING CHANGES ON
VOLCANOES USING GEODESY)**

ONLINE PUBLICATION DATE (20-MAY-2017)

doi:10.1016/j.jvolgeores.2017.04.014

Citation: Holden, L., Cas, R., Fournier, N., Ailleres, L., Modelling ground deformation patterns associated with volcanic processes at the Okataina Volcanic Centre, Journal of Volcanology and Geophysical Research, 2017. doi: 10.1016/j.jvolgeores.2017.04.014

4.1 Abstract

The Okataina Volcanic Centre (OVC) is one of two large active rhyolite centres in the modern Taupo Volcanic Zone (TVZ) in the North Island of New Zealand. It is located in a complex section of the Taupo Rift, a tectonically active section of the TVZ. The most recent volcanic unrest at the OVC includes the ~AD1315 Kaharoa and 1886 Tarawera eruptions. Current monitoring activity at the OVC includes the use of continuous GPS receivers (cGPS), lake levelling and seismographs. The ground deformation patterns preceding volcanic activity the OVC are poorly constrained and restricted to predictions from basic modelling and comparison to other volcanoes worldwide. A better understanding of the deformation patterns preceding renewed volcanic activity is essential to determine if observed deformation is related to volcanic, tectonic or hydrothermal processes. Such an understanding also means that the ability of the present day cGPS network to detect these deformation patterns can also be assessed.

The research presented here uses the finite element (FE) modelling technique to investigate ground deformation patterns associated with magma accumulation and diking processes at the OVC in greater detail. A number of FE models are produced and tested using Pylith software and incorporate characteristics of the ~1315 AD Kaharoa and 1886 Tarawera eruptions, summarised from the existing body of research literature. The influence of a simple ring fault structure at the OVC on the modelled deformation is evaluated. The ability of the present-day continuous GPS (cGPS) GeoNet monitoring network to detect or observe the modelled deformation is also considered. The results show the modelled horizontal and vertical displacement fields have a number of key features, which include prominent lobe based regions extending northwest and southeast of the OVC. The results also show that the ring fault structure increases the magnitude of the displacements inside the caldera, in particular in the vicinity of the southern margin. As a result, some of the cGPS stations in the vicinity of the OVC are more important for measuring deformation related to volcanic processes than others. The results have important implications for how any future observed deformation at the OVC is observed and interpreted.

4.2 Introduction

Large calderas must be continually monitored for time-dependent ground deformation to estimate magma chamber pressurization and assess their eruption potential (Galgana et al., 2014). However, the very long repose periods between eruptions at large calderas mean that the opportunity to directly observe deformation preceding volcanic unrest is limited. This means that at present there is also a limited understanding of precursory geophysical signals leading to major events (Ellis et al., 2007). This restricts the ability to

distinguish subtle precursory volcanic signals from local hydrothermal and regional tectonic signals (Cabral-Cano et al., 2008; Fournier and Chardot, 2012).

Numerical models can be used to forward model changes in the volcano system and simulate the resulting surface deformation field. For ‘simple’ sources, such as a magmatic dike or magma reservoir, analytical models, (e.g. Mogi, 1958; Okada, 1985, 1992; Mctigue, 1987), can be used. However, many volcano systems (particularly large calderas) are typically, 1) located in complicated rift settings, 2) co-located with active and energetic hydrothermal systems, and 3) have complex three dimensional structure (e.g. fracture systems linked to caldera collapse or complex layered crustal rheology). As a result the deformation field may be affected in an unpredictable way (DeNatale and Pingue, 1993; Bonaccorso et al., 2005) and differ from that modelled by analytical techniques. More flexible numerical techniques, such as the Finite Element (FE) technique are required to reflect this complexity.

Studies utilising the FE technique are diverse and include investigations of the influence of topography and heterogeneous rock properties on volcanic deformation (Trasatti et al., 2003; Bonaccorso et al., 2005; Manconi et al., 2007; Currenti et al., 2008, 2010; Long and Grosfils, 2009; Geyer and Gottsmann, 2010; Rochin et al., 2013), the presence of caldera boundary discontinuities (De Natale et al., 1997; Beauducel et al., 2004; Folch and Gottsmann, 2006), the relationship between hydrothermal activity and deformation (Todesco, 2009; Rinaldi et al., 2010; Rinaldi et al., 2011; Fournier and Chardot, 2012) and thermo-mechanical modelling (Hickey et al., 2015), to list a few examples. By simulating ground deformation, the FE technique can also be used to assess the ability of any in-situ continuous GPS (cGPS) network to observe or detect various magma system changes, such as dike intrusion at depth or chamber pressurization. This is also important to develop a monitoring network with a spatial resolution that is capable of distinguishing natural and anthropogenic sources of surface deformation (Eff-Darwich et al., 2008). However, studies that have applied this concept to real world volcano-monitoring using cGPS networks and/or other geodetic techniques (e.g. Fernández et al., 1999; Yu et al., 2000; Charco et al., 2007) are limited.

The Okataina Volcanic Centre (OVC) is one of two large active rhyolite centres in the modern Taupo rift, a tectonically active section of the TVZ (see Figure 4.1) in the North Island of New Zealand. Magma supply is considered plentiful in this part of the rift and has been linked to large-scale deformation patterns and variations in rift architecture (Rowland et al., 2010; Ellis et al., 2014; Hamling et al., 2015). The most recent volcanic unrest at the OVC includes the ~1315 CE Kaharoa and 1886 Tarawera eruptions, in which dike intrusion was a key eruption mechanism (Nairn and Cole, 1981; Sherburn and Nairn, 2001; Nairn et al., 2004, 2005). The OVC is presently monitored using continuous GPS (cGPS), seismographs and lake levelling

instrumentation. Surface deformation has been observed across the OVC (Scott, 1989; Hamling et al., 2015; Holden et al., 2015), however there is no clear evidence that it is linked to renewed volcanic unrest. Rather, studies indicate a relationship to large-scale magmatic and rifting processes (Ellis et al., 2014; Hamling et al., 2015; Holden et al., 2015).

As a result, the ground deformation patterns preceding volcanic activity at the OVC are poorly constrained and have only been considered in few studies (Sherburn and Nairn, 2001, 2004). Sherburn and Nairn, (2004) highlight that an outstanding problem at the OVC is whether magma bodies could exist or accumulate at depth without being detected using modern geophysical techniques. The aim of this research is to investigate (forward model) the hypothetical ground deformation patterns that might result as a result of volcanic activity at the OVC. The research presented here has followed the direction undertaken by Yu et al., (2000) who used analytical modelling (Okada, 1985, 1992) to consider the detection capabilities of the GPS monitoring network at Las Canadas caldera in Tenerife, published in this journal. Specifically, two research questions are addressed. These include 1) what are the key characteristics of the modelled surface deformation patterns, and 2) whether magma bodies could exist or accumulate at depth below the OVC without being detected by the existing cGPS monitoring network. The results of this study will have important implications for how any future observed deformation within the cGPS network at the OVC is interpreted.

4.3 Regional Geological Setting

The Taupo rift is a region of active tectonic extension (Darby et al., 2000; Wallace et al., 2004, Holden et al., 2015), high heat flow and magmatism (Bibby et al., 1995), and is one of the most productive regions of rhyolitic volcanism in the world (Wilson et al., 1995). Volcanism in this part of the rift is predominantly rhyolitic and the abundant magma supply is considered jointly responsible (alongside passive rifting processes) for deformation patterns and rift structure (Wallace et al., 2004; Rowland et al; 2010; Ellis et al., 2014; Hamling et al., 2015). The rift is divided into discrete segments with variable extension rates and styles (Rowland and Sibson, 2001; Acocella et al., 2003; Rowland et al., 2010). The OVC is located in the Okataina segment (see Figure 4.1 and Figure 4.2), which is considered to be either a structurally complex transfer zone related to local strain adjustment (Acocella et al., 2003; Cole and Spinks, 2009; Cole et al., 2010) or an accommodation zone that reflects stress field heterogeneity (Rowland and Sibson, 2001; Rowland et al., 2010). Extension rates across this part of the Taupo rift have been estimated using GPS data as between 10 to 12mm/yr⁻¹ (Wallace et al., 2004; Holden et al., 2015). Recent modelling by Ellis et al., (2014) and Hamling et al., (2015) suggests that localised magma intrusion and/or magma cooling may be responsible for change in rift structure and deformation patterns just south and outside of the OVC.

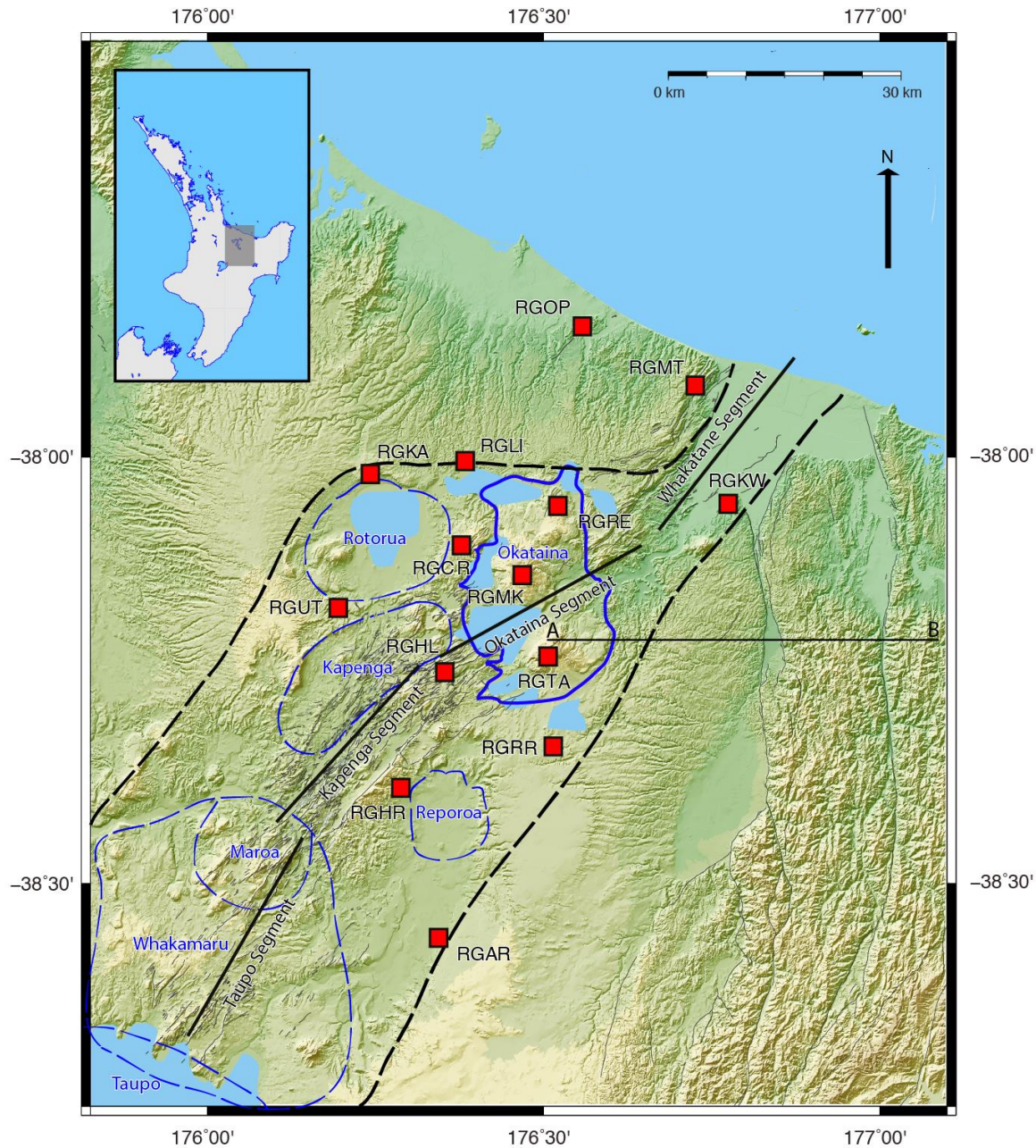


Figure 4.1 – Regional geological setting and location and distribution of all GPS stations used in this study. Locations of major TVZ calderas (from Spinks et al., 2005) are shown as blue dashed lines and their boundary locations are approximate. The Okataina Volcanic Centre (OVC) is shown as bold blue line. Modern TVZ boundaries are shown as dashed black lines from Cole (1990) and are approximate. GeoNet cGPS stations are shown as red squares. Rift segments are from Acocella et al., (2003) and shown approximately as solid black lines and labelled in the figure. The inset at the upper left shows the approximate location of the study area. The line A-B represents the profile used for later plots of modelled horizontal and vertical displacements.

4.4 The Okataina Volcanic Centre

The OVC is a 28 x 15 km rectangular caldera structure (with an eccentricity of 0.54), whose long axis trends roughly perpendicular to the Okataina segment axis (Spinks et al., 2005) (see Figure 4.2). It consists of overlapping and nested caldera structures filled with post-caldera rhyolites, which includes the larger Haroharo caldera, containing the Haroharo and Tarawera volcanic complexes (Nairn, 2002). Eruptive vents post 25ka are well mapped and define two broad linear zones; the Tarawera and Haroharo linear vent zones (Nairn, 2002). These lineations are roughly axial to the adjacent Whakatane and Kapenga segments and considered to mark their continuation into the Okataina area (Spinks et al., 2005).

Regional fault structures have strongly influenced OVC caldera structure (Cole et al., 2010; Seebeck et al., 2010). Gravity observations show that the north-west and south-east structural boundaries are controlled by normal rift faults (dip 55 to 75°), while the east and west boundaries are defined by near vertical north-south striking faults (dip 70 to 90°) (Seebeck et al., 2010). Other studies indicate that the depth of the collapse structure beneath the caldera is approximately 3 to 4 km and filled with volcanoclastic materials, underlain by a highly fractured greywacke basement (Bibby et al., 1995; Sherburn et al., 2003; Heise et al., 2007; Seebeck et al., 2010).

The OVC has erupted $\sim 80\text{km}^3$ of rhyolitic magma in the last 21ka (Nairn, 2002). An average recurrence interval between eruptions (2200 years) and average eruption rate of (0.004km^3) over this period relates to a chamber volume of 2000 km^3 (Jellinak and DePaulo, 2003). However, post caldera eruptions at the OVC are not considered to come from a single large magma chamber, but rather from diverse small to moderate magma sources (Charlier and Wilson, 2010). Most of these rhyolite magma bodies form at depths between 8 to 5 km beneath the Tarawera and Haroharo complexes (Villamor et al., 2011).

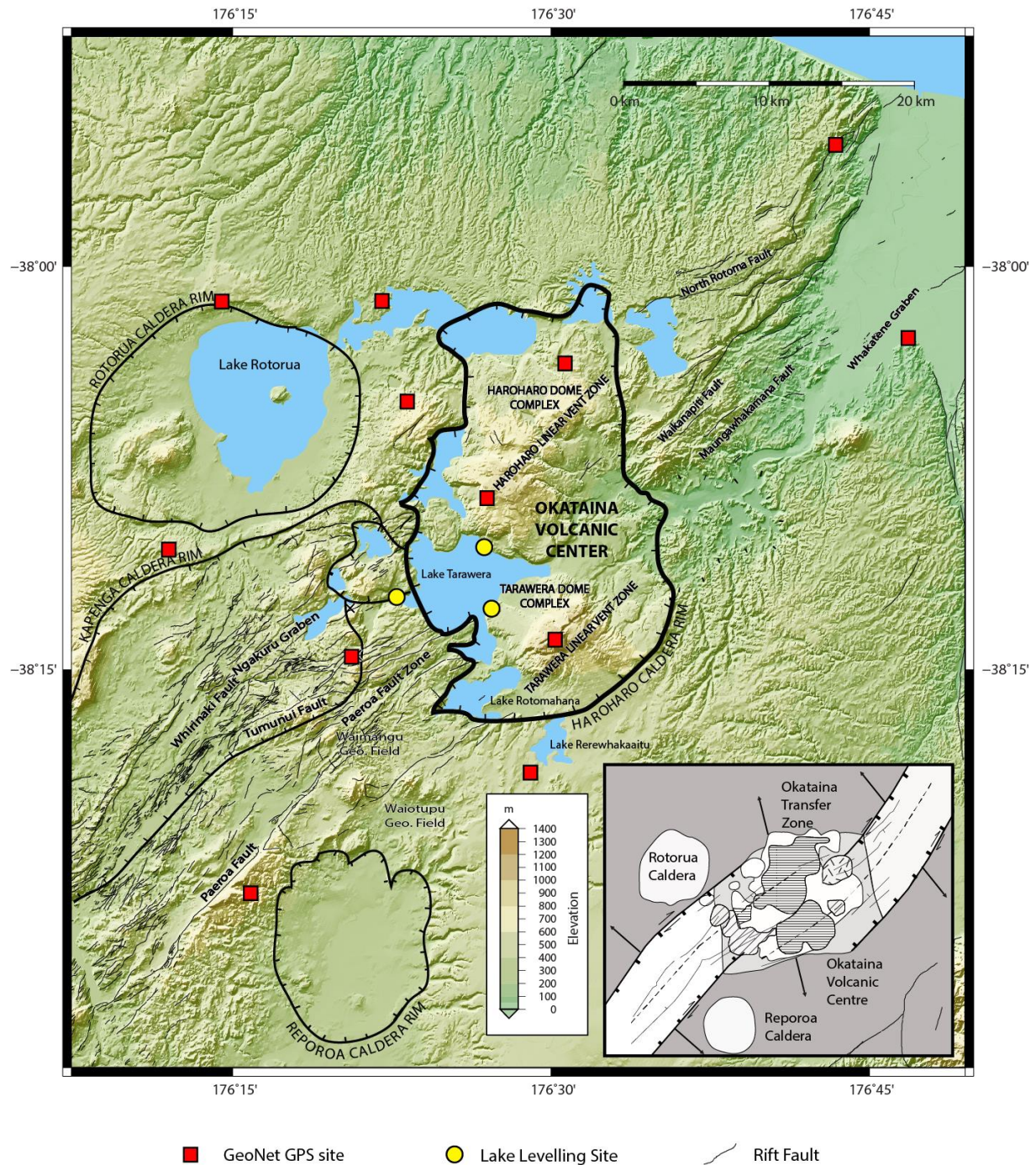


Figure 4.2 – Location map and structural details of the Okataina Volcanic Centre (OVC) from Nairn (2002). Caldera boundary locations are shown as black lines and from Spinks et al., (2005). Bottom right inset shows interaction of the Okataina rift segment and OVC with the neighbouring Kapenga and Whakatane rift segments from Cole et al., (2010). Locations of lake levelling sites are approximate and from Sherburn and Nairn, (2001). Rift faults from the GNS Science Active Faults Database.

4.4.1 Recent eruptive activity

Volcanic activity within the last 26ka has been linked to post-caldera rhyolitic dome building (Cole et al., 2010), primarily along the Tarawera and Haroharo linear vent zones (Nairn, 2002). Recent activity includes the ~AD 1315 Kaharoa rhyolite ($>5\text{km}^3$) and 1886 Tarawera basalt dike eruptions (Nairn, 2002). The Kaharoa eruption was primed and triggered by multiple basalt intrusions into an existing stratified rhyolitic magma body (Leonard et al., 2002; Nairn, 2002; Sherburn and Nairn, 2004). Nairn et al., (2004) propose that the pre-eruptive Kaharoa stratified magma body was 8km long, 1 km wide and 1.4 km high. Sherburn and Nairn (2001, 2004) indicate that the Kaharoa dike may have been 10m wide and may have reached the ground surface within four days. The 1886 CE Tarawera event involved the intrusion and eruption of en-echelon series of basalt dikes originally occurring within the Tarawera Rift, but shortly then after extending southwest into Lake Rotomahana (Nairn, 2002). Studies of exposed dike outcrops indicate that the average dike width along this length was 2m (Nairn and Cole, 1981).

4.4.2 Contemporary deformation at the OVC

Ground deformation at the OVC is monitored using various geodetic data by GNS Science (www.geonet.org.nz). Historically, this has included a horizontal strain network at both Lake Rotomahana and Tarawera rift summit (Scott, 1989; Sherburn and Nairn 2001). Today, monitoring of ground deformation is primarily achieved using a network of cGPS receivers within and around the caldera (see Figure 4.2). Three water level recorders are also situated on the east, west and north shores of Lake Tarawera (see Figure 4.2). Regional InSAR studies through the Taupo Rift (Samsonov et al., 2011; Hamling et al., 2015) have also provided some insight into vertical deformation in the OVC region.

These studies have identified significant deformation at the OVC (Scott, 1989; Hamling et al., 2015; Holden et al., 2015). Scott (1989) measured a regional tilt (0.9 micro radians per year at an azimuth of 72°) and shear strain and dilation across the strain networks. Using campaign and cGPS GNSS data, Holden et al., (2015) identified very large subsidence rates (up to 18 mm/yr^{-1}) in the south and south-western parts of the OVC caldera, and significant extension strain rates and shear strain rates in the vicinity of the Tarawera Rift. Large subsidence rates were identified using InSAR and cGPS through the central Taupo Rift (Hamling et al., 2015), including the OVC. There is no clear evidence that deformation is linked to volcanic unrest at the OVC. Rather, FE modelling by Hamling et al., (2015) links the large regional subsidence rates to cooling and deflation of large-scale magma body below the Taupo rift and TVZ. While Ellis et al., (2014), link strain rate heterogeneity at the south-west OVC boundary to a large accumulation of partial melt in this vicinity.

4.4.3 Previous FE modelling at the OVC

The FE technique has been applied in other studies for other locations in the TVZ, including Taupo caldera (Ellis et al., 2007; Peltier et al., 2009a), White Island volcano (Peltier et al., 2009b; Fournier and Chardot, 2012), as well as regionally (Hamling et al., 2015, 2016), but not specifically at the OVC. Sherburn and Nairn (2001, 2004) used the Mogi analytical model to predict ground deformation at the OVC. They model deformation related to a 1%, 5% and 15% volumetric increase in a 1.06 km spherical magma chamber at 6km depth. They conclude that the vertical deformation related to the 1% volumetric increase would be measureable across the lake levelling network, but if it were to occur at a steady rate across a number of years it would most likely be interpreted as tectonic in origin.

Sherburn and Nairn (2004), also consider the deformation field preceding a present day eruption similar to the Kaharoa 10m wide dike surface intrusion event. They consider that surface deformation linked to the rapidly increasing loss of magma at a deep reservoir would occur alongside deformation related to the dike intrusion at a shallower depth. As a result, they suggest that the total deformation signal would consist of a ‘deep, longer wavelength deflation signal, upon which was superimposed a shallow short wavelength inflation’. They then speculate that this would be detectable by the monitoring sites on the upper slopes of Mt. Tarawera (which would record uplift), but that more distant sites would observe subsidence due to deflation of the deeper magma source.

4.5 Materials and methods

4.5.1 FE Models

The FE modelling undertaken in this research builds on the results of Sherburn and Nairn (2001, 2004) and investigates in more detail the surface deformation patterns associated with hypothetical volcanic activity at the OVC. Using constraints from previous studies regarding the characteristics (e.g., source depth, chamber and dike dimensions etc.) of the Kaharoa and 1886 Tarawera eruptions, a number of FE models are constructed to forward model surface deformation. These incorporate a basic spherical magma chamber, a rectangular magma chamber and 1m wide dike.

The numerical computations are carried out using the Pylith software package (Williams et al., 2005; Williams, 2006; Aagaard et al., 2007, 2008). Pylith is an open source finite element code, available from the Computational Infrastructure for Geodynamics (CIG) organisation at <https://geodynamics.org>. Pylith allows

static and quasi-static crustal deformation modelling, and benchmarking results are presented in Aagaard et al., (2013a, 2013b). The application of Pylith for crustal deformation monitoring includes modelling co-seismic and post-seismic deformation (Hsu et al., 2011; Diao et al., 2014), fault rupture dynamics (Douilly et al., 2015), stress-strain and deformation at volcanoes (Nooner and Chadwick, 2009; Alparone et al., 2013) and rift diking events (Nooner et al., 2009), to list only a few examples.

Following initial benchmark testing of mesh and domain size, a 3D axisymmetric computational domain with dimensions of 200km x 200km x 100km depth was adopted. The very large domain size remains computationally efficient since a variable mesh resolution scheme was applied, in which the finest element size (approximately 50m) surrounds the deformation sources in the upper centre of the model and the largest elements are located at the domain boundaries away from the sources (see Figure 4.3). The elastic medium was considered to be uniform (homogeneous) in all cases, with a rigidity value of 30 GPa and Poisson ratio of 0.25. These values are in line with those adopted in other studies in the Taupo rift (Ellis et al., 2007; Peltier et al., 2009b). It is acknowledged that the inclusion of mechanical properties of different layers (including caldera infill) influences FE modelling results (e.g. Manconi et al., 2007; Geyer and Gottsmann, 2010). However, in this first attempt at modelling deformation using the FE technique in Pylith, this complexity is not addressed. Future research will incorporate this into the FE models, which may provide corrections on the results presented here.

Tetrahedral elements were used in the FE models in all cases. The average number of tetrahedral elements in the FE models is 215000. Zero horizontal and vertical Dirichlet boundary conditions were applied on the bottom and lateral faces of the domain. The upper surface was set as a free surface. The low (average) elevation topography across the OVC was not modelled on the free surface. Other studies have shown that relatively flat, smooth or low topography in relation to the source depth may not significantly influence the surface deformation field (Cayol and Cornet, 1998; Trassati et al., 2003; Newman et al., 2006; Galgana et al., 2014; Rochin et al., 2015).

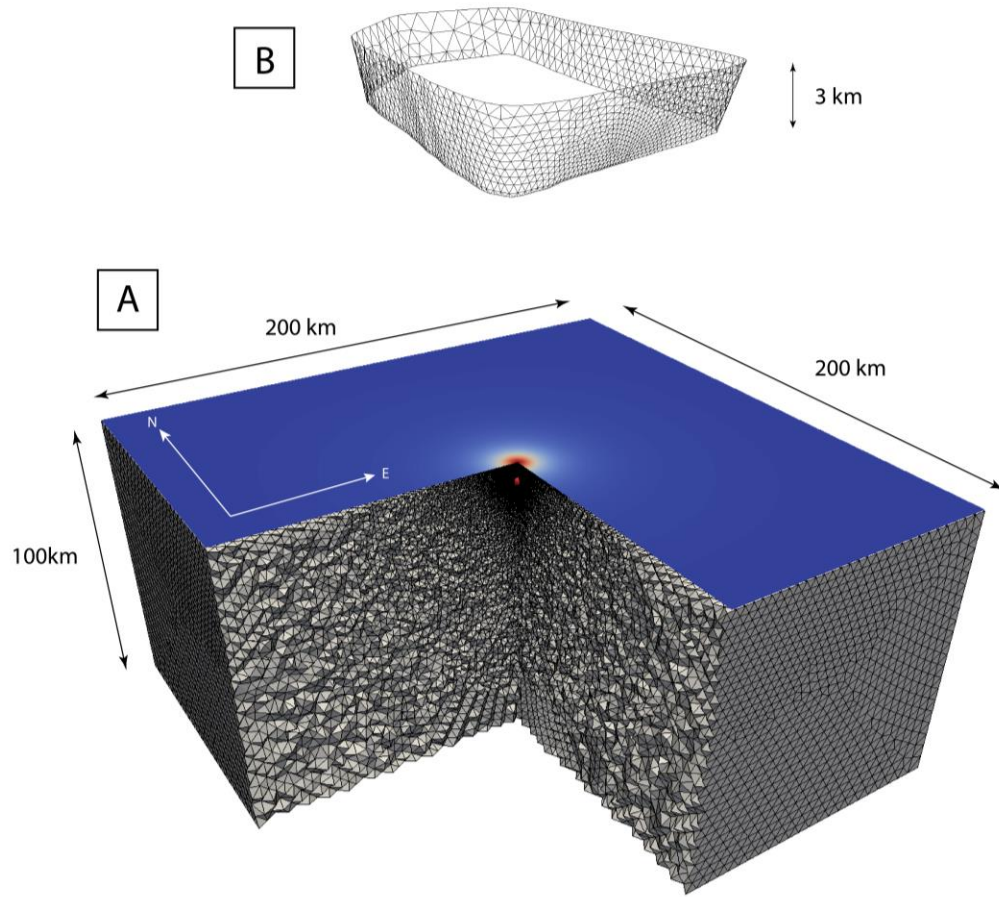


Figure 4.3 – A) Schematic 3D model of OVC ring fault structure used in the FE modelling (not to scale). Highest resolution cells are located around and above the various deformation sources at the centre of the domain. The domain size is 200km wide and 100km deep. B) Schematic 3D model of ring fault structure used in this research (see text for details). Note: dimensions are not to scale.

In Pylith, linear elastic equations are solved using the PETSc Krylov Solver Package (KSP) linear solver (Aagaard et al., 2013a). In the case of the spherical and rectangular magma chambers, ground deformation was assumed to follow 10 MPa overpressure, applied as a traction force on the chamber (Neumann boundary condition). This is considered sufficient to overcome the local overlying rock, which is considered to be 10-15 MPa at the nearby Taupo caldera (Rowland and Sibson, 2004; Ellis et al., 2007). In the case of the dike models, ground deformation was assumed to follow a 1m-dike intrusion. The McTigue (1987) and Okada (1985) analytical models were used to check the accuracy of the chamber and dike FE models respectively (see Figure 4.7A to Figure 4.7C in supplementary material A). These comparisons indicate the FE models have sufficient mesh resolutions to accurately estimate ground surface deformations in these instances.

Where possible, characteristics of the deformation sources (e.g. chamber and dike dimensions, depths and geometry etc.) were incorporated into the FE models using constraints from previous studies of the Kaharoa and 1886 Tarawera eruptions. For the spherical magma chambers, the radii tested are 1.38km and 1.06km. These correspond to the upper (11km^3) and lower (5km^3) magma chamber volume inferred to have existed prior to the Kaharoa eruption by Sherburn and Nairn (2004). The rectangular magma chamber has dimensions of 8km length, 1 km width and 1.4 km height. This matches the dimensions of the pre-Kaharoa chamber proposed by Nairn et al., (2004). The magma chambers were located at a depth of 6 km, following the modelling by Sherburn and Nairn (2001, 2004). This is representative of the estimated depth of the brittle/ductile layer in the vicinity of the OVC (Bibby et al., 1995; Bryan et al., 1999). In the FE models, the rectangular magma chamber was assumed to be directly below the Tarawera Rift.

The FE dike modelling was based on a vertical sheet of 8 km length and 1 km height with a leading vertical edge emplaced at 5km depth. An 8km length was adopted to match the length of the 8 km long rectangular magma chamber of Sherburn and Nairn (2001). It was assumed in this research that the dike body rises vertically above the roof of the magma chamber. The dike strikes at 57° north, which is aligned with mapped surface vents (Cole and Nairn, 1981), regional tectonic structure and is located directly below the Tarawera Rift.

4.5.2 FE ring fault structure

Acocella et al., (2003) note that the structure and shape of caldera collapse and resurgence may be controlled by existing caldera structure or rifting related structural discontinuities, such as normal faults. Nairn (1989) proposed the presence of such a structure or structures bounding the OVC, whose characteristics have been better constrained more recently using gravity and structural geology studies (Spinks et al., 2005; Seebeck et al., 2010; Cole et al., 2010). Utilising the major findings of these studies, a simple OVC ‘fracture system’ or ‘ring fault system’ was also included into the FE modelling (see Figure 4.3B), alongside the rectangular chamber and 1m wide dike geometries.

The geographic location of this feature in the FE models is based on the location of the inferred OVC caldera collapse geometry, presented in Spinks et al., (2005). The dip around the FE ring fault structure was based on the dip angles identified on the major northwest, southeast, east and west OVC boundary faults by Seebeck et al., (2010) (described in section 4.4 earlier). In the FE model, these are sub-vertical, and dip (inward) at 65° for the NW and SE sections and 80° (average values) on the east and west sections of the FE ring fault structure. The connecting corner faults dip at composite grades between these. The FE ring fault structure

extends to 3 km depth to meet the base of the caldera structure. Dynamic (spontaneous) slip on the ring structure fault plane is solved in Pylith using PETSc Scalable Nonlinear Equations Solvers (SNES) non-linear solver (Aagaard et al., 2013a). In this first attempt, fault surface friction and coefficient coefficients were set as zero to represent a mechanically weak (free slip) ring fault. Future research will incorporate more realistic fault friction coefficients along this structure.

4.6 Results

4.6.1 The FE spherical magma chamber model

The magnitude of the modelled displacements, as well as their spatial patterns is now examined. First, the spherical chamber results are discussed. The horizontal and vertical displacement fields in these cases are symmetric and a cross section (along profile A - B in Figure 4.1) is illustrated in Figure 4.4A and Figure 4.4B. The maximum modelled vertical displacement occurs directly above the chamber, in the Tarawera Rift. These include a 8mm and 18mm vertical displacement for the 1.06km and 1.38km chambers respectively. The maximum horizontal displacements (5mm and 7mm for the 1.06km and 1.38km chambers respectively) occur at approximately 3 to 4km surface distance from the origin of the chambers.

Following the approach of Charco et al., (2007), the limit of observable displacement at the local cGPS stations is considered by comparing the magnitude of modelled displacement with the daily coordinate solution precisions typical of cGPS instrumentation. Recent studies have shown that cGPS networks have the capability to provide a few millimetre level horizontal precisions and to 5 to 6mm vertical precisions (Ebner and Featherstone, 2008; Haasdyk, et al., 2010; Blewitt et al., 2013; Holden et al., 2016). In this study the daily cGPS coordinate solution precisions (or background or measurement noise) are assumed to be 2mm in the east and north components and 6 mm in the vertical component. These are represented as the horizontal dashed lines in Figure 4.4A and Figure 4.4B. For the 1.06 km spherical magma chamber, the approximate distance at which the modelled displacement is not greater than background noise is approximately 10 and 3km for the horizontal and vertical components respectively. For the 1.38km spherical magma chamber, these distances are approximately 17 and 6km, respectively.

In both cases, station RGTA would detect vertical displacement, since the magnitude of the displacement modelled in its proximity is well above background noise levels. At the next closest cGPS stations (RGMK and RGRR), the modelled vertical displacement might not be identified from background noise. Few other

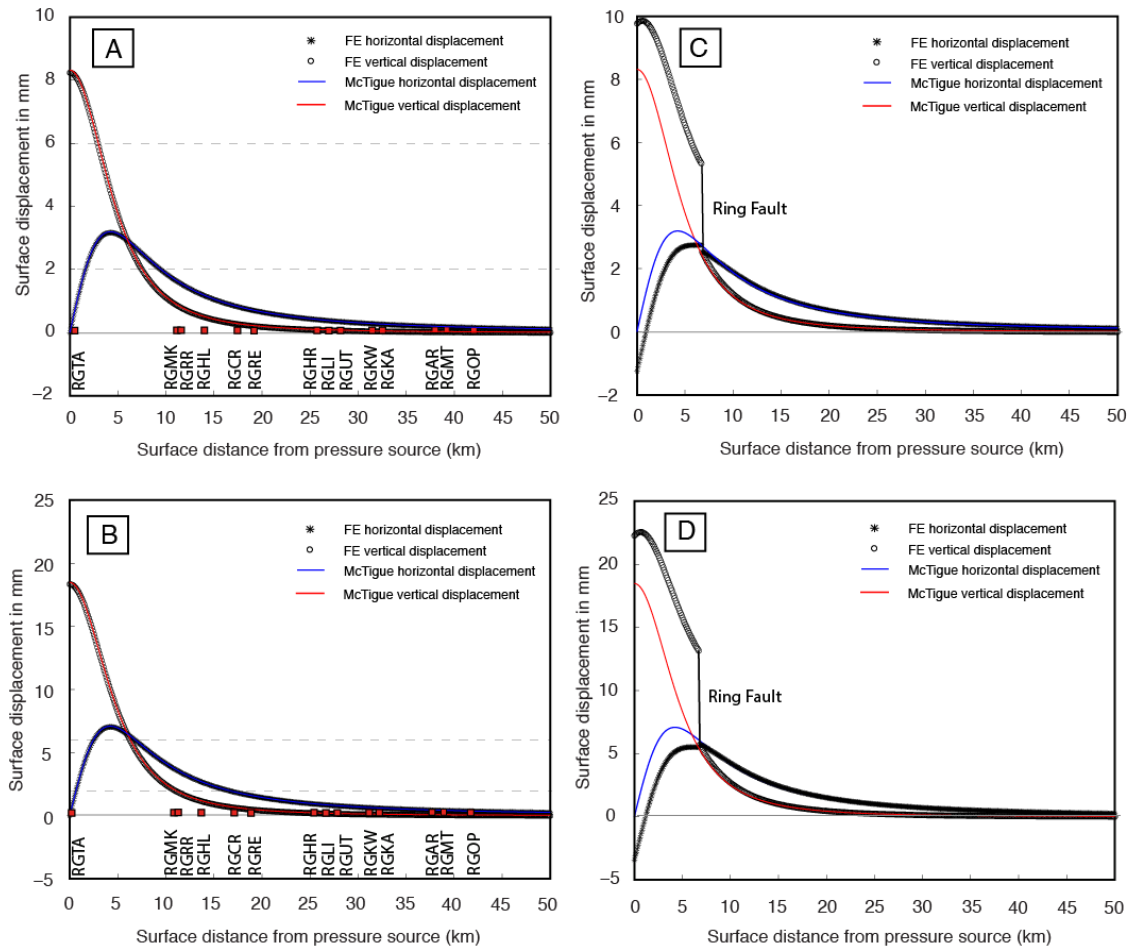


Figure 4.4 - A) Horizontal and vertical displacement associated with a spherical cavity of 1.06 km radius at 6km depth. B) Horizontal and vertical displacement associated with a spherical cavity of 1.38km at 6km depth. C) Horizontal and vertical displacement associated with 1.06km radius spherical cavity, with ring fault structure. D) Horizontal and vertical displacement associated with 1.38km radius spherical cavity, with ring fault structure. Poisson ratio is 0.25; overpressure is 10MPa and crustal shear modulus of 30 GPa. The dashed horizontal lines represent the assumed cGPS 2mm horizontal and 6mm vertical detectability limits. The red squares along the x-axis represent the regional cGPS stations at their appropriate ground distance from the Tarawera rift.

4.6.2 The FE rectangular magma chamber model

The horizontal and vertical displacements modelled for the rectangular chamber at 6km depth below the Tarawera Rift are shown in Figure 4.5A to Figure 4.5C. The maximum horizontal displacements in the east/west and north/south components (Figure 4.5A and Figure 4.5B respectively) are 7.4 and 9.3 mm, respectively. These figures also show that the modelled horizontal displacement field extends north-west and southeast to approximately 30 km distance from the Tarawera Rift, but that the limit of detectable displacement extends approximately 20 km. To the NW, this region contains stations RGCR, RGRE and RGMK. To the southwest this includes station RGRR. The maximum vertical displacement modelled (see Figure 4.5C) is 18.8mm uplift near the Tarawera rift. The most significant vertical displacement is contained within the vicinity of the OVC and detectable displacement occurs in the vicinity of station RGTA. At other nearby stations (e.g. RGMK and RGRR) the modelled vertical displacement is less than background noise.

4.6.3 The FE 1 m wide dike model

The modelled horizontal and vertical displacement associated with the 1 m wide dike at 5km depth is illustrated in Figure 4.5D to Figure 4.5F. The maximum horizontal displacement is 10mm and 13.8mm, for the east/west and north/south components respectively (see Figure 4.5D and Figure 4.5F). This occurs close to the Tarawera rift and in close proximity to the OVC. These figures also show that the horizontal displacements are broadly projected in lobe shaped regions trending between approximately NW and SE to NNW and SSE, or orthogonal to the orientation of the dike. As a result, the magnitude of horizontal displacement is greater than background noise at stations approximately 30km distance northwest of the OVC (e.g. RGMK, RGCR, RGRE and RGLI). With the exception of station RGRR, these stations are all located in the northwest of the OVC. The maximum vertical subsidence (see Figure 4.5F) is 6mm in the vicinity of the Tarawera Rift. At distances of approximately 10km northwest and southeast and parallel to the axis of the Tarawera Rift, a maximum of 11.8mm uplift is observed. Figure 4.5F also indicates that only station RGTA would clearly identify the modelled vertical displacement from background noise. For stations more distant than RGTA, the modelled uplift is smaller than background noise.

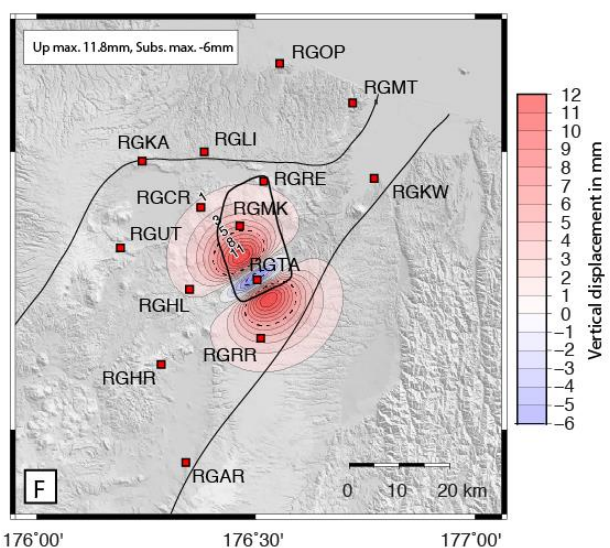
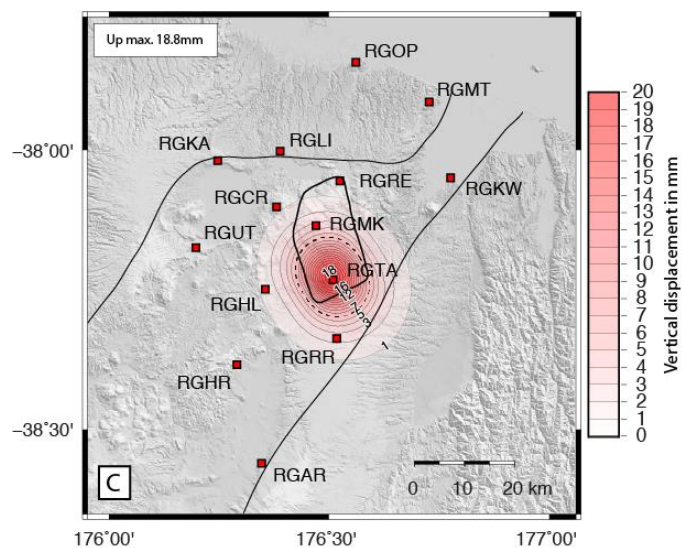
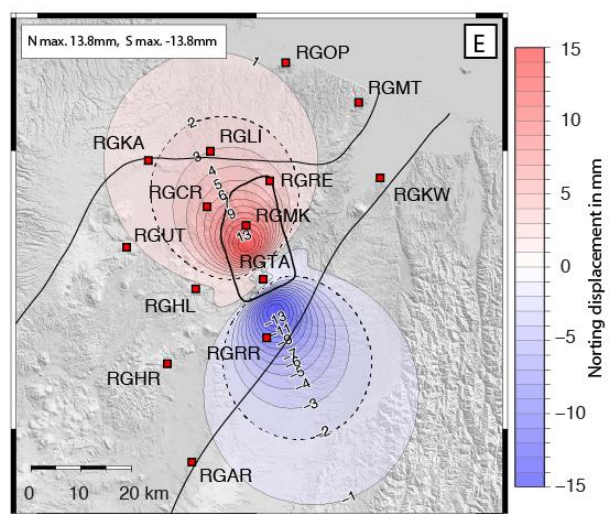
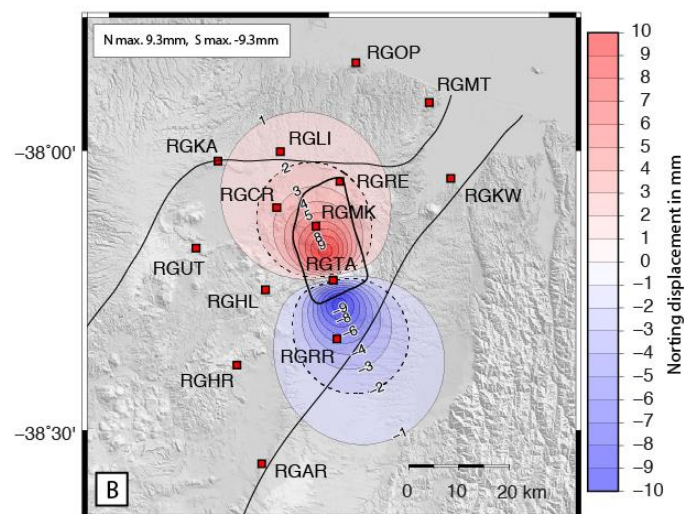
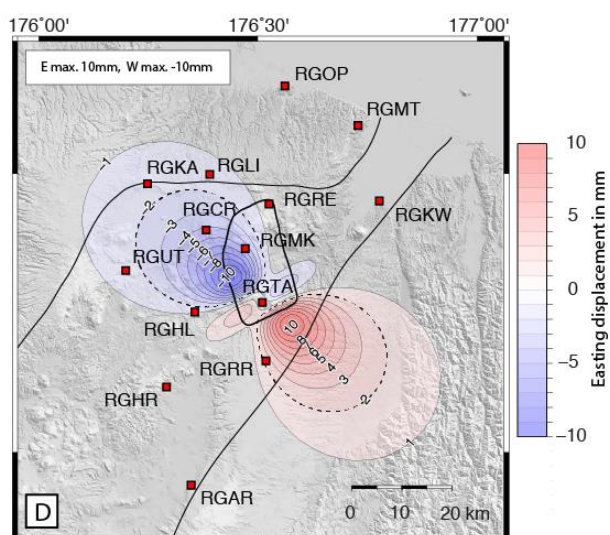
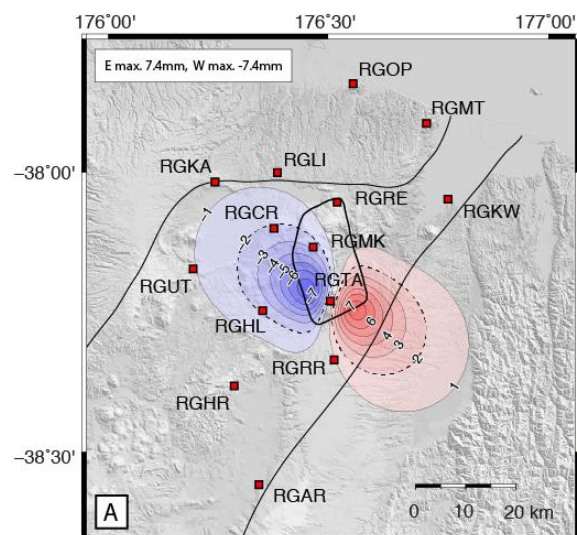


Figure 4.5 – The easting (A), northing (B) and vertical (C) displacement components associated with 10MPa overpressure of a rectangular magma chamber at 6km depth beneath the Tarawera Rift. The easting (D), northing (E) and vertical (F) displacement components associated with intrusion of a 1m wide vertical dike at 5km depth below the Tarawera Rift. The thin black lines represent the approximate location of the Taupo Rift at this location within the central North Island. The bold black line outlines the approximate location of the ring fault structure used in later modelling and is included in this figure for comparison. The cGPS stations are shown as red squares. Contour labels are in mm. The dashed contour lines represent the assumed horizontal (2mm) and vertical (6mm) detection limits described in the text. The maximum horizontal and vertical modelled displacements are shown at the top left in each figure. All units are in mm.

4.6.4 Deformation results with ring fault structure

The surface displacements modelled with the ring fault structure present and 10MPa overpressure within the two spherical chambers are illustrated in Figure 4.4 and Figure 4.8 and Figure 4.9 in supplementary material B and C. Figure 4.4C and Figure 4.4D illustrate the vertical and horizontal displacements along the transect A to B. Figure 4.8 and Figure 4.9 illustrate the full displacement fields modelled for the spherical chambers. The surface displacements modelled for the rectangular chamber at 6km depth and the 1 m dike (at 5km depth) with the ring fault structure, are presented in Figure 4.6A to Figure 4.6F. The results presented and discussed hereafter primarily focus on the results for the rectangular chamber and dike scenarios.

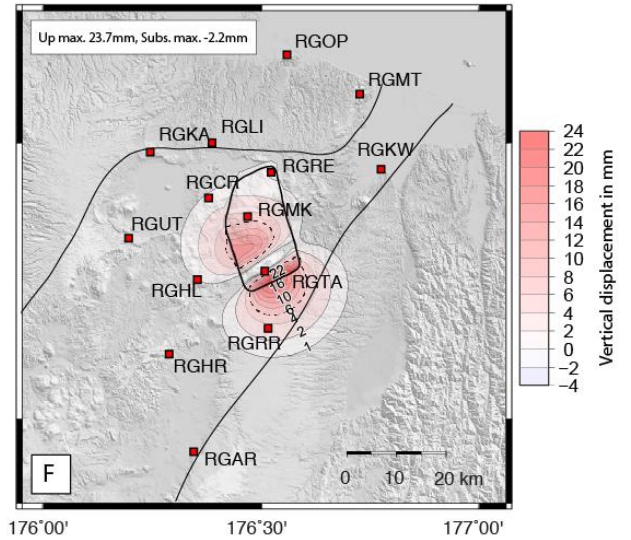
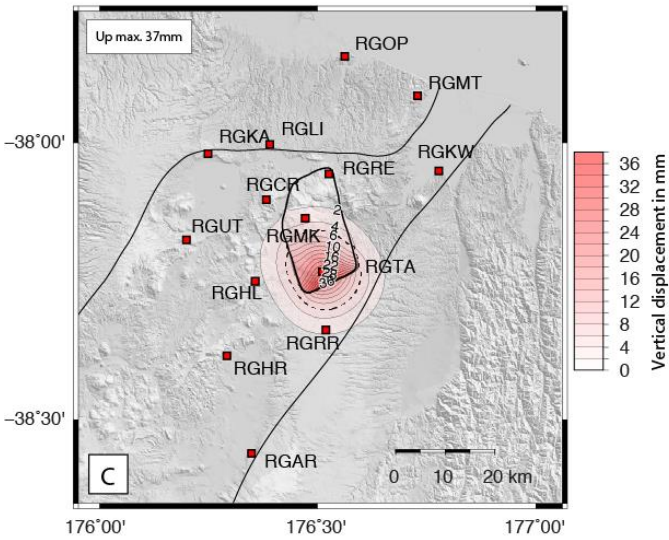
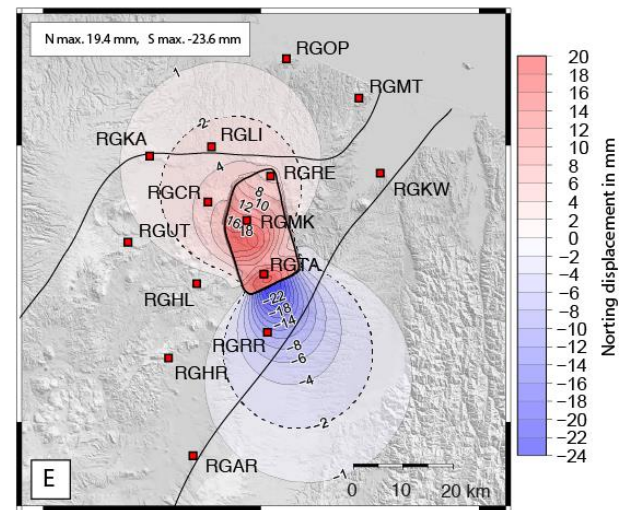
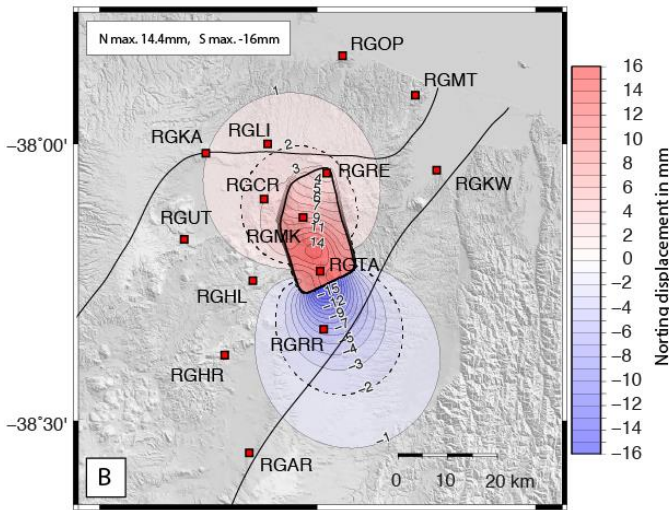
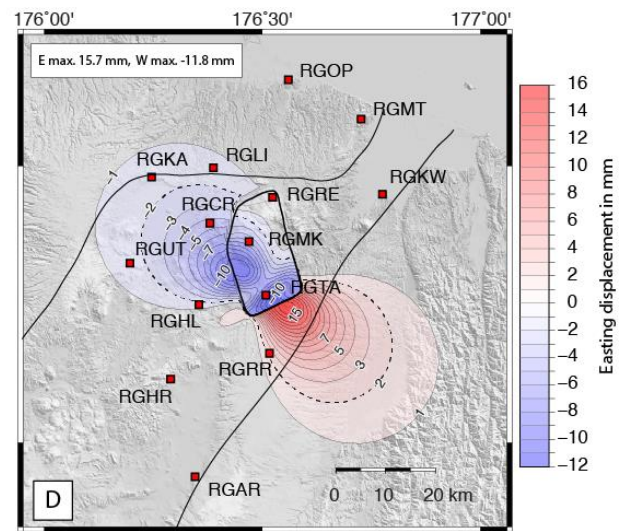
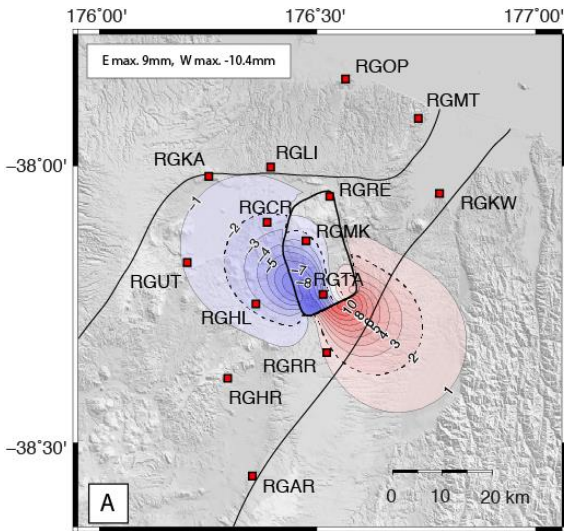
Some observations can be identified in these results before specific comments are made. First, the presence of the ring fault structure increases the modelled horizontal displacement and vertical uplift in various parts of the OVC region. In particular, this is more noticeable in the vicinity of the southern section of the ring fault structure (see Figure 4.6A, B, D, E) and also occurs on both sides of this structure (e.g. immediately south of the OVC). Second, the modelled vertical displacement decays rapidly across the ring fault boundary. This is particularly pronounced in the southern, south-eastern and south-western sections of the ring fault. This is evident in Figure 4.4C and Figure 4.4D. Due to the irregular shape of the ring fault structure, this is only representative along the A to B transect. The figures illustrate a significant change in vertical displacement (approximately 8mm) across the eastern boundary of ring fault structure for the 1.38 km spherical magma chamber and approximately 2mm change for the 1.06km radius chamber.

The horizontal displacements modelled in association with the rectangular chamber in the presence of the ring fault structure, are illustrated in Figure 4.6A and B. A maximum horizontal displacement of 9mm and 10.4 mm are modelled for the east/west and 14.4mm and 16mm for north/south components respectively. These

occur in the vicinity of the southern section of the ring fault structure. The maximum vertical displacement for the same scenario (see Figure 4.6C) is 37mm uplift inside the OVC region, near station RGTA. The horizontal displacements modelled for the 1m dike, with the ring fault structure are illustrated in Figure 4.6D and Figure 4.6E. A maximum horizontal displacement of 15mm and 12 mm are modelled for the east/west and 20mm and 23mm for the north/south components respectively. The maximum vertical displacement modelled for the dike (see Figure 4.6F), include 3mm subsidence in the vicinity of the Tarawera rift and up to 24 mm uplift, in proximity to the southern margin of the ring fault structure (see Figure 4.6F).

Finally, it is worth noting that the influence of the ring fault structure in the modelling is most pronounced for the displacements modelled in the vicinity of station RGTA. At this station, the magnitude of the modelled horizontal displacement without the ring fault structure is less than cGPS measurement noise (see Figure 4.5A, B, D and E). This is due to its location directly above the modelled displacement sources in the FE models. However, as shown in Figure 4.6A, B, C and D, the presence of the ring fault structure significantly increases the modelled horizontal displacements in the vicinity of station RGTA (e.g. up to approximately 18mm in Figure 4.6E). This would be readily detected in the cGPS coordinate solution at this location.

Figure 4.6 (over page) - The easting (A), northing (B) and vertical (C) displacement components associated with 10MPa overpressure of a rectangular magma chamber at 6km depth beneath the Tarawera Rift, in the presence of the OVC ring fault structure. The easting (D), northing (E) and vertical (F) displacement components associated with a 1m wide vertical dike at 5km depth below the Tarawera Rift in the presence of the OVC ring fault structure. The thin black lines represent the approximate location of the Taupo Rift at this location within the central North Island. The bold black line outlines the approximate location of the ring fault structure. The cGPS stations are shown as red squares. Contour labels are in mm. The dashed contour lines represent the assumed horizontal (2mm) and vertical (6mm) detection limits described in the text. The maximum horizontal and vertical modelled displacements are shown at the top left in each figure. All units are in mm



4.7 Discussion

4.7.1 Key characteristics of the modelling results

The horizontal and vertical ground displacements for the spherical geometry (see Figure 4.4A and Figure 4.4B) are symmetric in nature and should only be considered as a basic end-member representation of the expected displacement field relating to volcanic activity at the OVC. They do not represent new research, but rather reflect the implementation of a standard FE modelling approach (e.g. a spherical pressure source in a homogeneous elastic half space), in the OVC context. As a result, they closely match those expected from the analytical McTigue deformation model. Similarly, the dominant NW-SE trending ‘lobes’ of horizontal displacement evident in the 1m-wide dike ground displacement results (see Figure 4.5D and Figure 4.5E) match those expected from the Okada analytical model (although rotated to align with regional structure in the Taupo rift). This is also true for the vertical displacement field related to the 1m- wide dike. Nonetheless, both sets of results provide a useful start for considering expected displacement patterns linked to volcanic processes at the OVC and the sensitivity of the cGPS network.

The complex geometry of the pre-Kaharoa eruption rectangular magma chamber proposed by Nairn et al., (2004), cannot easily be accommodated by the McTigue or Okada analytical models. This research implemented the FE technique to achieve this. The resulting horizontal displacement field (in the absence of the ring fault structure) is similar to that for a 1m wide dike at 5km depth (e.g. Figure 4.5A, B, C and D); however the region of subsidence directly above the dike body is absent and replaced with uplift. This is an important distinction, which might reflect a unique geodetic signature of the two different scenarios in any future volcanic crisis at the OVC.

The inclusion of the ring fault structure in the FE models amplifies the magnitude of the modelled displacements, but this effect is primarily confined to within its margins (e.g. at the OVC), as well as immediately south of its southern margin. At much greater distance, the influence of the ring fault structure on the modelled displacement is marginal. These observations confirm earlier studies (De Natale and Pingue, 1993; De Natale et al., 1997; Orsi et al., 1999; Troise et al., 2004), which show the dominant influence of these structures on modelled displacement fields at other calderas. Other typical features identified here and in other ring fault studies, include a strong correlation between the caldera structure and displacement patterns, as well as a rapid decay of the vertical displacement across the ring structure fault (e.g. De Natale and Pingue, 1996; De Natale et al., 1997). A ‘raised’ region of uplift for the spherical and rectangular magma chambers is also evident near the Tarawera rift, constraining the most significant vertical displacement to within the

caldera (see Figure 4.6C). A similar feature was identified in the modelled surface displacements at nearby Taupo caldera by Ellis et al., (2007).

The results presented here that incorporate the ring fault structure illustrate an uneven distribution of the magnitude of the modelled displacements. Larger displacements are focussed across the southern part of the ring fault structure (compared to the northern section), as well as immediately outside the southern margin of this structure (see Figure 4.6). In this vicinity, the section of the ring fault is closer to, and its fault plane (approximately 65° dip) almost vertically above, the (various) displacement source at depth. Therefore, a combination of the proximity of the ring fault structure to the displacement source, as well as the elevated inward dipping fault dip angle, may promote greater interaction with the modelled stress field and may result in increased surface displacements in this vicinity. Similar relationships have been inferred by Folch and Gottsman (2006), however further investigation is required to more confidently constrain the nature of this relationship in the FE modelling undertaken here.

4.7.2 Can magma accumulation or emplacement occur at depth at the OVC without detection by the cGPS network?

Excluding the spherical magma chamber results, the dominant spatial feature in the modelled horizontal displacement fields presented here is the NW-SE trending ‘lobes’ pattern, which persist, even in the presence of the ring fault structure. This infers that displacements observed at cGPS stations NW and SE of the OVC (and within the OVC) are important for detecting magma accumulation and dike intrusion at depth at the OVC. However, since the magnitude of the modelled displacements decay (non-uniformly in the presence of the ring fault structure) away from the Tarawera rift through these regions, only some of the modelled displacement signal will be detected at these cGPS stations. Further, the present-day distribution of the cGPS around the Tarawera rift is not symmetric, with a greater number of stations towards the NW. This means that the modelled displacement field south-west of the OVC would only be observed by station RGRR. Nonetheless, the results presented here suggest that ground displacements related to magma accumulation or dike intrusion at depth beneath the OVC would be detected within the surrounding cGPS network. However this is mostly limited to stations in the caldera and to its NW. RGRR is the only cGPS station SW of the OVC that coincides with the modelled displacement there.

Specifically, for the horizontal displacements modelled without the ring fault structure, the range at which the displacement might remain apparent from background noise is approximately 15 to 20 km for the rectangular chamber (at 6km depth) and 25 to 30 km for the 1 m wide dike (at 5km depth). In the presence of the ring fault

structure, these ranges are approximately 20 to 25km and 30 km for the rectangular chamber and 1 m wide dike (at 5km depth) respectively. Therefore, considering the distribution of the cGPS stations, particularly in the NW of the OVC, RGLI represents the furthest cGPS station where the modelled horizontal displacement might be detected above measurement noise. Stations closer to the OVC, such as RGCR, RGMK, RGRE, RGTA and RGRR, would undergo horizontal displacement greater than background noise. However, these observations are only applicable for the specific (hypothetical) FE modelling undertaken here and only for the rectangular magma chamber and 1m dike at depth below the OVC.

In this modelling, the spatial extent of the detectable vertical displacement associated with the same scenarios, is chiefly limited to the proximity of Tarawera rift (approximately 10km NW and SE) and station RGTA. In all the modelling, station RGTA would experience vertical ground displacement (uplift or subsidence) within its detection capabilities, underlining its key importance for geodetic monitoring at the OVC. The modelled vertical displacements at the next closest stations (RGRT and RGMK) vary in magnitude, but typically just below their vertical detectability limits. Therefore in some scenarios vertical displacement might only be observed at station RGTA. However, measurable horizontal displacement would still be observed at these stations, which considered alongside the uplift observed at RGTA, would provide important insight into the source of the displacement.

In the southwest of the OVC, there are fewer cGPS stations (e.g. only RGRR) that coincide with the displacement modelled here. This region extends across the Reporoa caldera (see Figure 4.1 and Figure 4.2) and access to suitable locations for cGPS stations might be limited due to the presence of caldera infill and pyroclastic deposit. During any future unrest period at the OVC, it would be useful to place additional GPS instruments in this region. These would complement any remotely-sensed deformation dataset such as InSAR, which has already been successfully used through the Taupo Rift (Samsonov et al., 2011; Hamling et al., 2015). These two complementary datasets would better observe the modelled displacements southwest of the OVC and more useful in any attempt to invert measured surface displacement for deformation source parameters.

4.7.3 Limitations of this research and directions for further research

This research represents a first attempt to use FE modelling to consider deformation patterns associated with likely volcanic activity at the OVC. The results are considered in the context of the existing cGPS network and how this displacement might be observed. A number of simplifications and assumptions were adopted for practical purposes and software limitations. This includes the choice of an elastic medium with homogeneous material properties, which does not reflect the complex setting through the Okataina segment in the TVZ. Troise et al., (2004) note that the influence of structural discontinuities (such as ring faults) on modelled surface displacement is dominant in respect to the influence of elastic parameter heterogeneity. Therefore, some corrections to the modelled surface displacements presented here will be necessary when future FE modelling incorporates more realistic material properties.

The first attempt undertaken here assumed a single deformation source (with simple geometries) is present at depth beneath the OVC. A more realistic scenario might include the presence of a deflating magma chamber at depth, alongside an ascending vertical dike from the chamber (Sherburn and Nairn, 2004), a pipe like conduit from the chamber to the surface (Nairn et al., 2004) or vertical dikes extending much further distances outside the OVC, (Nairn, 2002; Nairn et al., 2005), all of which have all been associated with the Kaharoa and Tarawera eruptions. The surface deformation fields associated with these different scenarios will differ from those presented here. The FE modelling technique is capable of accounting for multiple deformation sources (Pascal et al., 2013), however preliminary attempts to achieve this (not presented here), were unable to produce FE models of sufficient mesh resolution and quality together with reasonable computational efficiency. Further attempts will be undertaken to improve the FE models used here to account for these multiple deformation sources and different geometries and compare their results to those presented here.

The inclusion of the ring fault structure in the modelling here has identified its important role in controlling surface displacement. However, this structure is represented in the FE model simply and the real world fracture system at the OVC is likely to be much more complex. Recent research has shown the benefits of using more flexible modelling techniques based on various information sources (Ronchin et al., 2013) to generate more complex three-dimensional geometry in FE modelling. Further, the initial assumption of free-slip along the ring-fault structure has likely influenced the resulting surface displacement field. More realistic fault cohesion and friction coefficients will also provide corrections to the modelled displacements presented here.

The research presented here focuses on the geodetic aspects of volcanic activity at the OVC (e.g. ground deformation, the regional cGPS network). However, some geological implications can be briefly considered. First, the modelled surface displacement patterns associated with the dike presented here represent an extensional environment (e.g., NW-SE orientated surface displacement radiating away from the Tarawera rift). If this reflects extension in the upper crust, it may be possible to use the approach adapted here to consider the contribution of diking processes at the OVC to the overall rifting (extension) budget in this section of the Taupo rift. Dike induced extension is considered an important mechanism for extension through this section of the Taupo rift (Seebeck and Nichol 2009; Rowland et al., 2010), but its contribution to the total extension budget is not well constrained.

There is no clear evidence of the modelled horizontal or vertical displacements (from this study) in the contemporary velocity and strain-rate fields recently documented at the OVC (e.g. Holden et al., 2015) or nearby vicinity (Wallace et al., 2004; Hamling et al., 2015). These studies suggest that present day deformation is dominated by the influence of regional magmatic and rifting processes rather than any volcanic processes within the OVC. How any future volcanic (geodetic) signal, such as those modelled here, may appear in this complex setting remains a challenging question and requires further research. This is important as any future geodetic data inversion at the OVC using numerical modelling techniques will have to account for these background signals (noise) in order to derive accurate deformation source parameters.

4.8 Conclusions

This study investigated the deformation fields that might occur due to renewed volcanic activity at the OVC. FE modelling was used to test a number of scenarios, in which magma may accumulate or migrate at depth below the Tarawera Rift. These incorporated constraints from published research regarding the ~AD1315 Kaharoa and 1886 Tarawera eruptions. This is the first time that the FE technique has been applied to consider surface displacements related to the pre-Kaharoa chamber geometry proposed by Sherburn and Nairn (2004). A simple ring fault structure was also introduced into the FE models. The results of the modelling were considered in relation to the detection capabilities of a modern permanent cGPS network in the vicinity of the OVC.

The major results of this research are to first show that FE modelling of the moderate overpressure of the pre-Kaharoa magma chamber of Sherburn and Nairn (2004) at 6km depth and the intrusion of a 1m-wide dike at 5km depth below the Tarawera rift would produce a horizontal displacement field that includes a distinct lobe-based pattern extending to the NW and SE of the OVC. The identification of this spatial pattern for the 1m-

wide dike matches that expected from the Okada analytical model and does not reflect new results. However, its application to the study area has provided some new insight into the expected magnitude and locations of displacements in the cGPS network and surrounding Taupo rift that might result from volcanic activity at the OVC. In the presence of the ring fault structure, this feature persists in the displacement fields, but also includes increased horizontal and vertical displacements in the vicinity of the southern margin of OVC ring fault structure. This highlights an important role of any existing caldera fracture system at the OVC for controlling ground deformation during future volcanic activity and requires further investigation.

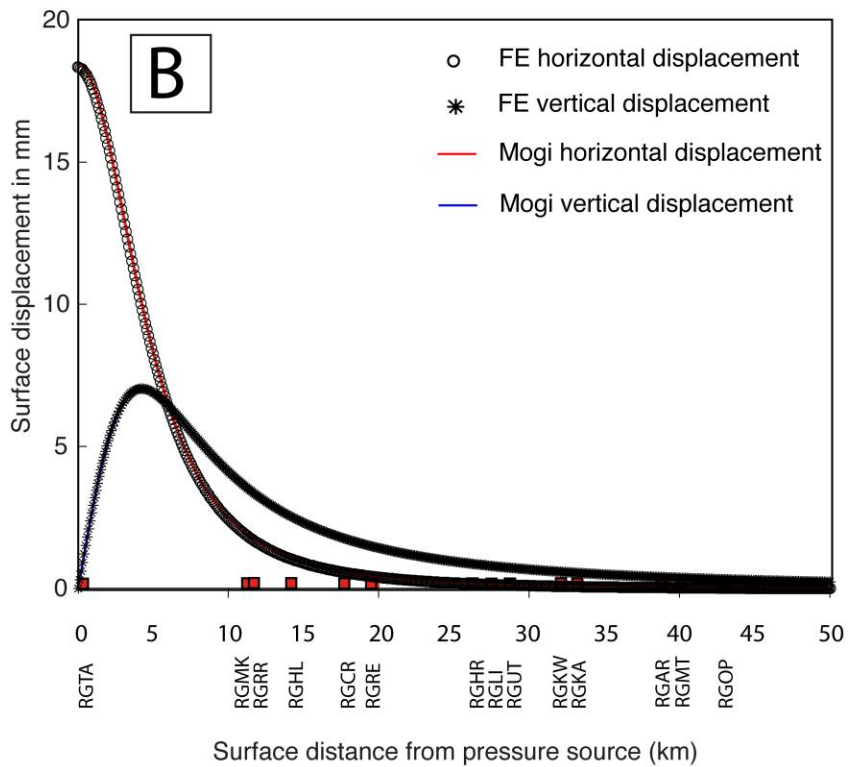
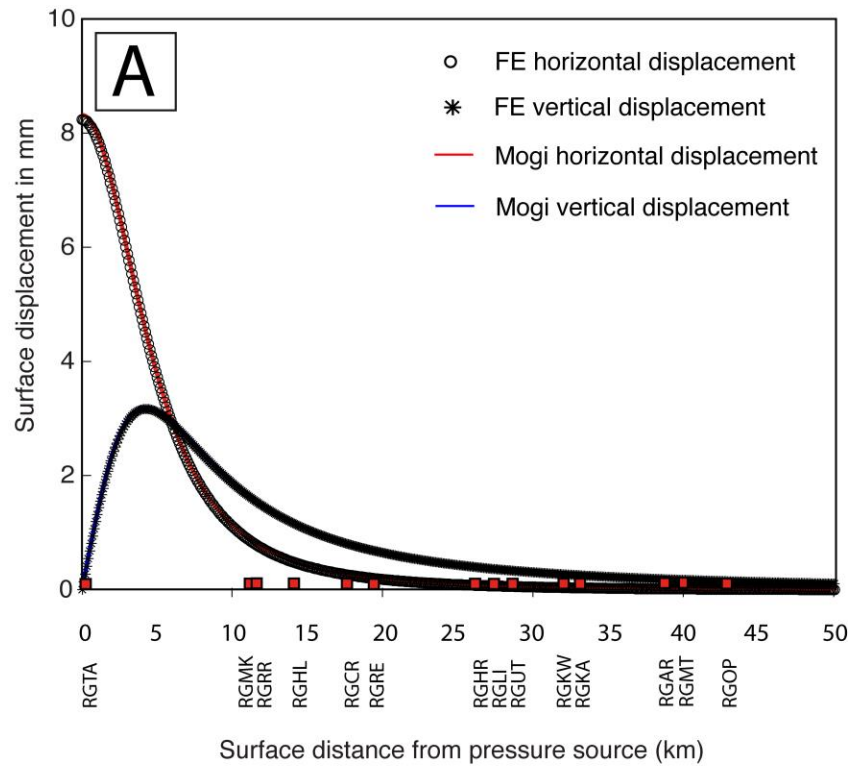
The second major result of this research is to indicate that the displacements modelled here would be detectable in nearby parts of the cGPS network. In particular, this includes stations approximately 20km to the northwest and southeast of the OVC. This suggests that it is unlikely that magma bodies, such as those tested here, could presently exist or accumulate beneath the OVC without being detected using combinations of modern geophysical techniques, such as geodetic (including InSAR) and seismic observations. However, further testing of different scenarios (too those tested here) is required to better constrain the sensitivity limitations of the present day cGPS network at the OVC. The results also show that only station RGRR would observe some measurable deformation southwest of the OVC. During future volcanic activity at the OVC, more GPS observations would be required in this region, or complemented with remotely sensed techniques such as InSAR. This confirms the importance of using different monitoring strategies at active and large calderas.

This first attempt using the FE technique for modelling displacement at the OVC, does not account for more realistic deformation source geometries and layered rock properties. As a result some corrections to the displacements modelled will be required. Further, the surface displacements modelled here only provide a limited picture of the surface deformation processes associated with volcanic activity at the OVC. However these results can still be used a first estimate of the location and magnitude of deformation that may follow renewed volcanic activity at the OVC, if its characteristics are similar to those of the most recent eruptions.

Acknowledgments: This research was conducted as part of a PhD research in the School of School of Earth, Atmosphere and Environment at Monash University in Melbourne Australia. We would like to thank the editor Professor Jurgen W. Neuberg for his patience and handling of the review process. Particular thanks are also given to the reviewers, Pietro Tizanni and Adelina Geyer. The quality of the manuscript has been greatly improved by their comments and suggestions. We would also like to thank Dr Susan Ellis at GNS Science and Jim Cole at the University of Canterbury, New Zealand for their discussions related to the models. We are also

grateful to Charles Williams at GNS Science for assistance with the Pylith software. All figures, except Fig. 3, Fig. 4, and Fig. 7 were produced using Generic Mapping Tools (Wessel and Smith, 1995) and further finished using Adobe Illustrator.

4.9 Electronic Supplementary Material



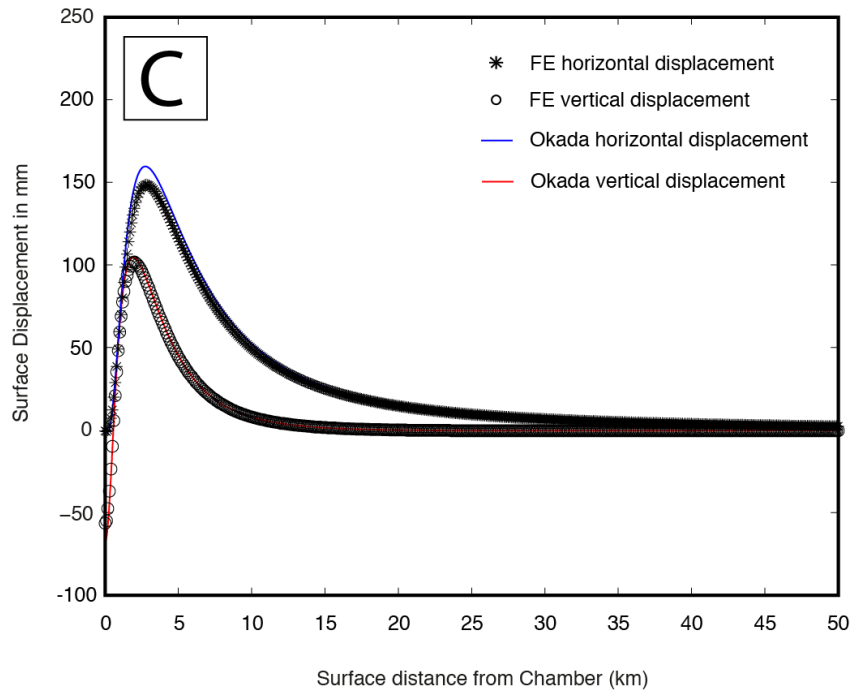
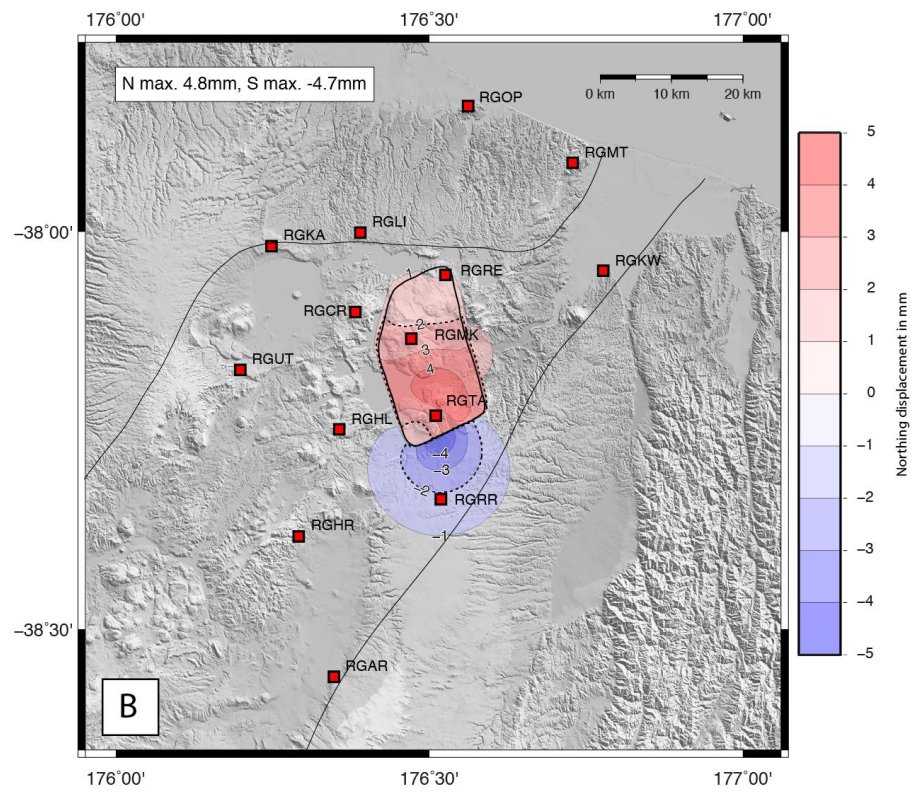
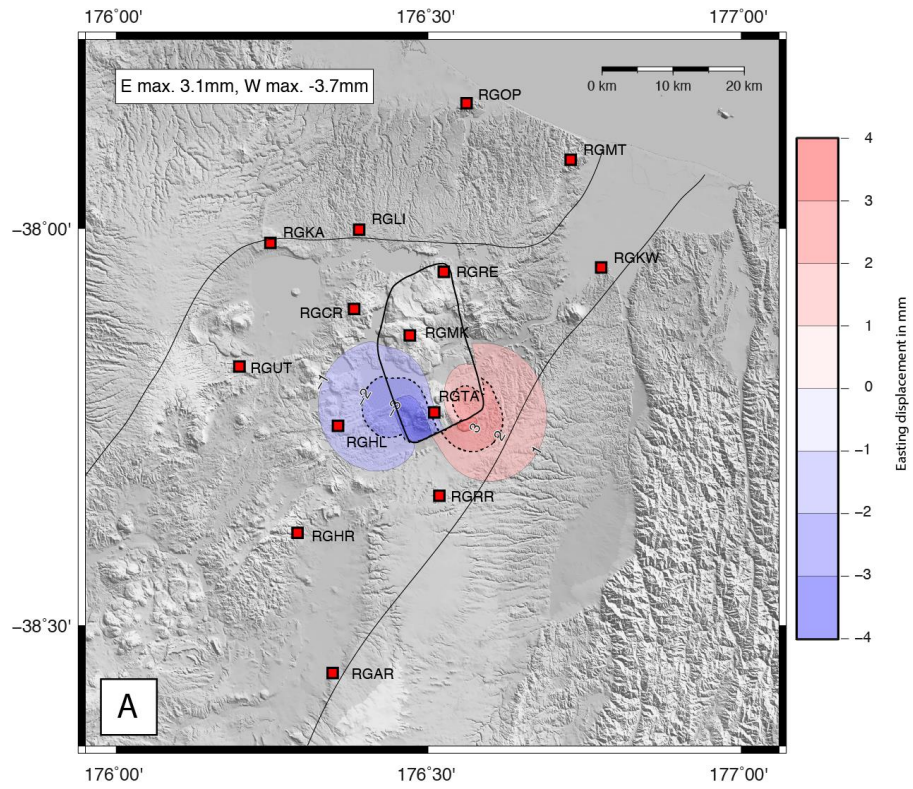


Figure 4.7 – **Supplementary Material A** – Comparison of horizontal (A) and vertical (B) displacements determined from Mogi analytical solution and Pylith FE solution for a 1.06 and 1.38 km radius spherical magma chamber (respectively) at 6 km depth. C - Comparison of horizontal and vertical displacements determined from Okada analytical solution and Pylith FE solution for a 4km long, 1m wide vertical dike from 5 to 1km depth.



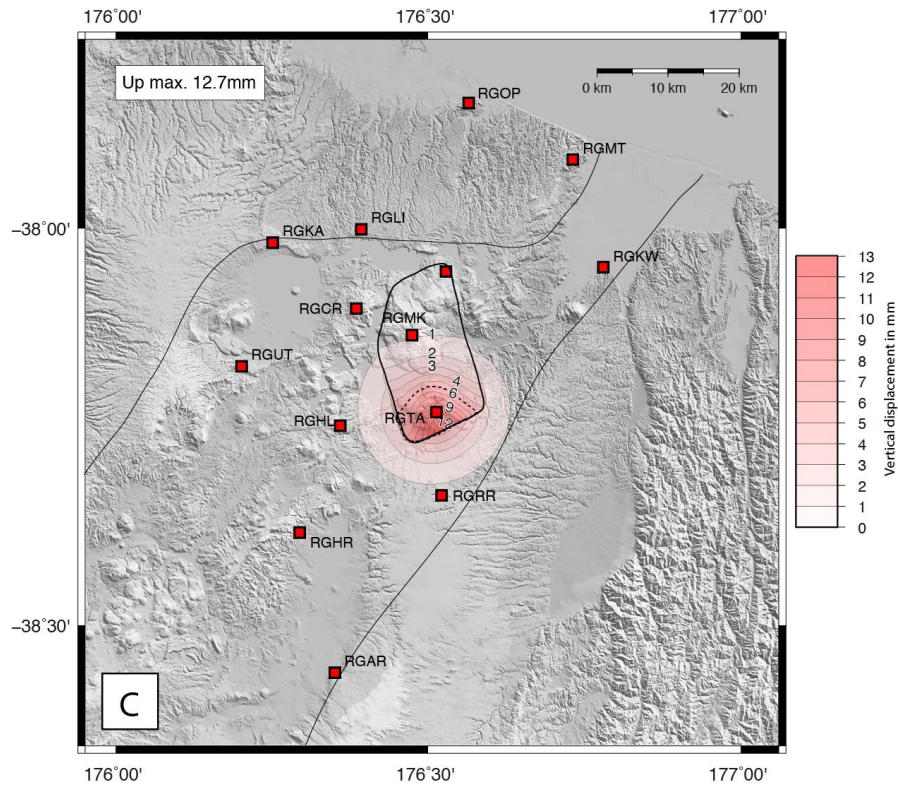


Figure 4.8 – **Supplementary Material B** – The easting (A), northing (B) and vertical (C) displacement components associated with 10MPa overpressure of a 1.06 km radius spherical magma chamber at 6km depth with the OVC ring fault structure. The thin black lines represent the approximate location of the Taupo Rift at this location within the central North Island. The bold black line outlines the approximate location of the ring fault structure and is included in this figure for comparison. The cGPS stations are shown as red squares. Contour labels are in mm. All units are in mm.

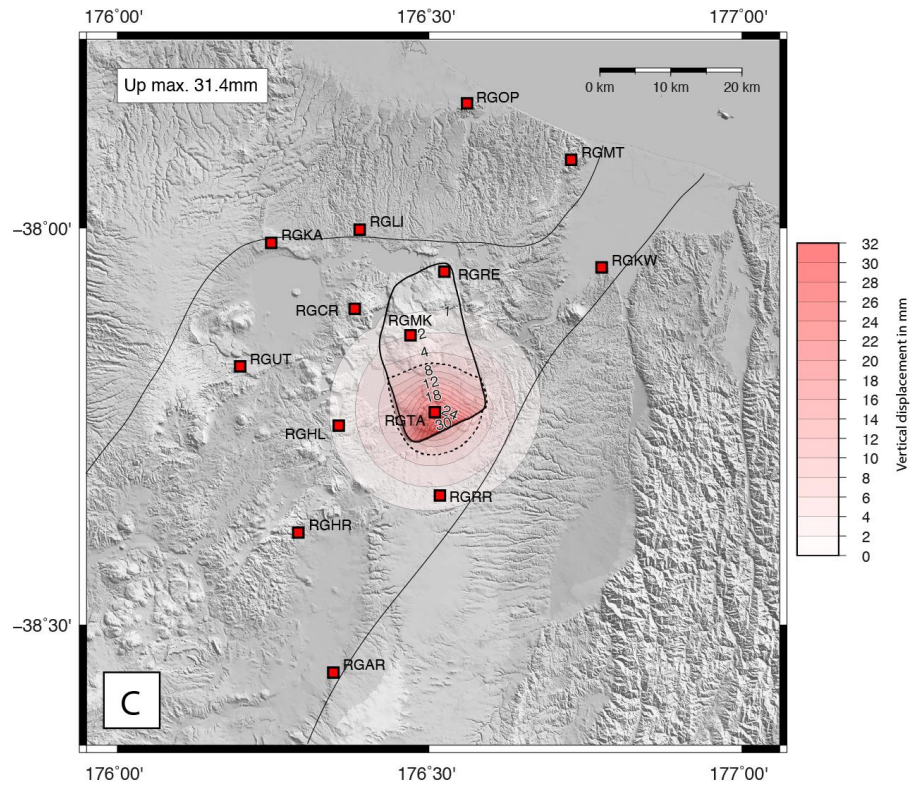


Figure 4.9 – **Supplementary Material C** – The easting (A), northing (B) and vertical (C) displacement components associated with 10MPa overpressure of a 1.38 km radius spherical magma chamber at 6km depth with the OVC ring fault structure. The thin black lines represent the approximate location of the Taupo Rift at this location within the central North Island. The bold black line outlines the approximate location of the ring fault structure and is included in this figure for comparison. The cGPS stations are shown as red squares. Contour labels are in mm. All units are in mm.

4.10 References

- Aagaard, B., Williams, C., Knepley, M., 2007. PyLith: a finite-element code for modeling quasi-static and dynamic crustal deformation. *Eos Trans. AGU* 8 (8(52)) (Fall Meet. Suppl., Abstract T21B-0592).
- Aagaard, B., Williams, C., Knepley, M., 2008. PyLith: a finite-element code for modeling quasi-static and dynamic crustal deformation. *Eos Trans. AGU* 89 (53) (Fall Meet. Suppl., Abstract T41A-1925).
- Aagaard, B., Kientz, S., Knepley, M., Strand, L., Williams, C., 2013. PyLith User Manual (Version 2.1.0. Davis), Computational Infrastructure of Geodynamics, CA.
http://geodynamics.org/cig/software/pylith/pylith_manual-2.1.0.pdf.
- Aagaard, B.T., Knepley, M.G., Williams, C.A., 2013. A domain decomposition approach to implementing fault slip in finite-element models of quasi-static and dynamic crustal deformation. *J. Geophys. Res. Solid Earth* 118. <http://dx.doi.org/10.1002/jgrb.50217>.
- Acocella, V., Spinks, K., Cole, J., Nicol, A., 2003. Oblique back arc rifting of Taupo Volcanic Zone, New Zealand. *Tectonics* 22 (4), 1045. <http://dx.doi.org/10.1111/j.1365-246X.2007.03345.x>.
- Alparone, S., Bonaccorso, A., Bonforte, A., Currenti, G., 2013. Long-term stress-strain analysis of volcano flank instability: the eastern sector of Etna from 1980 to 2012. *J. Geophys. Res. Solid Earth*, vol. 118 (9), 5098–5108. <http://dx.doi.org/10.1002/jgrb.50364>.
- Beauducel, F., de Natale, G., Obrizzo, F., Pingue, F., 2004. 3-D modelling of Campi Flegrei ground deformations: role of caldera boundary discontinuities. *Pure Appl. Geophys.* 161, 1329–1344. <http://dx.doi.org/10.1007/S00024-004-2507-4>.
- Bibby, H.M., Caldwell, T.G., Davey, F.J., Webb, T.H., 1995. Geophysical evidence on the structure of the Taupo Volcanic Zone and its hydrothermal circulation. *J. Volcanol. Geotherm. Res.* 68 (1–3), 29–58. [http://dx.doi.org/10.1016/0377-0273\(95\)00007-H](http://dx.doi.org/10.1016/0377-0273(95)00007-H).
- Blewitt, G., Kreemer, C., Hammond, W.C., 2013. EarthScope's Plate Boundary Observatory as the Mother of Invention. (Fall AGU, S24A-01, San Francisco, CA, Dec 9–13, 2013 [INVITED]).
- Bonaccorso, A., Cianetti, S., Giunchi, C., Trasatti, E., Bonafede, M., Boschi, E., 2005. Analytical and 3-D numerical modelling of Mt. Etna (Italy) volcano inflation. *Geophys. J. Int.* 163 (2), 852–862. <http://dx.doi.org/10.1111/j.1365-246X.2005.02777.x>.
- Bryan, C.J., Sherburn, S., Bibby, H.M., Bannister, S.C., Hurst, A.W., 1999. Shallow seismicity of the central Taupo Volcanic Zone, New Zealand: its distribution and nature. *N. Z. J. Geol. Geophys.* 42 (4), 533–542. <http://dx.doi.org/10.1080/00288306.1999.9514859>.
- Cabral-Cano, E., Correa-Mora, F., Meertens, C., 2008. Deformation of Popocatepetl volcano using GPS: regional geodynamic context and constraints on its magma chamber. *J. Volcanol. Geotherm. Res.* 170 (1–2), 24–34. <http://dx.doi.org/10.1016/j.jvolgeores.2007.09.008>.

- Cayol, V., Cornet, F., 1998. Effects of topography on the interpretation of the deformation field of prominent volcanoes - application to Etna. *Geophys. Res. Lett.* 25 (10), 1979–1982.
- Charco, M., Luzon, F., Fernández, J., Tiampo, K.F., Sanchez-Sesma, F.J., 2007. Three-dimensional indirect boundary element method for deformation and gravity changes in volcanic areas: application to Teide volcano (Tenerife, Canary Islands). *J. Geophys. Res.* 112 (B08409), 17.
<http://dx.doi.org/10.1029/2006JB004740>.
- Charlier, B.L.A., Wilson, C.J.N., 2010. Chronology and evolution of caldera-forming and post-caldera magma systems at Okataina Volcano, New Zealand from zircon U-Th model-age spectra. *J. Petrol.* 51 (5), 1121–1141. <http://dx.doi.org/10.1093/petrology/egq015>.
- Cole, J.W., 1990. Structural control and origin of volcanism in the Taupo Volcanic Zone, New Zealand. *Bull. Volcanol.* 52, 445–459. <http://dx.doi.org/10.1007/BF00268925>.
- Cole, J.W., Spinks, K.D., 2009. Caldera volcanism and rift structure in the Taupo Volcanic Zone, New Zealand. *Geol. Soc. Lond., Spec. Publ.* 327 (1), 9–29. <http://dx.doi.org/10.1144/SP327.2>.
- Cole, J.W., Spinks, K.D., Deering, C.D., Nairn, I.A., Leonard, G.S., 2010. Volcanic and structural evolution of the Okataina Volcanic Centre; dominantly silicic volcanism associated with the Taupo Rift, New Zealand. *J. Volcanol. Geoth. Res.* 190 (1–2), 123–135.
<http://dx.doi.org/10.1016/j.jvolgeores.2009.08.011>.
- Cole, J.W., Deering, C.D., Burt, R.M., Sewell, S., Shane, P.A.R., Matthews, N.E., 2014. Okataina Volcanic Centre, Taupo Volcanic Zone, New Zealand: a review of volcanism and synchronous pluton development in an active, dominantly silicic caldera system. *Earth Sci. Rev.* 128, 1–17.
<http://dx.doi.org/10.1016/j.earscirev.2013.10.008>.
- Currenti, G., Del Negro, C., Scandura, D., 2008. 3D numerical deformation model of the intrusive event forerunning the 2001 Etna eruption. *Phys. Earth Planet. Inter., Elsevier* 168 (1–2), 88–96.
<http://dx.doi.org/10.1016/j.pepi.2008.05.004>.
- Currenti, G., Bonaccorso, A., Del Negro, C., Scandura, D., Boschi, E., 2010. Elasto-plastic modeling of volcano ground deformation. *Earth Planet. Sci. Lett.* 296 (3–4), 311–318.
<http://dx.doi.org/10.1016/j.epsl.2010.05.013>.
- Darby, D.J., Hodgkinson, K.H., Blick, G.H., 2000. Geodetic measurement of deformation in the Taupo Volcanic Zone, New Zealand: the North Taupo network revisited. *N. Z. J. Geol. Geophys.* 43 (2), 157–170. <http://dx.doi.org/10.1080/00288306.2000.9514878>.
- De Natale, G., Pingue, F., 1993. Ground deformations in collapsed caldera structures. *J. Volcanol. Geotherm. Res.* 57 (1–2), 19–38. [http://dx.doi.org/10.1016/0377-0273\(93\)90029-Q](http://dx.doi.org/10.1016/0377-0273(93)90029-Q).
- De Natale, G., Pingue, F., Scarpa, R., 1996. Ground deformations modelling in volcanic areas. In: Tilling, R. (Ed.), *Monitoring and Mitigation of Volcano Hazards. IAVCEI Proceedings* pp. 365–388.

- http://dx.doi.org/10.1007/978-3-642-80087-0_11.
- De Natale, G., Petrazzuoli, M., Pingue, F., 1997. The effect of collapsed structures on ground deformations in calderas. *J. Volcanol. Geotherm. Res.* 57 (1–2), 19–38. <http://dx.doi.org/10.1029/97GL01600>.
- Diao, F., Xiong, X., Wang, R., Zheng, Y., Walter, T., Weng, Huihui, Li, J., 2014. Overlapping post-seismic deformation processes: afterslip and viscoelastic relaxation following the 2011 Mw 9.0 Tohoku (Japan) earthquake. *Geophys. J.Int.* 2014 (196(1)), 218–229. <http://dx.doi.org/10.1093/gji/ggt376>.
- Douilly, R., Aochi, H., Calais, E., Freed, A.M., 2015. Three-dimensional dynamic rupture simulations across interacting faults: the Mw7.0,2010, Haiti earthquake. *J. Geophys. Res. Solid Earth* 120 (2), 1108–1128. <http://dx.doi.org/10.1002/2014JB011595>.
- Ebner, R., Featherstone, W., 2008. How well can online GPS PPP post-processing services be used to establish geodetic survey control networks?. *J. Appl. Geodesy* 2(3), 149–157. <http://dx.doi.org/10.1515/JAG.2008.017>.
- Eff-Darwich, A., Grassin, O., Fernández, J., 2008. An upper limit to ground deformation in the Island of Tenerife, Canary Islands, for the period 1997–2006. *Pure Appl. Geophys.* 165, 104–1070. http://dx.doi.org/10.49.10.1007/978-3-7643-8907-9_4.
- Ellis, S.M., Wilson, C.J.N., Bannister, S., Bibby, H.M., Heise, W., Wallace, L., Patterson, N., 2007. A future magma inflation event under the rhyolitic Taupo volcano, New Zealand: numerical models based on constraints from geochemical, geological, and geophysical data. *J. Volcanol. Geotherm. Res.* 168 (1–4), 1–27. <http://dx.doi.org/10.1016/j.jvolgeores.2007.06.004>.
- Ellis, S.M., Heise, W., Kissling, W.M., Villamor, P., Schreurs, G., 2014. The effect of crustal melt on rift dynamics: case study of the Taupo Volcanic Zone. *N. Z. J. Geol. Geophys.* 57 (4), 453–458. <http://dx.doi.org/10.1080/00288306.2014.972961>.
- Fernández, J., Carrasco, J., Rundle, J., 1999. Geodetic methods for detecting volcanic unrest: a theoretical approach. *Bull. Volcanol.* 60 (7), 534–544. <http://dx.doi.org/10.1007/s004450050250>.
- Folch, A., Gottsmann, J., 2006. Faults and ground uplift at active calderas. In: Troise, C., De Natale, G., Kilburn, C.R.J. (Eds.), *Mechanisms of Activity and Unrest in Large Calderas*. Geological Society, Special Publications, London, pp.269,109–269,120. <http://dx.doi.org/10.1144/GSL.SP.2006.269.01.07>.
- Fournier, N., Chardot, L., 2012. Understanding volcano hydrothermal unrest from geodetic observations: insights from numerical modeling and application to White Island volcano, New Zealand. *J. Geophys. Res. Solid Earth* 117 (B11). <http://dx.doi.org/10.1029/2012JB009469>.
- Galgana, G.A., Newman, A.V., Hamburger, M.W., Solidum, R.U., 2014. Geodetic observations and modeling of time-varying deformation at Taal Volcano, Philippines. *J. Volcanol. Geotherm. Res.* 271, 11–23. <http://dx.doi.org/10.1016/j.jvolgeores.2013.11.005>.
- Geyer, A., Gottsmann, J., 2010. The influence of mechanical stiffness on caldera deformation and implications

- for the 1971–1984 Rabaul uplift (Papua New Guinea). *Tectonophysics* 483 (3–4), 399–412.
<http://dx.doi.org/10.1016/j.tecto.2009.10.029>.
- Haasdyk, J., Roberts, C., Janssen, V., 2010. Automated monitoring of CORSnet-NSW using the Bernese software. In: *Proceedings of XXIV FIG International Congress 2010, Sydney, Australia, 11–16 April*. (19 pp).
- Hamling, I.J., Hreinsdottir, S., Fournier, N., 2015. The ups and downs of the TVZ: geodetic observations of deformation around the Taupo Volcanic Zone, New Zealand. *J. Geophys. Res. Solid Earth* 120 (6), 4667–4679. <http://dx.doi.org/10.1002/2015JB012125>.
- Hamling, I.J., Hreinsdottir, S., Bannister, S., Palmer, N., 2016. Off-axis magmatism along a subaerial back-arc rift: observations from the Taupo Volcanic Zone, New Zealand. *Sci. Adv.* 2 (6), e1600288
<http://dx.doi.org/10.1126/sciadv.1600288>.
- Heise, W., Bibby, H.M., Caldwell, G., Bannister, S.C., Ogawa, Y., Takakura, S., Uchida, T., 2007. Melt distribution beneath a young continental rift: the Taupo Volcanic Zone, New Zealand. *Geophys. Res. Lett.* 34, L14313 <http://dx.doi.org/10.1029/2007GL029629>.
- Hickey, J., Gottsmann, J., Mothes, P., 2015. Estimating volcanic deformation source parameters with a finite element inversion: the 2001–2002 unrest at Cotopaxi volcano, Ecuador. *J. Geophys. Res. Solid Earth* 120 (3), 1473–1486. <http://dx.doi.org/10.1002/2014JB011731>.
- Holden, L., Wallace, L., Beavan, J., Fournier, N., Cas, R., Ailleres, L., Silcock, D., 2015. Contemporary ground deformation in the Taupo Rift and Okataina Volcanic Centre from 1998 to 2011, measured using GPS. *Geophys. J. Int.* 202 (3), 2082–2105. <http://dx.doi.org/10.1093/gji/ggv243>.
- Holden, L., Silcock, D., Choy, S., Cas, R., Ailleres, L., Fournier, N., 2016. Evaluating a campaign GNSS velocity field derived from an online precise point positioning service. *Geophys. J. Int.* 208 (1), 246–256. <http://dx.doi.org/10.1093/gji/ggw372>.
- Hsu, Y. J., Simons, M., Williams, C., Casarotti, E., 2011. Three-dimensional FEM derived elastic Green's functions for the co-seismic deformation of the 2005 Mw 8.7 Nias-Simeulue, Sumatra earthquake. *Geochem. Geophys. Geosyst.* 12(7), Q07013. <http://dx.doi.org/10.1029/2011GC003553>.
- Jellinek, A.M., DePaolo, D.J., 2003. A model for the origin of large silicic magma chambers: precursors of caldera-forming eruptions. *Bull. Volcanol.* 65 (5), 363–381. <http://dx.doi.org/10.1007/s00445-003-0277-y>.
- Leonard, G.S., Cole, J.W., Nairn, I.A., Self, S., 2002. Basalt triggering of the c. AD 1305 Kaharoa rhyolite eruption, Tarawera Volcanic Complex, New Zealand. *J. Volcanol. Geotherm. Res.* 115 (3–4), 461–486. [http://dx.doi.org/10.1016/S0377-0273\(01\)00326-2](http://dx.doi.org/10.1016/S0377-0273(01)00326-2).
- Long, S.M., Grosfils, E.B., 2009. Modelling the effect of layered volcanic material on magma reservoir failure and associated deformation, with application to Long Valley caldera, California. *J. Volcanol. Geotherm.*

Res. 186 (3–4), 349–360.

Manconi, A., Walter, T.R., Arnelung, F., 2007. Effects of mechanical layering on volcano deformation.

Geophys. J. Int. 170 (2), 952–958. <http://dx.doi.org/10.1111/j.1365-246X.2007.03449.x>.

McTigue, D.F., 1987. Elastic stress and deformation near a finite spherical magma body - resolution of the point-source paradox. J. Geophys. Res. Solid Earth 92 (B12), 12931–12940.

<http://dx.doi.org/10.1029/JB092iB12p12931>.

Mogi, K., 1958. Relations between the eruptions of various volcanoes and the deformation of the ground surface around them. Bull. Earthq. Res. Inst., Univ. Tokyo 36, 99–134.

Nairn, I.A., 2002. Geology of the Okataina Volcanic Centre. In: GNS Sciences, Institute of Geological and Nuclear Sciences Ltd., Lower Hut, New Zealand (Geological Map 25. 21 sheet). (156 pp.).

Nairn, I.A., Cole, J.W., 1981. Basalt dikes in the 1886 Tarawera Rift. N. Z. J. Geol. Geophys. 24 (5–6), 585–592. <http://dx.doi.org/10.1080/00288306.1981.10421534>.

Nairn, I.A., Shane, P.R., Cole, J.W., Leonard, G.J., Self, S., Pearson, N., 2004. Rhyolite magma processes of the similar to AD 1315 Kaharoa eruption episode, Tarawera volcano, New Zealand. J. Volcanol. Geotherm. Res. 131, 265–294. [http://dx.doi.org/10.1016/S0377-0273\(03\)00381-0](http://dx.doi.org/10.1016/S0377-0273(03)00381-0).

Nairn, I.A., Hedenquist, J.W., Villamor, P., Berryman, K.R., Shane, P.A., 2005. The similar to AD1315 Tarawera and Waiotapu eruptions, New Zealand: contemporaneous rhyolite and hydrothermal eruptions driven by an arrested basalt dike system?. Bull. Volcanol. 67 (2), 186–193. <http://dx.doi.org/10.1007/s00445-004-0373-7>.

Newman, A., Dixon, T., Gourmelen, N., 2006. A four-dimensional viscoelastic deformation model for Long Valley Caldera, California, between 1995 and 2000. J. Volcanol. Geotherm. Res. 1 (50(1–3)), 244–269. <http://dx.doi.org/10.1016/j.jvolgeores.2005.07.017>.

Nooner, S.L., Chadwick Jr., W.W., 2009. Volcanic inflation measured in the caldera of axial seamount: implications for magma supply and future eruptions. Geochem. Geophys. Geosyst. 10 (2), Q02002 <http://dx.doi.org/10.1029/2008GC002315>.

Nooner, S., Bennati, L., Calais, E., Buck, R., Hamling, I., Wright, T., Lewi, E., 2009. Post-rifting relaxation in the Afar region, Ethiopia. Geophys. Res. Lett. 36 (21), L21308 <http://dx.doi.org/10.1029/2009gl040502>.

Okada, Y., 1985. Surface deformation due to shear and tensile faults in a half-space. Bull. Seismol. Soc. Am. 75 (4), 1135–1154.

Okada, Y., 1992. Internal deformation due to shear and tensile faults in a half-space. Bull. Seismol. Soc. Am. 82 (2), 1018–1040.

Orsi, G., Civetta, L., Del Gaudio, C., de Vita, S., Di Vito, M.A., Isaia, R., Petrazzuoli, S.M., Ricciardi, G.P., Ricco, C., 1999. Short-term ground deformations and seismicity in the resurgent Campi Flegrei caldera (Italy): an example of active block-resurgence in a densely populated area. J. Volcanol. Geotherm. Res.,

- vol. 91 (2–4), 415–451. [http://dx.doi.org/10.1016/S0377-0273\(99\)00050-5](http://dx.doi.org/10.1016/S0377-0273(99)00050-5).
- Pascal, K., Neuberg, J., Rivalta, E., 2013. On precisely modelling surface deformation due to interacting magma chambers and dykes. *Geophys. J. Int.* 196 (1), 253–278. <http://dx.doi.org/10.1093/gji/ggt343>.
- Peltier, A., Hurst, T., Scott, B., Cayol, V., 2009. Structures involved in the vertical deformation at Lake Taupo (New Zealand) between 1979 and 2007: new insights from numerical modelling. *J. Volcanol. Geotherm. Res.* 181 (3–4), 173–184. <http://dx.doi.org/10.1016/j.jvolgeores.2009.01.017>.
- Peltier, A., Scott, B., Hurst, T., 2009. Ground deformation patterns at White Island volcano (New Zealand) between 1967 and 2008 deduced from levelling data. *J. Volcanol. Geotherm. Res.* 181 (3–4), 207–219. <http://dx.doi.org/10.1016/j.jvolgeores.2009.01.020>.
- Rinaldi, A.P., Todesco, M., Bonafede, M., 2010. Hydrothermal instability and ground displacement at the Campi Flegrei caldera. *Phys. Earth Planet. Inter.* 178 (3–4), 155–161. <http://dx.doi.org/10.1016/j.pepi.2009.09.005>.
- Rinaldi, A.P., Todesco, M., Vandemeulebrouck, J., Revil, A., Bonafede, M., 2011. Electrical conductivity, ground displacement, gravity changes, and gas flow at Solfatara crater (Campi Flegrei caldera, Italy): results from numerical modeling. *J. Volcanol. Geotherm. Res.* 207 (3–4), 93–105. <http://dx.doi.org/10.1016/j.jvolgeores.2011.07.008>.
- Ronchin, E., Masterlark, T., Molist, J.M., Saunders, S., Tao, W., 2013. Solid modeling techniques to build 3D finite element models of volcanic systems: an example from the Rabaul Caldera system, Papua New Guinea. *Comput. Geosci.* 52, 325–333. <http://dx.doi.org/10.1016/j.cageo.2012.09.025>.
- Ronchin, E., Geyer, A., Mart., J., 2015. Evaluating topographic effects on ground deformation: insights from finite element modeling. *J. Surv. Geophys.* 36, 513. <http://dx.doi.org/10.1007/s10712-015-9325-3>.
- Rowland, J.V., Sibson, R.H., 2001. Extensional fault kinematics within the Taupo Volcanic Zone, New Zealand: soft-linked segmentation of a continental rift system. *N. Z. J. Geol. Geophys.* 44 (2), 271–283. <http://dx.doi.org/10.1080/00288306.2001.9514938>.
- Rowland, J.V., Sibson, R.H., 2004. Structural controls on hydrothermal flow in a segmented rift system, Taupo Volcanic Zone, New Zealand. *Geofluids* 4 (4), 259–283. <http://dx.doi.org/10.1111/j.1468-8123.2004.00091.x>.
- Rowland, J.V., Wilson, C.J.N., Gravley, D.M., 2010. Spatial and temporal variations in magma-assisted rifting, Taupo Volcanic Zone, New Zealand. *J. Volcanol. Geoth. Res.* 190 (1–2), 89–108. <http://dx.doi.org/10.1016/j.jvolgeores.2009.05.004>.
- Samsonov, S., Beavan, J., Gonzalez, P., Tiampo, K., Fernández, J., 2011. Ground deformation in the Taupo Volcanic Zone, New Zealand, observed by ALOS PALSAR interferometry. *Geophys. J. Int.* 187 (1), 147–160. <http://dx.doi.org/10.1111/j.1365-246X.2011.05129.x>.
- Scott, B.J., 1989. Geodetic and geophysical monitoring of the 1886 Tarawera rift. In: Latter, J.H. (Ed.),

- Volcanic Hazards Assessment and Monitoring. IAVCEI Proceedings in Volcanology, Springer-Verlag, Berlin, pp. 575–584.
- Seebeck, H., Nicol, A., 2009. Dike intrusion and displacement accumulation at the intersection of the Okataina Volcanic Centre and Paeroa Fault zone, Taupo Rift, New Zealand. *Tectonophysics* 475 (3–4), 575–585. <http://dx.doi.org/10.1016/j.tecto.2009.07.009>.
- Seebeck, H., Nicol, A., Stern, T.A., Bibby, H.M., Stagpoole, V., 2010. Fault controls on the geometry and location of the Okataina Caldera, Taupo Volcanic Zone, New Zealand. *J. Volcanol. Geotherm. Res.* 190 (1–2), 136–151. <http://dx.doi.org/10.1016/j.jvolgeores.2009.04.011>.
- Sherburn, S., Nairn, I.A., 2001. A scenario of geophysical events inferred to have preceded the 1300 AD Kaharoa eruption: lessons for the future. *Inst. Geol. Nucl. Sci. (Science Report 2001/26 Lower Hutt, New Zealand)*. (57 pp).
- Sherburn, S., Nairn, I.A., 2004. Modelling geophysical precursors to the prehistoric c. AD1305 Kaharoa rhyolite eruption of Tarawera volcano, New Zealand. *Nat. Hazards* 32 (1), 37–58. <http://dx.doi.org/10.1023/B:NHAZ.0000026791.16566.96>.
- Sherburn, S., Bannister, S., Bibby, H., 2003. Seismic velocity structure of the central Taupo Volcanic Zone, New Zealand, from local earthquake tomography. *J. Volcanol. Geotherm. Res.* 122 (1–2), 69–88. [http://dx.doi.org/10.1016/S0377-0273\(02\)00470-5](http://dx.doi.org/10.1016/S0377-0273(02)00470-5).
- Spinks, K.D., Acocella, V., Cole, J.W., Bassett, K.N., 2005. Structural control of volcanism and caldera development in the transtensional Taupo Volcanic Zone, New Zealand. *J. Volcanol. Geotherm. Res.* 144 (1–4), 7–22. <http://dx.doi.org/10.1016/j.jvolgeores.2004.11.014>.
- Todesco, M., 2009. Signals from the Campi Flegrei hydrothermal system: role of a “magmatic” source of fluids. *J. Geophys. Res. Solid Earth* 114, B05201 <http://dx.doi.org/10.1029/2008JB006134>.
- Trasatti, E., Giunchi, C., Bonafede, M., 2003. Effects of topography and rheological layering on ground deformation in volcanic regions. *J. Volcanol. Geotherm. Res.* 122 (1–2), 89–110. [http://dx.doi.org/10.1016/S0377-0273\(02\)00473-0](http://dx.doi.org/10.1016/S0377-0273(02)00473-0).
- Troise, C., De Natale, G., Kilburn, C.R.J., 2004. Non-linear effects in ground deformation at calderas due to the presence of structural discontinuities. *Ann. Geophys.* 47 (4), 1513–1520.
- Villamor, P., Berryman, K.R., Nairn, I.A., Wilson, K., Litchfield, N., Reis, W., 2011. Associations between volcanic fields of the Okataina volcanic centre and surface rupture of nearby active vents. *Geol. Soc. Am. Bull.* 123 (7–8), 1383–1405. <http://dx.doi.org/10.1130/B30184.1>.
- Wallace, L.M., Beavan, J., McCaffrey, R., Darby, D., 2004. Subduction zone coupling and tectonic block rotations in the North Island, New Zealand. *J. Geophys. Res. Solid Earth* 109 (B12), B12406 <http://dx.doi.org/10.1029/2004JB003241>.
- Wessel, P., Smith, W.H.F., 1995. New version of the generic mapping tools released. *EOS Trans.* 76 (33), 329.

- Williams, C.A., 2006. Development of a package for modeling stress in the lithosphere. *Eos Trans. AGU* 87 (36) (Jt. Assem. Suppl., Abstract T24A-01).
- Williams, C.A., Aagaard, B., Knepley, M.G., 2005. Development of software for studying earthquakes across multiple spatial and temporal scales by coupling quasi-static and dynamic simulations. *Eos Trans. AGU* 86 (52) (Fall Meet. Suppl., Abstract S53A-1072).
- Wilson, C.J.N., Houghton, B.F., McWilliams, M.O., Lanphere, M.A., Weaver, S.D., Briggs, R.M., 1995. Volcanic and structural evolution of Taupo Volcanic Zone, New-Zealand – a review. *J. Volcanol. Geotherm. Res.* 68 (1–3), 1–28. [http://dx.doi.org/10.1016/0377-0273\(95\)00006-G](http://dx.doi.org/10.1016/0377-0273(95)00006-G).
- Yu, T., Fernández, J., Tseng, C.L., Sevilla, M.J., Arana, C., 2000. Sensitivity test of the geodetic network in the Las Canadas Caldera, Tenerife, for volcano monitoring. *J. Volcanol. Geotherm. Res.* 103, 397–407. [http://dx.doi.org/10.1016/S0377-0273\(00\)00233-X](http://dx.doi.org/10.1016/S0377-0273(00)00233-X).

5 Summary of results and research implications

5.1 Introduction

This research has considered contemporary surface deformation through the Okataina Volcanic Centre and surrounding Taupo Rift in the North Island of New Zealand. This is derived from repeated campaign and continuous GPS data collected from 2000 to 2011. Horizontal and vertical velocities are derived using an established and new processing technique. These velocities are considered in the context of regional tectonic, magmatic and/or hydrothermal processes. Deformation related to hypothetical volcanic activity at the OVC is modelled using the Finite Element technique in Pylith software. The results are used to consider the likely deformation patterns and whether the present geodetic monitoring network could detect these.

This chapter summarises the key results and findings and relates these to the research aims presented in Chapter 1. The implications for 1) understanding the nature of contemporary ground deformation within the OVC and the surrounding Taupo Rift and 2) for monitoring ground deformation using geodetic methods at the OVC are considered to assess their applicability at other large active calderas. Recommendations are presented regarding further research at the OVC. Chapter 1, which is introductory chapter, is not further discussed.

5.2 Summary of Chapter 2: Contemporary ground deformation in the Taupo Rift and Okataina Volcanic Centre from 1998 to 2011, measured using GPS.

This chapter presents a detailed picture of contemporary deformation at the Okataina Volcanic Centre (OVC) and within the surrounding Taupo rift. This is achieved by using existing and new GPS campaign and continuous GPS (cGPS) data collected between 1998 and 2011 by GNS Science New Zealand. The observed deformation is interpreted with the aim of resolving the distribution of deformation and strain rates within the Taupo rift and OVC, which have not previously been well constrained to a high level of detail. The main features of this chapter include:

- That ground deformation through the central Taupo rift and OVC region is not uniform in rate or distribution. This is indicated by the presence of a number of distinctive features, which include 1) significant contraction within the Kapenga segment and extension offset westwards from the zone of normal faulting; 2) rapid changes of principal strain rate axis orientations at the intersection of the Kapenga and Okataina segments; 3) elevated extension and shear strain rates at the Tarawera rift within the OVC; 4) very large subsidence rates in the central rift (up to -1.94 cm/yr^{-1}); and, 5) lower extensional strain rates than previously documented in the Whakatane graben (Wallace et al., 2004).
- The contraction within the normal fault system of the Ngakuru graben and near the Paeroa fault (within the Kapenga segment), and extension up to approximately 15 km west of the main rift axis do not agree with abundant geological estimates of normal faulting in the central rift. A magma cooling mechanism proposed by Hamling et al., (2015) would explain this mismatch. This would suggest that present day magmatic processes are masking geological observations of long-term normal faulting in the Kapenga segment and are also responsible for the observed extension west of the main rift axis.
- The deformation pattern at the intersection of the Kapenga and Okataina segments (and the south-western border of the OVC) likely reflects magmatic or hydrothermal processes at this location. This conclusion is supported by a good agreement between our principal strain rate axes rotations and those modelled just south of Okataina by Ellis et al., (2014). Our deformation field may also reflect a transition between different sets of hydrothermal and/or magmatic processes in this region.
- The highly heterogeneous strain rates and velocity field through the OVC include a broad scale clockwise rotation of horizontal principal strain rate axes across the caldera, localised elevated strain rates along the Tarawera rift (and vicinity) and large subsidence rates across Lake Tarawera, Lake Rotomahana, south of the OVC.
- This pattern shows no clear evidence of active volcanic processes. However, in the Tarawera rift the strain rate environment is highly suitable for magma migration and diking though the upper crust. It is not clear if this is related to volcanic and magmatic processes, given the nearby hydrothermal activity and likely influence of regional tectonic structure. However, given the recent history of volcanism in this part of the OVC, future deformation there must be interpreted cautiously.

The contents of this chapter are based on a peer reviewed paper published in the *Geophysical Journal International* (see Holden et al., 2015; doi:10.1093/gji/ggv243).

5.3 Summary of Chapter 3: Evaluating a Campaign GNSS Velocity Field Derived From an Online Precise Point Positioning Service.

This chapter investigates a new methodology for deriving geodetic velocities for use in studies of geophysical processes in the research community. The study involves re-processing the campaign and CORS GPS dataset used in Holden et al., (2015) with the online Jet Propulsion Laboratory (JPL) Automated Precise Positioning Service (APPS) service to derive station velocities. The two velocity datasets are then compared. The major contributions of this paper are to show that:

- Reliable horizontal and height solutions can be derived using the JPL APPS processing service.
- Reliable horizontal velocities can also be calculated from these solutions. The average uncertainty we estimate for the campaign data horizontal velocities derived from the APPS coordinate solutions ($\pm 1.7 \text{ mm/yr}^{-1}$) is similar to that of the Bernese horizontal velocities ($\pm 1.5 \text{ mm/yr}^{-1}$). Less reliability can be placed on the vertical velocities derived from the APPS height solutions, as in some cases their uncertainty is significantly larger than the magnitude of their velocity.
- The quality of the velocities derived from these positions indicates that they can be used to measure deformation related to a variety of geophysical processes. In general, the average level of uncertainty associated with calculated horizontal and vertical velocities presented in this research is generally less than the expected deformation rates associated with subsidence, volcanic, landslide and glacial processes. Therefore, the APPS and Bernese velocities could be used to measure deformation associated with these particular processes with a high level of confidence.
- The uncertainties associated with these must still be considered carefully in the context of the expected deformation associated with these processes. The average APPS and Bernese horizontal velocity uncertainties (± 1.5 and $\pm 1.7 \text{ mm/yr}^{-1}$ respectively) are of a similar magnitude to the velocities expected for inter-seismic and post-seismic deformation. This implies that they could measure inter- and post-seismic deformation, but that to achieve this with a suitable degree of confidence, careful field planning and practice, repeated GNSS campaigns and rigorous processing procedures must be used.

The contents of this chapter are based on a peer reviewed paper published in the *Geophysical Journal International* (see Holden et al., 2016; doi: 10.1093/gji/ggw372).

5.4 Summary of Chapter 4: Ground deformation patterns associated with magma migration beneath the Okataina Volcanic Centre.

This research uses the finite element (FE) modelling technique to model surface ground deformation patterns associated with magma accumulation and dike emplacement beneath the OVC in greater detail. The influence of caldera structure on the deformation field is investigated. This paper also considers the ability of the present-day GPS GeoNet monitoring network to detect or observe the deformation predicted from this modelling. This is achieved by comparing the magnitude of the modelled horizontal and vertical displacements to the detection capabilities of the cGPS network.

The main features of this research are;

- Several FE models were produced to reflect various magma migration scenarios at the Okataina Volcanic Centre. These include 1) a simple spherical magma chamber at 6km depth, 2) a rectangular sill chamber at 6 km depth and 3) a vertical dike emplaced at 5km depth below the OVC caldera. In the models, the magma chambers (in 1 and 2) are assumed to be over-pressurised from magma intrusion from greater depths below.
- In general, the modelled horizontal and vertical displacement fields are distributed in NW – SE ‘lobe’ based regions. The magnitude of the modelled displacements decay rapidly away from the Tarawera rift through these regions.
- The ring fault structure increases the modelled horizontal and vertical displacements in the OVC region, but particularly in the vicinity of the southern margin of the ring fault structure.
- In this region, the elevated modelled displacements may reflect the closer proximity of the ring fault structure to the displacement source and the elevated inward dipping fault dip angle of the ring fault structure there. This may promote greater interaction with the modelled stress field and increased surface displacements.
- The approximate limit of detectable horizontal displacement in the surrounding cGPS network for the scenarios modelled here extends to station RGLI (approximately 30km away from the Tarawera rift to its NW).
- The approximate limit of detectable vertical displacement in the surrounding cGPS network for the scenarios modelled here extends to approximately 10km from the Tarawera rift. Station RGTA within the OVC would clearly observe vertical displacement above its detection capabilities. At more distant cGPS stations the modelled vertical displacement is below their detection capabilities.

- The results of the modelling also show that only station RGRR would observe some measurable deformation southwest of the OVC for associated with the scenarios tested here. During future volcanic activity at the OVC, more GPS observations would be required in this region to enhance understanding of ground displacements recorded across the network. These observations would complement and ground truth space based techniques such as InSAR.

The contents of this chapter are based on a peer-reviewed paper that has been published in the Journal of Volcanology and Geothermal Research (JVGR).

5.5 Research Implications

5.5.1 Implications for rift processes and related deformation.

The identification of contractional strain and significant strain-rate heterogeneity in the geodetic **data** within the central Taupo Rift is unexpected. These features contrast with extensional strains documented from geological observations in the same region (Villamor and Berryman, 2001) and they have been linked to cooling of a large regional magma body (Hamling et al., 2015) and magma accumulation south of Okataina (Ellis et al., 2014). However, contractional structures in rift settings are considered to occur only locally (Lewis and Balbridge, 1994) and with limited preservation potential (Bubsy, 2012). Therefore, it is likely that in the longer term, these areas (e.g. those presently undergoing contraction and high strain rates) through the Taupo Rift might show extension reflecting more long-term tectonic processes. Nonetheless, our results suggest that in extensional rift settings, short-term transient processes can dominate the contemporary regional deformation signal within geodetic data. The presence of these processes may accommodate areas of trans-tension or transpression. If the principle axes of extension are not exactly orthogonal to the rift trend, trans-tension may result. In a terrain that is dismembered by faults (e.g. the central Taupo rift), the local areas of transpression will also accommodate heterogeneous strain distribution in the upper crust.

The mismatch suggests that the GPS velocities measured within the central Taupo Rift in this research do not represent long-term deformation. The discrepancy highlights the limitations of short-term geodetic observations to provide insight into structure and kinematics in rift settings in the presence of magmatic processes. This contrasts to more tectonic settings such as the Basin and Range province, where contemporary deformation derived from GPS is considered indicative of long-term deformation (Hammond and Thatcher, 2004). Only in the tectonic Whakatane graben, in the absence of magmatic processes (Wallace et al., 2004; Holden et al., 2015), is there a good correlation between geodetic and geological estimates of strain-rates.

Only there, can it be confidently concluded that deformation is linked to tectonic block rotation along the Hikurangi subduction zone (Wallace et al., 2004).

The mismatch also implies that numerical inversions using ground velocities (e.g. for elastic dislocation models, earthquake cycle models and block models) derived from geodetic data in rift settings should be undertaken with caution. The velocities in this research should not be used to model fault slip rates or distribution, infer rift structure or identify tectonic units within the central Taupo rift. This is due to the likely influence of magmatic processes or other transient motions. Similar caution must be observed when inverting geodetic data at intra-rift calderas for estimating deformation source parameters (e.g. chamber size, depth or overpressure).

5.5.2 Implications for volcanic processes at the OVC.

This research provides no geodetic evidence of any detectable volcanic activity at the OVC between 1998 and 2011. No regional uplift signal from magma accumulation or emplacement at depth, as speculated in previous research (Sherburn and Nairn, 2001; Sherburn and Nairn, 2004), or modelled in this research (see chapter 4), is evident in the deformation field surrounding the OVC. This implies that during the study period, 1) no volcanic activity occurred at the OVC, or 2) that the geodetic dataset was not able to detect any volcanic signal or 3) that the observed deformation in the OVC is a result of regional processes. This research favours the latter scenario and that present day deformation through the OVC reflects regional magmatic and/or tectonic processes outside the caldera. This is supported as the significant strain rate rotations and subsidence rates across the caldera, particularly in the SW, are similar to those observed through the central Taupo Rift. This implies that between periods of volcanic unrest at the OVC, deformation there most likely accommodates regional tectonic and magmatic processes.

At the Tarawera Rift, the co-location of high extension and shear strain rates with the location of the most recent volcanic activity (the 1886 Tarawera eruption) requires further investigation. These features suggest a present day environment through the Tarawera rift that is highly suitable for dike emplacement and any change in the style or rate of deformation there should be monitored closely. However, the lack of evidence of volcanic activity during the study period suggests that the observed extension through the Tarawera rift at present most likely accommodates regional processes outside the caldera, rather than volcanic processes within it during repose periods. This also suggests that historically, the timing of volcanic activity at the OVC may be linked to changes in regional processes. However, little insight can be gathered from the geodetic data presented here in this regard.

The ring fault structure used in the modelling in chapter 4 is a first order approximation; however it is representative of the numerous normal faults in this section of the rift and in the vicinity of the OVC. Other studies using numerical modelling (Walter, 2008; Rochin et al., 2013; Bathke et al., 2015) have shown that 1) the presence of, or slip on, ring fault structures may account for observed surface deformation at calderas and 2) that the geometry of these structures can be very complex. The results presented here support these findings and suggest that a ring fault structure at the OVC is likely to control surface deformation patterns associated with renewed volcanic activity.

In a detailed study of the link between ring faults and ring dikes during caldera subsidence, Walter (2008) showed that location of ring dikes may be controlled by tectonic and magmatic processes. He also emphasised the importance of understanding the volcanic-tectonic environment in these circumstances. The FE modelling results presented in chapter 4 (in this research), suggest that the presence of the ring-fault structure might provide an environment that promotes vertical magma ascent (diking) at shallow depths below the OVC caldera. Specifically, the results showed that the largest modelled horizontal surface displacements occurred across its southern margin, trending NW and SE approximately orthogonal to the fault plane at this section of the structure. This represents an extensional environment (at least on the surface) in the vicinity of the ring fault structure (near the Tarawera rift). Further FE modelling is required to determine whether this feature persists in the upper crust (upper few kilometres) beneath Tarawera (or the OVC). If this environment does exist in the shallow crust at the OVC, a ring fault structure may provide a future conduit for magma to ascend to the surface.

5.5.3 Implications for geodetic monitoring at the OVC and other calderas worldwide.

The station velocities presented here provide a baseline level of background deformation through the OVC from which possible precursory signals of renewed volcanic activity might be identified. However, since no volcanic activity has occurred at the OVC since the installation of geodetic instrumentation, little is known regarding the probable deformation signals resulting from magma accumulation and migration at depth at the OVC. This includes the magnitude and spatial extent of the surface deformation and the sensitivity of the cGPS monitoring network. The modelling presented in chapter 4 provides some new insights into these signals and adds to the limited body of knowledge regarding geodetic precursors at the OVC (Sherburn and Nairn 2001; Sherburn and Nairn 2004).

The surface displacements, modelled in chapter 4, are associated with magma accumulation or dike emplacement at depth below the OVC. The results show that the deformation would be detected within the

surrounding cGPS network, mostly limited to stations in the caldera and to its NW. RGRR is the only cGPS station SW of the OVC that coincides with the modelled displacement there. Further, cGPS station (RGTA) at the Tarawera rift is the only station in the OVC that might observe vertical deformation clearly above measurement noise. Deformation observed at this station must therefore be interpreted carefully, as this might appear as an anomalous vertical displacement (only observed at this station). However considered alongside the horizontal displacement observed at neighbouring stations (that the modelling indicated in chapter 4), it is likely that present-day cGPS network surrounding the OVC, would detect displacements associated with the volcanic scenarios tested in chapter 4. This is important since, the brittle/ductile zone beneath the central Taupo Rift is considered to be 6km (Bryan et al., 1999) and local seismographs might not observe an increase in seismicity above background levels linked to the magma accumulation. To improve the ability to monitor deformation related to volcanic activity at the OVC, it would be beneficial to obtain more cGPS observations (or high frequency campaign GNSS observations) in the SW, across the Reporoa caldera and Kaingaroa plains. This would not only complement any InSar data, but also better constrain deformation source parameters when performing numerical data inversion, during or following any period of renewed volcanic activity.

The results show that the spatial resolution of the present day cGPS network at the OVC is an important factor in order to properly observe the deformation fields modelled in chapter 4 and attempt to determine their source/s. In some cases, the inability to observe the modelled deformation is not necessarily due to the small magnitude of deformation, but rather the locations of the cGPS receivers. For example, it was identified that only station RGRR to the SW of the OVC would observe the modelled horizontal displacements for the scenarios testing in chapter 4. Further, chapter 4 shows that whether station RGTA (in the Tarawera rift) observes uplift or subsidence is a key difference between the rectangular chamber and vertical dike scenario. The modelling also shows that this uplift or subsidence may not necessarily be observed at nearby receivers. Thus, although the present day cGPS network is likely to observe some deformation related to the hypothetical scenario's modelled in chapter 4, it would be difficult to identify which of the two scenario's is responsible.

This is problematic, since the likely location of any future volcanic activity within the caldera is not well constrained. This also highlights the importance of complementing cGPS monitoring networks, with other monitoring techniques, including seismograph networks and remote sensing techniques such as InSAR. However, this study suggests that more GPS observations SW of the OVC would enhance understanding of ground movement data patterns. Repeated campaign GNSS surveys are conducted through this region, however their temporal resolution is low.

5.5.4 Implications for GNSS data processing and field surveys.

The methodology presented in chapter 3 provides an alternative method to determine station velocities using an online PPP service. It has broad implications for both GNSS fieldwork and GNSS data processing in geophysical studies. The novelty of this approach includes the need for significantly less personnel and resources in the field. This significantly reduces operating costs and greater flexibility to when the fieldwork could be conducted. Further, less training in scientific GNSS software and post-processing would be required. This would benefit various organisations, particularly Government scientific organisations in developing countries, where the number of personnel appropriately trained in GNSS data processing is often limited. Also, deformation surveys can be conducted without the need for CORS networks. This provides for easier field surveys to be undertaken in remote locations, such glacial movement in the arctic regions. The approach also provides field survey flexibility that can be used to significantly increase the spatial and temporal resolution of ground based geodetic surveys. Since the PPP solution is absolute (earth centred), GNSS receivers need not be deployed simultaneously. As a result, transient processes or anomalous deformation signals can be investigated in greater detail than from bi-annual (or longer) repeated campaign GNSS surveys. Rather, a dedicated receiver (or receivers) could occupy a number of geodetic monuments many times over a year.

This approach could be used to investigate the large subsidence signals (larger than those expected from rifting) identified through the hydrothermal fields at the SW boundary of the OVC. Subsidence rates there have been measured using InSAR (Hamling et al., 2015) and campaign GNSS data (Holden et al., 2015) as 15mm/yr^{-1} and up to 20mm/yr^{-1} respectively. However, whether these rates are steady or transient over the observation period cannot be resolved due to the low temporal resolution of the data. Further, cGPS data availability is very limited and not of sufficient spatial resolution in this vicinity. Using the approach highlighted in chapter 3, a number of GNSS receivers could be regularly deployed on geodetic monuments and then reoccupy these monuments, over shorter periods and the data processed more rapidly. Such a survey could be undertaken by a single individual. A similar approach could be utilised to better constrain the deformation identified at the Tarawera Rift in the OVC.

5.5.5 Suggestions for further research

This research has contributed a more detailed picture of the velocity and strain-rate field through the central Taupo Rift and OVC, than previously documented. This has provided a clearer picture of present day deformation within the OVC and some insight into its relationship to regional geological processes. The evaluation of an online GNSS processing service for obtaining ground deformation estimates using campaign

GNSS dataset indicated that reliable station velocities could be obtained. Detailed models exploring ground deformation related to various volcanic scenarios at the OVC were developed. However, there still remain outstanding research topics that need to be addressed in the future. These topics include the following:

- ***Incorporate new GNSS campaign data from the central Taupo Rift into the velocity and strain rate estimates.*** GNS science conducts campaign GNSS surveys every approximately four years through the central Taupo rift. The inclusion of new geodetic data to derive updated station velocities would further constrain deformation rates in the OVC as well as reduce velocity and strain rate uncertainties. Particularly in the vicinity of the hydrothermal fields at the SW, where deformation is likely to be highly episodic. The deployment of more GNSS receivers through the OVC caldera would be beneficial, particularly across the Tarawera Rift. This would better constrain the extensional strain rates observed there in this research and complement recent InSAR studies (Hamling et al., 2015), which are at present limited at the OVC.
- ***Further investigate the uncertainties associated with velocities derived from online PPP services.*** The uncertainties associated with the station velocities derived from campaign data and the online JPL PPP service was estimated in chapter 3. The application of this approach to different geophysical processes is limited by the magnitude of the velocity uncertainties. Therefore, more research is required to determine if the uncertainties are associated with the quality of the campaign GNSS dataset and/or the capabilities of the online PPP processing service. This would best be accomplished using an independent campaign GNSS datasets, from independent sources. This includes different methodologies (e.g. occupation times), field practices and GPS receiver types.
- ***Improved FE modelling.*** This FE modelling undertaken here has highlighted the need to undertake further modelling. This should address more realistic deformation source and caldera ring fault geometries, multiple deformation sources and layered rock properties beneath the OVC. The results would better constrain the detection capabilities of the existing cGPS network as well as the surface deformation patterns associated with a wider range of volcanic scenarios. This extended modelling may also provide some insight into the role of the ring fault structure in accommodating extensional processes at the Tarawera rift and the whether its presence promotes the passage of magma to shallow depths at the OVC. For instance, the co-location of measured high extension and shear strain rates with maximum FE modelled surface displacements at the location of the most recent volcanic activity

in the OVC (e.g. the Tarawera rift) is intriguing. This suggests a causal relationship between magmatic/volcanic processes and ground deformation at the OVC, which must be investigated further.

- ***Reconcile modelled deformation at the OVC with background regional deformation.*** An omission of this research is an investigation of how the modelled displacements at the OVC in chapter 4, would appear within the present day observed heterogeneous strain field and large subsidence rates present in the central Taupo Rift. This could be achieved through incorporating rifting rates through in the OVC region into the FE modelling. The FE modelling approach may be adapted to consider the contribution of diking processes at the OVC to the overall rifting (extension) budget in this section of the Taupo rift. Dike induced extension is considered an important mechanism for extension through this section of the Taupo rift (Seebeck et al., 2009; Rowland et al., 2010), but its contribution to the total extension budget is not well constrained. In particular this would include modelling deformation related to the emplacement or ascent of dikes at shallower depths below the OVC.

5.6 References

- Acocella, V., Spinks, K., Cole, J., Nicol, A., 2003. Oblique back arc rifting of Taupo Volcanic Zone, New Zealand. *Tectonics* 22 (4), 1045. <http://dx.doi.org/10.1111/j.1365-246X.2007.03345.x>.
- Bathke, H., Nikkhoo, M., Holohan, E.P., Walter, T.R., 2015. Insights into the 3D architecture of an active caldera ring-fault at Tendürek volcano through modeling of geodetic data, *Earth and Planetary Science Letters*, 422(157-168). doi:10.1016/j.epsl.2015.03.041.
- Busby, C. J., Azor, A., (Eds.), *Tectonics of Sedimentary Basins: Recent Advances*, Blackwell Publishing Ltd. (2012), pp. 382–404
- Ellis, S. M., Heise, W., Kissling, W.M., Villamor, P., Schreurs, G., 2014. The effect of crustal melt on rift dynamics: case study of the Taupo Volcanic Zone. *N. Z. J. Geol. Geophys.*, 57(4): 453-458; doi: 10.1080/00288306.2014.972961
- Hamling, I. J., Hreinsdottir, S., Fournier, N., 2015. The ups and downs of the TVZ: geodetic observations of deformation around the Taupo Volcanic Zone, New Zealand. *J. Geophys. Res. Solid Earth* 120 (6), 4667–4679. <http://dx.doi.org/10.1002/2015JB012125>.
- Holden, L., Wallace, L., Beavan, J., Fournier, N., Cas, R., Ailleres, L., Silcock, D., 2015. Contemporary ground deformation in the Taupo Rift and Okataina Volcanic Centre from 1998 to 2011, measured using GPS. *Geophys. J. Int.* 202 (3), 2082–2105. <http://dx.doi.org/10.1093/gji/ggv243>.
- Lewis, C. J., Baldridge, W. S., 1994. Crustal extension in the Rio Grande Rift, New Mexico: Half-grabens, accommodation zones and shoulder uplifts in the Ladron Peak-Sierra Lucero area, *in* Keller, G.R., and Cather, S.M., (Eds), *Basins of the Rio Grande Rift: Structure, Stratigraphy, and Tectonic Setting*: Boulder, Colorado, Geological Society of America Special Paper 291.
- Ronchin, E., Masterlark, T., Molist, J.M., Saunders, S., Tao, W., 2013. Solid modeling techniques to build 3D finite element models of volcanic systems: an example from the Rabaul Caldera system, Papua New Guinea. *Comput. Geosci.* 52, 325–333. <http://dx.doi.org/10.1016/j.cageo.2012.09.025>.
- Rowland, J. V., Sibson, R. H., 2001. Extensional fault kinematics within the Taupo Volcanic Zone, New Zealand: soft-linked segmentation of a continental rift system. *N. Z. J. Geol. Geophys.* 44 (2), 271–283. <http://dx.doi.org/10.1080/00288306.2001.9514938>.
- Rowland, J. V., Sibson, R. H., 2004. Structural controls on hydrothermal flow in a segmented rift system, Taupo Volcanic Zone, New Zealand. *Geofluids* 4 (4), 259–283. <http://dx.doi.org/10.1111/j.1468-8123.2004.00091.x>.
- Rowland, J. V., Wilson, C. J. N., Gravley, D. M., 2010. Spatial and temporal variations in magma-assisted rifting, Taupo Volcanic Zone, New Zealand. *J. Volcanol. Geoth. Res.* 190 (1–2), 89–108. <http://dx.doi.org/10.1016/j.jvolgeores.2009.05.004>.

- Sherburn, S., Nairn, I. A., 2001. A scenario of geophysical events inferred to have preceded the 1300AD Kaharoa eruption: lessons for the future, Inst. Geol. Nucl. Sciences Science Report 2001/26, 57 pp. Lower Hutt, New Zealand.
- Sherburn, S., Nairn, I. A., 2004. Modelling geophysical precursors to the prehistoric c. AD1305 Kaharoa rhyolite eruption of Tarawera volcano, New Zealand. *Nat. Hazards* 32 (1), 37–58.
<http://dx.doi.org/10.1023/B:NHAZ.0000026791.16566.96>.
- Wallace, L. M., Beavan, J., McCaffrey, R., Darby, D., 2004. Subduction zone coupling and tectonic block rotations in the North Island, New Zealand. *J. Geophys. Res. Solid Earth* 109 (B12), B12406
<http://dx.doi.org/10.1029/2004JB003241>.
- Walter, T.R., 2008. Facilitating dike intrusions into ring-faults. *Dev. Volcanol.* 10, 351–374.
 doi:10.1016/S1871-644X(07)00009-5
- Villamor, P., Berryman, K., 2001. A late Quaternary extension rate in the Taupo Volcanic Zone, New Zealand, derived from fault slip data. *N. Z. J. Geol. Geophys.*, 44(2), 243–269.
- Villamor, P., Berryman, K.R., 2006. Evolution of the southern termination of the Taupo Rift, New Zealand. *N. Z. J. Geol. Geophys.*, 49(1), 23–37.